Experimental Evaluation of Knee Exoskeleton Interface Mechanisms

Kaleb Mannion

Thesis submitted to the University of Ottawa in partial fulfillment of the requirements for the Master of Applied Science in Biomedical Engineering

Ottawa – Carleton Institute for Biomedical Engineering

Department of Mechanical Engineering

Faculty of Engineering

University of Ottawa

ABSTRACT

Mobility loss or impairment, whether due to injury, disease, or aging, affects quality of life, leads to poorer healthcare outcomes, diminished life satisfaction, and increased healthcare costs. Exoskeletons, mechanical devices worn to assist or augment the wearer's capabilities, are a method to mitigate these negative outcomes. They can reduce strain and injuries associated with physical activities or restore mobility to those affected by impairments.

A major challenge for exoskeletons is ensuring user comfort. Literature indicates that comfort is crucial for their adoption. Discomfort often arises from a mismatch between the user's natural motion and the mechanical motion of the exoskeleton, causing excessive compression or shear on the user's limbs. One proposed solution is to add passive degrees of freedom between the user and the exoskeleton to better match their movements. While this has shown promise in simulations, experimental verification is lacking.

This research experimentally verified if adding passive degrees of freedom to knee exoskeletons improves user comfort and to determine their optimal stiffness and orientation. To test this, modular connection mechanisms were developed to allow motion between the exoskeleton frame and cuffs in one degree of freedom while restricting others. These mechanisms could be configured to add some stiffness to the active degree of freedom. The connection mechanisms were tested on both a leg phantom and on a human participant. During testing, interface pressures between the limb and the cuff, as well as limb and exoskeleton positions, were measured to compare different configurations.

The results support adding passive translation along the axis of the shank as well as in the transverse axis of the shank. However, the leg phantom had limited predictive ability, highlighting the need for human studies to be conducted where possible. Further research is necessary to better characterize the effect of passive degrees of freedom through human trials.

ACKNOWLEDGEMENTS

Thanks to Dr. Doumit and Emelie for their help in preparing and editing my thesis and conference paper.

Thanks to my parents, Kevin and Dayle, for supporting me during my studies. I couldn't have done this without your support and love.

Thanks to Hasini, for listening to, supporting, motivating and being there for me.

TABLE OF CONTENTS

List of Figures

List of Tables

Nomenclature

Acronym	Definition
ADC	Analogue to digital converter
CM	Connection mechanism
DOF	Degree of freedom
fps	Frames per second
ICR	Instantaneous centre of rotation
IM	Interface material
IO	Input/output
PDT	Pressure discomfort threshold
PLA	Polylactic acid
PPT	Pressure pain threshold
RMSE	Root mean squared error
ROM	Range of motion
VAS	Visual analogue scale

Chapter 1 Introduction

Mobility affects nearly all facets of daily life. Those with mobility impediments, be it from injury, illness, or aging, tend to have worse healthcare outcomes, higher healthcare expenditures, and poorer life satisfaction [1], [2], [3]. Some of these adverse effects can be mitigated by interventions that promote mobility [1]. Exoskeletons are an emerging technology capable of restoring mobility and preventing injuries that can lead to mobility challenges.

Exoskeletons are mechanical devices designed to be worn. Typically, they consist of a mechanism that mimics the motion of the body parts to which they are attached. When worn, an exoskeleton can support or augment the capabilities of the individual based on their needs. These capabilities have led to various applications for exoskeletons, such as rehabilitation, restoring mobility, protecting, and augmenting industrial workers physical abilities. While often neglected in exoskeleton research and development, comfort plays a crucial role in exoskeleton usage and adoption [4], [5], [6], [7].

This work focuses on evaluating a method to improve the comfort of knee exoskeletons. The knee bears the weight of the body throughout gait and is particularly vulnerable to diseases and injuries that lead to mobility loss. Consequently, significant research and development has been dedicated to knee exoskeletons. By addressing comfort, this research aims to enhance the practicality and user acceptance of knee exoskeletons, thereby improving their effectiveness in real world applications.

1.1 Rationale

The body of research into exoskeleton development and its applications is extensive however, exoskeleton comfort has yet to be studied comprehensively. This is despite research that suggests comfort is of primary value for many users and will affect their adoption [4], [5], [7], [8], [9]. While numerous factors can contribute to an individual's comfort, one common research focus is kinematic incompatibility between the limb and exoskeleton. Most research looking to address kinematic incompatibility does so by altering the exoskeleton joint, often resulting in complex designs. Furthermore, few studies perform human testing to verify that the proposed designs improve kinematic compatibility and the underlying goal of comfort.

First proposed in orthosis research in the 1970s, and more recently reintroduced into exoskeleton research is the concept of passive degrees of freedom (DOF) [10], which solves the problem of kinematic incompatibility between the exoskeleton and limb joints by enabling some relative motion through a connection mechanism (CM). Passive DOFs were theoretically and experimentally verified on upper limbs to reduce kinematic incompatibility [10]; however, despite the promise of passive DOFs, little research has been done to test their performance on knee exoskeletons. . Recent simulation studies have shown that passive DOFs improve comfort, and the passive DOF stiffness has an influence on comfort [11], [12].

Passive DOFs, like many proposed designs to improve exoskeleton comfort, are rarely tested with human participants to verify the simulations' predictions. This is mainly attributed to the challenges related to human variability and added complexity. Limb surrogates can be an intermediate step between computer simulations and human testing.

1.2 Objectives and Contributions

The primary objective of this research is to enhance the comfort of a knee exoskeleton by developing passive DOF mechanisms to be applied at the connection between the shank and the thigh. The following ancillary objectives support the research into the primary objective:

(1) Design and build a knee exoskeleton with modular CMs capable of adding passive DOF with varying stiffnesses between the exoskeleton and limb.

(2) Design and build inexpensive pressure sensors capable of measuring the pressure distribution at the shank and thigh interface.

(3) Design and build a leg surrogate and jig to predict and analyse human-exoskeleton interactions.

(4) Test the kinematic and interface pressure affect of all six DOF under different connection stiffnesses at both the shank and thigh interface.

(5) Conduct preliminary human trials to evaluate the kinematic, interface pressure and comfort effect of the DOFs.

The work carried out to achieve these objectives, resulted in the following contributions:

(1) A comprehensive literature review[13] was conducted to analyse human comfort, determine how exoskeleton mechanisms effect comfort, and identify approaches to improving exoskeleton comfort.
(2) A leg phantom and testing jig were developed to measure human-exoskeleton interaction behaviour. The jig incorporated an advanced joint design to recreate the knee instant axis movement.
(3) A modular knee exoskeleton capable of adding passive DOFs to the CM between the exoskeleton and leg was developed.
(4) Initial human testing showed that the addition of some passive DOFs can reduce shearing and pressure at the shank interface.

1.3 Thesis Outline

This thesis is divided into six chapters: introduction, literature review, brace design methodology, experimental methodology, results and discussion, and conclusion. The introduction in Chapter 1 outlines the motivation, objectives, and contributions of this research. Chapter 2 reviews the necessary background information to facilitate a proper understanding of this research. Chapter 3 outlines the design and manufacturing process of the knee exoskeleton. Chapter 4 presents the experimental equipment, methodology and data processing. Chapter 5 presents the data analysis, the conclusions drawn from the results of the experiments, addresses some of the limitations of the work, and insights for future research. Chapter 6 concludes the thesis with a brief summary of the research, results and recommendations.

Chapter 2 Literature Review

This literature review provides the foundational knowledge necessary to understand this thesis. Overviews of knee joint anatomy and the causes of discomfort provide a background for understanding the mechanisms of exoskeletons discomfort and common approaches to improving comfort.

2.1 Knee Joint

The knee is complex, composed of two joints with a single joint cavity and several ligaments. Depending on the activity, the knee supports loads up to several times the individual's body weight. The high loads placed upon the knee and its relatively unstable structure make it more susceptible to injury than other joints, which is of particular concern because knee injuries can limit an individual's mobility.

The knee has a passive flexion range of motion between 130° and 140° [14]. However, the knee can achieve 160° of flexion under certain circumstances [15]. During normal walking, the knee requires 60° to 70° of flexion, while ascending stairs requires about 80° of flexion while sit-to-stand motions requires roughly 90° of flexion [14]. At approximately 90° of flexion, the range of longitudinal rotation is the greatest, at roughly 35° [15].

While the primary motion produced by the knee is flexion and extension as well as some medial-lateral rotation while flexed, due to the geometry of the articulating surfaces as well as the elasticity of the ligaments restraining the knee, motion in all axes is possible to a certain extent [16]. The knee is not a true revolute joint, knee flexion and extension is accompanied by translation and rotation in other directions [17]; the joint's axis of rotation translates and rotates throughout flexion and extension [18]. This axis is often denoted as the instant axis. The motion of the instant axis is often approximated as a two-dimensional translation of an instantaneous center of rotation (ICR), neglecting the rotation of the instant axis.

2.2 Exoskeleton Comfort

2.2.1 Comfort

Comfort is a subjective experience, making it is difficult to define and quantify. Generally, comfort can be described as the absence of pain, and of being relaxed, however, this does not necessarily imply that discomfort is the presence of pain or stress. Discomfort can be defined as a negative physical state causing unpleasant sensations [19]. Discomfort is often associated with pain, fatigue, itching, and temperature, among other factors [19]. What is considered comfortable varies between individuals and can change over time.

Discomfort can be measured using a visual analogue scale (VAS) or a numeric rating scale (NRS) [19]. The VAS and NRS provide ordinal measurements of discomfort, and data analysis must be done using non-parametric statistics [20]. Due to the limitations of ordinal data, many exoskeleton studies focus instead on measurable sources of discomfort, such as pressure or force. While force can be used to analyze discomfort, pressure is more commonly used and is a superior metric, because the area upon which the force is applied is a key factor.

For the purposes of this research, comfort will be defined in terms of pressure and shear force applied to an individual's soft tissues. Subjective measures of user comfort were recorded, however due to the limited sample size they have little statistical value and are omitted. Lower pressures and less shearing are considered to be more comfortable.

2.2.2 Human Pressure Tolerance

For safety, three aspects of pressure need to be considered: magnitude, duration and location. If pressure is applied for enough time, tissues can undergo ischemia and necrosis. Generally, continuous 30 mmHg is considered the safe threshold; however, depending on the location and individual, the threshold may be as low as 20 mmHg or as high as 80 mmHg [21]. Intermittently reducing pressure below the safe threshold roughly every two hours for at least ten minutes can prevent tissue necrosis and injury [21].

While the safe pressure threshold may be 30 mmHg, the pressure discomfort threshold (PDT) and pressure pain threshold (PPT) can be much higher. Only the PDT will be considered in this research because exoskeletons should avoid causing pain. Furthermore, while general PPT values can be defined for limbs and areas, their utility is questionable because PPT varies greatly between individuals, the device and the task [22]. For the lower limb, the PDT ranges from 12000 mmHg on the sole of the foot [23] to 105 mmHg on the thigh and calf [24]. In everyday use, an exoskeleton should remain below the PDT.

Ideally, an exoskeleton attached to a user's limb would apply only the pressure necessary to provide the desired assistance; however, this is difficult to achieve in practice. Intuitively, the best compromise would be to reduce the pressure applied, which can be achieved by either increasing the area where the device applies force or by decreasing the force applied by the device. While this is generally a good approach, research by Goonetilleke et al.[25] has shown that above a critical force value, discomfort and surface area have a “U-relationship”; increasing the surface area, and thereby reducing the pressure, causes more discomfort than concentrating the pressure over a smaller area [25]. They attribute this effect to how the nervous system performs spatial summing of stimuli [25], where forces applied over a larger area cause a more intense sensory response than when applied over a small area.

2.2.3 Human Shear Tolerance

Much less understood is the relationship between shear and comfort. A previous study identified that the threshold for pressure to cause ischemia is reduced when accompanied by shear forces [26]. However, the literature does not offer a safe shear-pressure relationship and how it changes between individuals and locations. A study analyzing the contact behaviour of a lower limb exoskeleton during gait found that, based on a porcine skin model, shear was liable to cause injuries to some participants within a few seconds of normal gait [27]. A porcine model for blister development proposed by Mao et al.[28] can be applied to humans and suggests that injuries due to shear are both a function of the shear magnitude and the time over which it is applied [28].

Most of the studies considering shear stress in exoskeletons do so in the context of preventing injuries, typically blisters [27], [29], rather than in the context of comfort. This is likely due to the lack of research into a shear discomfort threshold with which results can be compared. Nevertheless, these results are still useful for setting an upper limit to the shear stress that an exoskeleton can apply. Massardi et al. suggested that research in this area is hampered by technological capabilities in measuring shear stress on the limbs [22].

2.3 Kinematic Incompatibility

Kinematic incompatibility arises when two different kinematic chains, such as a series of linkages and revolute joints, are coupled together in such a manner that motion is restricted. When an exoskeleton is coupled to an individual’s limb, kinematic incompatibility can occur. However, because the individual’s soft tissues are not rigid, motion can still occur by deforming the individual’s soft tissues, which causes discomfort [30], [31]. Additionally, the interaction forces introduced by coupling the user's limb to the exoskeleton can limit or alter the range of limb motion [30]. Multiple factors are known to contribute to kinematic incompatibility in exoskeleton-limb systems.

- **Kinematic Mismatch**: The exoskeleton's DOFs are not sufficient to follow the user's limb motion. This typically occurs when simplifying the motion of human joints to traditional mechanical joints (e.g. revolute joints, prismatic joints, spherical joints). As previously discussed, the knee joint's axis of rotation changes throughout rotation, leading to kinematic incompatibility and discomfort. Further complicating matters is anatomical variability between users, which requires that exoskeleton designs be tailored to individuals as ICR movement profiles, limb lengths, and diameters differ.
- **Joint Axis Offset**: The user's limb joints and the corresponding joints on the exoskeleton are misaligned. Misalignment can occur either from initial offset during exoskeleton donning, or from exoskeleton migration during use. In practice, it is not possible to perfectly align an exoskeleton's joints with the user's, meaning some degree of offset is inevitable.

2.4 Existing Approaches to Improving Comfort

Fundamentally, all approaches to improving exoskeleton comfort revolve around the interaction forces between the exoskeleton and user's limb and how they are distributed over the user's skin. From this, there are two approaches that can be taken to improving comfort, reducing the force applied to the user by the exoskeleton and changing how the applied force is transferred to the user. In this section, we present three approaches related to either distributing interaction forces across the user's tissues or reducing the interaction forces.

2.4.1 Interface material

The interface material (IM) distributes the interaction forces over the user's skin, generally a padding or foam of some kind. In this section, two design parameters of the IM, the geometry and stiffness, are discussed in the context of altering how the interaction forces are applied to the user's limb. While not considered here, because the IM is in direct contact with the user's skin, its thermal properties, moisture/air permeability, and texture are also important to consider.

Numerous papers have investigated methods to tailor the IM geometry to the user and its effects. In 2014, Reimer et. al. tested tailored interfaces against non tailored interfaces on the forearms of participants and found that by tailoring the interfaces to the participants, maximum pressure at the interface decreased by at least 5% while also increasing the surface area over which the applied force is dissipated [32]. In more recent research, two approaches to designing tailored interfaces for a lower limb exoskeleton were tested; 3D scanner based design and iterative design [33]. In the iterative design method, the participant's limb geometry was approximated through an iterative design process [33]. They found inconsistent results, with the 3D scanner based approach reducing interface migration for the thigh, while the iterated based approach was better for the shank [33]. While the study had a small sample size, when considered with the results from Reimer et. al. it suggests that tailoring the interface geometry in general is a good strategy for improving pressure distribution and this is shown in practice for prosthetic and orthotic devices.

The IM thickness can be altered, however increasing the thickness of the IM has not been observed to have a significant impact on comfort nor force distribution [34], [35].

The stiffness of the interface also has an effect on both pressure distribution and interface migration. In multiple papers by Levesque et al. stiffer materials were found to improve pressure distribution [33], [34]. Despite this, based on results by Kozinc et. al., where various foams and paddings were evaluated against no padding on an aluminium applicator, the foams and paddings were found to increase the pain threshold by 10-38% [35] compared to the bare aluminum, with aluminum being much stiffer than the foams and paddings used, it suggests a limit at which increasing stiffness will decrease comfort.

While many methods to improve how the IM dissipates forces over the user's skin have been investigated in the literature, few have investigated if the methods also improve user comfort. When evaluating materials for their effect on discomfort and pain thresholds, Kozinc et. al. found significant intersubject variability in the discomfort threshold between different IMs and suggested that the IM be tailored to the individual [35], similar to the conclusions put forth by Reimer et. al. about utilizing an individualized approach [32].

2.4.2 Joint designs

The joint between the thigh and shank frames of the exoskeleton is the primary contributing factor to kinematic incompatibility, therefore many joint designs have been proposed in the literature to address this issue. In general, these joint designs fall into one of three categories [36], [37], shown in Figure 2.1;

- **Single Axis:** Composed of a single rotational DOF placed in parallel with the knee joint.
- **Polycentric:** Allow for the rotational axis to move along a predetermined path.
- **Polycentric Self-aligning:** Enables free translation of the axis of rotation to minimize the misalignment between the joint axis and the ICR.

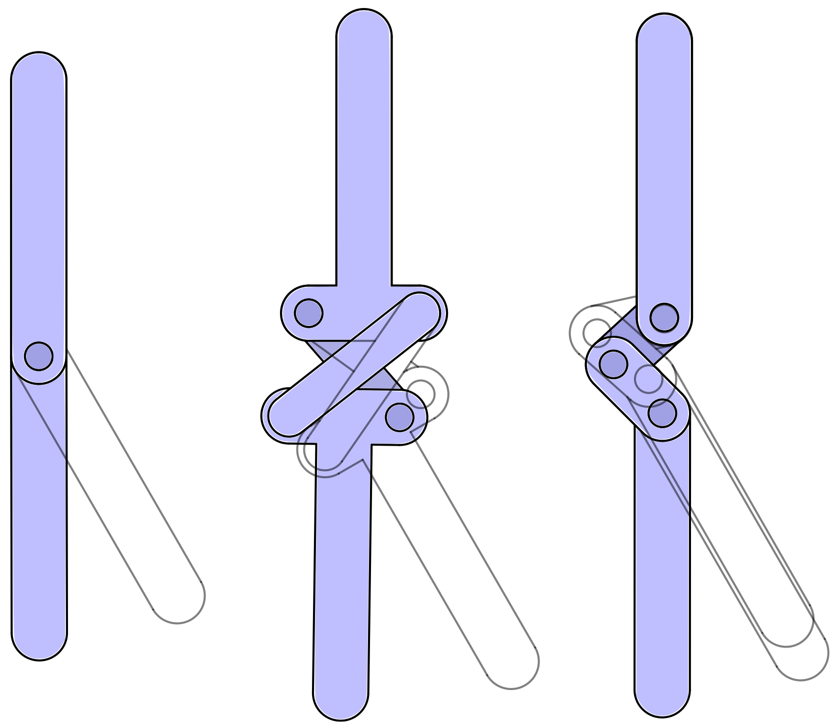

Figure 2.1: Left : Single axis joint. Centre: Polycentric joint. Right: Polycentric self aligning.

Each of these approaches has its own advantages and disadvantages. Single axis joints are mechanically the simplest joints and provide the most rigid connection. Polycentric joints require more design consideration; depending on the design, different joint motion profiles can be produced, some of which may have a stronger resemblance to the knee's ICR motion. Polycentric self aligning joints can be more mechanically complex than the other joints and may not provide as rigid a connection as the other joints. In theory, polycentric self aligning joints should be the most kinematically compatible and thereby the most comfortable, while single axis joints are the least, in practice it is more complicated. In a study by Patrick et al. comparing the relative performance of each category of joints in terms of interaction forces and device migration, it was found that single axis joints can outperform polycentric joints with both lower interaction forces and lower device migration [36]. The authors suggested that the performance of polycentric joints may depend on the individual, with tailoring the joint to the user necessary to improve performance [36]. Conversely, the polycentric self aligning joint performed as expected, with the lowest interaction forces and device migration [36]. Similar results were obtained in another study in which a polycentric self aligning joint was evaluated against itself with the self aligning component disabled [38]. With the self aligning mechanism enabled, joint tracking performance improved by 38% while comfort improved by 15.3% [38].

2.4.3 Connection Mechanisms

The mechanical link between the exoskeleton frame and the IM is the connection mechanism (CM). For most exoskeletons the connection mechanism is a rigid connection that does not allow any relative motion. However, in an approach first proposed in the 1970s, passive DOF can be added to exoskeletons to address kinematic incompatibility when being worn [31]. An example of passive degrees of freedom added between kinematic chains is shown in Figure 2.2, with the addition of passive DOF.

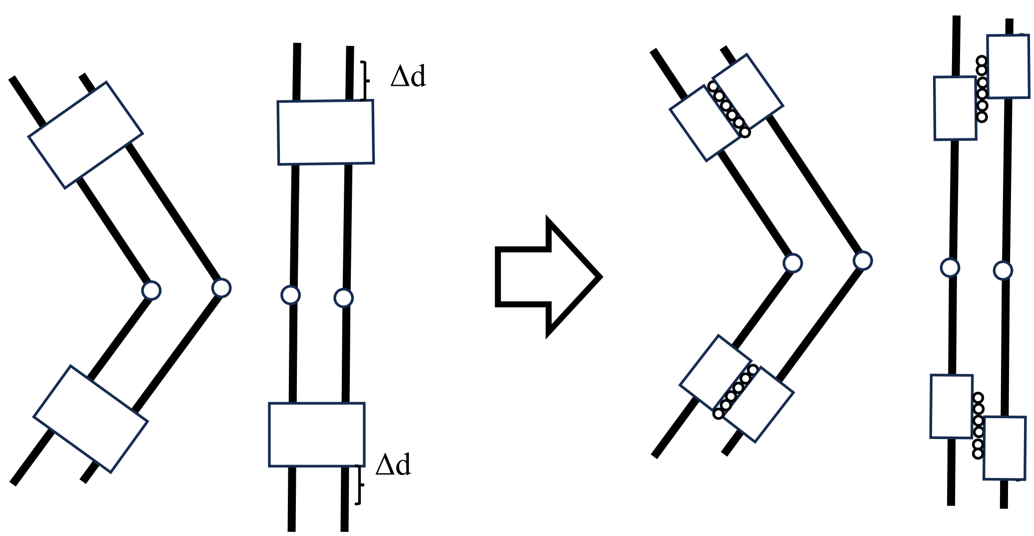

Figure 2.2: The addition of passive DOF to the coupling removes kinematic incompatibility.

In work by Jarrasse et. al., passive DOFs were mathematically proven to eliminate kinematic incompatibility and the associated interaction forces. Furthermore they tested and verified this approach on an upper limb exoskeleton [31]. Passive DOFs again proved to work for upper limb exoskeletons in work done by Lee et. al., where interaction forces between the limb and exoskeleton were found to be significantly decreased with the implementation of passive DOF in the connection mechanism [39].

Despite its promise in improving kinematic compatibility in upper limb exoskeletons, little research into the application of passive DOF to the CMs of lower limb exoskeletons has been performed. Two simulation studies performed by Shafiei and Behzadipour added passive DOF to the CM of lower limb exoskeletons. In one study the passive DOF were able to move freely [11] while in the other each degree of freedom had added stiffness [12]. In the study examining the freely mobile passive DOFs, longitudinal rotation with longitudinal translation on the shank was found to improve the performance in terms of discomfort and tracking by an average of 97% [11]. No significant improvements to performance were found by implementing passive DOFs to the thigh CM [11]. Similarly, in the study incorporating some stiffness into the CM passive DOFs, no significant improvements were found by adding passive DOFs to the thigh CM[12], while the stiffness of the shank longitudinal rotation and longitudinal translation stiffnesses improved performance by 47% [12]. Contrary to the results of Shafiei and Behzadipour, when adding longitudinal translation and rotation on the shank of an exoskeleton, Levesque observed poorer joint tracking, comfort and pressure were not reported [33]. These inconsistent results, the lack of human trials with passive DOFs on lower limbs and the promise based on upper limb performance emphasize the necessity of further research.

Chapter 3 Brace Design Methodology

This chapter presents the design and construction of the knee brace, along with the CMs to experimentally evaluate the effect of passive DOFs in the CM. The brace was designed with modular CMs, each configured to allow motion in a single DOF and to test the effect of passive DOFs. The brace was instrumented with sensors to record the pressures at the interface between the limb and brace. The design, development and calibration of the pressure sensors is also discussed in this chapter.

3.1 Brace Design

These brace design criteria are directly informed by the primary research objective, which is to determine whether adding passive degrees of freedom (DOF) to the shank and thigh components improves user comfort.

The brace needed to reproduce the kinematic mismatch between a leg and a typical knee exoskeleton with a single revolute joint between the shank and thigh portions. This ensures that the conclusions drawn are representative of typical knee exoskeletons. The brace should be lightweight, easy to wear, and capable of supporting its weight through the cuffs alone. To accommodate a variety of individuals, it was essential for the brace to be adjustable.

The connection mechanism (CM) between the brace frame and cuffs needed to be modular, allowing for the testing of various degrees of freedom (DOFs). Specifically, both a rigid CM and CMs enabling motion along the primary anatomical axes were necessary. Each CM adding a DOF had to be capable of optionally including springs for stiffness adjustment. Collectively, the CMs needed to facilitate six DOFs, encompassing rotation and translation about the sagittal, transverse, and longitudinal axes of the leg. Consequently, the design criteria are:

1. The brace must use a single revolute joint between the thigh and shank portions.
2. The mass of the brace should be minimized.
3. The brace should not be cumbersome.
4. The brace must support its own weight through the cuffs alone.
5. The brace must allow the replacement of modular connection mechanisms.
6. The brace must be adjustable.
7. The connection mechanisms must limit the motion to one of the six DOF.

8. The connection mechanisms must allow for adjustable stiffness.

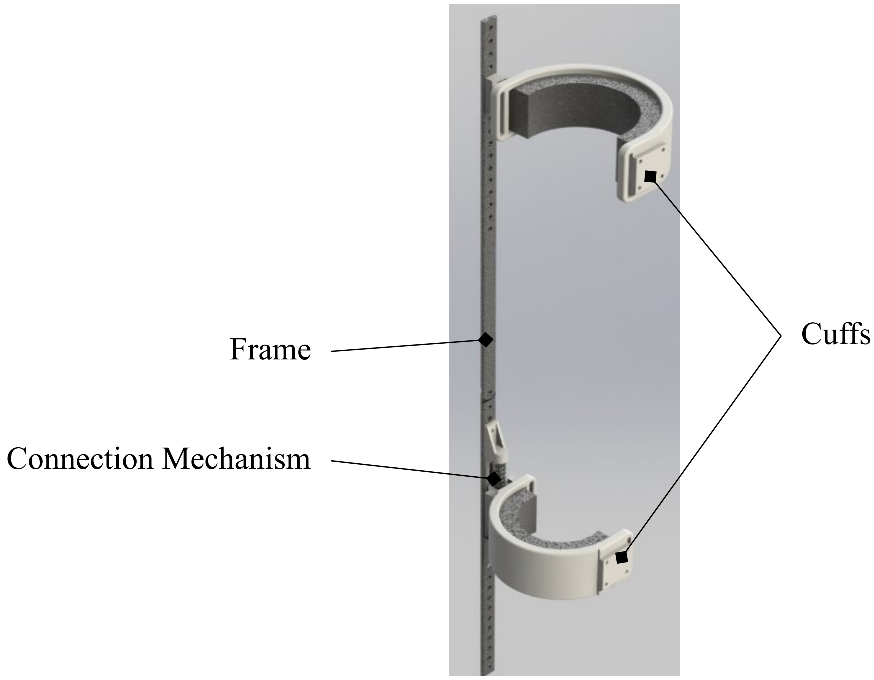

Figure 3.1: Overview of the brace showing the three subsystems.

The design of the brace was divided into three subsystems: the frame, the CMs and the cuffs shown above in Figure 3.1. Several conceptual designs were achieved for each subsystem; however based on the evaluation criteria, the following final subsystems designs were retained.

3.1.1 Frame

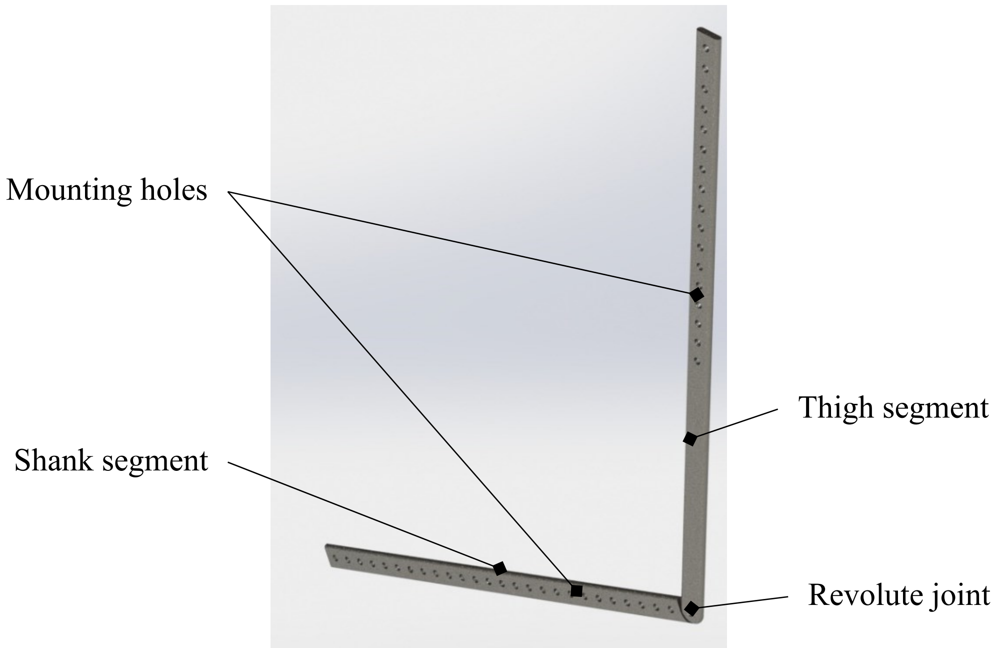

Figure 3.2: Brace frame showing the mounting holes and revolute joint.

The frame, shown in Figure 3.2, includes a revolute joint as well as a mounting system, allowing for adjustments to accommodate various subjects. The frame was constructed from a modified stainless steel orthotic knee upright (Becker model 1002). Regularly spaced holes were drilled into the upright to allow for adjustments to the positioning of the connection mechanism. Initially, the design included both medial and lateral uprights, however, the medial upright was eliminated to reduce bulk and simplify the design. The thigh and shank portions of the upright were connected by a revolute joint.

3.1.2 Connection Mechanism

To create the different DOFs, three distinct connection mechanisms were developed. Figure 3.3 shows the six DOFs at the thigh and shank studied in this research. Two mechanisms were designed specifically for the transverse DOFs, while a single versatile mechanism was designed to provide the remaining four DOFs through multiple configurations. The CMs connected the frame to the cuffs, enabling relative motion in one of the DOFs between the cuff and frame. The CMs were used interchangeably on either the thigh or shank cuffs to test various DOF conditions. Initially, the goal was to design a single mechanism that could produce any combination of the six DOFs. However, this requirement was simplified to focus on individual DOFs based on revised experiment objectives. Consequently, three distinct mechanisms were developed to collectively produce all six DOFs. This approach reduced the number of necessary parts, simplifying both the design and assembly process. One CM, built around a cylindrical joint was used to create both translation and rotation in the longitudinal and sagittal axes, while the two transverse DOFs were created using two separate CMs due to limited space.

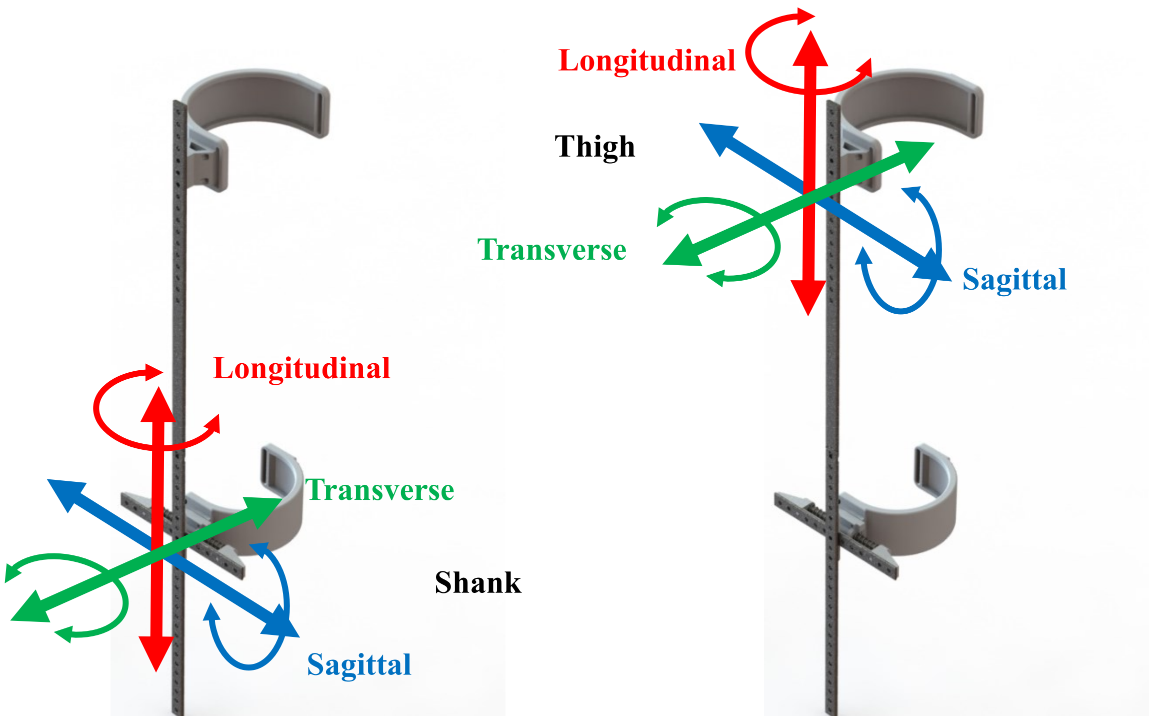

Figure 3.3: Diagram of the six DOF created by the CMs at the shank (left) and thigh (right) interfaces.

Longitudinal and Sagittal Mechanism

By employing a cylindrical joint, both rotational and translational DOFs could be achieved in a single CM. During testing, the unneeded DOF could be locked, turning the cylindrical joint into either a prismatic or a revolute joint. Additionally, the cylindrical joint could be rotated to align with the longitudinal or sagittal axes of the limb, reducing the number of mechanisms needed to achieve all six DOF. However, there were two issues with this design: locking the DOF and incorporating adjustable stiffness for each DOF.

The cylindrical joint, shown in Figure 3.4, was constructed using a carbon steel shaft (Grainger Canada WWG3DWL3) cut to length and a bronze bushing (Grainger Canada

WWG1X871). The shaft is affixed to the frame through two 3D printed PLA shaft end mounts while a carriage is mounted on the bushing, allowing for a total of 74mm of translation, and approximately 60 degrees of rotation.

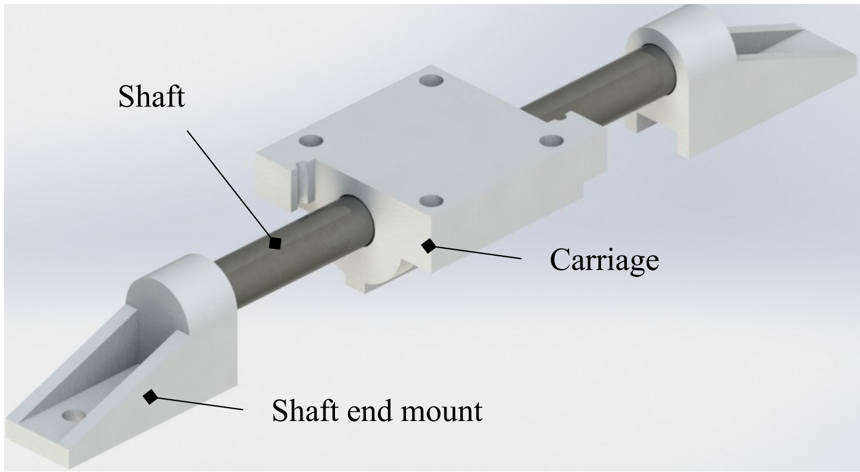

Figure 3.4: Longitudinal and sagittal cylindrical joint for translational and rotational DOFs.

To lock the rotational DOF, a 3D printed guide rail was made. Similarly, the translational DOF is locked using 3D printed guide blocks at the ends of the slider. The carriage has corresponding geometry to interface with either set of guides. The PLA construction of both the carriage and the guides has a relatively low coefficient of friction, minimizing its effect on the slider kinetics. The translational and rotational guides are shown in Figure 3.5.

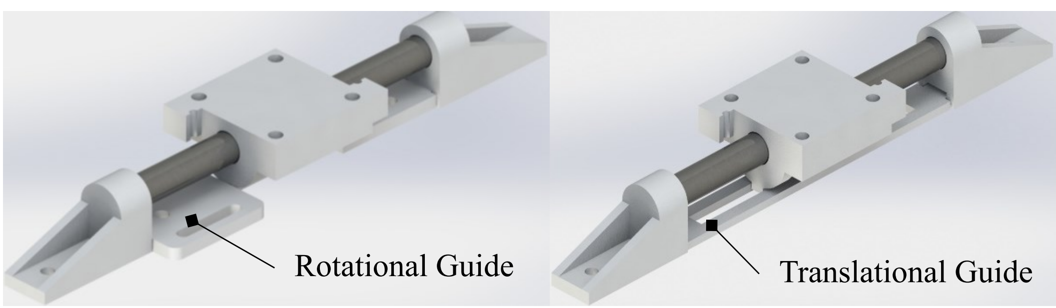

Figure 3.5: Translational and rotational guides for longitudinal and sagittal DOF.

Springs were used to adjust the CM stiffness. The springs for the translational DOF were installed on the shaft between the shaft end mounts and the carriage. Carriage translation in either direction would compress the springs. The springs for the rotational DOF were installed on the shaft, tensioning between the carriage and the rotational guides. Spacers were placed within the rotational springs to keep them concentric with the shaft. Both the rotational and translational DOF springs were placed in pairs to provide stiffness in both directions as shown in Figure 3.6.

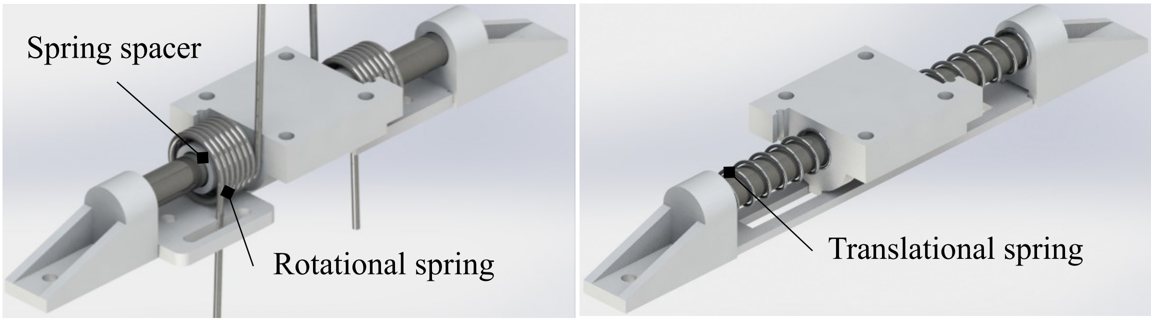

Figure 3.6: Opposing springs for rotational(left) and translational(right) DOF of the longitudinal and sagittal mechanism.

To install the CM for sagittal DOFs, an aluminum flat was cut to length and had mounting holes drilled for the shaft end mounts. A mounting hole was drilled and tapped in the center of the aluminum flat to connect to the frame. Rotation of the aluminum flat was constrained using two 3D printed PLA stops. Both the sagittal and longitudinal configurations of the mechanism are shown in Figure 3.7.

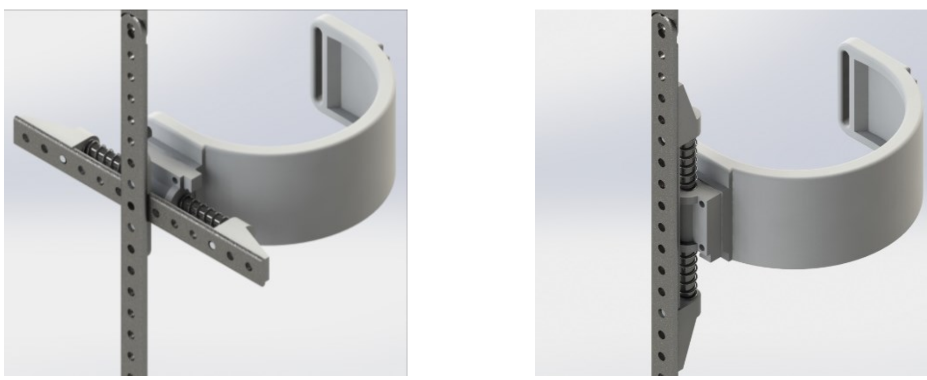

Figure 3.7: Sagittal(left) and longitudinal(right) mechanisms in their translational configuration.

Transverse Translation

Translation along the transverse axis was created using a pair of cylindrical joints, shown in Figure 3.8. These joints were formed by two 5x50 mm(Grainger Canada EBP41KR10) stainless steel dowel pins passing through a 3D printed PLA guide on the brace mounting plate. The pins were rigidly connected to the cuff mounting plate while they were able to translate through the brace mounting plate and brace.

Springs could be installed on both pins to adjust the stiffness. The spring were connected to both the cuff and brace mounting plates, enabling them to function in both compression and tension. A screw was used to limit the joint travel, providing approximately 3cm of travel distance.

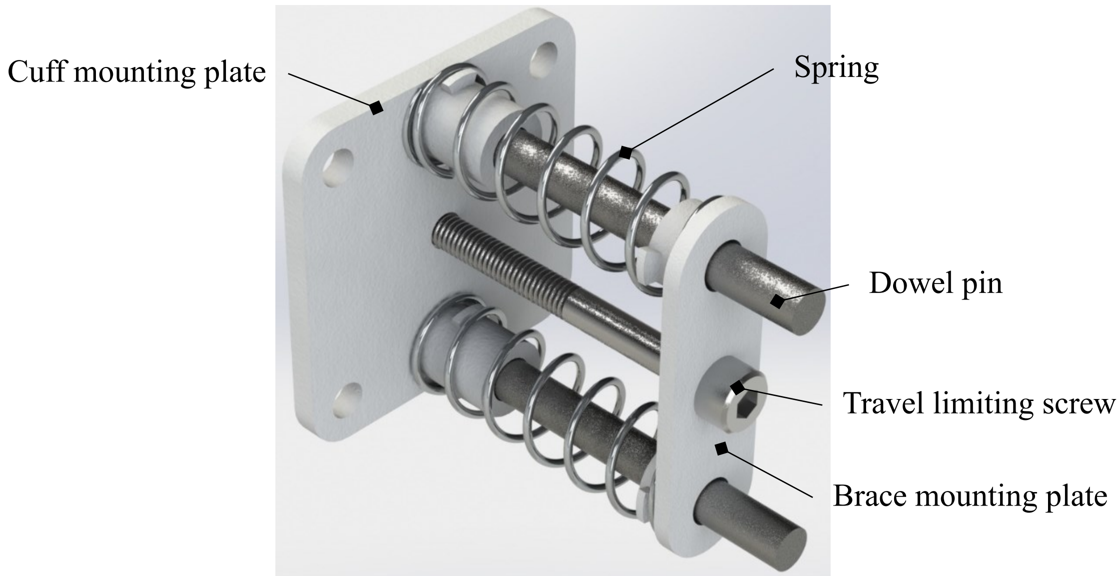

Figure 3.8: Transverse translation CM showing the cylindrical joints and the travel limiting screw.

Transverse Rotation

Rotation about the transverse axis was created using a revolute joint. The joint consisted of four 3D printed PLA parts: a cuff mounting plate, a frame mounting plate, a lateral spring mounting plate and an end cap, all of which are shown in Figure 3.9. The cuff and frame mounting plates have mating cylindrical geometry, enabling rotation about their axis. A screw passed through the center to enable rotation, but not translation. Springs are installed around the revolute joint on both sides of the frame with tensioning geometry incorporated into the three mounting plates. This setup allowed approximately 110 degrees of rotation.

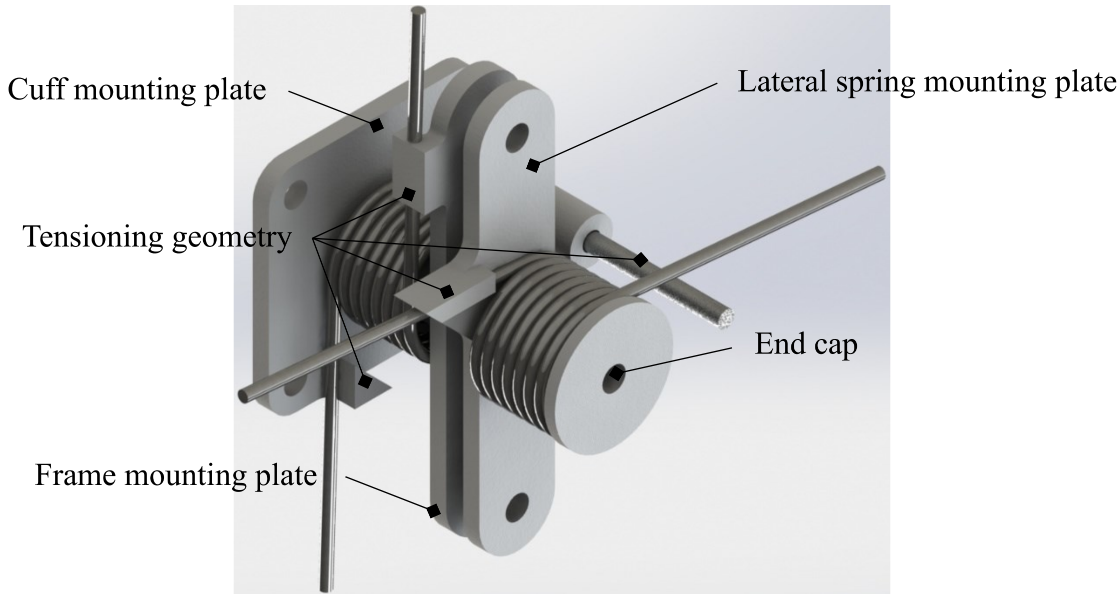

Figure 3.9:Design of the transverse rotation CM, showing the revolute joint and spring installation.

3.1.3 Cuffs

The cuffs were designed to apply sufficient pressure to the limb to ensure the brace remained securely in place during testing. The cuffs were designed as rigid semi-circular shells slightly larger than the participant's thigh and shank, with a slot for installing padding. The rigid cuffs were 3D printed from PLA and incorporated nuts embedded within the print to enable fastening to the CMs. Each cuff included two slots for hook and loop straps, allowing for the fit to be adjusted.

Polyurethane foam (Grainger Canada WWG5GCU7) is used as padding, secured within the slot using adhesive backed hook and loop strips. This allowed for the padding to be easily replaced. Faux leather vinyl (VViViD Bycast65) was placed between the foam and the limb to provide a comfortable interface. The complete cuff assembly is shown in Figure 3.10.

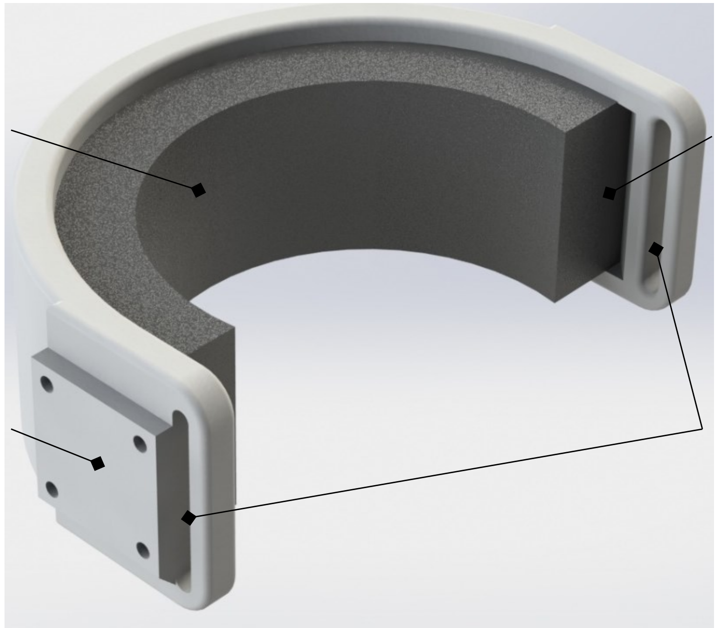

Figure 3.10: Design of the cuff showing the padding, its slot, mounting holes and strap slots.

3.2 Sensors

Great consideration was given to the design of the pressure sensor because the pressure data was a key metric used to evaluate the different CMs. The pressure sensor needs to be flexible to deform with the underlying padding material. Additionally, they also needed to provide reliable measurements while deformed. Ideally, the pressure sensor would be capable of providing high resolution pressure readings throughout the interface, to enable a more detailed characterization of the interface pressure distribution. The sensing system needed to be wireless to facilitate human trials, capable of synchronizing with the external motion capture system being used, and provide high frequency measurements to match the motion capture system.

Consequently, the design criteria were established:

1. The sensor needs to be flexible.
2. The sensor needs to function while deformed.
3. The sensor needs a spatial resolution of at least 1 samples/4cm²
4. The sensor system needs to be wireless
5. The sensor system needs to be compatible with external synchronization
6. The sensor system needs to be capable of sampling the pressure distribution at 200 samples per second

7. The sensor system needed to be affordable

The sensor design is composed of three primary subsystems: pressure sensors, data transmission and data recording. The pressure sensors were constructed using a piezoresistive material and an array of anodes and cathodes. A microcontroller reads the sensor array and wirelessly transmits the data via a 2.4GHz transceiver module. Another microcontroller receives the data, synchronizes it with the motion capture system and sends it to a computer for recording and analysis.

3.2.1 Pressure Sensors

Due to the specific requirements of the sensors, a custom pressure sensing solution was developed for this research. The pressure sensors were designed using a piezoresistive textile; Velostat (Adafruit Industries 1361). Velostat was chosen for its affordability, durability, flexibility, affordability and prior success in similar applications. The resistance of Velostat is dependant on the pressure applied to it, this was used to create an array of pressure sensor elements using a single sheet of Velostat. The array was formed by perpendicular rows of anode and cathode strips on opposite sides of the Velostat sheet as shown in Figure 3.11.

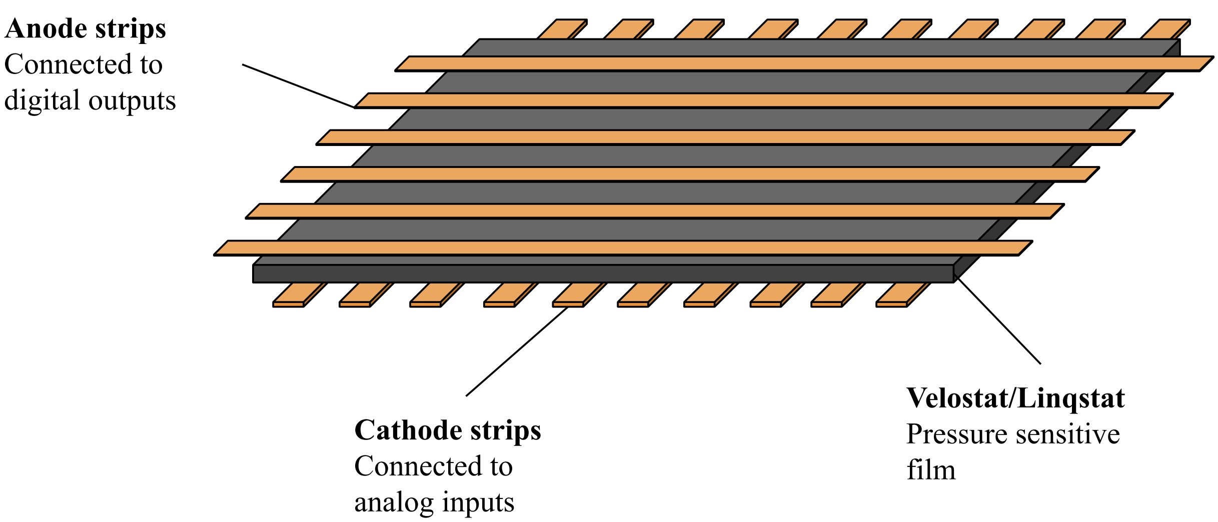

Figure 3.11: Velostat pressure sensing array construction.

When the sheet is compressed, the resistance of the material between the anodes and cathodes changes. To measure the resistance change, a variable voltage divider is formed by connecting each cathode to ground through a resistor, the voltage of the cathode is read by the

ADC of the microcontroller. Row-column scanning was used to read the individual pressure sensing elements in the matrix. One of the anodes is set to high (5V) by the controller while the voltage of one of the cathodes is read by the ADC of the controller, this results in the resistance at the intersection of the anode and cathode strips being read. To prevent the inactive digital inputs from drawing current when they were set to low, they were made high impedance using 1N4148 diodes.

The array consisted of five anodes and twelve cathodes, forming a total of sixty pressure sensor elements. The cuff padding was 5cm tall, with the desired resolution of 1 sample/4cm², the padding could be up to 48cm wide, fitting a thigh or shank up to 30cm in diameter, well in excess of the expected participant anatomy.

The cathode and anode strips were made from 5 mm conductive copper tape backed with a conductive adhesive (Sparkfun 13827). The first design of the pressure sensor matrix used the conductive adhesive to connect the strips to the Velostat, however this resulted in inconsistent pressure measurements. The final pressure sensor matrix design used a vinyl backing for the copper tape to adhere to while the Velostat sheet was placed in-between the two sheets of vinyl, as shown in Figure 3.12. The resistance of the Velostat ranged from 3kΩ to 20kΩ.

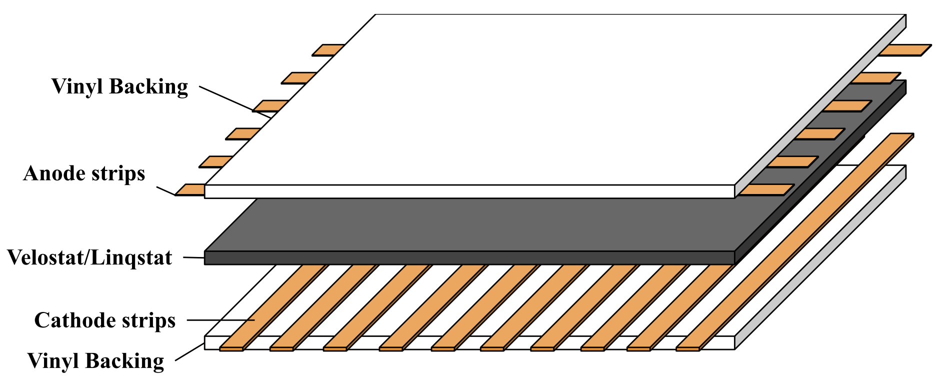

Figure 3.12: Arrangement of the layers of the pressure sensor.

The circuit that read the pressure sensor matrix needed to balance the pressure dynamic range against the pressure sensitivity. Figure 3.13 depicts a simplified structure for each voltage divider, the fixed resistors are shared among the voltage dividers for each cathode, as shown in Figure 3.15. To tune the matrix, two variables were adjusted: the fixed resistor in the voltage divider and the analogue reference voltage. Both the dynamic range and sensitivity depended on the fixed resistor and analogue reference voltage. A larger reference voltage would increase the dynamic range the ADC could measure, at the cost of reduced sensitivity. Conversely, a smaller fixed resistor increased sensitivity, but reduced dynamic range. The resistance of the fixed resistor was chosen to maximize the dynamic range of the voltage divider, while the voltage reference was chosen to maximize the sensitivity of the sensors. Equation (3.1) describes the relationship between the voltage out (V_{out}), the Velostat resistance (A) and the fixed resistor resistance (B).

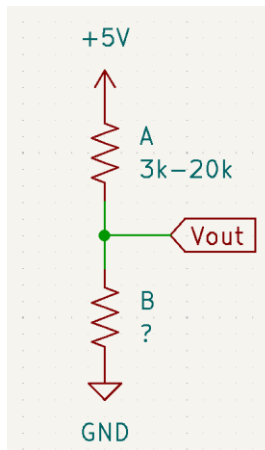

Figure 3.13: Individual voltage divider formed by the Velostat (A) and the fixed resistor (B).

$$V_{out}(A, B) = 5V \frac{B}{A + B} \tag{3.1}$$

The dynamic range of the fixed resistor is found with equation (3.2). While it is possible to determine the resistance that would maximize equation (3.2), achieving that exact resistance would have been difficult as resistors generally have wide tolerances and are only available at specific values.

$$V_{out}(3k\Omega, B) - V_{out}(20k\Omega, B) = DR(B) = 5V\left(\frac{B}{3k\Omega + B} - \frac{B}{20k\Omega + B}\right)$$

$$DR(B) = 5V\left(\frac{B}{3k\Omega + B} - \frac{B}{20k\Omega + B}\right) \tag{3.2}$$

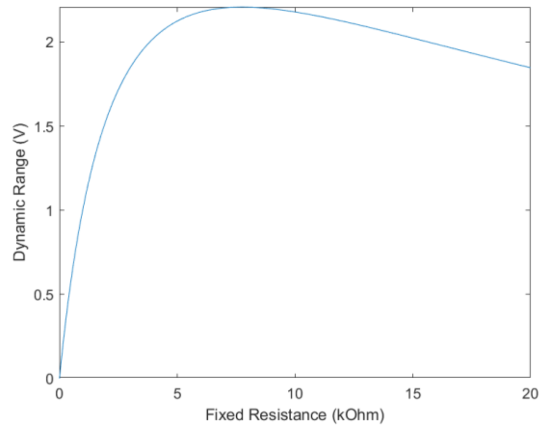

Figure 3.14: Dynamic range of pressure sensor matrix elements for fixed resistance values from 0-20kΩ.

As shown in Figure 3.14, a 10kΩ resistor achieves nearly the same dynamic range as the ideal resistance. The expected dynamic range is less than 2.5V, which allows the analogue reference voltage to be set to 3.3V, increasing the sensitivity of the pressure readings. The final circuit for the pressure sensor matrix is shown in Figure 3.15.

Figure 3.15: Pressure sensing matrix circuit.

3.2.2 Sensor Microcontroller

Arduino boards were considered for the microcontrollers due to their affordability, ease of implementation, and extensive documentation. The Arduino MEGA microcontroller was selected for the sensor controller because it had enough IO pins for the sensor matrix, wireless transceiver, status LEDs, and any other devices that may need to be connected.

Every 0.005s, the microcontroller needed to read the sixty pressure sensors and write the results to the data buffers on the transmitter module. The default ADC configuration on the Arduino results in 0.0001s per conversion. At this speed, fifty of the pressure sensors could be read within the allotted time, while leaving no time to transmit the readings. To reduce the conversion time, the ADC clock pre-scaler was changed from 128 to 16, resulting in each reading taking 1/8th the time. The precision loss due to the faster ADC clock was negligible. The code could have been further optimized by enabling asynchronous ADC conversion, however there was a concern that the interrupts generated may interfere with the operation of the transceiver.

The final program, available in Appendix B, has two phases: setup and data streaming. In the setup phase, the status LED and sensor pins are enabled, the ADC clock pre-scaler and reference voltage are configured, the nRF24L01 is initialized as a transmitter with the maximum data rate, power, and amplification possible. Once initialization is completed, the program enters the data streaming loop. The loop consists of reading the sensor array and transmitting results. The sensor elements are iterated through, with the readings being stored in a buffer 31 bytes long. The sensor array readings are divided into four packets of fifteen readings as the maximum packet size of the transceiver is 32 bytes while the readings are each two bytes. The extra byte in the packet denotes which array elements are in the packet. Once the buffer is full, it is written to the transmitter's buffer to be transmitted. The acknowledgment packet sent by the receiver is used to set the status LEDs.

3.2.3 Data Transmission

The transceiver needed to continuously transmit the readings from all sixty sensor elements within one frame of the motion capture system. The motion capture system recording frame rate was 200 fps, while each sensor reading was two bytes, the necessary bandwidth could be calculated using equation (3.3).

$$bandwidth = 200\frac{frames}{s} \times 60\ \frac{readings}{frame} \times 2\frac{bytes}{reading} \tag{3.3}$$

$$bandwidth = 24000\ bytes/s$$

Based on this requirement, the nRF24L01 with power amplifier and low noise amplifier module (CANADUINO) was chosen. The nRF24L01 module could achieve 2Mbps data transfer rates, well in excess of what was required.

Various transmission protocols were considered and tested. Originally, the transmitted data would include error correction codes, the timestamp of the readings, and the reading location, in addition to allowing the receiver to respond with status information such as begin recording, end recording. Due to the difficulty of implementing and testing these features, the design was simplified. The final communication protocol had the transmitter continuously sending the same data packet until the packet was acknowledged. The acknowledgement packets were used to convey status information.

3.2.4 Receiver Microcontroller

The transmitted data was received by another nRF24L01 module connected to an Arduino Uno. The Uno was used as the receiving microcontroller only needed a few IO pins for the transceiver and external synchronization hardware. The synchronization hardware for the motion capture system, the eSync2, was used to synchronize the pressure readings with the motion capture cameras.

The eSync2 was configured to pull one of the microcontroller pins HIGH while the cameras were exposing. When the pin fell to LOW at the end of the camera exposure, an interrupt was generated on the microcontroller. The interrupt triggered the microcontroller to send the most recent set of pressure readings along with the frame number to the connected computer. A MATLAB program running on the computer received the data and recorded it in a file for later processing.

3.3 Pressure Sensor Calibration

The pressure sensors underwent an initial loading process where weight was applied for 24 hours, allowing the Velostat's properties to settle. The pressure sensor arrays were calibrated by measuring their response to a series of increasing masses, as shown in Figure 3.16. The mass increased in roughly 25-50g increments to a total of roughly 1.5kg. To create a uniform pressure distribution across the sensor array, the mass was placed on a rigid piece of fiber board on the back of the padding while the sensors were on the front of the padding.

Figure 3.16: Calibration setup for pressure sensor matrices.

The array was given at least five seconds to settle after each mass increase. For each mass, the sensor array was sampled a thousand times. The response data was fitted with exponential and polynomial curves to compare and decide which calibration curve to use. The average adjusted R^2 and total root mean squared error (RMSE) of the fitted curves across all sensor elements are shown in Table 3-1 and Table 3-2.

Table 3-1: Average goodness of fit results for the thigh cuff sensor matrix.

Fit	**Adjusted R^2**	**Root mean squared error**
Exponential	0.9281	218
1st Degree Polynomial	0.7328	433
2nd Degree Polynomial	0.8859	276
3rd Degree Polynomial	0.9744	130

Table 3-2: Average goodness of fit results for the shank cuff sensor matrix.

Fit	**Adjusted R^2**	**Root mean squared error**
Exponential	0.8991	91
1st Degree Polynomial	0.8909	94
2nd Degree Polynomial	0.9305	74
3rd Degree Polynomial	0.9504	59

While the third-degree polynomial fits resulted in better adjusted R^2 and RMSE, the exponential fit was chosen because the relationship was expected to be similar to an exponential curve and the 3rd degree polynomials appeared to be overfitted. The final fitted curves are shown in Figure 3.18.

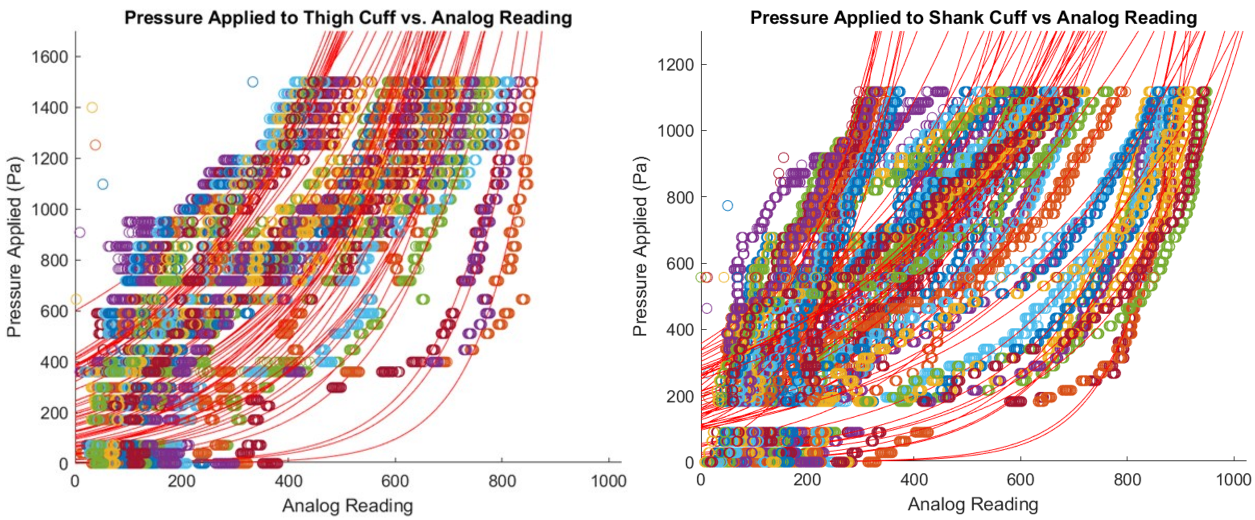

Figure 3.18: Pressure applied vs. analogue reading for thigh and shank sensor matrices.

Chapter 4 Experimental Methodology

In this chapter, the instrumentation, methodology and data processing techniques used to evaluate the CMs are presented. A specialized jig was developed to test the brace and CMs in a repeatable manner. The motion tracking system used to measure the kinematics of the brace and limb is also detailed.

4.1 Jig Design

For experimental evaluation, a jig was used to simulate the human leg and exoskeleton system. The jig allowed for trials to be conducted in a repeatable manner that would be difficult to achieve with human participants. To ensure that the jig was predictive of human results, it needed to model key properties of the human leg.

Two key properties of the human leg were modeled: the relative motion of the thigh and shank, and the stiffness of the soft tissues of the thigh and shank. The relative motion was modeled because the relative motion caused by the ICR movement is associated with discomfort, as reported in the literature. The stiffness of the soft tissues was modeled because it directly affects the interface pressure distribution. Based on these requirements, the design criteria for the jig were:

1. The jig must emulate the relative motion of the thigh and shank.
2. The jig's knee analogue must be capable of producing a ROM greater than 70° in flexion.
3. The jig must produce a consistent motion.
4. The soft tissue analogue must have a stiffness between 10.4kPa and 89.2kPa[40].

The jig design was separated into four sub-systems: soft tissue analogues, knee joint analogue, actuation, and frame. The knee joint analogue reproduced the relative motion of the thigh and shank along with the necessary range of motion, the soft tissue analogue reproduced human tissue stiffness, the actuator created a consistent motion, and the frame connected all the systems and held the jig securely in place during testing. For each subsystem, several design concepts were considered. The final jig is shown in Figure 4.1.

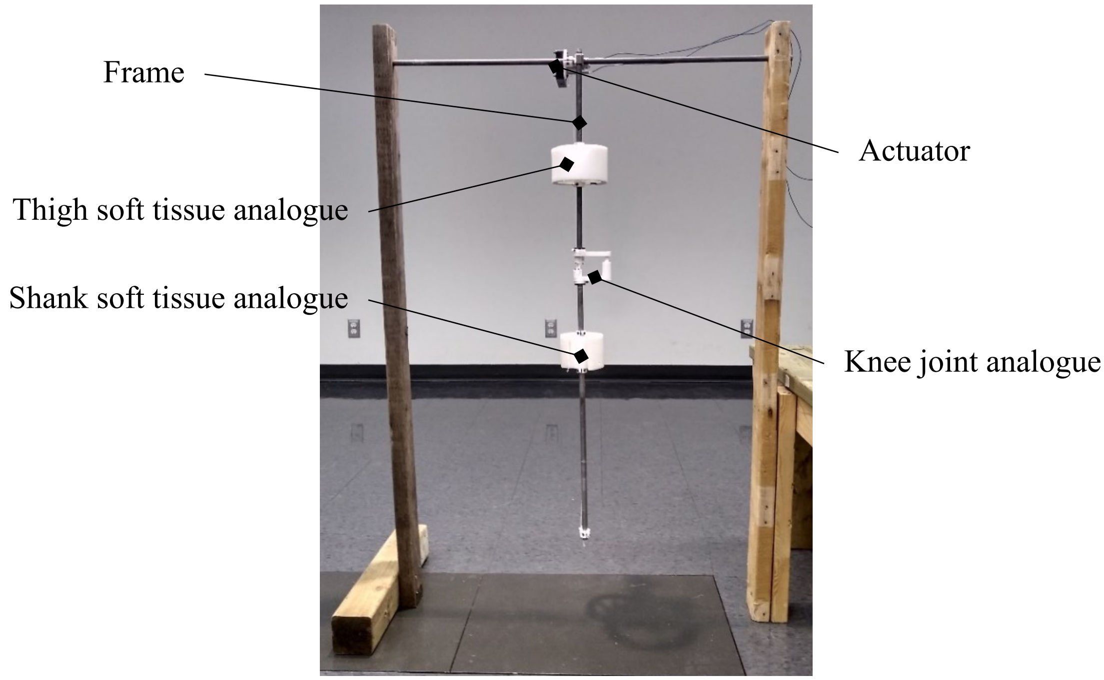

Figure 4.1: The assembled jig.

4.2.1 Soft Tissue Analogue

The soft tissue analogue was constructed from a 3D printed PLA core wrapped in foam. Based on the stiffness requirement, Volara 2A with a compression strength of 34 kPa at 25% compression and 97 kPa at 50% compression [41] was selected. The foam reproduced the soft tissue stiffness while the PLA core was used to save material and simplify the fabrication over layering several sheets of foam. Although the actual stiffness of the analogue was likely higher due to the stiffer PLA core, this was a reasonable approximation. The foam was glued to the core with 3M Super 77 Multipurpose Spray Adhesive. Analogues were created for both the thigh and shank. The thigh and shank were simplified to be cylinders, the diameter of the thigh was130.5 mm while the shank was 105 mm, and lengths of 76.2 mm. The thigh analogue connected to the frame in the centre while the shank analogue was offset from the center to emulate leg physiology. The final analogues are shown in Figure 4.2.

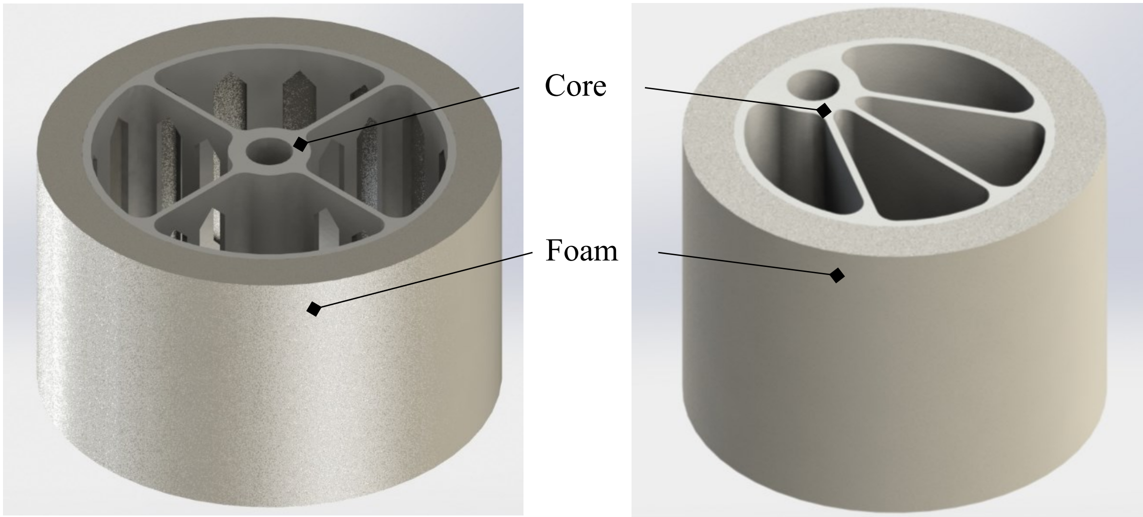

Figure 4.2: Soft tissue analogues for thigh (left) and shank (right)

3.2.2 Knee Joint Analogue

The knee joint analogue used a non-planar four-bar mechanism. The mechanism used a ball joint to replicate the nearly spherical motion of the knee while two links model the constraints imposed by the cruciate ligaments. This spherical mechanism produces a one degree of freedom joint that better models the knee than traditional planar four-bar mechanisms [42]. These spherical mechanisms are proposed by Sancisi et al.[42].

The spherical mechanism was reproduced in SolidWorks, it is formed by four primary components: the thigh and shank heads, and two links. The coordinates for the spherical joint, the link attachment points and lengths were based on specimen two in Sancisi et al.[42]. Early prototypes of the printed joint suffered from the spherical ends of the links coming dislodged from their sockets, which was addressed by adding caps to the sockets. Cutouts to allow the motion of the links are incorporated into the sockets. The thigh and shank heads are connected to the frame with slots and adjustable collars tightened around the frame. The complete mechanism is shown in Figure 4.3.

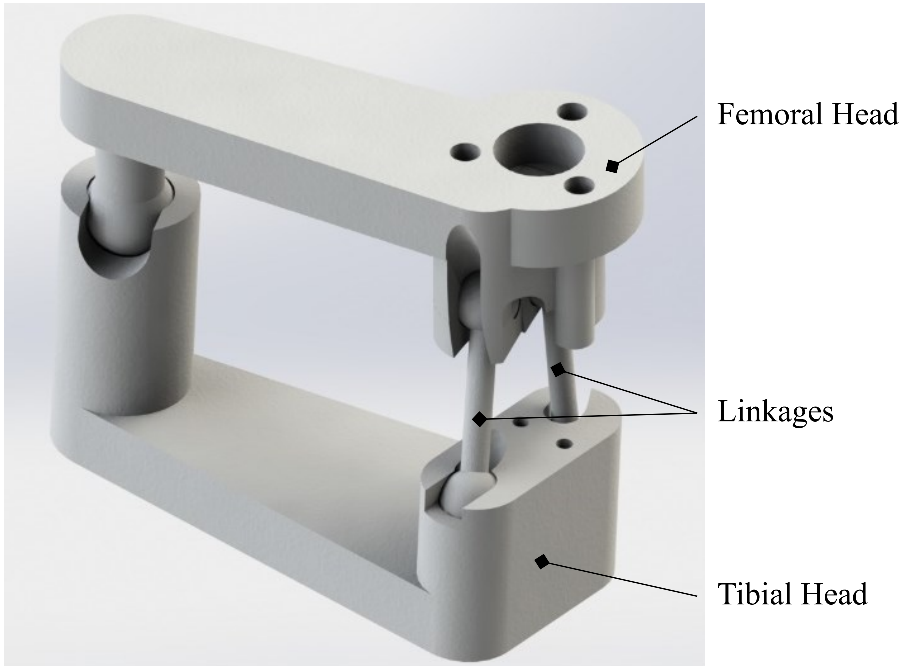

Figure 4.3: Knee joint analogue.

4.2.3 Actuation

Actuation of the jig was provided through a winch. The motor wound a cable connected to the distal end of the shank frame. Running the motor wound the cable, pulling the distal end of the shank frame upward.

A 9V gear motor was mounted to the jig frame using 3D printed PLA mounts. A 3D printed PLA spool was attached to the motor shaft for winding the cable. The distal end of the cable was fastened to the shank frame through a 3D printed PLA tie point. Power was supplied to the motor using an external adjustable DC power supply (Kaiweets PS-3010F). The assembly is shown in Figure 4.4.

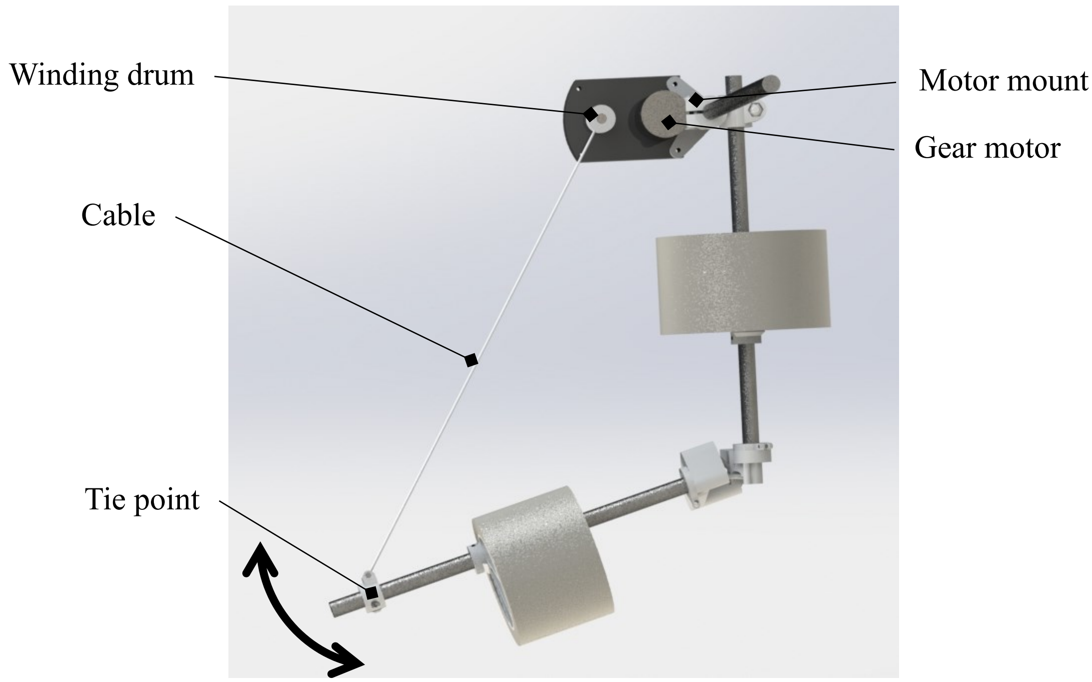

Figure 4.4: Jig actuation setup showing the motor, cable and tie point.

The motor was controlled using the sensor microcontroller. Upon receiving an acknowledgement packet indicating that recording had begun, would raise the winch. The microcontroller used a pair of relays to control the motor. An H-bridge was constructed from the pair of relays, using both the normally open and normally closed pins, as shown in Figure 4.5. The H-bridge allowed the microcontroller to control the motor direction, enabling both raising and lowering of the winch.

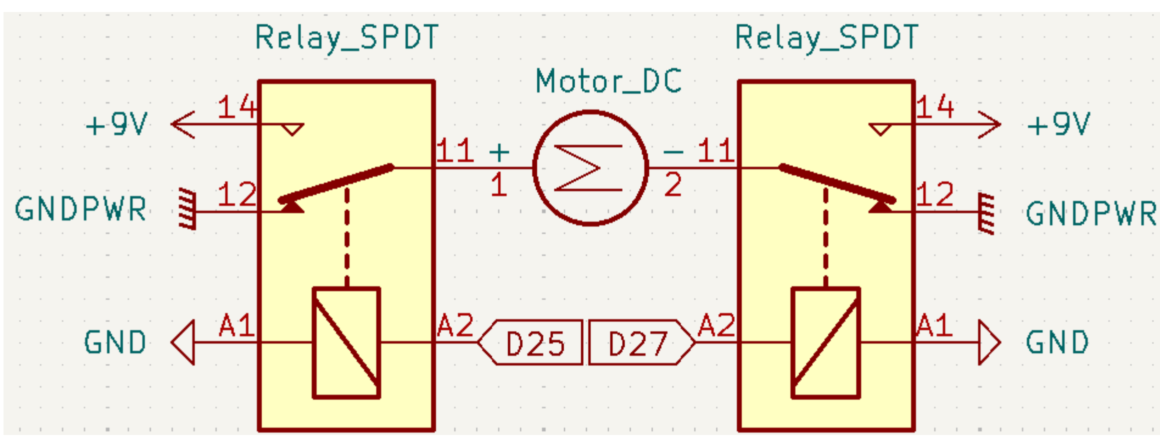

Figure 4.5: Motor relay H-bridge circuit configuration for controlling jig motor.

4.2.4 Frame

The frame to connect all the components was constructed using aluminum rods. Parts were affixed to the frame through 3D printed PLA clamps. This construction allowed for easy adjustment of the location and orientation of each part while being lightweight and simple to construct. The frame was suspended by wooden supports.

4.2 Motion Tracking

Infrared marker-based motion tracking was used to track the motion of the shank, thigh, and brace. The motion tracking system used eight infrared PrimeX 13 cameras (NaturalPoint Inc.) placed around the capture volume. Five of the cameras were mounted on the walls approximately 2m high, while three were mounted on portable tripods closer to the participant or jig to ensure markers were continuously tracked. The cameras were synchronized using an external eSync2 device. The cameras were configured to capture pictures at 200fps. The cameras streamed their video feeds over ethernet to a desktop computer running the software, Motive (NaturalPoint Inc.), which reconstructed the 3D position of the markers.

Within Motive, four rigid bodies were defined using the sets of markers: the thigh brace, the shank brace, the thigh, and the shank. The marker placement on the jig and brace are shown in Figure 4.6. For trials conducted on the human participant, the femoral markers were placed on the medial and lateral epicondyles and the femoral greater trochanter, while the shank markers were placed on the lateral condyle of the tibia, as well as the medial and lateral malleoli.

The motion capture system was calibrated with most of the wanding performed in the centre of the control volume, and continuous system calibration was enabled. The coordinate system of the motion capture system was aligned with the sagittal axis of the participant.

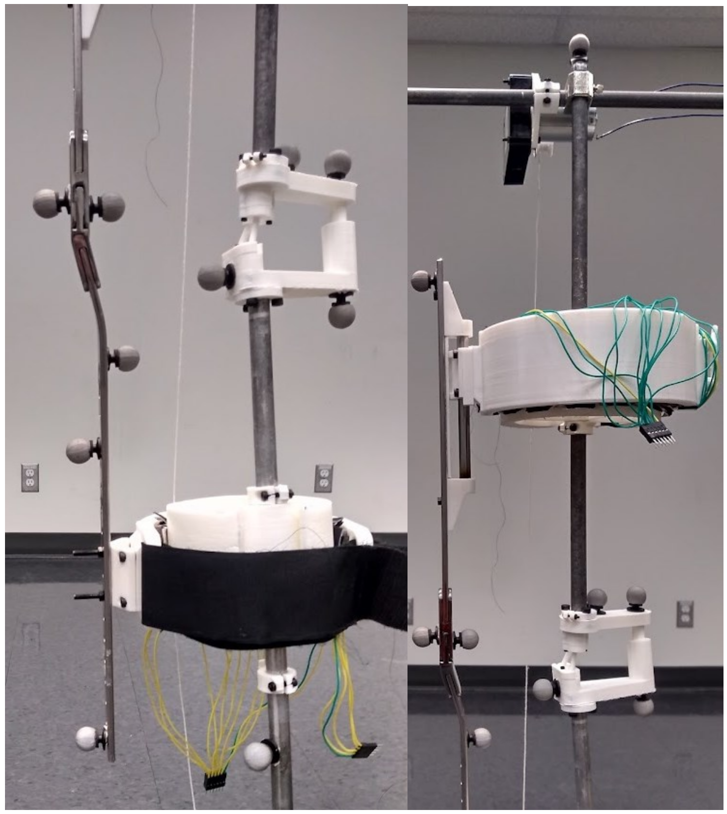

Figure 4.6: Placement of the markers on the jig and brace.

4.3 Experiment Methodology

The experiment was split into two phases. In the first phase, CM tests were conducted using the jig. The results of the jig trials were then analyzed and used to guide the human testing phase. Only the promising CMs, along with those suggested by the literature, were selected for further testing. In the second phase, CM tests were conducted with a human participant.

4.3.1 Jig Trials

The brace was placed on the jig and fastened in place using the hook and loop straps, which were tightened until the brace remained securely attached as the jig rotated through its range of motion. The straps were tightened to minimize the sliding of the brace across the soft tissue analogue, ensuring the kinematic incompatibility between the brace and the jig was primarily compensated for by the material of the soft tissue analogue. Before each set of trials, the jig joint and the CM was lubricated. A few test runs were performed to ensure all systems were functioning as intended. The consistency of the jig was verified by demonstrating consistent behaviour across multiple trials.

For the control trials, the thigh and shank CMs were configured with the fixed CM. The tests were conducted in two phases. In the first phase, the fixed CM was installed on the thigh, while the mobile CMs were installed at the shank. In the second phase, this setup was reversed, with the fixed CM on the shank and the mobile CMs on the thigh.

Each of the nine DOFs produced by the CMs, was tested with three different stiffness settings: free, 0.6N/rad and 1.2N/rad for the rotational DOFs, and free, 1kN/m and 2kN/m for the translational DOFs. The pressures on the thigh and shank were recorded in separate sets of trials as the pressure measuring system could only read one cuff at a time. Each CM configuration was tested 60 times, half of which had the pressure measuring system active on the thigh, while the other half the pressure measuring system was active on the shank. The tension of the cuff strap was not adjusted between trials to maintain consistent conditions.

Each trial began with the jig at or close to its fully extended state. During each trial, the motion capture system and pressure measurement system recorded data and saved it for later analysis. The motion capture system ended the trials after 8s, at which the jig achieved approximately 70° of flexion. Between trials the jig was lowered to the starting position.

4.3.2 Human Trials

Participants were recruited for this research under the ethics certificate H-06-23-9326 issued by the University of Ottawa Office of Research Ethics and Integrity, shown in Appendix E. The participants had to meet the following requirements:

(1) In good health.
(2) No history of lower limb injury resulting in permanent changes to their gait.
(3) Not currently experiencing or having experienced within the past month any symptoms related to a lower limb injury affecting their gait.
(4) Not have a neurological disorder.
(5) Not taking medication that affects their perception of comfort or pain.

One participant was recruited and provided their informed consent to participate in the human trials. The participant was female, 24 years old, 163 cm tall, and weight of 53 kg.

Before arrival, the participant was requested to wear tight fitting shorts to prevent occluding the motion capture markers and to facilitate their attachment. The participant had the exoskeleton attached to their leg with the knee joint and exoskeleton aligned visually by minimizing the difference in joint centers as they rotated. The cuff straps were tightened such that they didn't cause immediate discomfort to the user while minimizing sliding of the brace across the user's limb, ensuring that only tissue shearing could accommodate kinematic incompatibility between the brace and limb. Markers were placed on the medial and lateral epicondyles of the femur, femoral greater trochanter, lateral condyle of the tibia, and the medial and lateral malleoli. The marker placement was facilitated by palpating the joints and bony prominences along with the participant flexing and extending the knee.

The participant stood in the center of the capture volume while three motion capture cameras were positioned on tripods around them to avoid the participant's motion occluding the markers. The participant was provided with a post to help with balance should they need it during the trials.

For each trial, the participant would listen for the computer to announce the beginning of the recording, at which point they would bend their knee past 90° within 2 seconds at which point the recording automatically ended.

The participant tested five different CM configurations: control, and longitudinal translation at the shank at 0 N/m and 1 kN/m levels of CM stiffness, and sagittal translation at the shank with 0 N/m and 1 kN/m levels of CM stiffness. Because the jig results did not clearly indicate optimal configurations to test, these configurations were selected based on the results from Shafiei and Behzadipour [11], [12]. Due to time constraints on the human trials, and the pressure measurement system only being capable of recording the pressure at one interface at a time, only the shank interface pressures were measured. The shank interface was chosen as the work by Shafiei and Behzadipour [11], [12] indicated this is where most of the improvements would be found. The participant performed thirty trials with each CM configuration. Following each set of trials on a CM configuration the participant was asked walk around the room for 10 minutes after which they evaluated the comfort at both the shank and thigh interfaces separately on a visual analogue scale (VAS).

4.4 Data Analysis

A MATLAB script, presented in Appendix A, was written to perform the data analysis. The data analysis pipeline can be simplified to the following steps:

1. Importing pressure and motion capture data
2. Raw data processing
3. Fitting interface pressure and relative motion data
4. Plotting interface pressure and relative motion curves

Raw data processing had two components: data cleaning and data processing. The same cleaning process was applied to both the pressure and motion capture data. The specific processing done to the kinematic and pressure data is presented in sections 4.5.1 and 4.5.2.

Data cleaning began with the removal of outliers and missing data. Both individual points within a trial and entire trials could be outliers. Individual data points that deviated more than three scaled median absolute deviations from the median were classified as outliers and replaced with the median of the ten-element window surrounding the outlier. These outlier points were typically the result of measurement errors or issues in data transmission and recording. Removing these points reduced the noise in the data, leading to more accurate fits of the underlying relationship. Frames of the motion capture recording during which the cameras lost track of any marker were removed from the analysis. Anomalous trials, which significantly deviated from the rest of the set, were manually removed as outliers. Removing a few outlier trials ensured that only trials exhibiting typical behaviour were included. Given the large number of trials, the typical behaviour could be reliably identified. Of the 180 human trials conducted, 24 were removed as outliers, while for the 2220 jig trials, 124 were removed as outliers.

The data was fitted with curves to identify relationships and calculate statistical metrics. Linear regressions were used to fit polynomial curves to the data. To determine the effect of the CMs and their stiffnesses, the trial conditions were used as a categorical variable in the regressions. To avoid overfitting or underfitting the data, the polynomial degree was iteratively increased to achieve the maximum adjusted R^2, with a fourth order polynomial as the highest degree permitted. Each regression was plotted and statistics such as adjusted R^2 and RMSE were recorded.

The p-values and F-statistics are omitted from this report because they were all found to be significant, with MATLAB reporting the p-values to be zero or nearly zero. This was likely due to the number of trials conducted and the consistency within them. Because the statistical measures showed that all the CMs were statistically significantly different from the control, a measure of effect size was used to identify specific configurations that had the largest effect. A modified Cohen's D, shown in equation (4.1), was calculated as a measure of the effect size. Cohen's D compares the difference between two means in relation to their pooled standard deviation, in the context of the kinematics and pressure data, the average difference between the control, $M_{control}$, and the test conditions, M_{test}, was used for the means while the pooled RMSE was used in the placed of the standard deviation.

$$\mathrm{d} = \frac{M_{control} - M_{test}}{RMSE_{pooled}} \tag{4.1}$$

When evaluating the performance of the jig, we consider the predictive power of the jig. The predictive power represents the ability of the jig to produce

4.4.1 Kinematic Processing

From the motion capture data, the relative displacement of the exoskeleton was calculated. Relative displacement refers to the change in relative position of the limb and exoskeleton segments relative to the initial difference in position between the two, shown in Figure 4.7. This calculation was performed in two steps: first, calculating the relative displacement in world coordinates, and second, converting the relative displacement to the reference frame of the limb segment. Converting the relative displacement to the limb segment's coordinate system aids in interpreting the results.

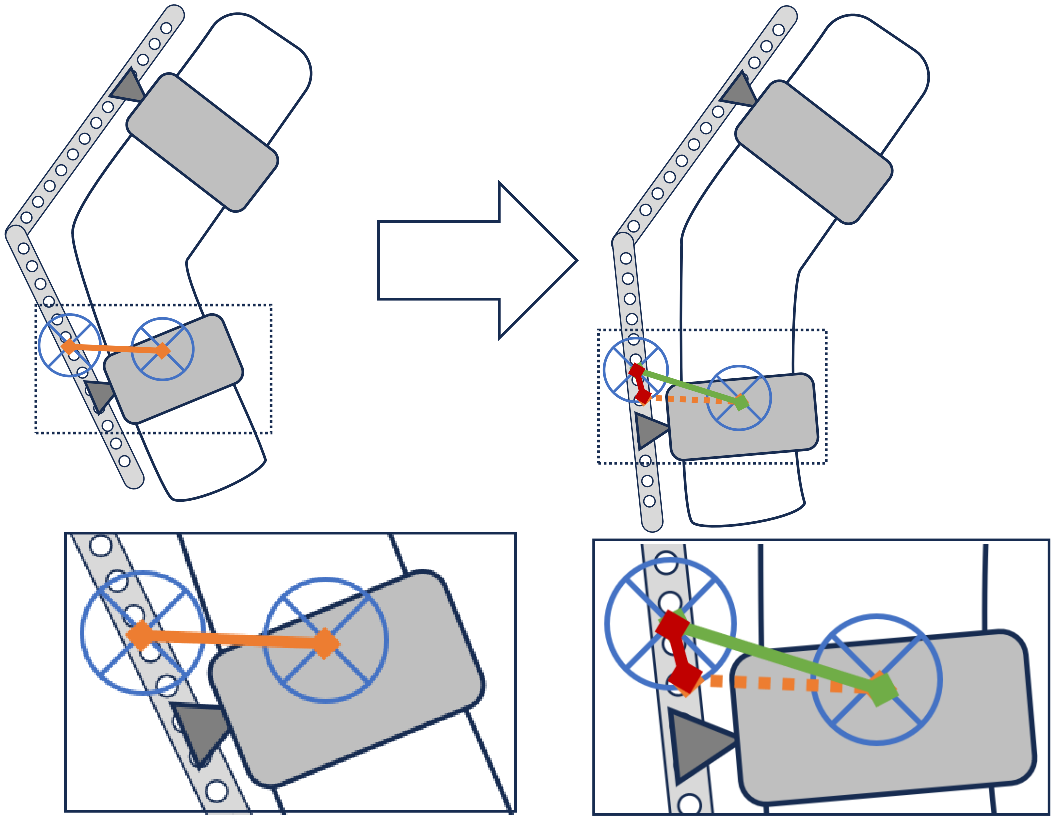

Figure 4.7: Leg with brace in two positions, showing the centers of the shank and shank brace segments, along with the displacement (orange and green) between them and the relative displacement (red) between the first(left) and second(right) positions.

The relative displacement of the shank for each datapoint in a trial, $\Delta\vec{S}$, and thigh, $\Delta\vec{T}$, with respect to the brace shank and thigh segments are calculated using equations (4.2) and (4.3). $\vec{S}$ represents the shank position while $\vec{T}$ represents the thigh position, $\overrightarrow{SB}$ represents the shank brace position and $\overrightarrow{TB}$ represents the thigh brace position; and $\Delta\vec{S}_{10°}$ is the shank relative displacement and $\Delta\vec{T}_{10°}$ is the thigh relative displacement, both at 10° of flexion. Each of these positions is defined as the geometric center of the motion capture markers placed on each segment, which is consistent across trials. The $\Delta\vec{S}_{10°}$ and $\Delta\vec{T}_{10°}$ terms serve to zero the data to enable comparison between trials and were interpolated from the adjacent datapoints for each trial. 10° of flexion was used as the zero-reference point because not all trials began from exactly 0° of flexion.

$$\Delta\vec{S} = \vec{S} - \overrightarrow{SB} - \Delta\vec{S}_{10°} \quad (4.2)$$

$$\Delta\vec{T} = \vec{T} - \overrightarrow{TB} - \Delta\vec{T}_{10°} \quad (4.3)$$

To convert the coordinate system from the room to the reference frame of the shank and thigh segments, the reference frame was rotated and the points positions calculated using equations (4.4) and (4.5), where $\Delta\vec{S}'$ and $\Delta\vec{T}'$ are the points in the new reference frame, q_s and q_T are the quaternions representing the rotation of the shank and thigh limb segments respectively.

$$\Delta\vec{S}' = q_s * \Delta\vec{S} q_s \quad (4.4)$$

$$\Delta\vec{T}' = q_T * \Delta\vec{T} q_T \quad (4.5)$$

4.4.2 Pressure Processing

Pressure processing involved converting the raw analogue voltage readings of the pressure sensors into pressures and spatially averaging the sensors.

The sensor calibration curves were used to convert the analogue voltage readings to pressures. The pressure data was not zeroed, because zeroing would remove the effect of the CM configuration on the baseline pressure.

The sixty pressure sensors were spatially averaged into six pressure zones: proximal and distal rows of lateral, central, and medial zones. The pressures zones are shown in Figure 4.8. Averaging the pressure sensors into larger zones reduced the noise from individual sensors and facilitated the presentation and interpretation of the results. Because the sensor matrix was composed of five rows of twelve sensor elements, the central row contributed to both the proximal and distal pressure zones. To compensate for the overlap, the contribution of the central row was divided by two.

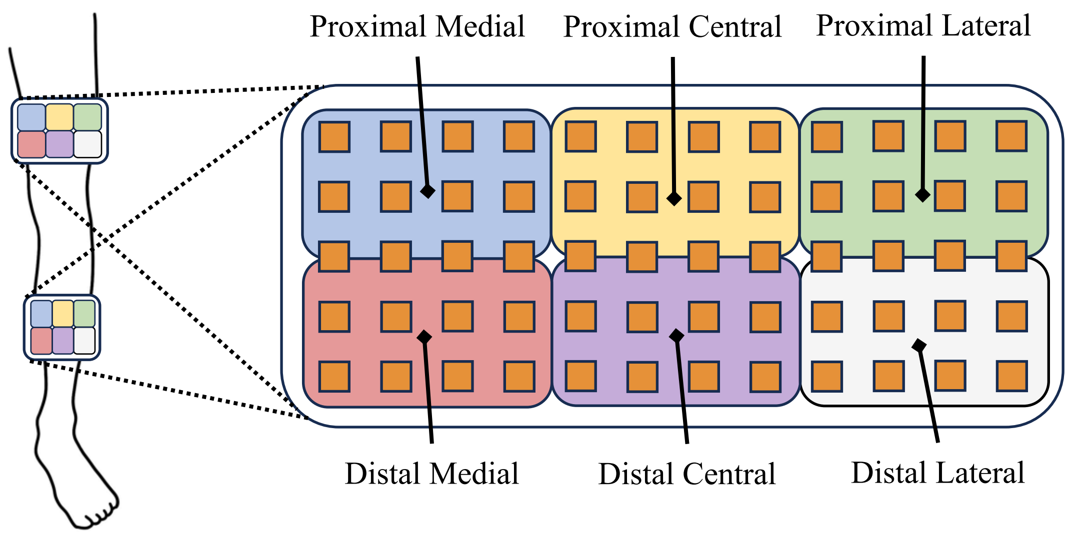

Figure 4.8: Leg and pressure sensor cuffs showing the sensor elements (orange squares) and the pressure zones along with their locations.

Chapter 5 Results and Discussion

This chapter presents the results of the interface pressures and relative displacement analyses, accompanied by a detailed discussion. The chapter is organized into three main sections: the effect of added DOFs on the shank, the effect of added DOFs at the thigh, and a comprehensive discussion of the overall findings from both the jig and human trials. Additionally, the limitations of this work and potential sources of error are explored. A summary table of trials conducted is shown below in Table 5-1.

Table 5-1: Summary of trials conducted.

Location and Passive DOF	Stiffnesses	Jig Trials	Human Trials
Control	N/A	☒	☒
Shank Longitudinal Rotational	1.2N/rad	☒	☐
	0.6N/rad	☒	☐
	0N/rad	☒	☐
Shank Longitudinal Translational	2kN/m	☒	☐
	1kN/m	☒	☒
	0N/m	☒	☒
Shank Sagittal Rotational	1.2N/rad	☒	☐
	0.6N/rad	☒	☐
	0N/rad	☒	☐
Shank Sagittal Translational	2kN/m	☒	☐
	1kN/m	☒	☒
	0N/m	☒	☒
Shank Transverse Rotational	1.2N/rad	☒	☐
	0.6N/rad	☒	☐
	0N/rad	☒	☐
Shank Transverse Translational	2kN/m	☒	☐
	1kN/m	☒	☐
	0N/m	☒	☐
Thigh Longitudinal Rotational	1.2N/rad	☒	☐
	0.6N/rad	☒	☐
	0N/rad	☒	☐
Thigh Longitudinal Translational	2kN/m	☒	☐
	1kN/m	☒	☐
	0N/m	☒	☐

Thigh Sagittal Rotational	1.2N/rad	☒	☐
	0.6N/rad	☒	☐
	0N/rad	☒	☐
Thigh Sagittal Translational	2kN/m	☒	☐
	1kN/m	☒	☐
	0N/m	☒	☐
Thigh Transverse Rotational	1.2N/rad	☒	☐
	0.6N/rad	☒	☐
	0N/rad	☒	☐
Thigh Transverse Translational	2kN/m	☒	☐
	1kN/m	☒	☐
	0N/m	☒	☐

5.1 Added Degrees of Freedom to the Shank

To facilitate comparison, the results from the human trials are presented alongside those from the jig trials for both longitudinal and sagittal translational DOFs. For each DOF, three sets of fitted curves are presented: the shank interface pressures, the thigh interface pressures, and finally the relative displacement of the two interfaces. The 95% prediction bounds for each fitted curve are shown as a shaded region around the curve. Tables of the fit statistics are presented in Appendix C.

5.1.1 Longitudinal Rotational

The brace and limb segment relative displacements are shown in Figure 5.1 while the pressures at the thigh and shank interfaces are shown in Figure 5.2 and Figure 5.3 respectively.

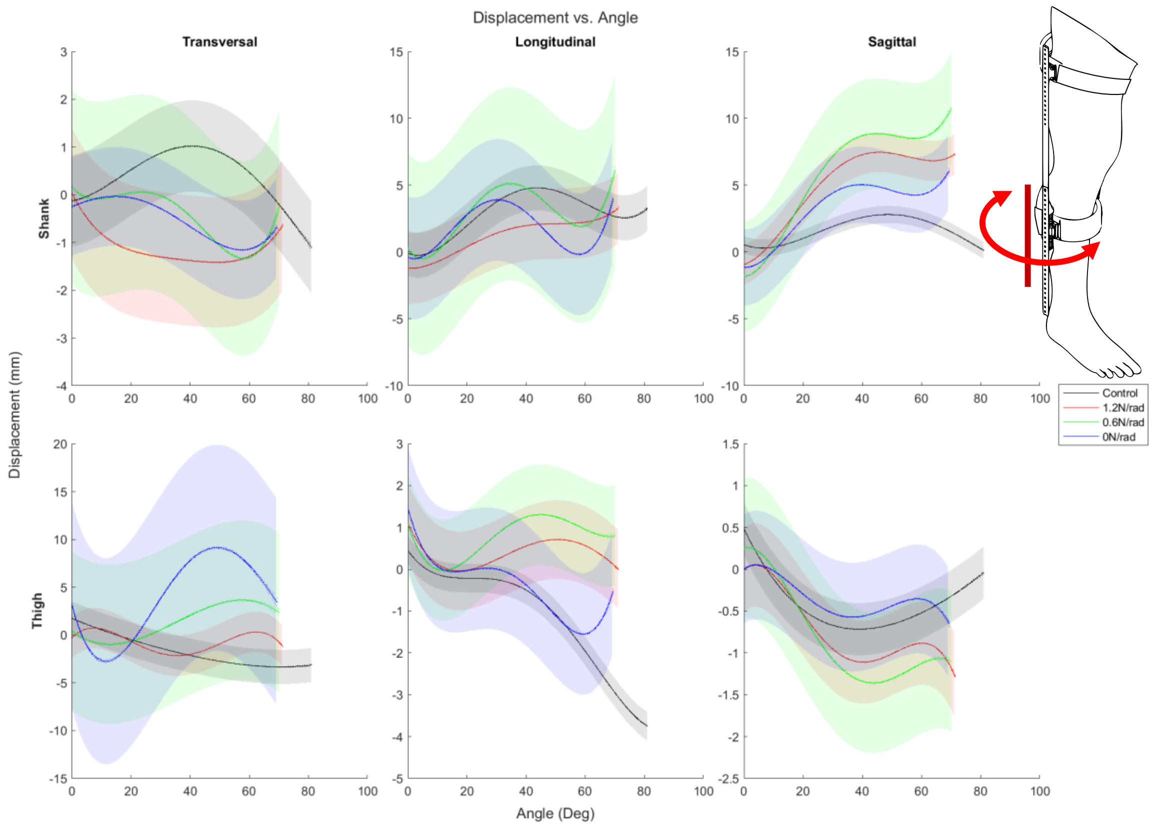

Figure 5.1: Relative displacement of the limb segments and brace with longitudinal rotation at the shank interface permitted. Shaded areas are 95% prediction bounds. Dotted lines are 95% confidence bounds

Adding longitudinal rotation to the shank CM led to the expected behaviour of increasing shank displacement in the sagittal direction. The increase in sagittal displacement does not strongly depend on the stiffness of the CM. At the thigh interface longitudinal displacement decreased, conversely, in the transverse direction displacement increased. The no stiffness trials were expected to have the most variance, followed by the medium stiffness trials, which is seen in the thigh relative displacement, however in the shank relative displacement, the medium stiffness trials had more variance.

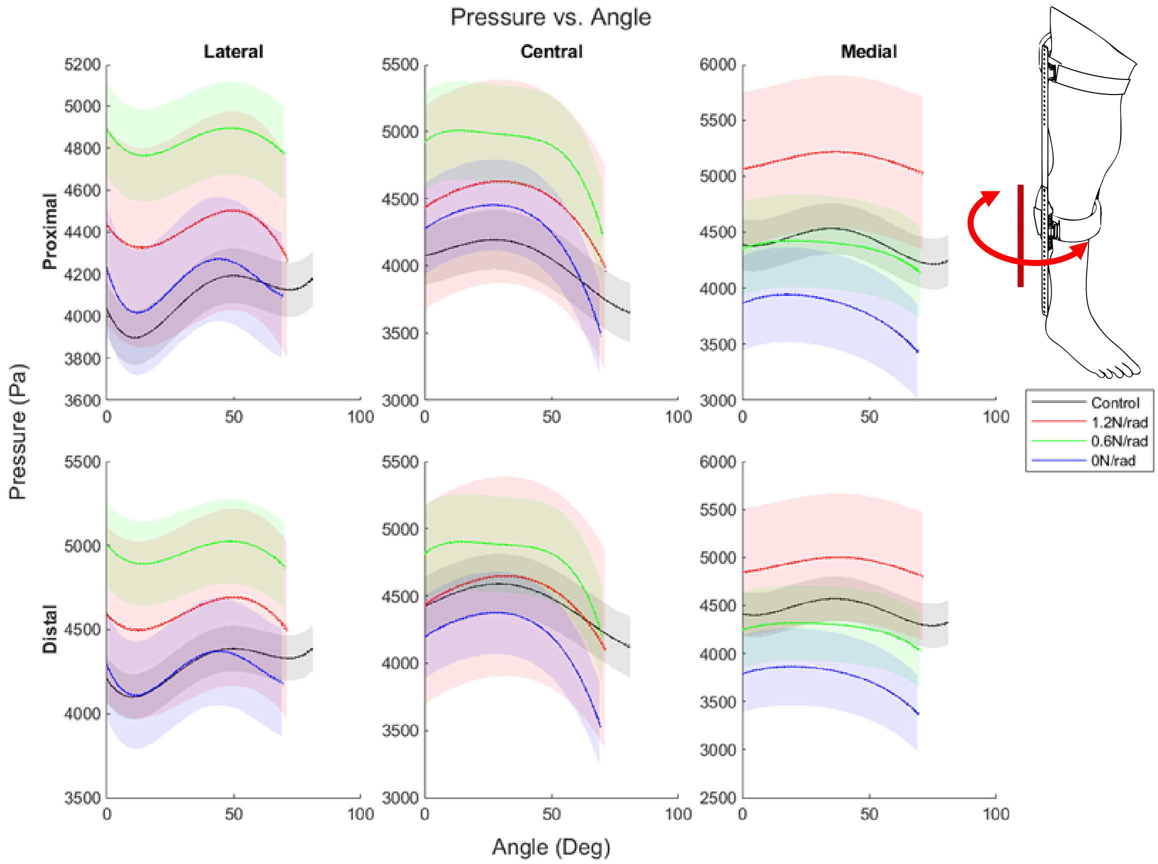

Figure 5.2: Fitted curves for thigh pressures with longitudinal rotation permitted at the shank. Shaded areas are 95% prediction bounds. Dotted lines are 95% confidence bounds

Adding longitudinal rotation to the shank CM led to an increase in pressures in the lateral and central regions while pressure decreased in the medial regions. The trials with no stiffness in the CM had the lowest observed pressures, while the trials with some stiffness increased interface pressures. Unexpectedly, the high stiffness trials had the greatest variability.

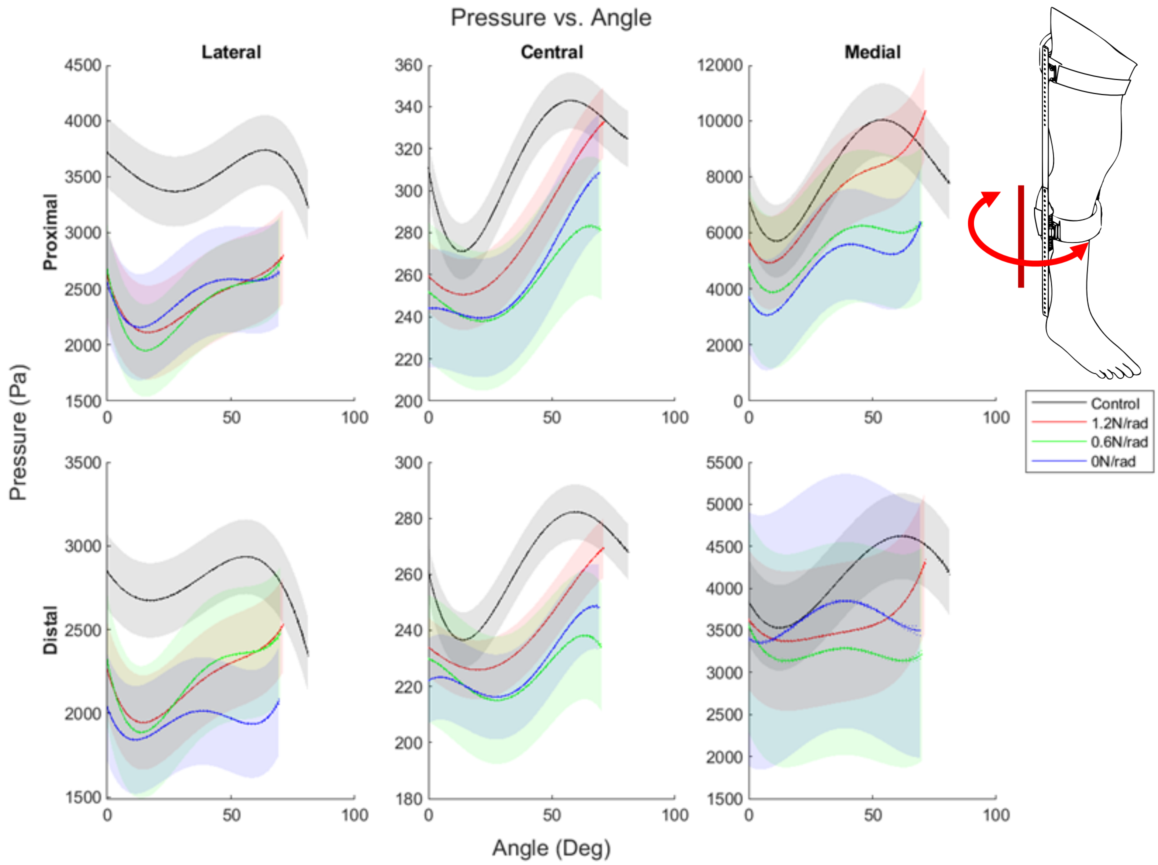

Figure 5.3: Fitted curves for shank pressures with longitudinal rotation permitted at the shank. Shaded areas are 95% prediction bounds. Dotted lines are 95% confidence bounds

Adding longitudinal rotation at the shank CM led to a consistent decrease in shank interface pressures. The medium and no stiffness trials had the largest reduction in pressures. Similar variability was observed across the stiffness configurations.

5.1.2 Longitudinal Translational

The relative displacements of the brace and limb segments are shown in Figure 5.4 while the pressures at the thigh and shank interfaces are shown in Figure 5.5 and Figure 5.6 respectively. The human trials are presented alongside the jig trials to facilitate a robust comparison.

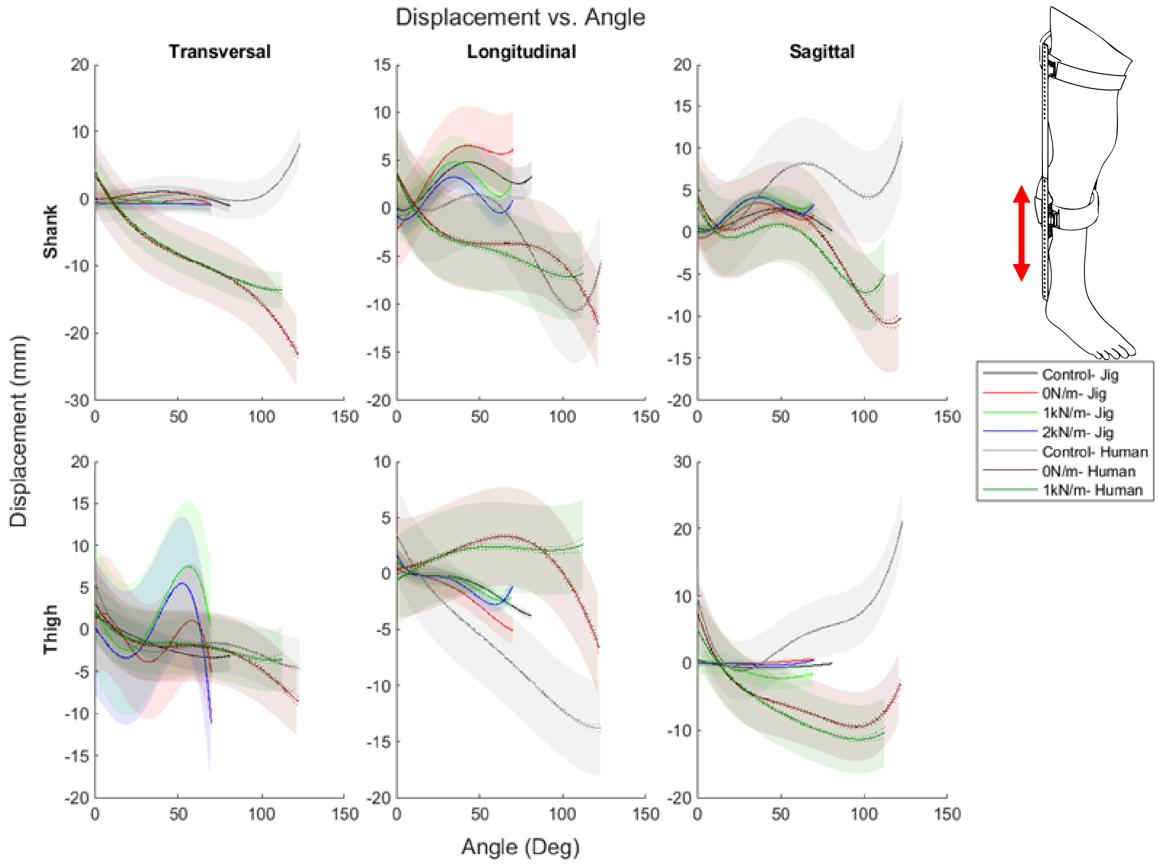

Figure 5.4: Relative displacement of the limb segments and brace with longitudinal translation at the shank interface permitted. Shaded areas are 95% prediction bounds. Dotted lines are 95% confidence bounds

Jig Trials

Adding longitudinal translation to the shank CM led to small changes in shank longitudinal translation. In the medium and no stiffness trials, longitudinal translation decreased while in the high stiffness trials longitudinal translation increased, however the magnitude of these changes are small.

Human Trials

Adding longitudinal translation to the shank CM led to changes in displacement greater than 2cm at both the shank and thigh interfaces. The added DOF resulted in drastic and consistent changes in behaviour across the CM stiffnesses. Thigh longitudinal translation increased at all angles. Shank transverse and sagittal translations, along with thigh sagittal translations differed markedly from the control and expectations.

The jig did not have strong predictive power for the human trials. The jig underestimated the degree of relative motion, and the shape of the displacement-angle curves did not match those from the human trials. Consequently, the jig was unable to predict many of the observations made for the human trials.

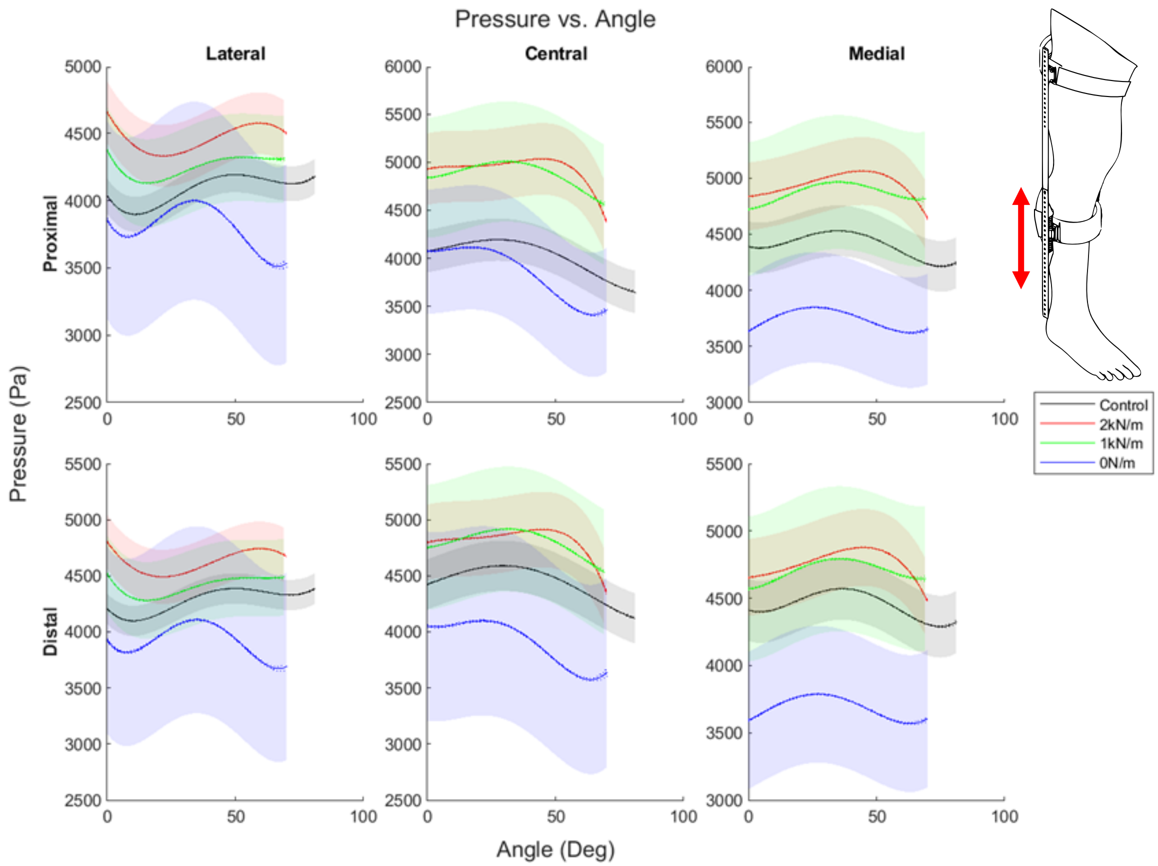

Figure 5.5: Fitted curves for thigh pressures with longitudinal translation permitted at the shank. Shaded areas are 95% prediction bounds. Dotted lines are 95% confidence bounds

Adding longitudinal translation to the shank CM had inconsistent effects on thigh interface pressures. The control trials and the trials with no stiffness had the lowest interface pressures; it was expected that the two trials with some stiffness would fall between these two. Regardless of the conditions, the fitted curves have similar behaviours, with the primary difference between the conditions being the initial pressure.

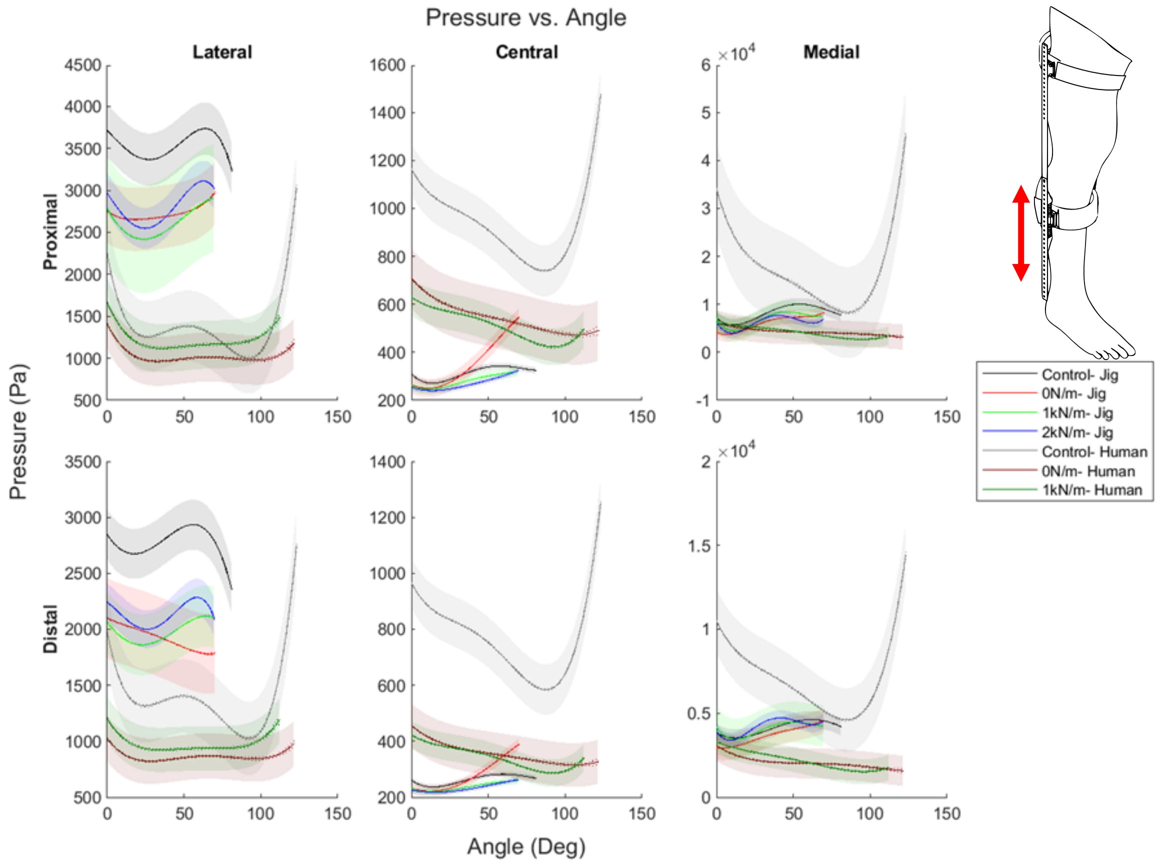

Figure 5.6: Fitted curves for shank pressures with longitudinal translation permitted at the shank. Shaded areas are 95% prediction bounds. Dotted lines are 95% confidence bounds

Jig Trials

Adding longitudinal translation to the shank CM led to large decrease in the pressure at the lateral side of the interface. The stiffness of the CM did not appear to have a consistent effect across the pressure zones.

Human Trials

Adding longitudinal translation to the shank CM led to a reduction in interface pressures. The added DOF resulted in a consistent change to the relationship between angle and pressure, the most notable difference occurring at angles above ~90 degrees, where the large pressure spike was reduced. The pressure reduction supports the addition of longitudinal translation to exoskeleton CMs.

The jig did not have strong predictive power for the shank interface pressures.

5.1.3 Sagittal Rotational

The relative displacements of the brace and limb segments are shown in Figure 5.7 while the pressures at the thigh interface is shown in Figure 5.8 and shank interface is shown in and Figure 5.9,

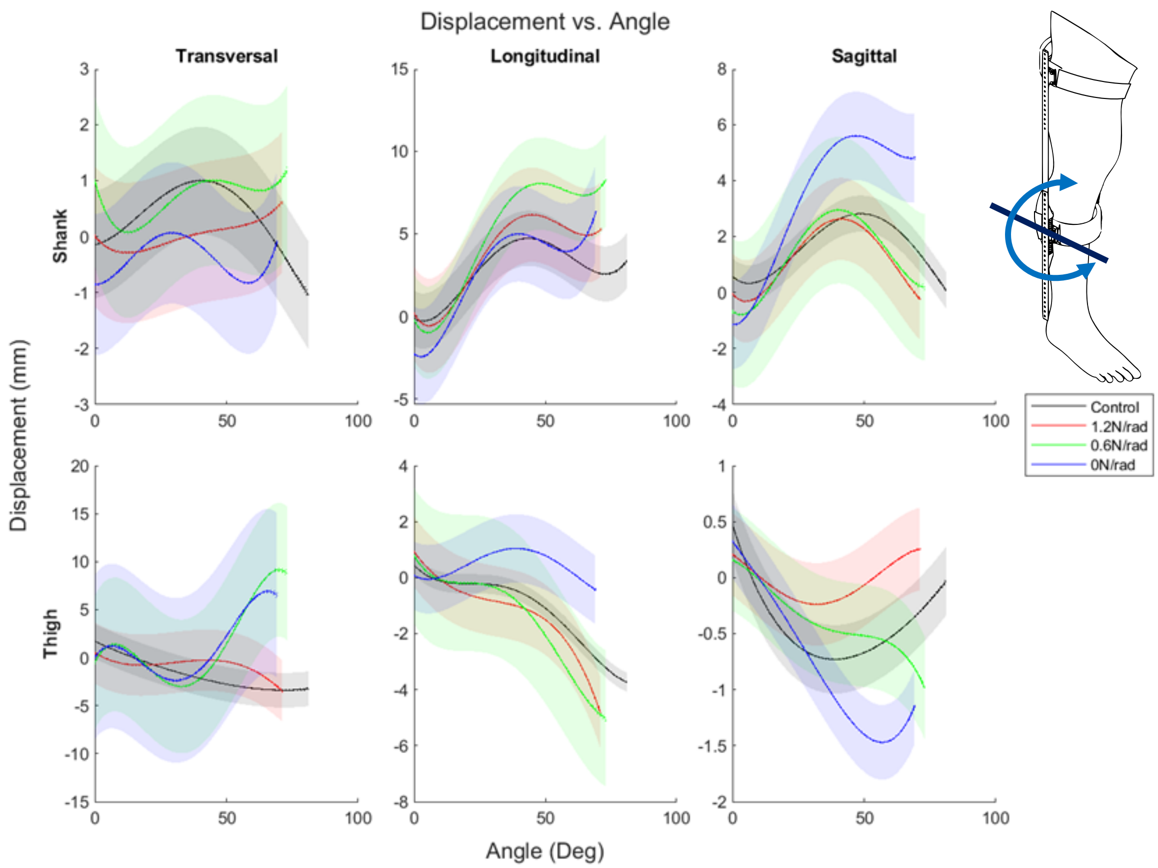

Figure 5.7: Relative displacement of the limb segments and brace with sagittal rotation at the shank interface permitted. Shaded areas are 95% prediction bounds. Dotted lines are 95% confidence bounds

Adding sagittal rotation to the shank CM led to small increases in longitudinal translation at the shank, which was expected, however the large increase in sagittal translation under the no stiffness condition was unexpected. At the thigh interface, transverse and longitudinal translation increased, however there was no discernable pattern across the stiffnesses.

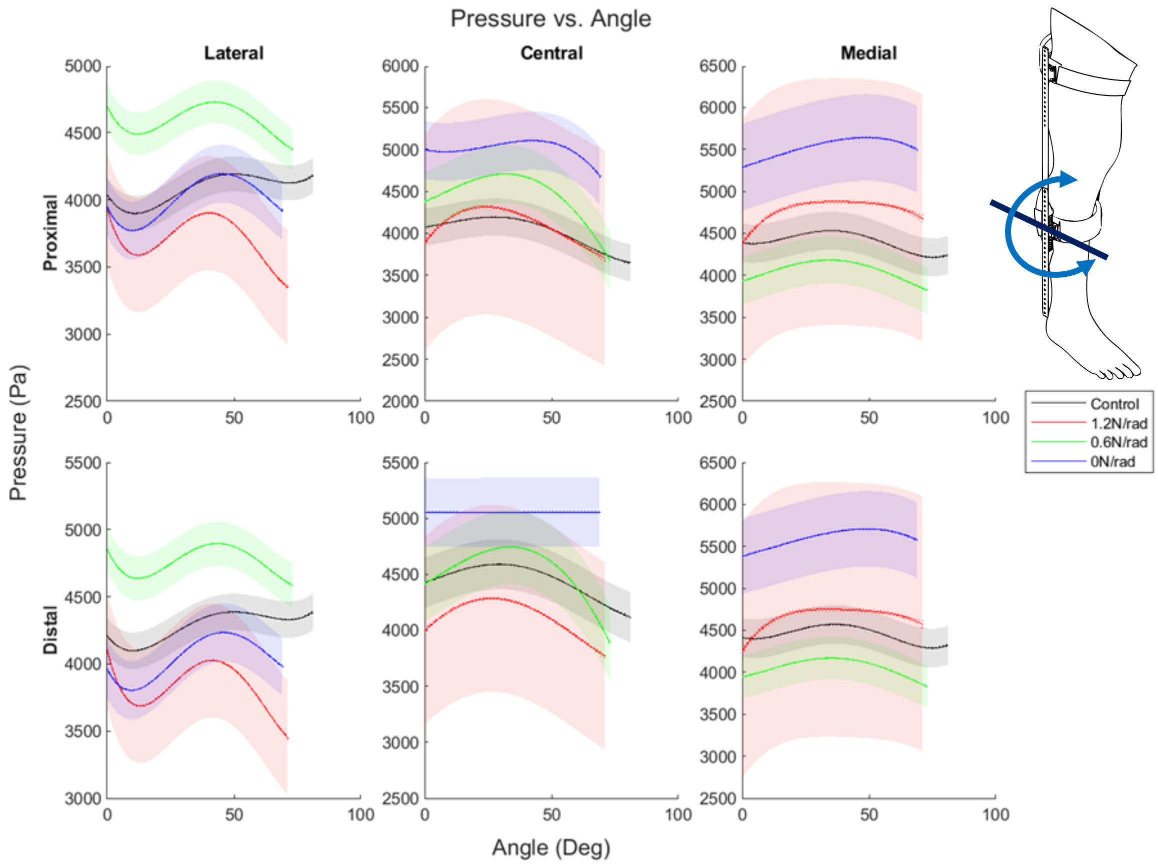

Figure 5.8: Fitted curves for thigh pressures with sagittal rotation permitted at the shank. Shaded areas are 95% prediction bounds. Dotted lines are 95% confidence bounds

Adding sagittal rotation to the shank CM resulted in inconsistent changes in thigh interface pressures, making drawing conclusions difficult. The pressures of the three different stiffness configurations had inconsistent relative performance across the pressure zones, for instance the 1.2N/rad stiffness configuration had the lowest pressures on the medial side, while the 0.6N/rad had the lowest pressure on the lateral side. The relative performance of the configurations does not appear to follow a trend from the lowest to highest stiffness. Additionally, contrary to expectations, the high stiffness trials had a large amount of variance compared to the no and medium stiffness trials.

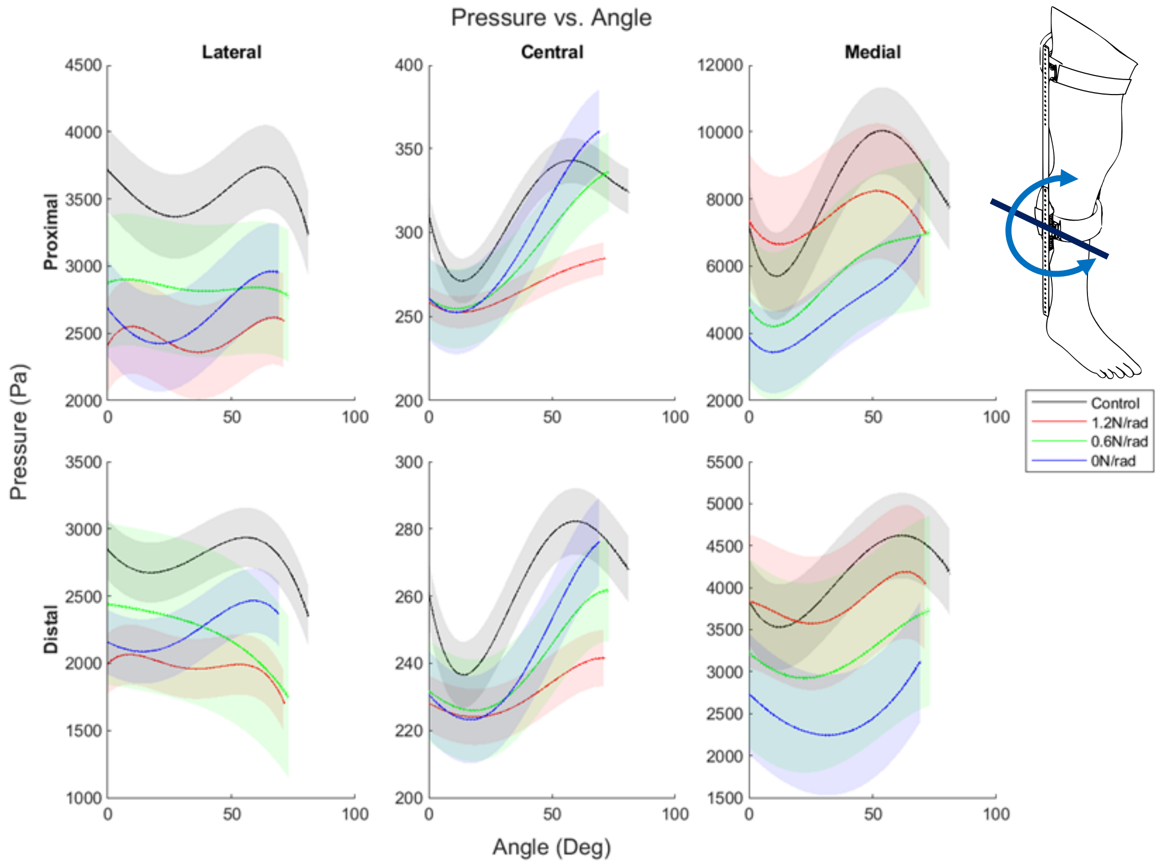

Figure 5.9: Fitted curves for shank pressures with sagittal rotation permitted at the shank. Shaded areas are 95% prediction bounds. Dotted lines are 95% confidence bounds

Adding sagittal rotation to the shank CM led to decreased pressures at the shank interface. The stiffness of the DOF does not appear to have a large influence on the magnitude of the pressure decrease.

5.1.4 Sagittal Translational

The relative displacements of the brace and limb segments are shown in Figure 5.10 while the pressures at the thigh and shank interfaces are shown in Figure 5.11 and Figure 5.12 respectively. The human trials are presented alongside the jig trials to facilitate a robust comparison.

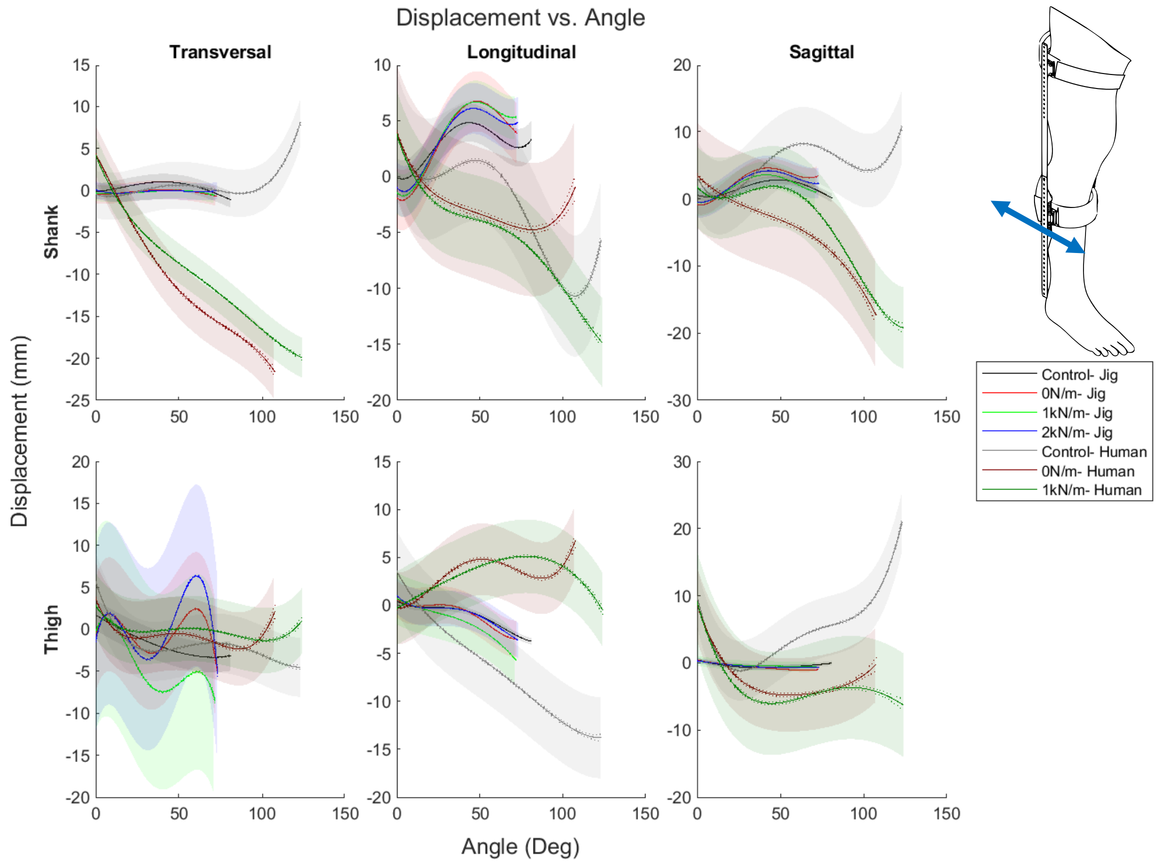

Figure 5.10: Relative displacement of the limb segments and brace with sagittal translation at the shank interface permitted. Shaded areas are 95% prediction bounds. Dotted lines are 95% confidence bounds

Jig Trials

Adding sagittal translation to the shank CM led to a small increase in sagittal translation at the shank as well as an unexpected small increase in shank longitudinal translation. Thigh transverse translation appears to have increased; however the prediction bounds show that it is not greater than the variance. The displacement curves across all trials remained relatively similar.

Human Trials

Adding sagittal translation to the shank CM led to an increase in sagittal translation at the shank and decrease in sagittal translation at the thigh as expected. The increase in longitudinal translation at the thigh and transverse translation at the shank was unexpected.

Similar to the results obtained from longitudinal translation permitted at the shank, the jig results do not have strong predictive power for the human results. The jig underestimated the degree of relative motion, and the shape of the displacement-angle curves did not match those from the human trials. Consequently, the jig was unable to predict many of the observations made for the human trials.

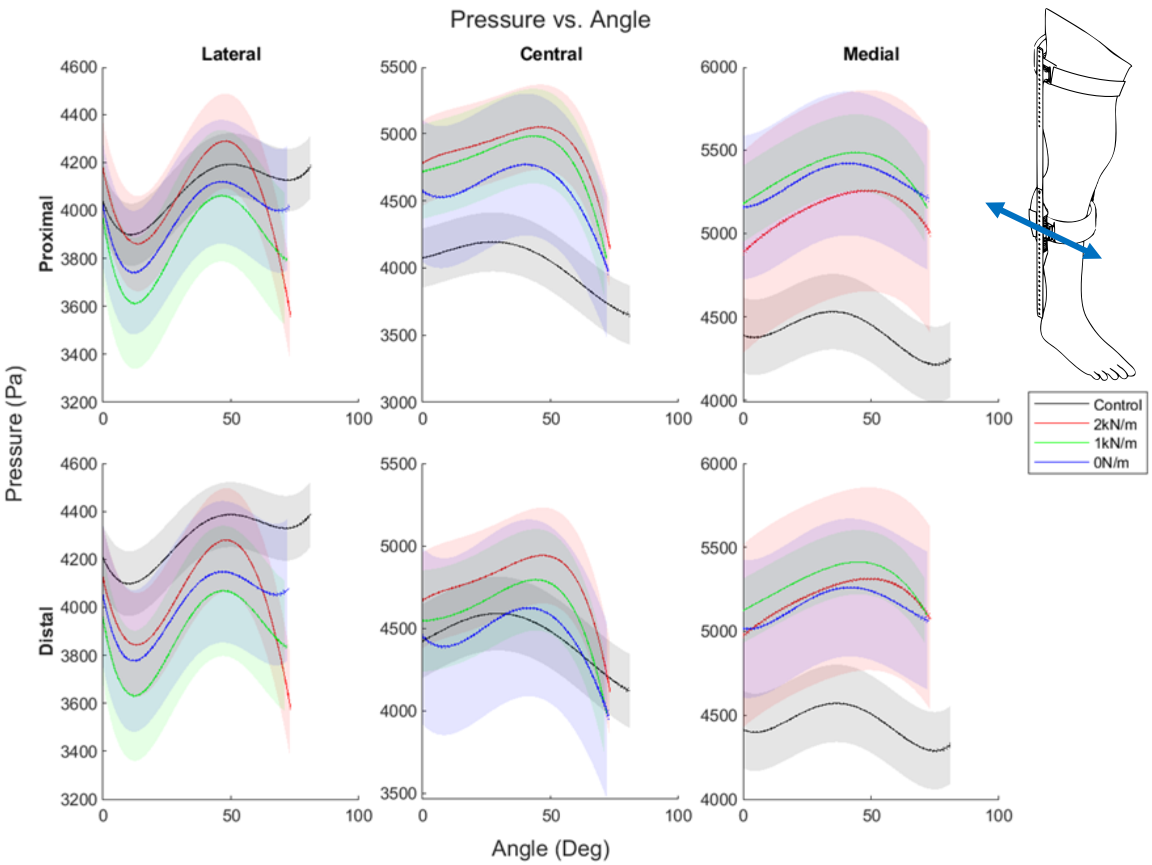

Figure 5.11: Fitted curves for thigh pressures with sagittal translation permitted at the shank. Shaded areas are 95% prediction bounds. Dotted lines are 95% confidence bounds

Adding sagittal translation to the shank CM led to an increase in central and medial thigh interface pressures that did not depend on the CM stiffness.

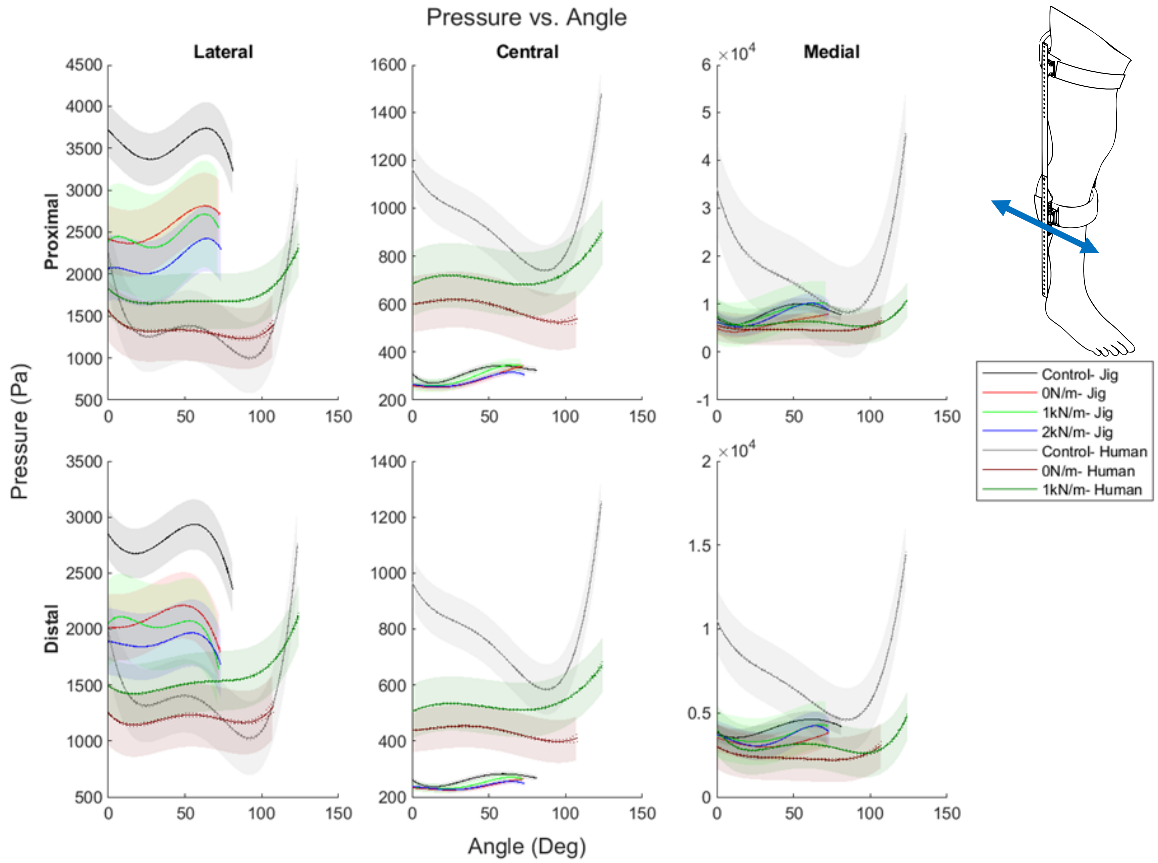

Figure 5.12: Fitted curves for shank pressures with sagittal translation permitted at the shank. Shaded areas are 95% prediction bounds. Dotted lines are 95% confidence bounds

Jig Trials

Adding sagittal translation led to a reduction of approximately 1000-1500 Pa in lateral interface pressures while pressures in other zones experienced only small reductions. The no stiffness case resulted in the lowest pressures, which was the expected outcome. The magnitude of the reduction was small, potentially limiting its utility.

Human Trials

Adding sagittal translation led to a decrease in pressures in the central and medial zones. The no stiffness condition resulted in a larger reduction in interface pressure compared to the medium stiffness condition. The effect on the behaviour was similar, with both conditions reducing the sharp increase in pressure associated with flexion greater than ~90 degrees. These observations support the addition of sagittal translation to exoskeleton CMs.

The jig did not have strong predictive power for the human results. The behaviour of the curves did not match nor did the changes between the control and the trials with the added DOF.

5.1.5 Transverse Rotational

The relative displacements of the brace and limb segments are shown in Figure 5.13 while the pressures at the thigh and shank interfaces are shown in Figure 5.14 and Figure 5.15 respectively.

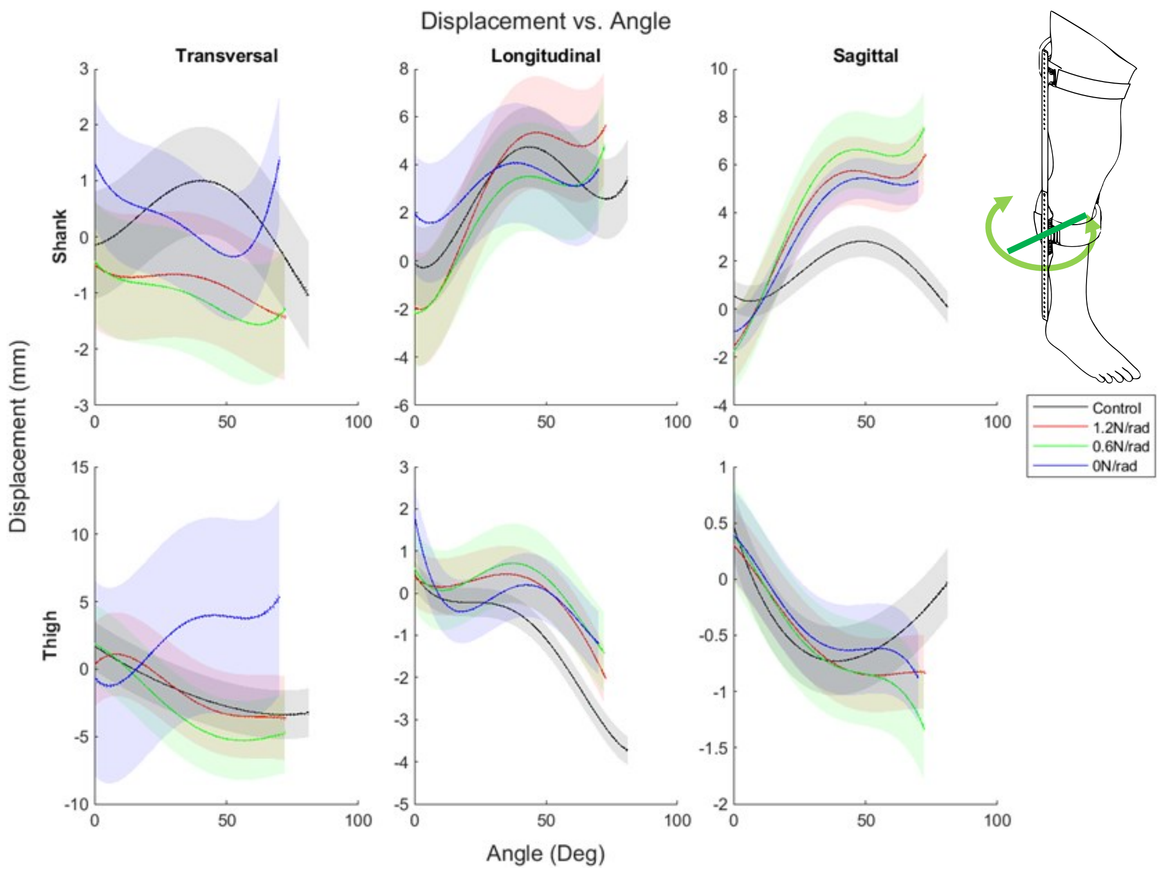

Figure 5.13: Relative displacement of the limb segments and brace with transverse rotation at the shank interface permitted. Shaded areas are 95% prediction bounds. Dotted lines are 95% confidence bounds

Adding transverse rotation to the shank CM led to increased translation in the longitudinal and sagittal directions as expected. Most of the increase occurred in the sagittal direction and was consistent across CM stiffness. At the thigh, longitudinal translation decreased somewhat, while transverse translation increased only under the no stiffness condition, however the prediction bounds suggest a large amount of variability.

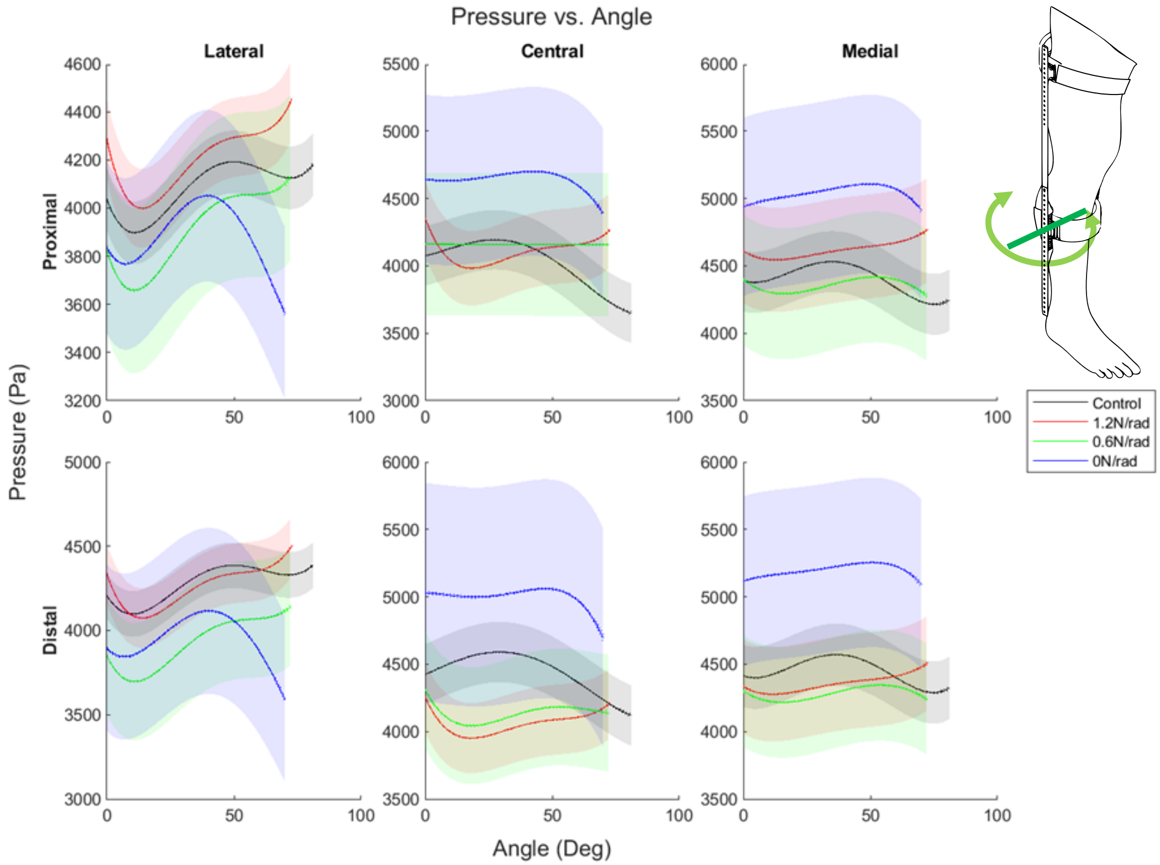

Figure 5.14: Fitted curves for thigh pressures with transverse rotation permitted at the shank. Shaded areas are 95% prediction bounds. Dotted lines are 95% confidence bounds

Adding transverse rotation to the shank CM led inconsistent results in thigh interface pressures. The medium and high stiffness trials generally had similar performance to the control while the no stiffness trials had higher pressures and larger variability.

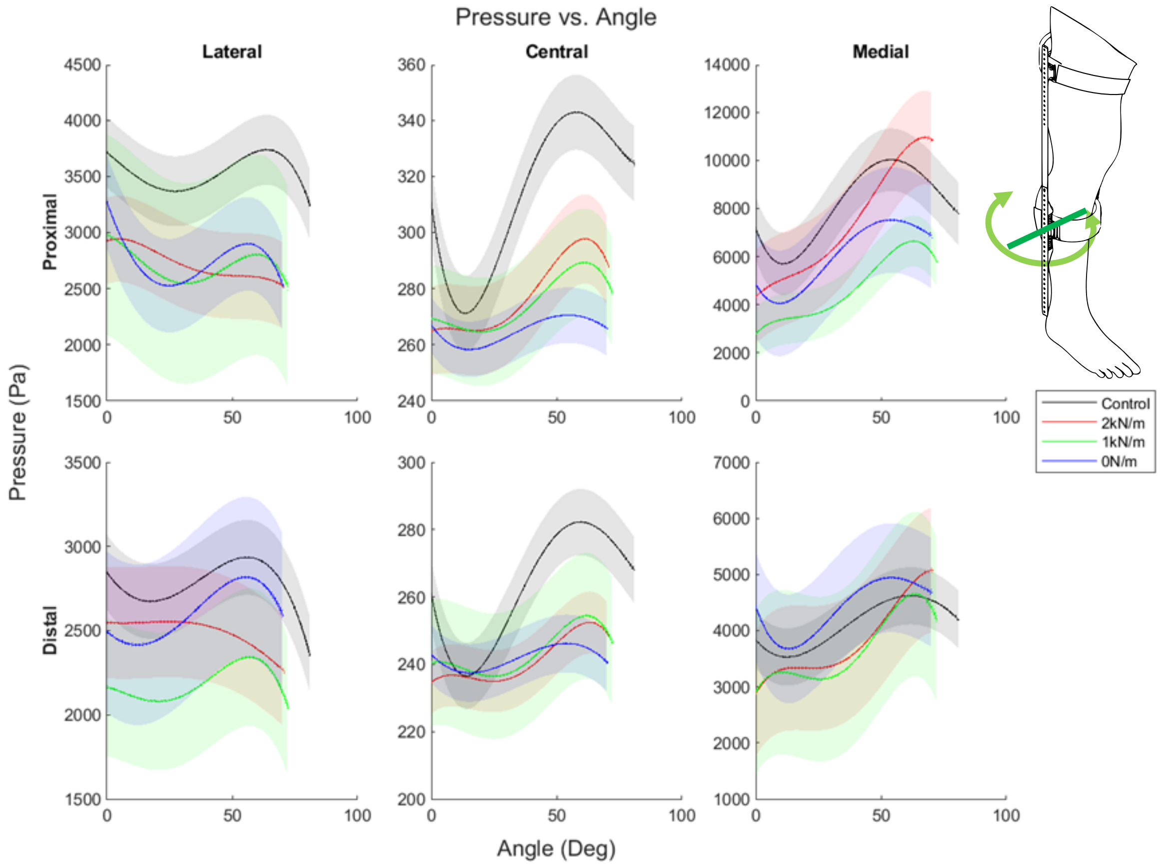

Figure 5.15: Fitted curves for shank pressures with transverse rotation permitted at the shank. Shaded areas are 95% prediction bounds. Dotted lines are 95% confidence bounds.

Adding transverse rotation to the shank CM led to a reduction in pressure in all zones except the medial-central one. The two conditions with some stiffness in the CM had similar behaviours. The no stiffness condition had the most variable results across the pressure zones. Despite the inconsistency between the stiffness conditions, these results support the addition of transverse rotation to exoskeleton CMs.

5.1.6 Transverse Translational

The relative displacements of the brace and limb segments are shown in Figure 5.16 while the pressures at the thigh interface are shown in Figure 5.17 and the shank interface pressures are shown in and Figure 5.18.

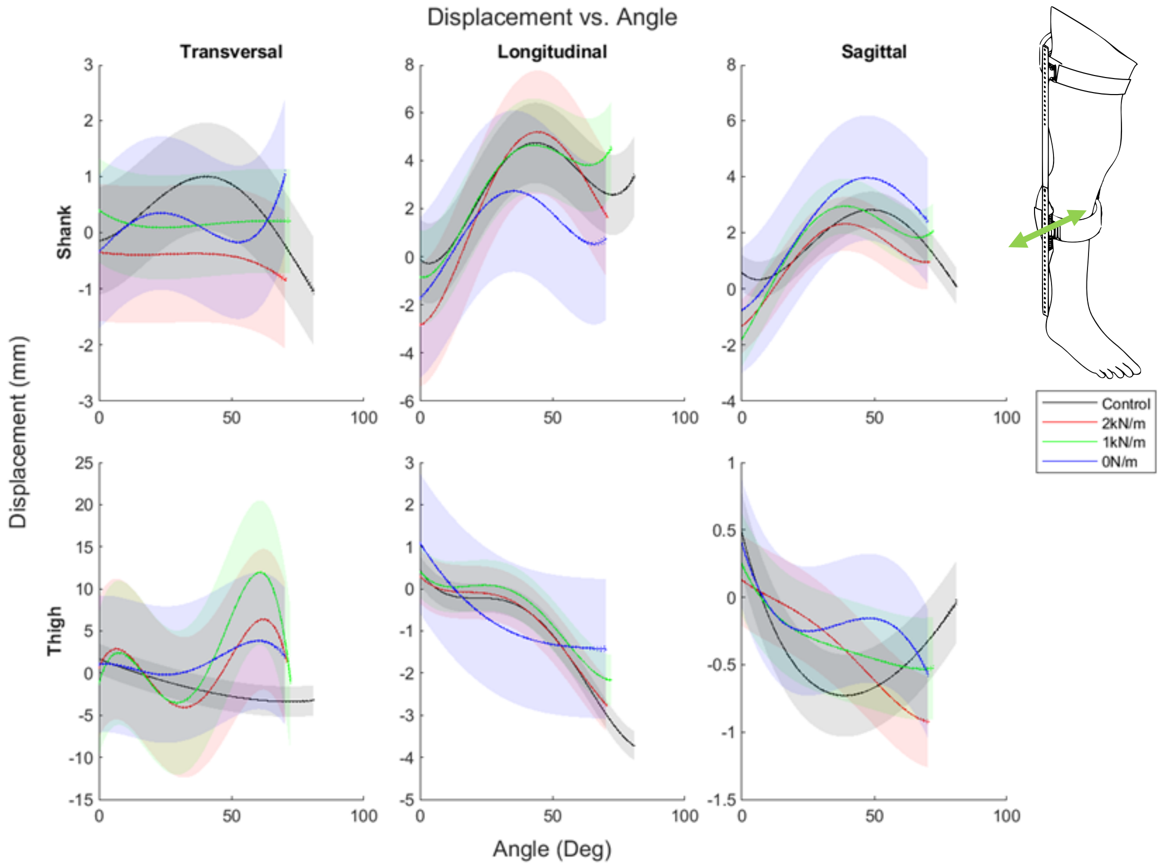

Figure 5.16: Relative displacement of the limb segments and brace with transverse translation at the shank interface permitted. Shaded areas are 95% prediction bounds. Dotted lines are 95% confidence bounds

Adding transverse translation to the shank CM led to very little change in behaviour. Most stiffness conditions had similar results to the control, and where they differed the differences were small. Large differences were also accompanied by increased variability.

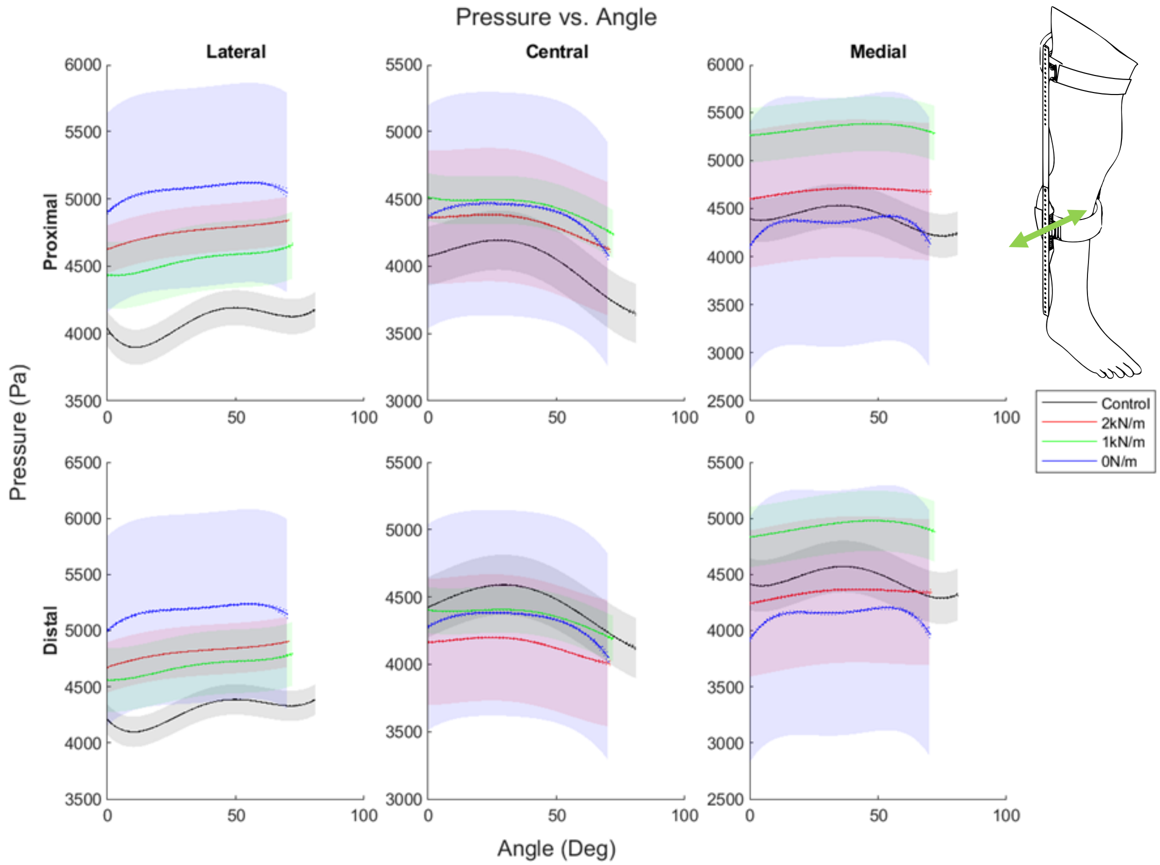

Figure 5.17: Fitted curves for thigh pressures with transverse translation permitted at the shank. Shaded areas are 95% prediction bounds. Dotted lines are 95% confidence bounds

Adding transverse translation to the shank CM led to no real change in relative displacement. Most stiffness configurations had similar results to the control while those that differed had a large amount of variability.

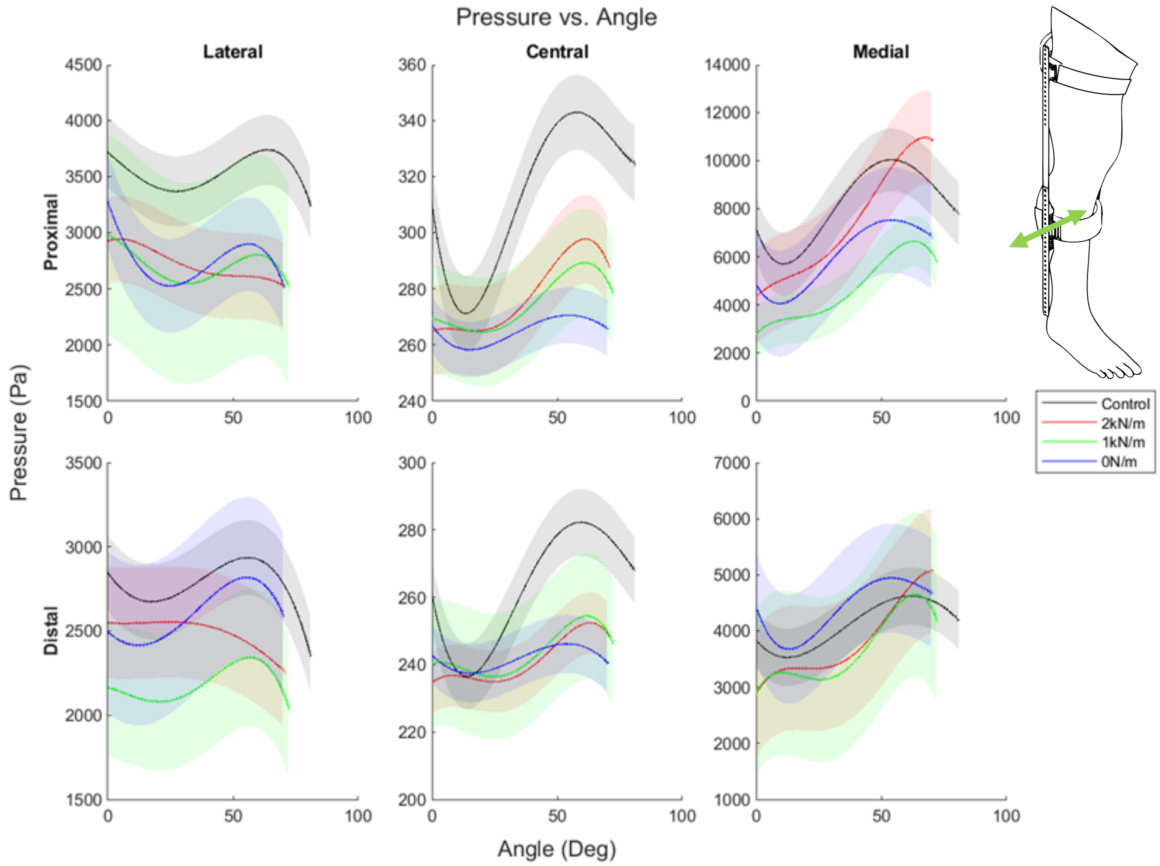

Figure 5.18: Fitted curves for shank pressures with transverse translation permitted at the shank. Shaded areas are 95% prediction bounds. Dotted lines are 95% confidence bounds

Adding transverse translation to the shank CM led to a reduction in shank interface pressure, concentrated on the lateral side of the interface. The stiffness configuration did not have a consistent effect across all the pressure zones.

5.2 Added Degrees of Freedom to the Thigh

For each DOF, three sets of fitted curves are presented: the shank interface pressures, the thigh interface pressures, and finally the relative displacement of the two interfaces. The 95% prediction bounds for each fitted curve are shown as a shaded region around the curve. Tables of the fit statistics are presented in Appendix C.

5.2.1 Longitudinal Rotational

Relative displacements of the brace and limb segments are shown in Figure 5.19 while the pressures at the thigh and shank interfaces are shown in Figure 5.20 and Figure 5.21 respectively.

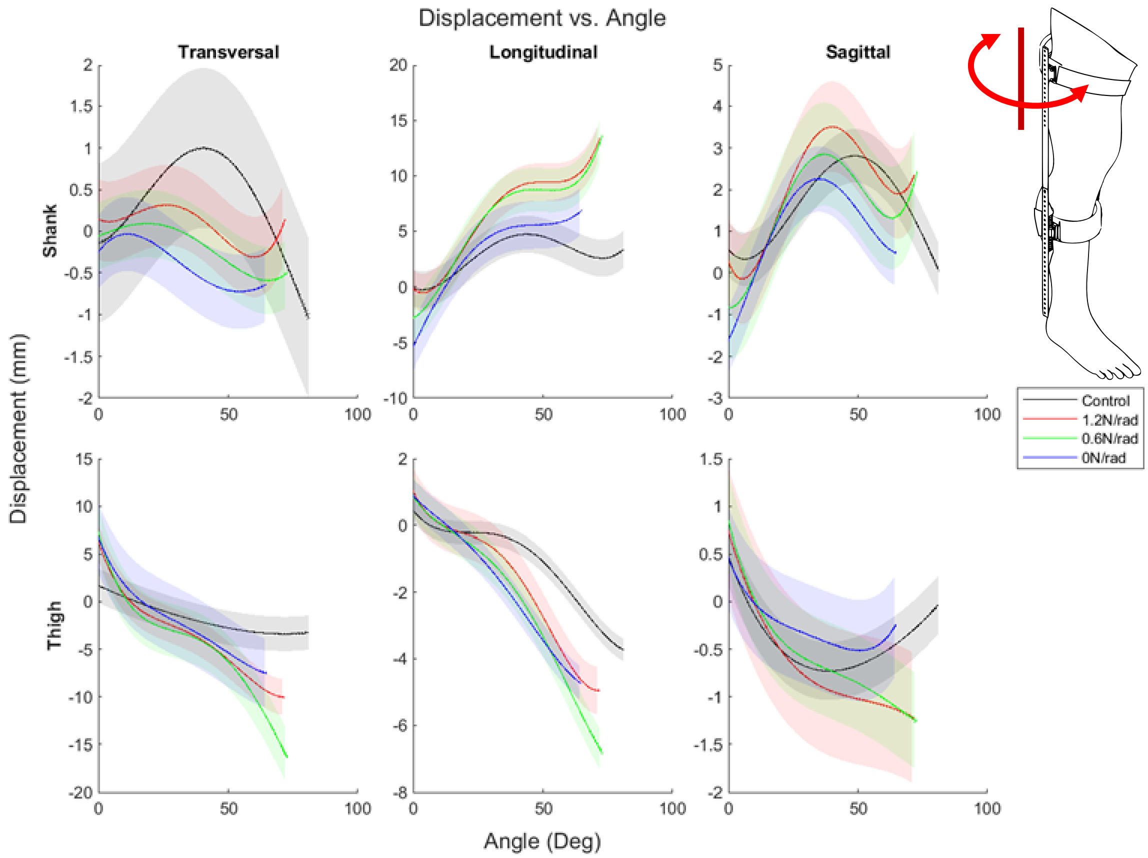

Figure 5.19: Relative displacement of the limb segments and brace with longitudinal rotation at the thigh interface permitted. Shaded areas are 95% prediction bounds. Dotted lines are 95% confidence bounds.

Adding longitudinal rotation to the thigh CM led to an increase in thigh transverse translation. Unexpectedly, thigh sagittal translation did not increase, and thigh longitudinal translation increased.

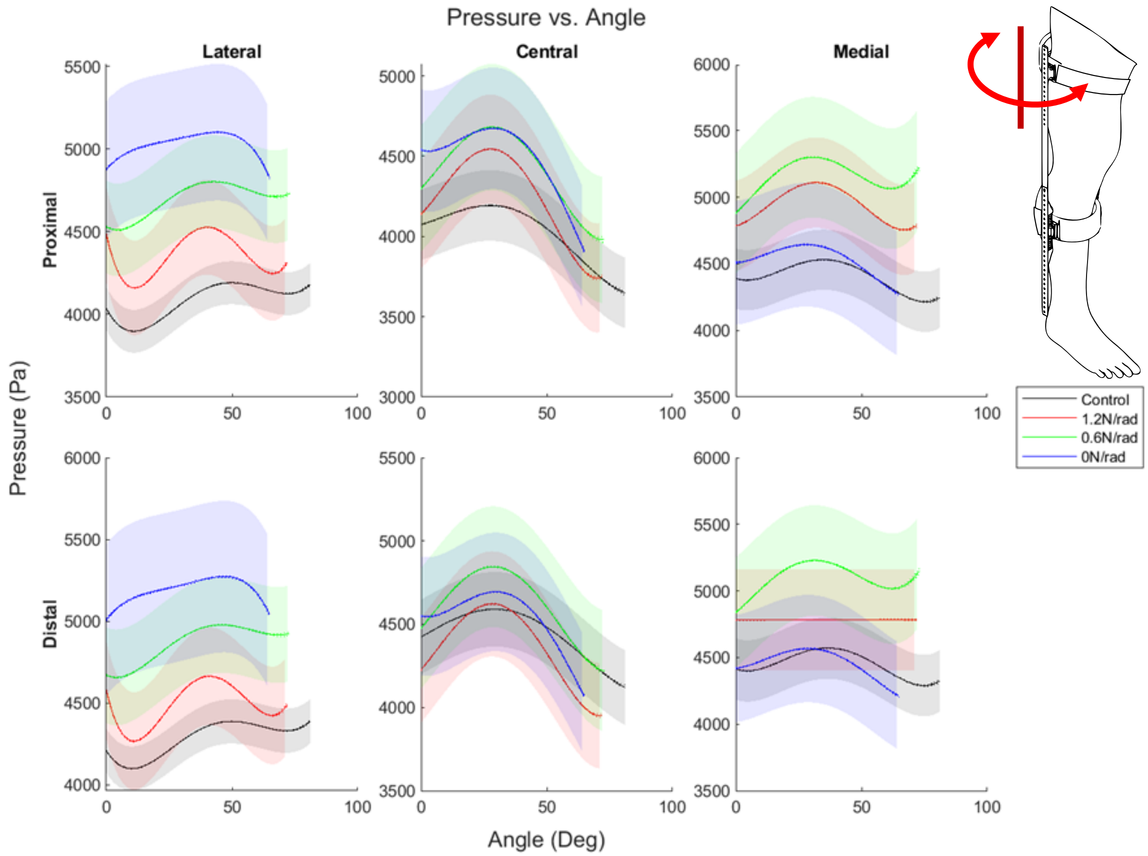

Figure 5.20: Fitted curves for thigh pressures with longitudinal rotation permitted at the thigh. Shaded areas are 95% prediction bounds. Dotted lines are 95% confidence bounds

Adding longitudinal rotation to the thigh CM led to increased thigh interface pressures. This outcome was contrary to the expectation that thigh pressures would decrease when the CM was applied to the thigh interface. The relative performance of the different stiffness configurations suggests that stiffness in longitudinal rotation should be maximized to minimize thigh interface pressures.

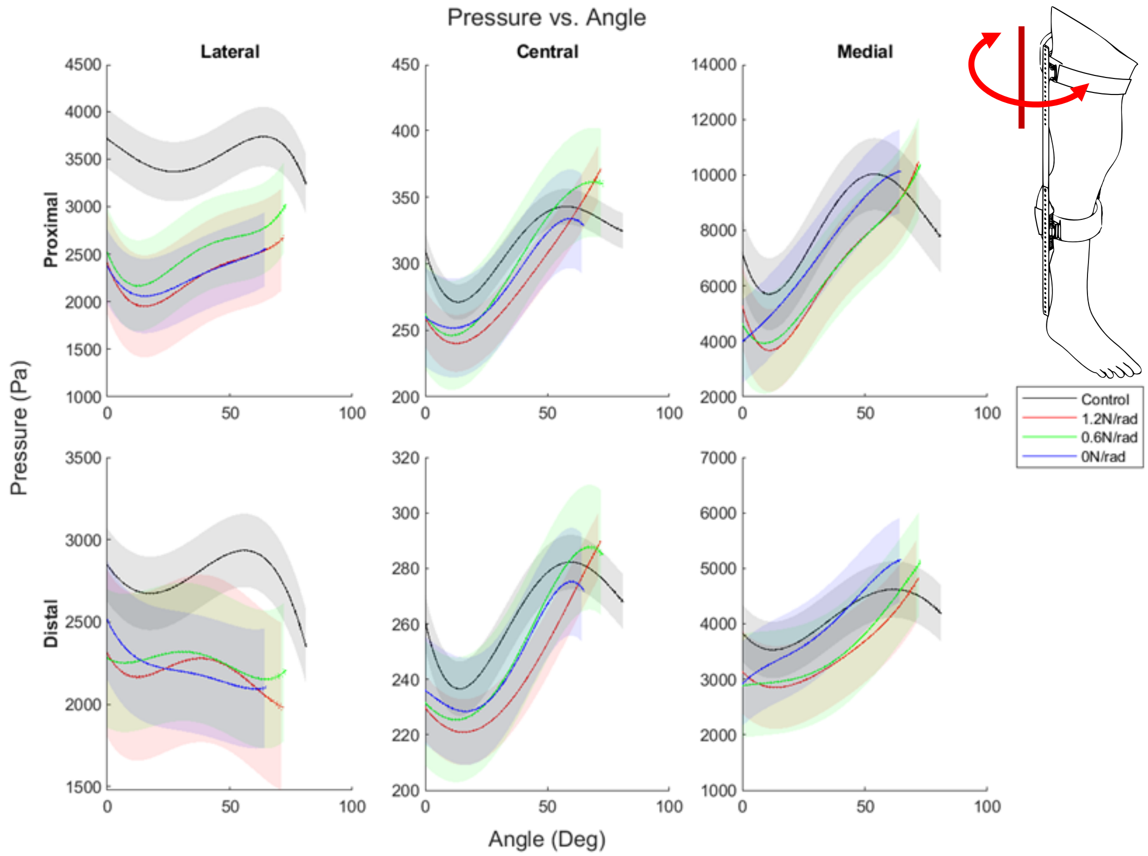

Figure 5.21: Fitted curves for shank pressures with longitudinal rotation permitted at the thigh. Shaded areas are 95% prediction bounds. Dotted lines are 95% confidence bounds.

Adding longitudinal rotation to the thigh CM led to a decrease in shank interface pressures. The behaviour across stiffness configurations appeared similar, with the primary differences in shank interface pressures arising from the initial pressure.

5.2.2 Longitudinal Translational

The relative displacements of the brace and limb segments are shown in Figure 5.22 while the pressures at the thigh and shank interfaces are shown in Figure 5.23 and Figure 5.24 respectively.

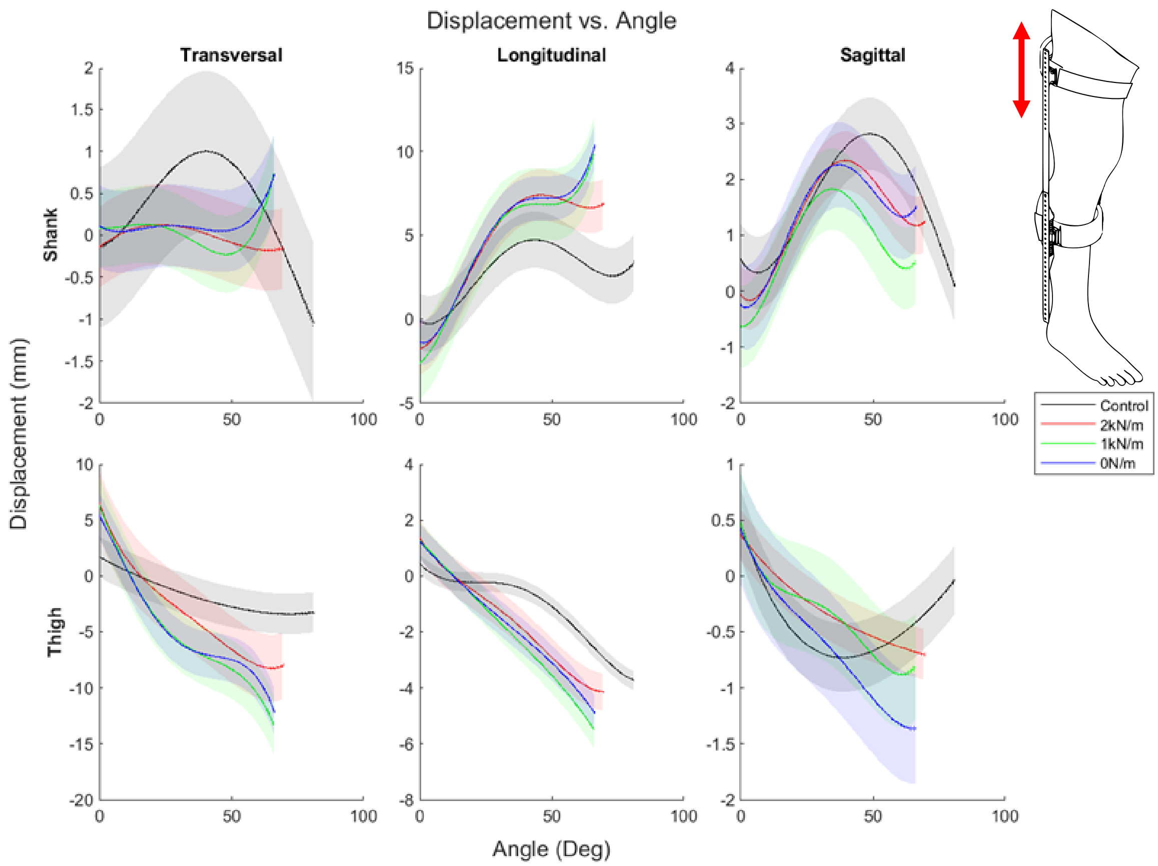

Figure 5.22: Relative displacement of the limb segments and brace with longitudinal translation at the thigh interface permitted. Shaded areas are 95% prediction bounds. Dotted lines are 95% confidence bounds

Adding longitudinal translation to the thigh CM led to increased longitudinal translation at the thigh interface and increased transversal translation of the thigh interface. The transversal translation at the thigh interface was not expected. Shank longitudinal translation increased as well.

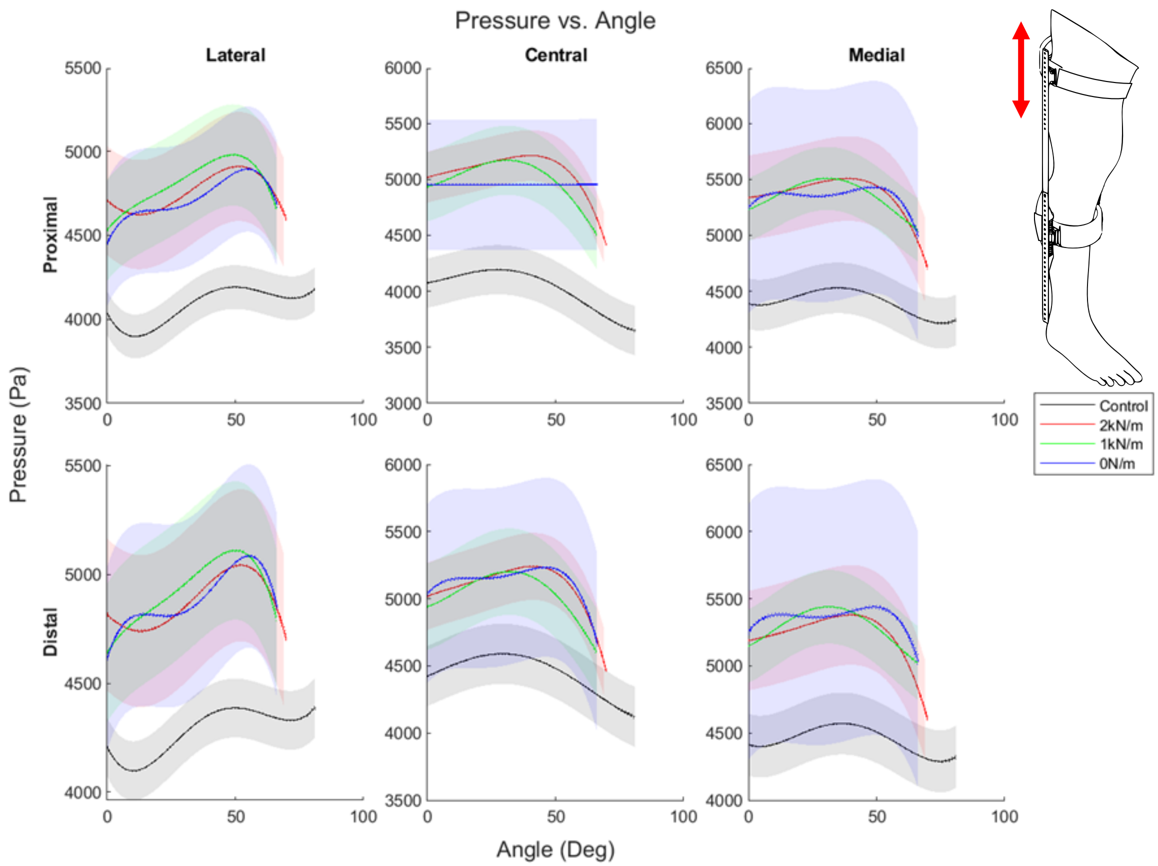

Figure 5.23: Fitted curves for thigh pressures with longitudinal translation permitted at the thigh. Shaded areas are 95% prediction bounds. Dotted lines are 95% confidence bounds.

Adding longitudinal translation to the thigh CM led to increased thigh interface pressures. The increase was similar regardless of the stiffness conditions, suggesting that longitudinal translation should not be added to the thigh CM of an exoskeleton.

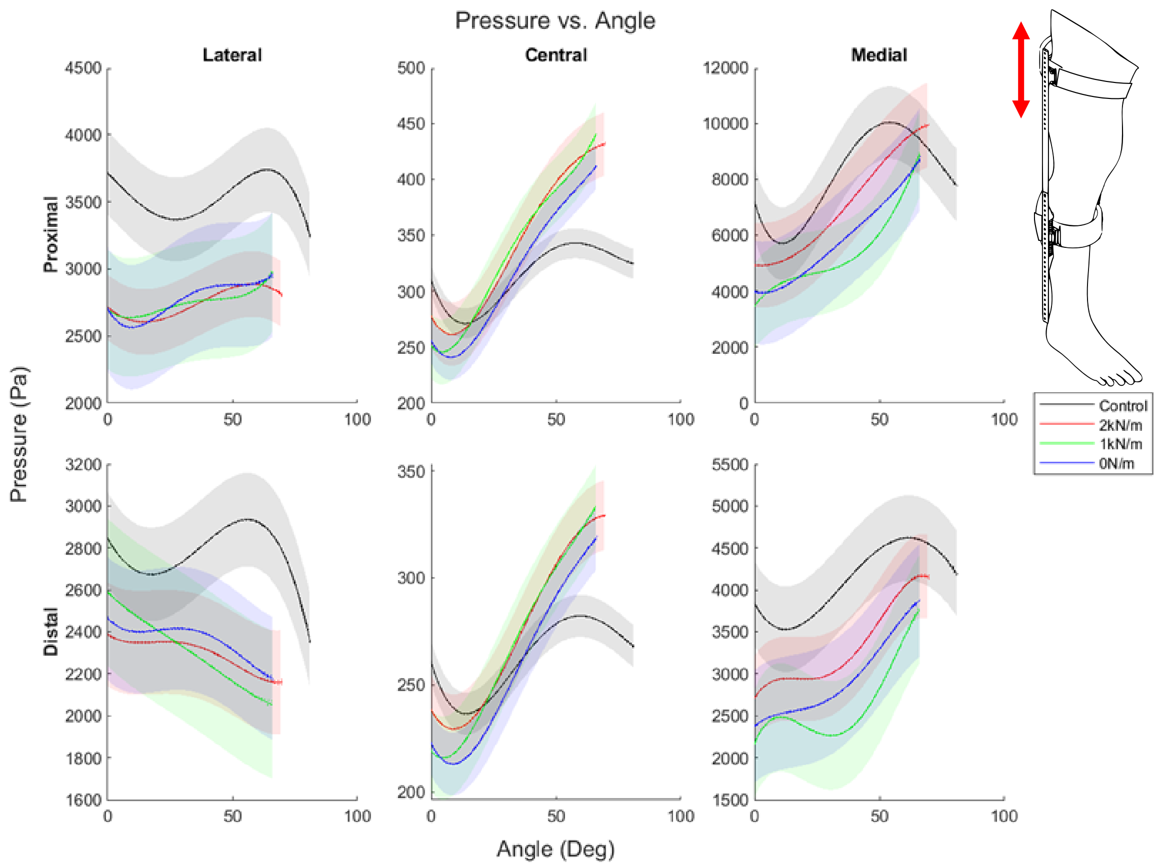

Figure 5.24: Fitted curves for shank pressures with longitudinal translation permitted at the thigh. Shaded areas are 95% prediction bounds. Dotted lines are 95% confidence bounds.

Adding longitudinal translation to the thigh CM led to a decrease in shank interface pressures in the medial and lateral zones. The central zones had lower initial pressures; however, they exceeded the control pressures above roughly 30 degrees. All stiffness conditions behaved similarly.

5.2.3 Sagittal Rotational

The relative displacements of the brace and limb segments are shown in Figure 5.25 while the pressures at the thigh and shank interfaces are shown in Figure 5.26 and Figure 5.27 respectively.

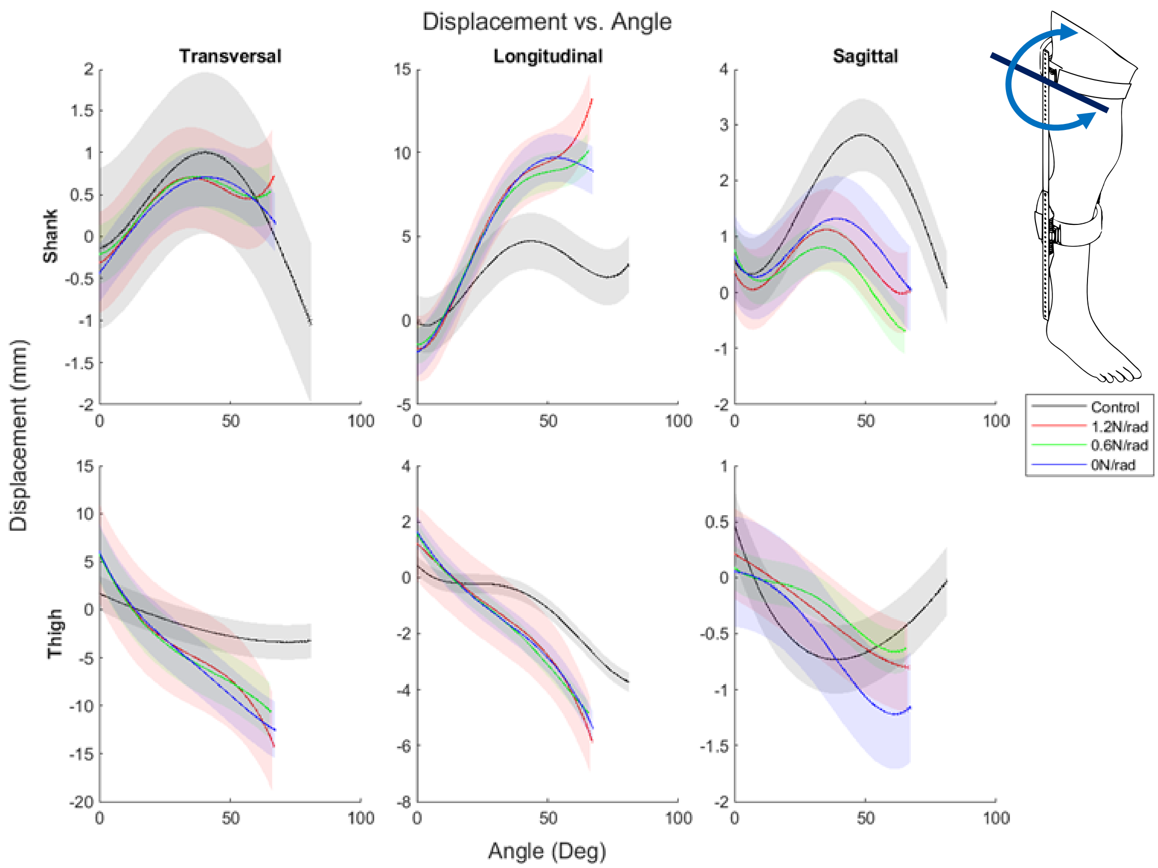

Figure 5.25: Relative displacement of the limb segments and brace with sagittal rotation at the thigh interface permitted. Shaded areas are 95% prediction bounds. Dotted lines are 95% confidence bounds.

Adding sagittal rotation to the thigh CM led to increased longitudinal and transverse translation at the thigh, which was expected. Conversely, shank longitudinal translation increased.

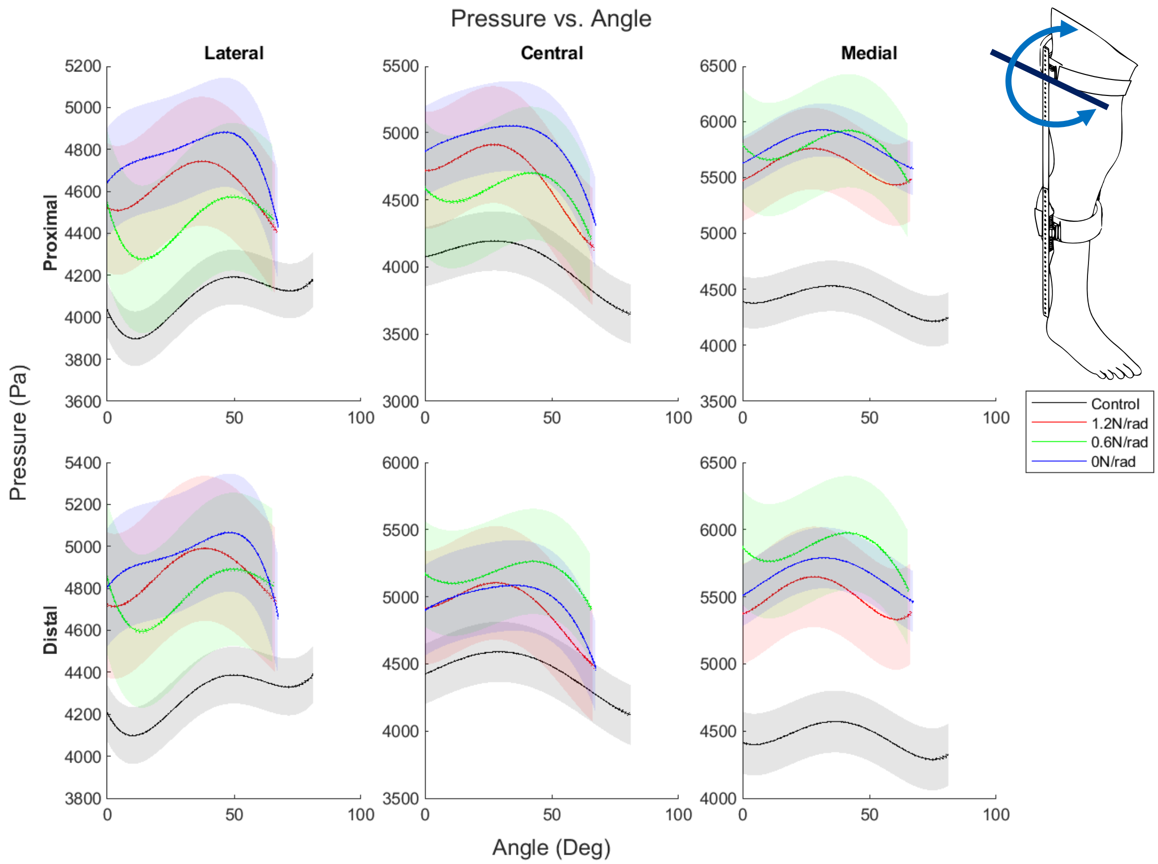

Figure 5.26: Fitted curves for thigh pressures with sagittal rotation permitted at the thigh. Shaded areas are 95% prediction bounds. Dotted lines are 95% confidence bounds.

Adding sagittal rotation to the thigh CM led to an increase in thigh interface pressures. Similar increases and behaviour occurred across the stiffness configurations. These results do not support the addition of sagittal rotation to exoskeleton thigh CMs.

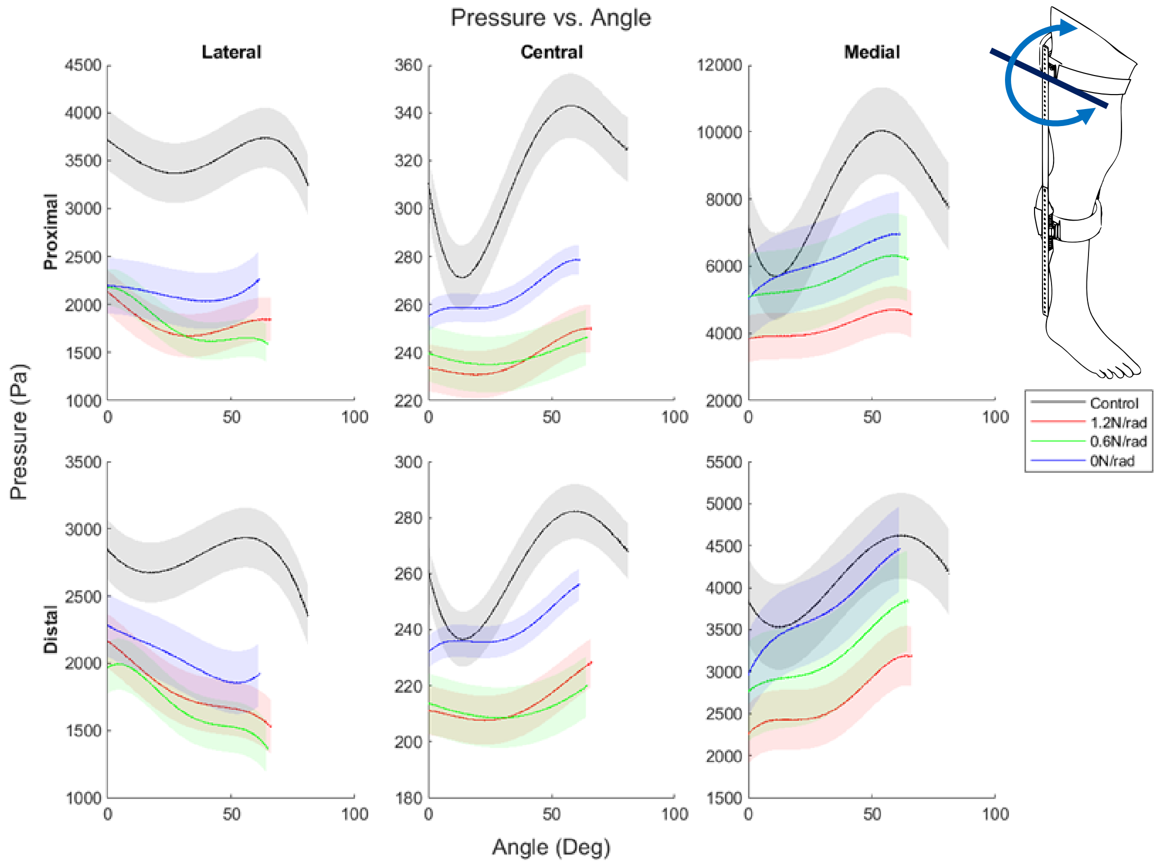

Figure 5.27: Fitted curves for shank pressures with sagittal rotation permitted at the thigh. Shaded areas are 95% prediction bounds. Dotted lines are 95% confidence bounds.

Adding sagittal rotation to the thigh CM led to reduced shank interface pressures. Regardless of the stiffness configuration, the reduction and behaviour were similar. The prediction bounds indicate the change is consistent. The consistency could be explained by the variability introduced by a added DOF acting at the thigh, the distance of the shank from the added DOF reduces the variability.

5.2.4 Sagittal Translational

The relative displacements of the brace and limb segments are shown in Figure 5.28 while the pressures at the thigh and shank interfaces are shown in Figure 5.29 and Figure 5.30 respectively.

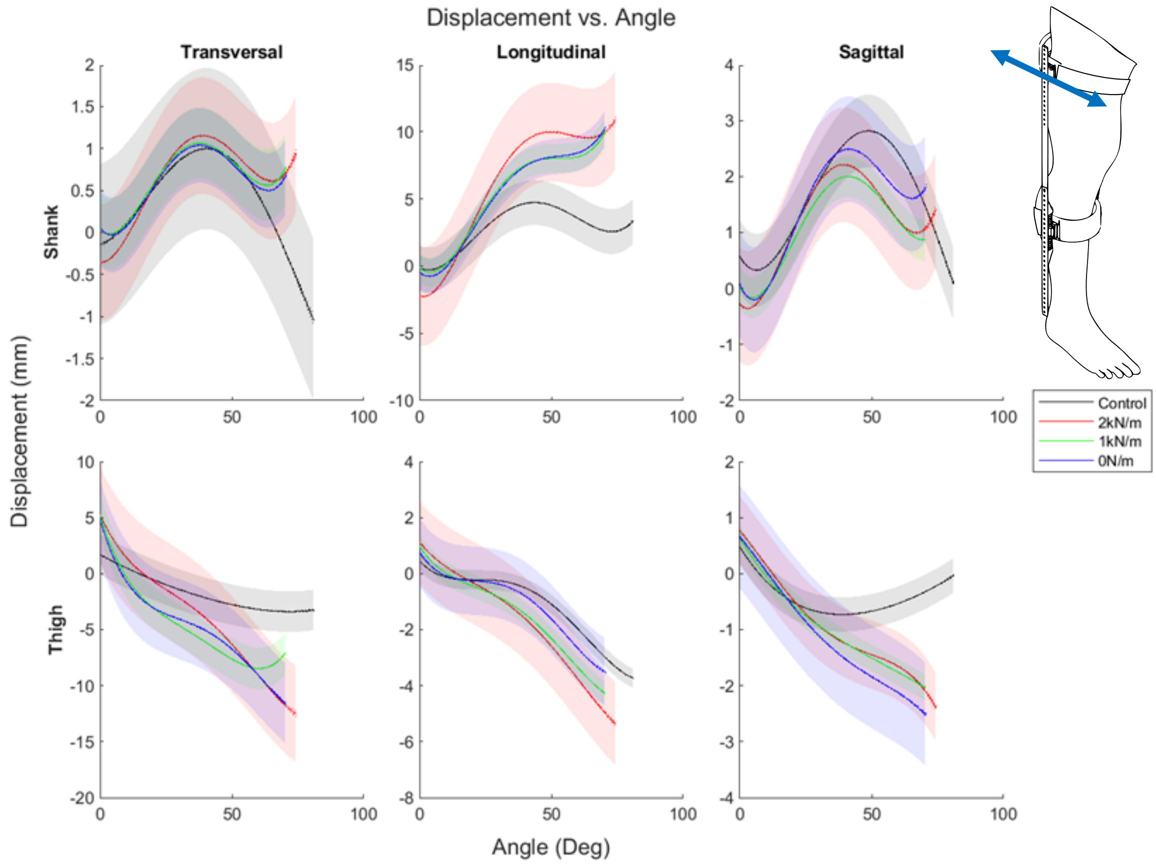

Figure 5.28: Relative displacement of the limb segments and brace with sagittal translation at the thigh interface permitted. Shaded areas are 95% prediction bounds. Dotted lines are 95% confidence bounds.

Adding sagittal translation to the thigh CM led to the expected increase in thigh sagittal translation, however this was accompanied by unexpected translation in the transverse axis as well. While shank sagittal translation did not change, longitudinal translation increased unexpectedly.

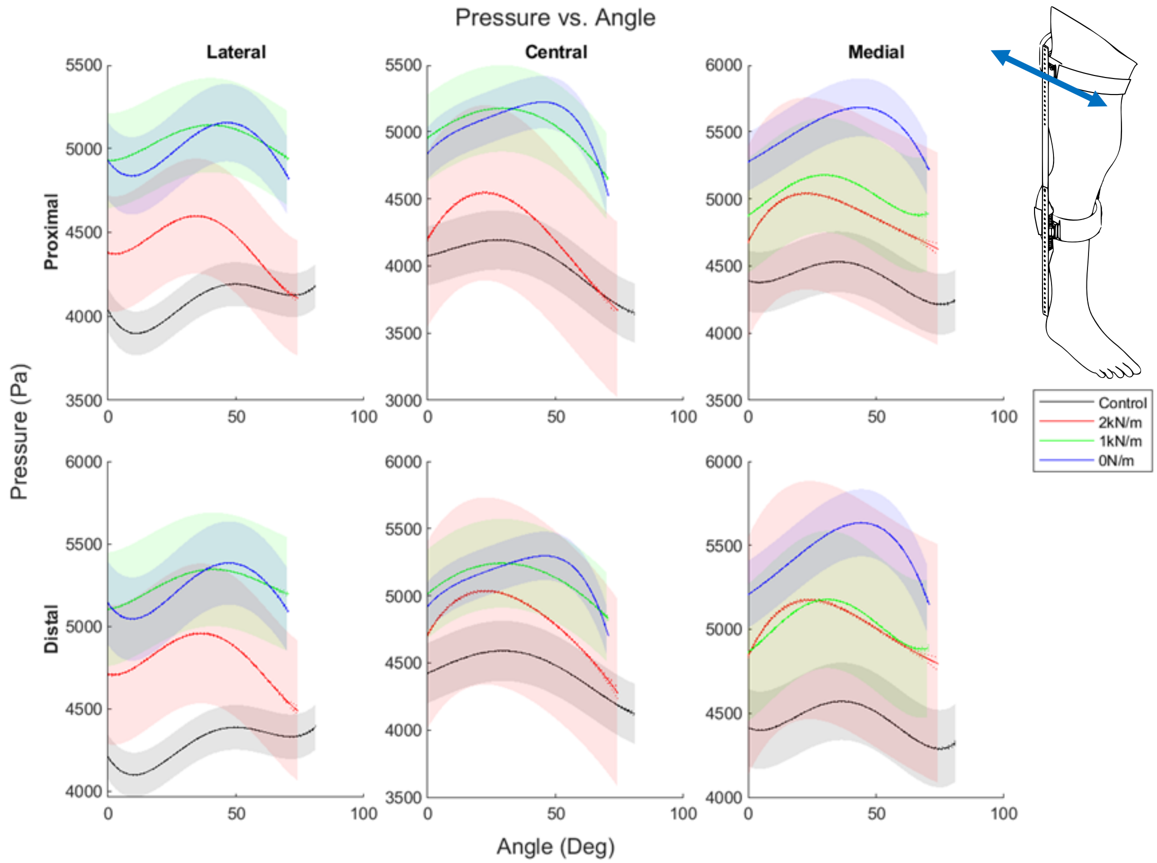

Figure 5.29: Fitted curves for thigh pressures with sagittal translation permitted at the thigh. Shaded areas are 95% prediction bounds. Dotted lines are 95% confidence bounds.

Adding sagittal translation to the thigh CM led to an increase in thigh interface pressures. The higher stiffness conditions had the smallest increase in interface pressures, suggesting that sagittal translation should not be added to exoskeleton thigh CMs.

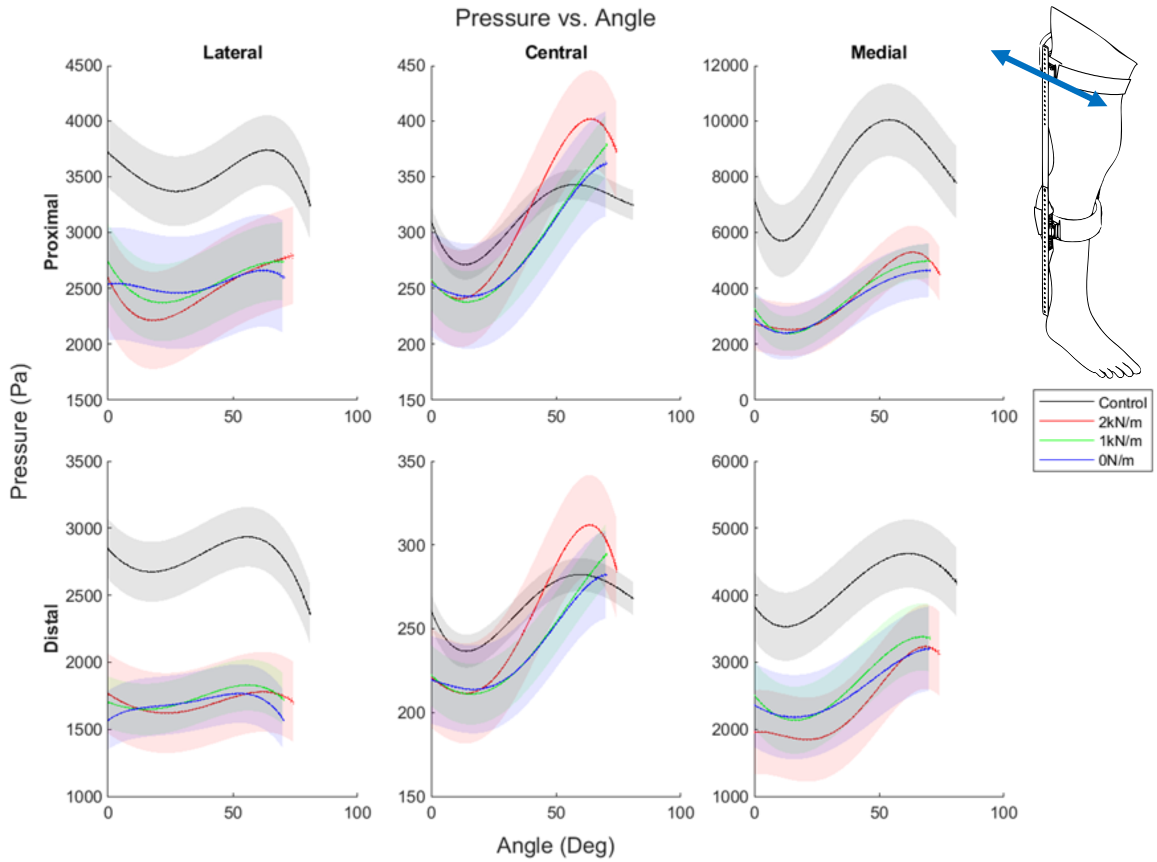

Figure 5.30: Fitted curves for shank pressures with sagittal translation permitted at the thigh. Shaded areas are 95% prediction bounds. Dotted lines are 95% confidence bounds.

Adding sagittal translation to the thigh CM led to a reduction in shank interface pressures. Similar reductions in pressure and behaviour were observed across the stiffness conditions. In the central zones, the control trial outperformed the trials with the added DOF above 50 degrees of flexion.

5.2.5 Transverse Rotational

The relative displacements of the brace and limb segments are shown in Figure 5.31 while the pressures at the thigh and shank interfaces are shown in Figure 5.32 and Figure 5.33 respectively.

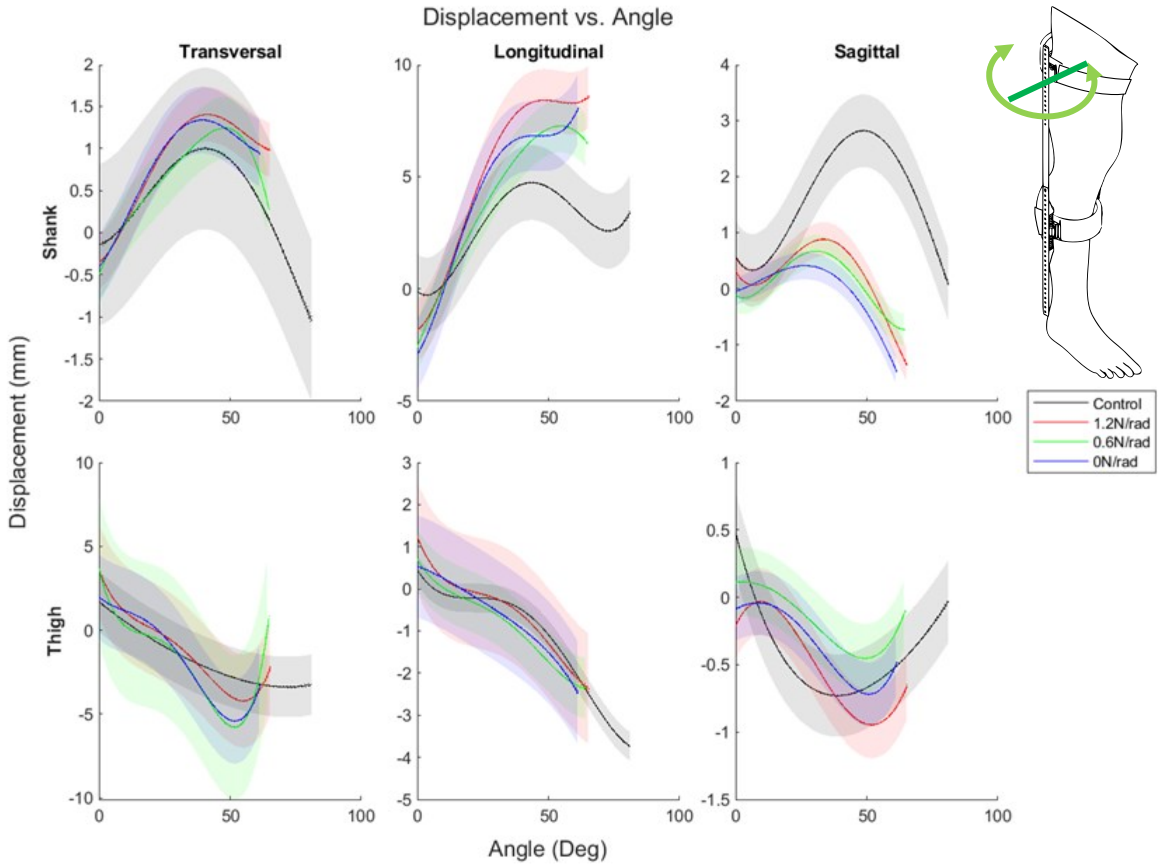

Figure 5.31: Relative displacement of the limb segments and brace with transverse rotation at the thigh interface permitted. Shaded areas are 95% prediction bounds. Dotted lines are 95% confidence bounds.

Adding transverse rotation to the thigh CM led to an unexpected increase in transverse translation at the thigh, while the expected changes of increased longitudinal and sagittal translation did not occur. This suggests that CM did not function as intended. At the shank interface, longitudinal translation increased while sagittal translation decreased.

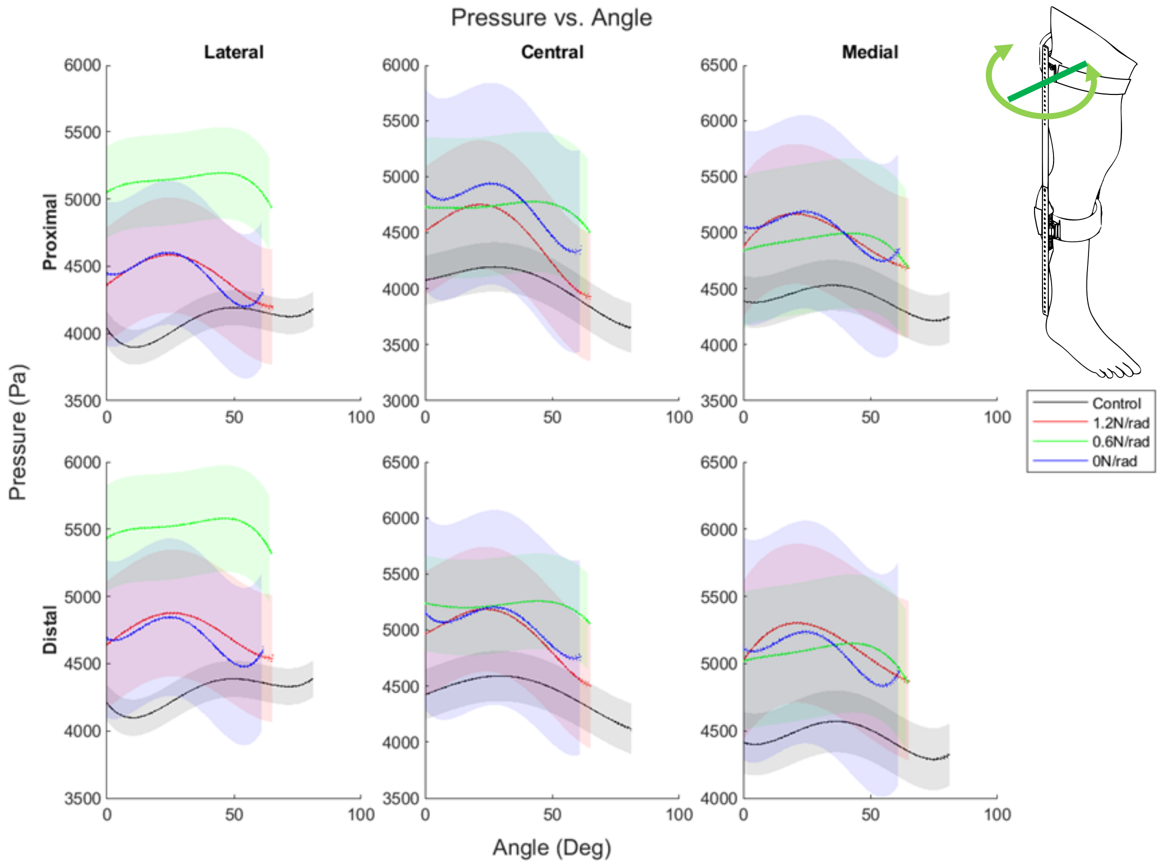

Figure 5.32: Fitted curves for thigh pressures with transverse rotation permitted at the thigh. Shaded areas are 95% prediction bounds. Dotted lines are 95% confidence bounds.

Adding transverse rotation to the thigh CM led to increased pressures at the thigh interface. While the amount of pressure increase was not consistent across the stiffness conditions, the results do not support the addition of transverse rotation to the thigh CM of an exoskeleton.

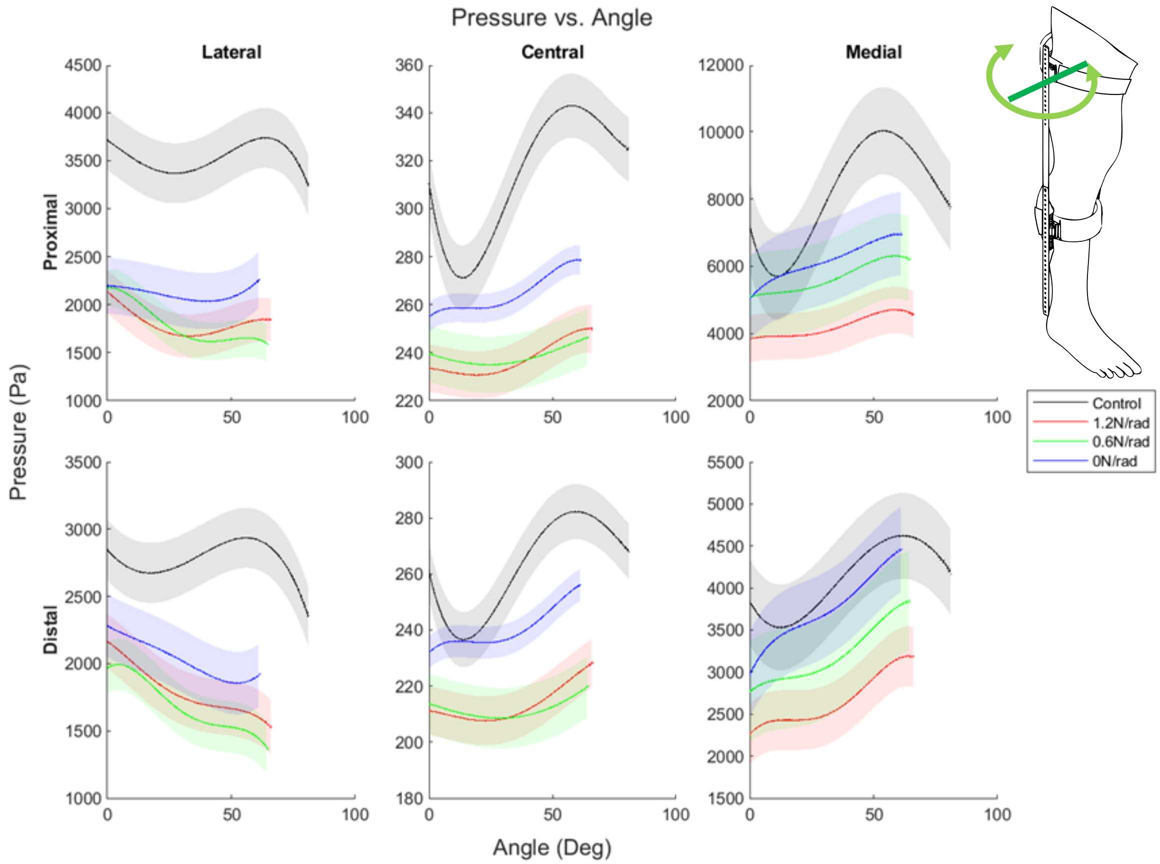

Figure 5.33: Fitted curves for shank pressures with transverse rotation permitted at the thigh. Shaded areas are 95% prediction bounds. Dotted lines are 95% confidence bounds.

Adding transverse rotation to the thigh CM led to a reduction in shank interface pressures. Counter to expectations, the no-stiffness condition had the highest interface pressures, however it was still below the control. The stiffest condition resulted in the largest reduction in interface pressures.

5.2.6 Transverse Translational

The relative displacements of the brace and limb segments are shown in Figure 5.34 while the pressures at the thigh and shank interfaces are shown in Figure 5.35 and Figure 5.36 respectively.

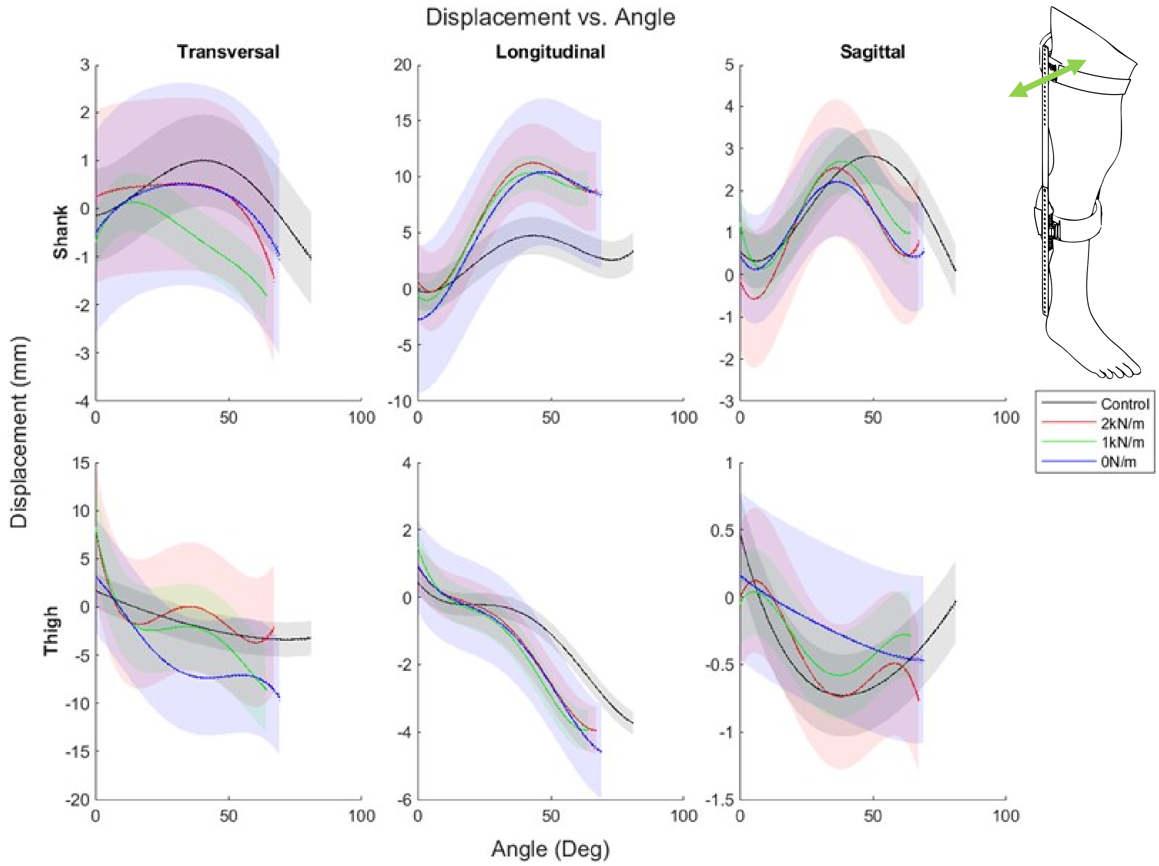

Figure 5.34: Relative displacement of the limb segments and brace with transverse translation at the thigh interface permitted. Shaded areas are 95% prediction bounds. Dotted lines are 95% confidence bounds.

Adding transverse translation to the thigh CM led to increased transverse translation at the thigh as expected, with more translation occurring with lower CM stiffness. Shank and thigh longitudinal translation increased unexpectedly.

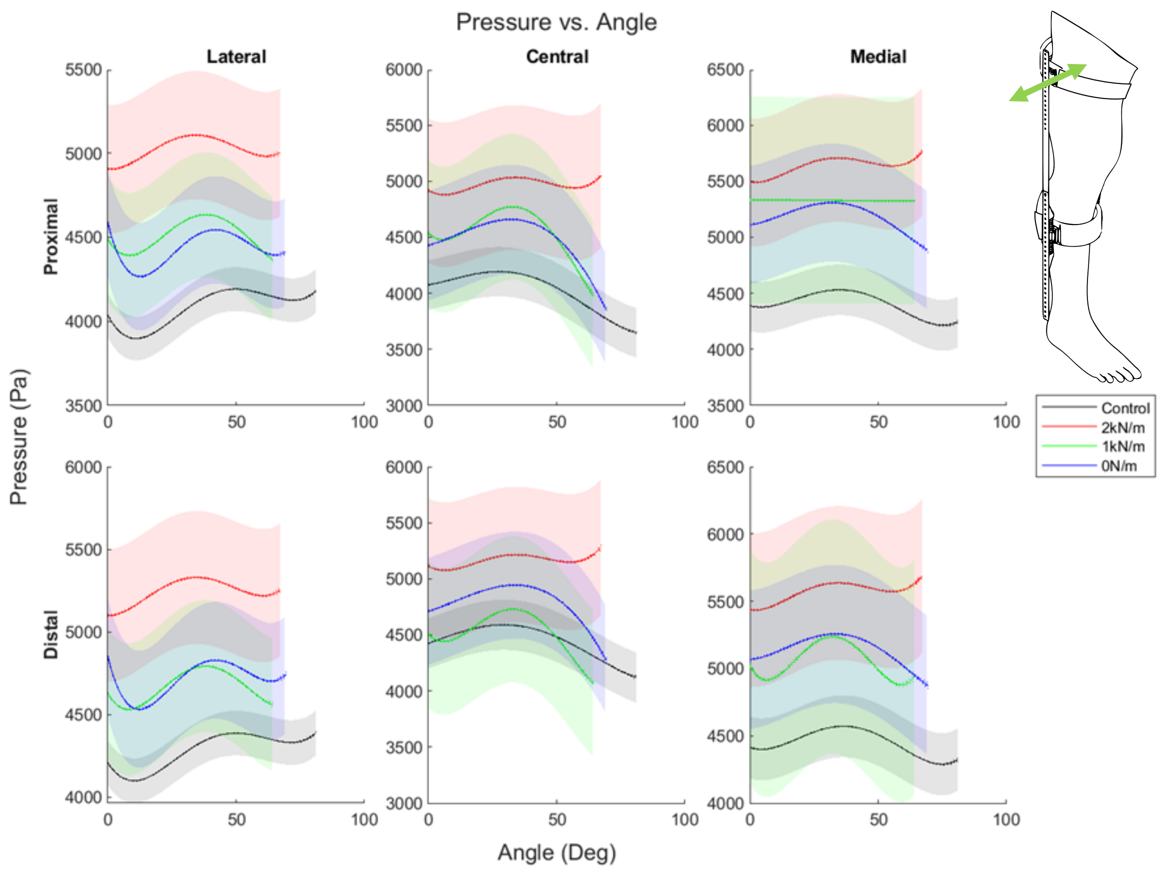

Figure 5.35: Fitted curves for thigh pressures with transverse translation permitted at the thigh. Shaded areas are 95% prediction bounds. Dotted lines are 95% confidence bounds.

Adding transverse translation to the thigh CM led to increased thigh interface pressures. The two lower stiffness conditions resulted in similar pressure increases, however, the increase was smaller than that caused by the stiffest condition, which is unexpected.

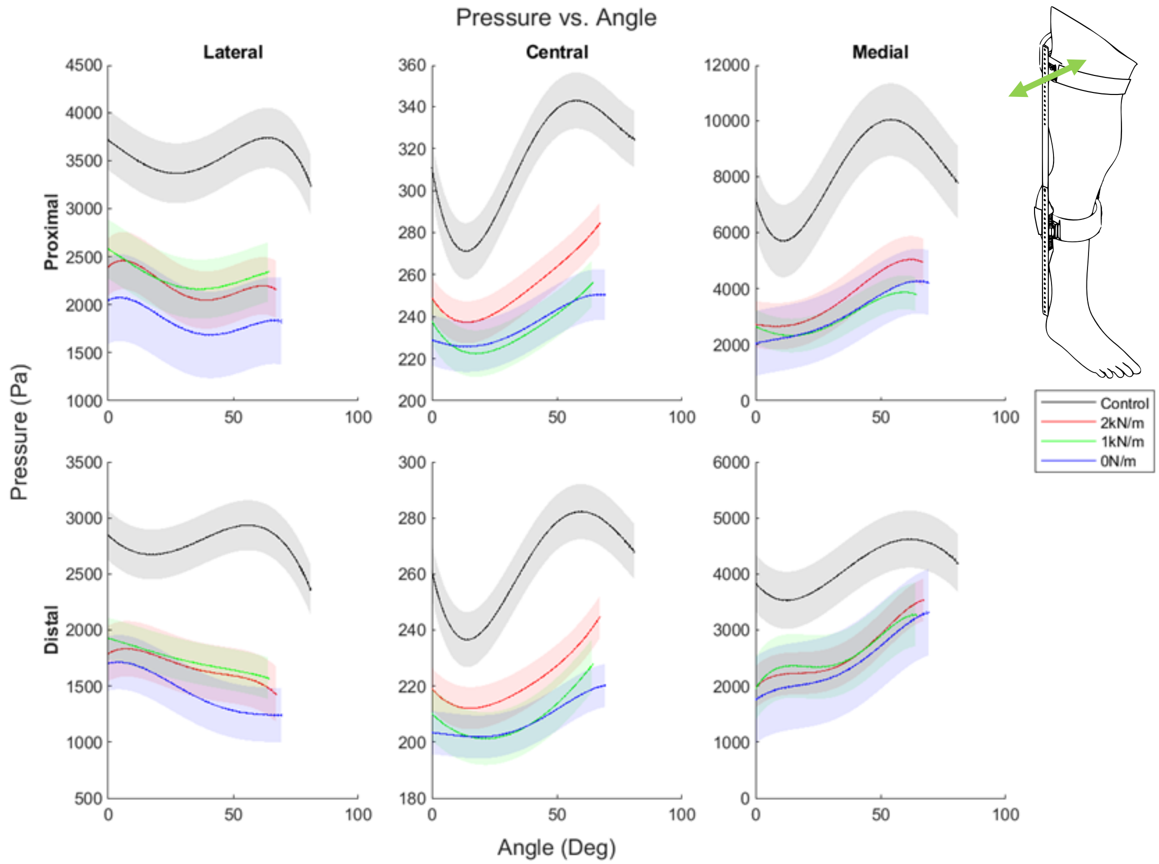

Figure 5.36: Fitted curves for shank pressures with transverse translation permitted at the thigh. Shaded areas are 95% prediction bounds. Dotted lines are 95% confidence bounds.

Adding transverse translation to the thigh CM led to reduced shank interface pressures. The three stiffness conditions had similar behaviours and pressure reductions.

5.3 Comfort Scores

The comfort scores reported by the participant are presented below in Table 5-2. Due to the limited sample size no meaningful statistical evaluations can be performed.

Table 5-2: Reported VAS scores of each CM configuration.

	VAS Scores
Control Thigh	8
Control Shank	3.2
Axial Translation 1kN/m Thigh	6
Axial Translation 1kN/m Shank	5.3
Axial Translation 0N/m Thigh	3.4

Axial Translation 0N/m Shank	3.7
Sagittal Translation 1kN/m Thigh	6.1
Sagittal Translation 1kN/m Shank	7.3
Sagittal Translation 0N/m Thigh	6.8
Sagittal Translation 0N/m Shank	6.7

5.4 Discussion

This section provides a comprehensive discussion of the results. First, the conclusions drawn from the jig trials are presented, followed by the conclusions of the human trials, including an assessment of the predictive power of the jig for the human trials. Finally, the limitations of the research and sources of error are discussed.

5.4.1 Jig Results

Adding passive DOFs to the shank CM generally led to an increase in both shank and thigh translation. Adding passive DOFs to the thigh CM generally led to an increase in thigh longitudinal and transversal translation and shank longitudinal translation

Adding a passive DOF generally led to a reduction in shank interface pressures. The stiffness of the passive DOF had an inconsistent effect; for some configurations the stiffest configuration had the largest pressure reduction while for others the no stiffness configuration had the largest pressure reduction. The results were inconsistent across the pressure zones as well. This suggests the addition of the passive DOF is sufficient to reduce interface pressures and that the stiffnesses selected were too similar for a consistent difference in effect to be detected. Most of the pressure reduction at the shank interface appears to be a result of the reduced initial pressure, as the pressure curves have similar shapes. The added passive DOF appeared to allow better passive alignment, but they did not change the overall shape of the pressure curves. The better passive alignment could be used to reduce the impact of misalignment occurring during donning of the exoskeleton.

Adding a passive DOF generally led to an increase in thigh interface pressures. Similar to the shank, the stiffness of the passive DOF had an inconsistent effect. The initial thigh pressures were consistently higher than the control, contrary to the behaviour found at the shank interface. While increasing interface pressures is generally undesirable, due to the increased PDT of the thigh relative to the shank, it could be preferable to shift the interface pressures to the thigh by adding a passive degree of freedom.

As shown by the prediction bounds, most added DOFs result in increased variability in relative displacement and interface pressures. This is likely due to the passive DOF creating more kinematic “solutions” when rotating the knee, resulting in more variability between trials. More variability for the interface pressures and relative displacement was observed when the passive DOF was at the shank, suggesting that passive DOFs have a larger effect at the shank. Generally, the stiffer configurations had less variability, however this was not always the case.

5.4.2 Human Results

For the human trials, adding either longitudinal or sagittal translation to the shank CM resulted in increased translation at the shank interface and decreased translation at the thigh interface. The added passive DOF decreased shank interface pressures by similar amounts regardless of the CM stiffness, the zero stiffness trials did have slightly lower pressures overall. In general, this was also associated with reduced shank interface pressures, however, the effect on comfort could not be verified with the limited participant pool. These results support the hypothesis that adding passive DOF to the CM can reduce interface pressures, however whether that improves user comfort is not known.

The human trials had much larger relative translations that did not behave like the jig trials. This suggests that the jig has limited predictive power for human trials. This could be a result of the jig simplifying the leg too much or due to the knee the jig joint was modelled after having different kinematics than the participant’s knee. Similarly, the jig had limited predictive power for the shank interface pressures as well. While the jig did predict the reduction in interface pressure, it was unable to predict the pressure curve in relation to the joint angle. This is likely due to a combination of the jig joint not reflecting the participant’s joint and the compliance and shape of the jig shank and thigh segments. Work by Postolka et al. found that knee joint kinematics varies significantly between individuals[43], suggesting that the jig joint should have been modelled after the participant’s individual knee kinematics. Compared to the jig trials, the variability of the human trials was relatively consistent between the control trial and the trials with the passive DOF.

5.4.3 Limitations and Sources of Error

The sensors used to measure the pressure have numerous issues that limit the reliability of the pressure results obtained. The Velostat used to form the pressure sensor matrix has poor time response and hysteresis characteristics[44], resulting in it being unable to measure large sudden changes in pressure. Since the pressures were not expected to greatly change over the duration of each trial, the effect of the poor hysteresis and time response was considered negligible. While the non-linearity of the sensor could be accommodated through calibration curves, properly calibrating the response curves was difficult due to the low forces applied and the shape of the sensor. As such the pressure values found in this research should only be used to compare pressures within the same pressure zones of the same sensor and not as an absolute measure of the interface pressure. While the sensor matrix did address some of the short comings of force sensitive resistors expressed in previous work by Levesque[45], further work is necessary to find reliable methods of measuring interface pressures.

The jig used as a leg phantom had limited predictive capabilities for the human trials. There are numerous factors that could be improved or altered to better reflect human kinetics and tissue behaviour. The jig knee joint may not reflect the kinematics of the participant's knee, should the jig be used in further research, multiple knee joint mechanisms based on different knee anatomies should be tested. Furthermore, the soft tissue analogues of the thigh and shank could easily be refined by improving the geometry to better mimic a human leg. Replicating the stiffness of a human leg would be more difficult as it varies based on location and muscle flexion.

Two effects likely resulted in exaggerated relative motion recorded in the human trials. The markers were placed on bony prominences; however, some skin motion is inevitable, some of which can be compensated for by comparing to the control, but some inconsistency remains. Additionally, the exoskeleton was likely not in the same position between human trials as some sliding is inevitable during use, compared to the jig trials where the position of the cuffs could easily be verified.

Chapter 6 Conclusion

A leg phantom and testing jig were developed as well as an exoskeleton with modular connection mechanisms. Sensors for measuring the shank and thigh interface pressures between a limb and the exoskeleton were designed and built. Motion capture equipment was used to measure relative motion between the exoskeleton and limb segments. Jig and human trials measured the kinematic and interface pressure of added passive DOFs to the CMs of the shank and thigh. The results were analyzed to determine if the added passive DOFs altered the kinematics to improve user comfort or analogues for user comfort. Additionally, the results were used to determine if the jig developed was able to predict the results from the human trials.

For the jig trials, added passive DOFs to the shank tended to increase both thigh and shank relative motion, while for the human trials it decreased thigh relative motion. Similarly, added DOFs to the thigh increased relative motion at both interfaces in the jig trials.

For the jig trials, regardless of the passive DOF added or its location, shank pressures tended to decrease while the thigh pressures tended to increase. Similarly, for the human trials shank pressures tended to decrease. The effect of the stiffness of the added passive DOF was inconsistent for the jig trials while for the human trials the pressure reduction was similar regardless of the stiffness. These results suggest that added passive DOF do reduce shank interface pressures and that the stiffness of the passive DOF does not have an effect provided it is in the range of 0-2kN/m or 0-1.2N/rad.

More work is necessary to build a leg phantom capable of predicting human-exoskeleton interaction behaviour. More knee joint analogue mechanisms can be created easily with 3D printing and used in testing for a wider range of limb kinematic behaviour. The soft tissues of the limb could be better approximated in both geometry and in material properties. Measuring interface pressures has shown to be difficult in both this work and in previous work, further development of sensors is necessary. Sensors capable of measuring shearing at the exoskeleton-limb interface need to be developed and used to evaluate the effect of shear on comfort, as the effect of shear on comfort is relatively unexplored in the literature. The human trial results for longitudinal and sagittal translation at the shank show some promise of reducing interface pressures however further testing is necessary to both verify the reduction in interface pressures and to confirm it results in a subjective improvement in user comfort.

References

[1] S. Musich, S. S. Wang, J. Ruiz, K. Hawkins, and E. Wicker, “The impact of mobility limitations on health outcomes among older adults,” *Geriatr. Nur. (Lond.)*, vol. 39, no. 2, pp. 162–169, Mar. 2018, doi: 10.1016/j.gerinurse.2017.08.002.

[2] “Exploring the Health of Women with Mobility Impairments,” *Women Health*, Accessed: Apr. 24, 2024. [Online]. Available: https://www.tandfonline.com/doi/abs/10.1080/03630240802131981

[3] “Disparities in mental health, social support and coping among individuals with mobility impairment,” *Disabil. Health J.*, vol. 14, no. 2, p. 101047, Apr. 2021, doi: 10.1016/j.dhjo.2020.101047.

[4] E. Swinnen and E. Kerckhofs, “Compliance of patients wearing an orthotic device or orthopedic shoes: A systematic review,” *J. Bodyw. Mov. Ther.*, vol. 19, no. 4, pp. 759–770, Oct. 2015, doi: 10.1016/j.jbmt.2015.06.008.

[5] S. A. Elprama, S. D. Bock, R. Meeusen, K. D. Pauw, B. Vanderborght, and A. Jacobs, “Design and Implementation Requirements for Increased Acceptance of Occupational Exoskeletons in an Industrial Context: A Qualitative Study,” *Int. J. Human–Computer Interact.*, vol. 0, no. 0, pp. 1–16, 2023, doi: 10.1080/10447318.2023.2247597.

[6] W. B. Mortenson, A. Pysklywec, L. Chau, M. Prescott, and A. Townson, “Therapists’ experience of training and implementing an exoskeleton in a rehabilitation centre,” *Disabil. Rehabil.*, vol. 44, no. 7, pp. 1060–1066, Mar. 2022, doi: 10.1080/09638288.2020.1789765.

[7] B. S. Rupal, S. Rafique, A. Singla, E. Singla, M. Isaksson, and G. S. Virk, “Lower-limb exoskeletons: Research trends and regulatory guidelines in medical and non-medical applications,” *Int. J. Adv. Robot. Syst.*, vol. 14, no. 6, p. 1729881417743554, Nov. 2017, doi: 10.1177/1729881417743554.

[8] I. Tijjani, S. Kumar, and M. Boukheddimi, “A Survey on Design and Control of Lower Extremity Exoskeletons for Bipedal Walking,” *Appl. Sci.-BASEL*, vol. 12, no. 5, Mar. 2022, doi: 10.3390/app12052395.

[9] J. Wolff, C. Parker, J. Borisoff, W. B. Mortenson, and J. Mattie, “A survey of stakeholder perspectives on exoskeleton technology,” *J. NeuroEngineering Rehabil.*, vol. 11, no. 1, p. 169, Dec. 2014, doi: 10.1186/1743-0003-11-169.

[10] N. Jarrassé and G. Morel, “A formal method for avoiding hyperstaticity when connecting an exoskeleton to a human member,” in *2010 IEEE International Conference on Robotics and Automation*, May 2010, pp. 1188–1195. doi: 10.1109/ROBOT.2010.5509346.

[11] M. Shafiei and S. Behzadipour, “Adding backlash to the connection elements can improve the performance of a robotic exoskeleton,” *Mech. Mach. Theory*, vol. 152, p. 103937, Oct. 2020, doi: 10.1016/j.mechmachtheory.2020.103937.

[12] M. Shafiei and S. Behzadipour, “The Effects of the Connection Stiffness of Robotic Exoskeletons on the Gait Quality and Comfort,” *J. Mech. Robot.-Trans. ASME*, vol. 12, no. 1, Feb. 2020, doi: 10.1115/1.4044841.

[13] K. Mannion, É. Séguin, and M. Doumit, “A Review of Knee Exoskeleton Design Aspects for Improving User Comfort,” in *2024 IEEE 4th International Conference on Human-Machine Systems (ICHMS)*, May 2024, pp. 1–7. doi: 10.1109/ICHMS59971.2024.10555841.

[14] P. J. Rowe, C. M. Myles, C. Walker, and R. Nutton, “Knee joint kinematics in gait and other functional activities measured using flexible electrogoniometry: how much knee

motion is sufficient for normal daily life?," *Gait Posture*, vol. 12, no. 2, pp. 143–155, Oct. 2000, doi: 10.1016/S0966-6362(00)00060-6.

[15] P. K. Levangie and C. C. Norkin, *Joint Structure and Function A Comprehensive Analysis: A Comprehensive Analysis*. Philadelphia, UNITED STATES: F. A. Davis Company, 2011. Accessed: May 24, 2023. [Online]. Available: http://ebookcentral.proquest.com/lib/ottawa/detail.action?docID=2038737

[16] J. Goodfellow and J. O'Connor, "The mechanics of the knee and prosthesis design," *J. Bone Joint Surg. Br.*, vol. 60-B, no. 3, pp. 358–369, Aug. 1978, doi: https://doi.org/10.1302/0301-620X.60B3.581081.

[17] H. Iwaki, V. Pinskerova, and M. a. R. Freeman, "Tibiofemoral movement 1: the shapes and relative movements of the femur and tibia in the unloaded cadaver knee," *J. Bone Joint Surg. Br.*, vol. 82-B, no. 8, pp. 1189–1195, Nov. 2000, doi: 10.1302/0301-620X.82B8.0821189.

[18] M. A. R. Freeman and V. Pinskerova, "The movement of the normal tibio-femoral joint," *J. Biomech.*, vol. 38, no. 2, pp. 197–208, Feb. 2005, doi: 10.1016/j.jbiomech.2004.02.006.

[19] S. Ashkenazy and F. DeKeyser Ganz, "The Differentiation Between Pain and Discomfort: A Concept Analysis of Discomfort," *Pain Manag. Nurs.*, vol. 20, no. 6, pp. 556–562, Dec. 2019, doi: 10.1016/j.pmn.2019.05.003.

[20] P. Kersten, A. A. Küçükdeveci, and A. Tennant, "The use of the Visual Analogue Scale (VAS) in rehabilitation outcomes," *J. Rehabil. Med.*, vol. 44, no. 7, pp. 609–610, Jun. 2012, doi: 10.2340/16501977-0999.

[21] J. Tamez-Duque, R. Cobian-Ugalde, A. Kilicarslan, A. Venkatakrishnan, R. Soto, and J. L. Contreras-Vidal, "Real-Time Strap Pressure Sensor System for Powered Exoskeletons," *Sensors*, vol. 15, no. 2, pp. 4550–4563, Feb. 2015, doi: 10.3390/s150204550.

[22] S. Massardi, D. Rodriguez-Cianca, D. Pinto-Fernandez, J. C. Moreno, M. Lancini, and D. Torricelli, "Characterization and Evaluation of Human–Exoskeleton Interaction Dynamics: A Review," *Sensors*, vol. 22, no. 11, Art. no. 11, Jan. 2022, doi: 10.3390/s22113993.

[23] T. W. Weerasinghe, R. S. Goonetilleke, and U. Reischl, "Pressure thresholds and stiffness on the plantar surface of the human foot | Scholars Portal Journals," vol. 60, no. 7, Jul. 2017, doi: 10.1080/00140139.2016.1229042.

[24] T. Kermavnar, K. J. O'Sullivan, V. Casey, A. De Eyto, and L. O'Sullivan, "Circumferential tissue compression at the lower limb during walking, and its effect on discomfort, pain and tissue oxygenation: Application to soft exoskeleton design," *Appl. Ergon.*, vol. 86, p. 103093, Jul. 2020, doi: 10.1016/j.apergo.2020.103093.

[25] R. S. Goonetilleke and T. J. Eng, "Contact Area Effects on Discomfort," *Proc. Hum. Factors Ergon. Soc. Annu. Meet.*, vol. 38, no. 10, pp. 688–690, Oct. 1994, doi: 10.1177/154193129403801032.

[26] A. A. Manorama, S. Baek, J. Vorro, A. Sikorskii, and T. R. Bush, "Blood perfusion and transcutaneous oxygen level characterizations in human skin with changes in normal and shear loads — Implications for pressure ulcer formation," *Clin. Biomech.*, vol. 25, no. 8, pp. 823–828, Oct. 2010, doi: 10.1016/j.clinbiomech.2010.06.003.

[27] X. Wan, Y. Liu, Y. Akiyama, and Y. Yamada, "Monitoring Contact Behavior during Assisted Walking with a Lower Limb Exoskeleton," *IEEE Trans. Neural Syst. Rehabil. Eng.*, vol. 28, no. 4, pp. 869–877, 2020, doi: 10.1109/TNSRE.2020.2979986.

[28] X. Mao, Y. Yamada, Y. Akiyama, S. Okamoto, and K. Yoshida, “Safety verification method for preventing friction blisters during utilization of physical assistant robots,” *Adv. Robot.*, vol. 31, no. 13, pp. 680–694, Jul. 2017, doi: 10.1080/01691864.2017.1318716.
[29] Y. Akiyama, S. Okamoto, Y. Yamada, and K. Ishiguro, “Measurement of Contact Behavior Including Slippage of Cuff When Using Wearable Physical Assistant Robot,” *IEEE Trans. Neural Syst. Rehabil. Eng.*, vol. 24, no. 7, pp. 784–793, Jul. 2016, doi: 10.1109/TNSRE.2015.2464719.
[30] J. L. Pons, *Wearable Robots: Biomechatronic Exoskeletons*. New York, UNITED KINGDOM: John Wiley & Sons, Incorporated, 2008. Accessed: Jan. 17, 2023. [Online]. Available: http://ebookcentral.proquest.com/lib/ottawa/detail.action?docID=351664
[31] N. Jarrasse and G. Morel, “Connecting a Human Limb to an Exoskeleton,” *IEEE Trans. Robot.*, vol. 28, no. 3, pp. 697–709, Jun. 2012, doi: 10.1109/TRO.2011.2178151.
[32] S. M. F. Reimer, T. C. Lueth, and L. T. D’Angelo, “Individualized arm shells towards an ergonomic design of exoskeleton robots,” in *2014 IEEE International Conference on Systems, Man, and Cybernetics (SMC)*, Oct. 2014, pp. 3958–3965. doi: 10.1109/SMC.2014.6974550.
[33] L. Levesque and M. Doumit, “Study of human-machine physical interface for wearable mobility assist devices,” *Med. Eng. Phys.*, vol. 80, pp. 33–43, Jun. 2020, doi: 10.1016/j.medengphy.2020.03.008.
[34] L. Levesque, S. Pardoel, Z. Lovrenovic, and M. Doumit, “Experimental comfort assessment of an active exoskeleton interface,” in *2017 IEEE International Symposium on Robotics and Intelligent Sensors (IRIS)*, Oct. 2017, pp. 38–43. doi: 10.1109/IRIS.2017.8250095.
[35] Ž. Kozinc, J. Babič, and N. Šarabon, “Human pressure tolerance and effects of different padding materials with implications for development of exoskeletons and similar devices,” *Appl. Ergon.*, vol. 93, p. 103379, May 2021, doi: 10.1016/j.apergo.2021.103379.
[36] S. Patrick, N. Anil Kumar, and P. Hur, “Evaluating Knee Mechanisms for Assistive Devices,” *Front. Neurorobotics*, vol. 16, 2022, Accessed: Oct. 26, 2022. [Online]. Available: https://www.frontiersin.org/articles/10.3389/fnbot.2022.790070
[37] É. Séguin and M. Doumit, “Review and Assessment of Walking Assist Exoskeleton Knee Joints,” in *2020 IEEE International Conference on Systems, Man, and Cybernetics (SMC)*, Oct. 2020, pp. 1230–1235. doi: 10.1109/SMC42975.2020.9283152.
[38] S. Sarkisian, M. Ishmael, and T. Lenzi, “Self-Aligning Mechanism Improves Comfort and Performance With a Powered Knee Exoskeleton,” *IEEE Trans. NEURAL Syst. Rehabil. Eng.*, vol. 29, pp. 629–640, 2021, doi: 10.1109/TNSRE.2021.3064463.
[39] B. Lee, S. C. Lee, and C. Han, “Design of Fixations for an Exoskeleton Device with Joint Axis Misalignments,” *Int. J. Precis. Eng. Manuf.*, vol. 21, no. 7, pp. 1291–1298, Jul. 2020, doi: 10.1007/s12541-019-00311-w.
[40] Y. Zheng and A. F. T. Mak, “Effective elastic properties for lower limb soft tissues from manual indentation experiment,” *IEEE Trans. Rehabil. Eng.*, vol. 7, no. 3, pp. 257–267, Sep. 1999, doi: 10.1109/86.788463.
[41] “Volara Data Sheet | Foam Factory, Inc. - Canada.” Accessed: Mar. 06, 2024. [Online]. Available: https://canada.foambymail.com/volara-foam-sheet.html
[42] N. Sancisi, D. Zannoli, V. Parenti-Castelli, C. Belvedere, and A. Leardini, “A one-degree-of-freedom spherical mechanism for human knee joint modelling,” *Proc. Inst. Mech. Eng. [H]*, vol. 225, no. 8, pp. 725–735, Aug. 2011, doi: 10.1177/0954411911406951.

[43] B. Postolka *et al.*, “Tibio-femoral kinematics of the healthy knee joint throughout complete cycles of gait activities,” *J. Biomech.*, vol. 110, p. 109915, Sep. 2020, doi: 10.1016/j.jbiomech.2020.109915.
[44] A. Dzedzickis *et al.*, “Polyethylene-Carbon Composite (Velostat®) Based Tactile Sensor,” *Polymers*, vol. 12, no. 12, p. 2905, Dec. 2020, doi: 10.3390/polym12122905.
[45] L. D. B. Levesque, “Experimental Evaluation and Characterization of a Mobility Assist Device Physical Interface,” Université d’Ottawa / University of Ottawa, 2018. Accessed: Mar. 12, 2024. [Online]. Available: http://hdl.handle.net/10393/37365

Appendix A – MATLAB Code

Data Analysis and Processing

```
analyzeData("Jig Results",["Fixed-Fixed","LongitudinalRotational-Fixed_1.2Nprad","LongitudinalRotational-Fixed_0.6Nprad","LongitudinalRotational-Fixed_0Nprad"],["Control","1.2N/rad","0.6N/rad","0N/rad"], "LongitudinalRotational-Fixed",false, true,"Shank");
analyzeData("Jig Results",["Fixed-Fixed","TransverseRotational-Fixed_1.2Nprad","TransverseRotational-Fixed_0.6Nprad","TransverseRotational-Fixed_0Nprad"],["Control","1.2N/rad","0.6N/rad","0N/rad"], "TransverseRotational-Fixed",false, true,"Thigh");
analyzeData("Jig Results",["Fixed-Fixed","FrontalRotational-Fixed_1.2Nprad","FrontalRotational-Fixed_0.6Nprad","FrontalRotational-Fixed_0Nprad"],["Control","1.2N/rad","0.6N/rad","0N/rad"], "FrontalRotational-Fixed",false, true,"Thigh");
analyzeData("Jig Results",["Fixed-Fixed","LongitudinalTranslational-Fixed_2kNpm","LongitudinalTranslational-Fixed_1kNpm","LongitudinalTranslational-Fixed_0Npm"],["Control","2kN/m","1kN/m","0N/m"], "LongitudinalTranslational-Fixed",false, true,"Thigh");
analyzeData("Jig Results",["Fixed-Fixed","TransverseTranslational-Fixed_2kNpm","TransverseTranslational-Fixed_1kNpm","TransverseTranslational-Fixed_0Npm"],["Control","2kN/m","1kN/m","0N/m"], "TransverseTranslational-Fixed",false, true,"Thigh");
analyzeData("Jig Results",["Fixed-Fixed","FrontalTranslational-Fixed_2kNpm","FrontalTranslational-Fixed_1kNpm","FrontalTranslational-Fixed_0Npm"],["Control","2kN/m","1kN/m","0N/m"], "FrontalTranslational-Fixed",false, true,"Thigh");

analyzeData("Jig Results",["Fixed-Fixed","Fixed-LongitudinalRotational_1.2Nprad","Fixed-LongitudinalRotational_0.6Nprad","Fixed-LongitudinalRotational_0Nprad"],["Control","1.2N/rad","0.6N/rad","0N/rad"], "Fixed-LongitudinalRotational",false, true,"Thigh");
analyzeData("Jig Results",["Fixed-Fixed","Fixed-TransverseRotational_1.2Nprad","Fixed-TransverseRotational_0.6Nprad","Fixed-TransverseRotational_0Nprad"],["Control","1.2N/rad","0.6N/rad","0N/rad"], "Fixed-TransverseRotational",false, true,"Thigh");
analyzeData("Jig Results",["Fixed-Fixed","Fixed-FrontalRotational_1.2Nprad","Fixed-FrontalRotational_0.6Nprad","Fixed-FrontalRotational_0Nprad"],["Control","1.2N/rad","0.6N/rad","0N/rad"], "Fixed-FrontalRotational",false, true,"Thigh");
```

```
analyzeData("Jig Results",["Fixed-Fixed","Fixed-
LongitudinalTranslational_2kNpm","Fixed-LongitudinalTranslational_1kNpm","Fixed-
LongitudinalTranslational_0Npm"],["Control","2kN/m","1kN/m","0N/m"], "Fixed-
LongitudinalTranslational",false, true,"Thigh");
analyzeData("Jig Results",["Fixed-Fixed","Fixed-
TransverseTranslational_2kNpm","Fixed-TransverseTranslational_1kNpm","Fixed-
TransverseTranslational_0Npm"],["Control","2kN/m","1kN/m","0N/m"], "Fixed-
TransverseTranslational",false, true,"Thigh");
analyzeData("Jig Results",["Fixed-Fixed","Fixed-FrontalTranslational_2kNpm","Fixed-
FrontalTranslational_1kNpm","Fixed-
FrontalTranslational_0Npm"],["Control","2kN/m","1kN/m","0N/m"], "Fixed-
FrontalTranslational",false, true,"Thigh");

compareHumanJig(["Fixed-Fixed","LongitudinalTranslational-
Fixed_0Npm","LongitudinalTranslational-Fixed_1kNpm","LongitudinalTranslational-
Fixed_2kNpm"],["Control","0N/m","1kN/m","2kN/m"],"Compare-
LongitudinalTranslational");
compareHumanJig(["Fixed-Fixed","FrontalTranslational-
Fixed_0Npm","FrontalTranslational-Fixed_1kNpm","FrontalTranslational-
Fixed_2kNpm"],["Control","0N/m","1kN/m","2kN/m"],"Compare-FrontalTranslational");

function compareHumanJig(conditionDirectories, conditionNames, rootSaveName)
[jigData,~] = analyzeData("Jig Results",conditionDirectories,conditionNames, "Jig-
"+rootSaveName,false,true, "Shank");
[humanData,~] = analyzeData("Subject
1",conditionDirectories(1:3),conditionNames(1:3),"Human-"+rootSaveName,true,
false,"Shank");
pressureData = [jigData.pressureFits(1:4,:);humanData.pressureFits(1:3,:)];
displacementData =
[jigData.displacementFits(1:4,:);humanData.displacementFits(1:3,:)];
plotLegend = conditionNames + ["- Jig";"- Human"];
plotDataSets(pressureData, "Angle (Deg)","Pressure (Pa)","Pressure vs.
Angle",["Lateral" "Central" "Medial"], ["Proximal" "Distal"],
plotLegend.',rootSaveName+"-PresureComponents-ComparisonPoints");
plotDataSets(displacementData, "Angle (Deg)","Displacement (mm)","Displacement vs.
Angle",["Transversal" "Longitudinal" "Sagittal"], ["Shank" "Thigh"],
plotLegend.',rootSaveName+"-TranslationComponents-ComparisonPoints");
plotFitSets(pressureData, "Angle (Deg)","Pressure (Pa)","Pressure vs.
Angle",["Lateral" "Central" "Medial"], ["Proximal" "Distal"],
plotLegend.',rootSaveName+"-PresureComponents-ComparisonFits");
plotFitSets(displacementData, "Angle (Deg)","Displacement (mm)","Displacement vs.
Angle",["Transversal" "Longitudinal" "Sagittal"], ["Shank" "Thigh"],
plotLegend.',rootSaveName+"-TranslationComponents-ComparisonFits");
end

function [fits,raw] = analyzeData(rootDirectory, conditionDirectories,
conditionNames,rootSaveName,isRotY, hasTimeStamp, pressureLocation)
motionData = importMotionData(rootDirectory, conditionDirectories, conditionNames,
isRotY);
pressureData = importPressureData(rootDirectory, conditionDirectories,
conditionNames, pressureLocation,hasTimeStamp);
data = innerjoin(motionData,pressureData,'Keys',["FrameNo","trialNo","condition"]);
dispComponentFits =
fitData(data,conditionNames,'angle','ShankTransversalDisplacement');
```

```
dispComponentFits =
[dispComponentFits,fitData(data,conditionNames,'angle','ShankLongitudinalDisplaceme
nt')];
dispComponentFits =
[dispComponentFits,fitData(data,conditionNames,'angle','ShankSagittalDisplacement')
];
dispComponentFits =
[dispComponentFits,fitData(data,conditionNames,'angle','ThighLongitudinalDisplaceme
nt')];
dispComponentFits =
[dispComponentFits,fitData(data,conditionNames,'angle','ThighTransversalDisplacemen
t')];
dispComponentFits =
[dispComponentFits,fitData(data,conditionNames,'angle','ThighSagittalDisplacement')
];
pressureFits = fitData(data,conditionNames,'angle','topLeft');
pressureFits = [pressureFits,fitData(data,conditionNames,'angle','topCenter')];
pressureFits = [pressureFits,fitData(data,conditionNames,'angle','topRight')];
pressureFits = [pressureFits,fitData(data,conditionNames,'angle','bottomLeft')];
pressureFits = [pressureFits,fitData(data,conditionNames,'angle','bottomCenter')];
pressureFits = [pressureFits,fitData(data,conditionNames,'angle','bottomRight')];
individualFitOffset = 0;
if length(conditionNames) > 1
    individualFitOffset = 1;
end
plotDataSets(dispComponentFits(1:end-individualFitOffset,:), "Angle
(Deg)","Displacement (mm)","Displacement vs. Angle",["Transversal" "Longitudinal"
"Sagittal"], ["Shank" "Thigh"], conditionNames,rootSaveName+"-
TranslationComponentsPoints");
plotFitSets(dispComponentFits(1:end-individualFitOffset,:), "Angle
(Deg)","Displacement (mm)","Displacement vs. Angle",["Transversal" "Longitudinal"
"Sagittal"], ["Shank" "Thigh"],
conditionNames,rootSaveName+"TranslationComponentsFits");
plotDataSets(pressureFits(1:end-individualFitOffset,:), "Angle (Deg)","Pressure
(Pa)","Pressure vs. Angle",["Lateral" "Central" "Medial"], ["Proximal" "Distal"],
conditionNames,rootSaveName+"-"+pressureLocation+"-PressurePoints");
plotFitSets(pressureFits(1:end-individualFitOffset,:), "Angle (Deg)","Pressure
(Pa)","Pressure vs. Angle",["Lateral" "Central" "Medial"], ["Proximal" "Distal"],
conditionNames,rootSaveName+"-"+pressureLocation+"-PressureFits");
locations = ["Shank Transverse";"Shank Longitudinal";"Shank Sagittal";"Thigh
Transverse";"Thigh Longitudinal";"Thigh Sagital"];
statExport(dispComponentFits,locations,conditionNames,rootSaveName+"-
DisplacementStatSummary");
statExport(pressureFits,locations,conditionNames,rootSaveName+"-
"+pressureLocation+"-PressureStatSummary");
fits = table();
fits.pressureFits = pressureFits;
fits.displacementFits = dispComponentFits;
raw = data;
end

function motionData = importMotionData(rootDirectory,conditionDirectories,
conditionNames,isRotY)
motiveData = cell(1,length(conditionDirectories));
for j = 1:length(conditionDirectories)
```

```
    fileNames = dir("..\..\"+rootDirectory+"\Shank\" + conditionDirectories(j) +
"\");
    fileNames = struct2table(fileNames(4:end));%skip the .. and . files as well as
the first test (it usually has weird results)
    pressureFiles = fileNames.name(~contains(fileNames.name,["~" "Motive"]));
    motionFiles = strrep(pressureFiles,"Arduino","Motive");
    for i = 1:size(motionFiles,1)
        %% reading the file in, renaming the variables and trimming uneeded
        %% data
        motiveData{i,j} = readtable("..\..\"+rootDirectory+"\Shank\" +
conditionDirectories(j) + "\"+
motionFiles(i),'VariableDescriptionsLine',7,'VariableNamesLine',4,'NumHeaderLines',
7); %get angles
        motiveData{i,j} = rmmissing(motiveData{i,j},"DataVariables",[1:66]);
        motiveData{i,j} =
renamevars(motiveData{i,j},["Var1","Shank_4","Shank_5","Shank_6","Shank","Shank_1",
"Shank_2","Shank_3", ...

"ShankFrame_4","ShankFrame_5","ShankFrame_6","ShankFrame","ShankFrame_1","ShankFram
e_2","ShankFrame_3", ...
            "Thigh_4","Thigh_5","Thigh_6","Thigh","Thigh_1","Thigh_2","Thigh_3",
...

"ThighFrame_4","ThighFrame_5","ThighFrame_6","ThighFrame","ThighFrame_1","ThighFram
e_2","ThighFrame_3"], ...
            ["FrameNo",
"shankX","shankY","shankZ","shankrX","shankrY","shankrZ","shankrW", ...

"shankFrameX","shankFrameY","shankFrameZ","shankFramerX","shankFramerY","shankFrame
rZ","shankFramerW", ...
            "thighX","thighY","thighZ","thighrX","thighrY","thighrZ","thighrW", ...

"thighFrameX","thighFrameY","thighFrameZ","thighFramerX","thighFramerY","thighFrame
rZ","thighFramerW"]);
        motiveData{i,j} = motiveData{i,j}(:,[1,3:30]);
        if(isRotY)%human trials were done with the axes rotated 90 degrees about Y,
rotate to match with jig
            motiveData{i,j} =
renamevars(motiveData{i,j},["shankX","shankrX","shankFrameX","shankFramerX","shankZ
","shankrZ","shankFrameZ","shankFramerZ","thighX","thighrX","thighFrameX","thighFra
merX","thighZ","thighrZ","thighFrameZ","thighFramerZ"],["shankZ","shankrZ","shankFr
ameZ","shankFramerZ","shankX","shankrX","shankFrameX","shankFramerX","thighZ","thig
hrZ","thighFrameZ","thighFramerZ","thighX","thighrX","thighFrameX","thighFramerX"])
;
            motiveData{i,j}.shankZ = -motiveData{i,j}.shankZ;
            motiveData{i,j}.shankrZ = -motiveData{i,j}.shankrZ;
            motiveData{i,j}.shankFrameZ = -motiveData{i,j}.shankFrameZ;
            motiveData{i,j}.shankFramerZ = -motiveData{i,j}.shankFramerZ;
            motiveData{i,j}.thighZ = -motiveData{i,j}.thighZ;
            motiveData{i,j}.thighrZ = -motiveData{i,j}.thighrZ;
            motiveData{i,j}.thighFrameZ = -motiveData{i,j}.thighFrameZ;
            motiveData{i,j}.thighFramerZ = -motiveData{i,j}.thighFramerZ;
        end
        %% Labelling the trial number and the conditions
```

```
        fileNo = regexp(pressureFiles(i),'[0-9]{3}','match');%get the file number,
used to place in array in correct position for numbering
        fileNo = str2double(fileNo{1});
        motiveData{i,j}.trialNo(:) = fileNo;
        motiveData{i,j}.condition(:) = conditionNames(j);
        %% Finding angles between parts
        thighQuat =
quaternion(motiveData{i,j}.thighrW,motiveData{i,j}.thighrX,motiveData{i,j}.thighrY,
motiveData{i,j}.thighrZ);
        shankQuat =
quaternion(motiveData{i,j}.shankrW,motiveData{i,j}.shankrX,motiveData{i,j}.shankrY,
motiveData{i,j}.shankrZ);
        thighFrameQuat =
quaternion(motiveData{i,j}.thighFramerW,motiveData{i,j}.thighFramerX,motiveData{i,j
}.thighFramerY,motiveData{i,j}.thighFramerZ);
        shankFrameQuat =
quaternion(motiveData{i,j}.shankFramerW,motiveData{i,j}.shankFramerX,motiveData{i,j
}.shankFramerY,motiveData{i,j}.shankFramerZ);
        [angle,~,~,~] = parts(quatmultiply(quatconj(thighQuat),shankQuat));
        angle(angle>1)=1;%rounding the values slightly above 1 to 1.
        motiveData{i,j}.angle = 2*acosd(angle);
        motiveData{i,j}.angle = motiveData{i,j}.angle-
min(motiveData{i,j}.angle);%setting 0 degrees to be the first frame the body is
visible, rather than the frame it was defined on.
        [thighToFrameAngle,~,~,~] =
parts(quatmultiply(quatconj(thighQuat),thighFrameQuat));
        thighToFrameAngle(thighToFrameAngle>1)=1;%rounding the values slightly
above 1 to 1.
        motiveData{i,j}.thighToFrameAngle = 2*acosd(thighToFrameAngle);
        [shankToFrameAngle,~,~,~] =
parts(quatmultiply(quatconj(shankQuat),shankFrameQuat));
        shankToFrameAngle(shankToFrameAngle>1)=1;%rounding the values slightly
above 1 to 1.
        motiveData{i,j}.shankToFrameAngle = 2*acosd(shankToFrameAngle);
        %% Trimming down to only include flexion
        [~,endIndex] = max(motiveData{i,j}.angle);
        motiveData{i,j} = motiveData{i,j}(1:endIndex,:);
        if size(motiveData{i,j},1) < 4
            motiveData{i,j} = table();
            break;
        end
        %% Relative Motion
        zeroAngle = 10;
        [angleUnique, uniqueIndices,~] = unique(motiveData{i,j}.angle(:));
        thighQuat =
quaternion(motiveData{i,j}.thighrW,motiveData{i,j}.thighrX,motiveData{i,j}.thighrY,
motiveData{i,j}.thighrZ);
        shankQuat =
quaternion(motiveData{i,j}.shankrW,motiveData{i,j}.shankrX,motiveData{i,j}.shankrY,
motiveData{i,j}.shankrZ);
        firstInterpQuatIndex = find(motiveData{i,j}.angle ==
interp1(angleUnique,angleUnique,zeroAngle,'previous'));
        secondInterpQuatIndex = find(motiveData{i,j}.angle ==
interp1(angleUnique,angleUnique,zeroAngle,'next'));
```

```
        quatIntervalFraction = (zeroAngle-
motiveData{i,j}.angle(firstInterpQuatIndex))/(motiveData{i,j}.angle(secondInterpQua
tIndex)-motiveData{i,j}.angle(firstInterpQuatIndex));
        interpQuat =
quatinterp(shankQuat(firstInterpQuatIndex),shankQuat(secondInterpQuatIndex),quatInt
ervalFraction,'slerp');
        %if isempty(interpQuat)
        %    break;
        %end
        shankRefDisplacement =
rotateframe(interpQuat,interp1(angleUnique,motiveData{i,j}{uniqueIndices,["shankX",
"shankY","shankZ"]}-
motiveData{i,j}{uniqueIndices,["shankFrameX","shankFrameY","shankFrameZ"]},zeroAngl
e,"linear","extrap"));
        interpQuat =
quatinterp(thighQuat(firstInterpQuatIndex),thighQuat(secondInterpQuatIndex),quatInt
ervalFraction,'slerp');
        thighRefDisplacement =
rotateframe(interpQuat,interp1(angleUnique,motiveData{i,j}{uniqueIndices,["thighX",
"thighY","thighZ"]}-
motiveData{i,j}{uniqueIndices,["thighFrameX","thighFrameY","thighFrameZ"]},zeroAngl
e,"linear","extrap"));
        shankDisplacement = rotateframe(shankQuat,
motiveData{i,j}{:,["shankX","shankY","shankZ"]}-
motiveData{i,j}{:,["shankFrameX","shankFrameY","shankFrameZ"]});
        thighDisplacement = rotateframe(thighQuat,
motiveData{i,j}{:,["thighX","thighY","thighZ"]}-
motiveData{i,j}{:,["thighFrameX","thighFrameY","thighFrameZ"]});
        shankRelDisplacement = shankDisplacement-shankRefDisplacement;
        thighRelDisplacement = thighDisplacement-thighRefDisplacement;
        motiveData{i,j}.shankBodyRelDisplacement =
filloutliers(shankRelDisplacement,"linear",'movmedian',10);
        motiveData{i,j}.thighBodyRelDisplacement =
filloutliers(thighRelDisplacement,"linear",'movmedian',10);
        motiveData{i,j}.totalShankRelDisplacement =
sqrt(motiveData{i,j}.shankBodyRelDisplacement(:,1).^2+motiveData{i,j}.shankBodyRelD
isplacement(:,2).^2+motiveData{i,j}.shankBodyRelDisplacement(:,3).^2);
        motiveData{i,j}.totalThighRelDisplacement =
sqrt(motiveData{i,j}.thighBodyRelDisplacement(:,1).^2+motiveData{i,j}.thighBodyRelD
isplacement(:,2).^2+motiveData{i,j}.thighBodyRelDisplacement(:,3).^2);
        motiveData{i,j}.normalizedShankDisplacement =
sqrt(shankDisplacement(:,1).^2+shankDisplacement(:,2).^2+shankDisplacement(:,3).^2)
./sqrt(shankRefDisplacement(1)^2+shankRefDisplacement(2)^2+shankRefDisplacement(3)^
2);
        motiveData{i,j} =
splitvars(motiveData{i,j},{'shankBodyRelDisplacement','thighBodyRelDisplacement'},'
NewVariableNames',{{'ShankTransversalDisplacement','ShankLongitudinalDisplacement',
'ShankSagittalDisplacement'},{'ThighTransversalDisplacement','ThighLongitudinalDisp
lacement','ThighSagittalDisplacement'}});
    end
end
motionData = vertcat(motiveData{:,:});
end
```

```
function pressureData = importPressureData(rootDirectory, conditionDirectories,
conditionNames, location, hasTimeStamp)
%% Read in the calibration data based on the location being imported, fit the data
calibrationData = [];
if location == "Shank"
    load("shankCalRaw.mat");
elseif location == "Thigh"
    load("Thigh3Raw.mat");
end
for i = 1:size(calibrationRaw,1)
    pressures(1:size(calibrationRaw{2,2},1),1) = calibrationRaw{i,1};
    responses = calibrationRaw{i,2};
    pressureResponse = [pressures,responses];
    calibrationData = vertcat(calibrationData,pressureResponse);
end
sensorFits = cell(60,1);
for i = 2:61
    [sensorFits{i-1},~] = fit(calibrationData(:,i),calibrationData(:,1),'exp1');
end
pressureData = cell(1,length(conditionDirectories));
%% Import the trial data
for j = 1:length(conditionDirectories)
    files = dir("..\..\"+rootDirectory+"\"+location+"\" + conditionDirectories(j) +
"\");
    files = struct2table(files(4:end));%skip the .. and . files as well as the
first test (it usually has weird results)
    pressureFiles = files.name(~contains(files.name,["~" "Motive"]));
    for i = 1:size(pressureFiles,1)
        pressureData{i,j} = readtable("..\..\"+rootDirectory+"\"+location+"\" +
conditionDirectories(j) + "\"+ pressureFiles(i));
        %% Adding Labels
        pressureDataOffset = 1;
        if(hasTimeStamp)
            pressureData{i,j} = renamevars(pressureData{i,j},['Var1'],['FrameNo']);
        else
            pressureData{i,j}.FrameNo = transpose([1:height(pressureData{i,j})]-1);
            pressureDataOffset = 0;
        end
        fileNo = regexp(pressureFiles(i),'[0-9]{3}','match');
        fileNo = str2double(fileNo{1});
        pressureData{i,j}.trialNo(:) = fileNo;
        pressureData{i,j}.condition(:) = conditionNames(j);
        %% Convert analog readings to pressures
        for k = 1:60
            pressureData{i,j}.("Var"+string(k+pressureDataOffset)) =
feval(sensorFits{k}, pressureData{i,j}{:,"Var"+string(k+pressureDataOffset)});
            pressureData{i,j}.("Var"+string(k+pressureDataOffset)) =
filloutliers(pressureData{i,j}{:,"Var"+string(k+pressureDataOffset)},"linear",'movm
edian',10);
        end
        %% Combine into Zones
        pressureData{i,j}.topLeft = (sum(pressureData{i,j}{:,"Var"+string([1 2 6 7
11 12 16 17]+pressureDataOffset)},2) + 0.5*sum(pressureData{i,j}{:,"Var"+string([3
8 13 18]+pressureDataOffset)},2))/10;
```

```
        pressureData{i,j}.topCenter = (sum(pressureData{i,j}{:,"Var"+string([21 22
26 27 31 32 36 37]+pressureDataOffset)},2) +
0.5*sum(pressureData{i,j}{:,"Var"+string([23 28 33 38]+pressureDataOffset)},2))/10;
        pressureData{i,j}.topRight = (sum(pressureData{i,j}{:,"Var"+string([41 42
46 47 51 52 56 57]+pressureDataOffset)},2) +
0.5*sum(pressureData{i,j}{:,"Var"+string([43 48 53 58]+pressureDataOffset)},2))/10;
        pressureData{i,j}.bottomLeft = (sum(pressureData{i,j}{:,"Var"+string([4 5 9
10 14 15 19 20]+pressureDataOffset)},2) +
0.5*sum(pressureData{i,j}{:,"Var"+string([3 8 13 18]+pressureDataOffset)},2))/10;
        pressureData{i,j}.bottomCenter = (sum(pressureData{i,j}{:,"Var"+string([24
25 29 30 34 35 39 40]+pressureDataOffset)},2) +
0.5*sum(pressureData{i,j}{:,"Var"+string([23 28 33 38]+pressureDataOffset)},2))/10;
        pressureData{i,j}.bottomRight = (sum(pressureData{i,j}{:,"Var"+string([44
45 49 50 54 55 59 60]+pressureDataOffset)},2) +
0.5*sum(pressureData{i,j}{:,"Var"+string([43 48 43 48]+pressureDataOffset)},2))/10;
    end
end
pressureData = vertcat(pressureData{:,:});
end

function fits = fitData(data,conditionNames, predictor, response)
fits = cell(1);
%% Individual fits
maxOrder = 0;
for i = 1:length(conditionNames)
    %% filter out the trial data
    trials = data(data.condition == conditionNames(i),string({predictor, response,
"trialNo"}));
    adjR2 = 0;
    order = 0;
    while 1 %wish matlab had do while but this is a work around
        fits{i,1} = fitlm(trials, response + "~"+predictor+"^"+string(order));
        if (fits{i,1}.Rsquared.Adjusted < adjR2) || (order >= 4)
            break;
        else
            adjR2 = fits{i,1}.Rsquared.Adjusted < adjR2;
            order = order + 1;
        end
    end
    if order > maxOrder
        maxOrder = order;
    end
end
if(length(conditionNames)>1)
    trimmedData = data(:,string({"condition",predictor, response}));
    fits{length(conditionNames)+1,1} = fitlm(trimmedData,response+"~
condition*"+predictor+"^"+string(maxOrder));
end
end

function plotDataSets(fits, plotXlabel, plotYlabel, plotTitle, plotColumnNames,
plotRowNames, conditions, saveName)
tiled = tiledlayout(2,3);
fig = gcf;
fig.Position(3:4) = fig.Position(3:4)*1.5;
```

```matlab
fig.Position(1:2) = [0,0];
tiled.TileSpacing = 'compact';
tiled.Padding = 'compact';
title(tiled, plotTitle);
ylabel(tiled, plotYlabel);
xlabel(tiled, plotXlabel);
colours = [ 0,0,0;
            1,0,0;
            0,1,0;
            0,0,1;
            0.5,0.5,0.5;
            0.5,0,0;
            0,0.5,0];
for i = 1:size(fits,1)
    for j = 1:6
        nexttile(j);
        hold on;
        h = plot(fits{i,j});
        for k = 1:4
            h(k).Color = colours(i,:);
        end
        h(3).Annotation.LegendInformation.IconDisplayStyle = "off";
        h(4).Annotation.LegendInformation.IconDisplayStyle = "off";
        delete(h(2));
        delete(h(3));
        delete(h(4));
        title("");
        xlabel("");
        ylabel("");
        legend("off");
    end
end
lg = legend(conditions,'Location','best');
if(conditions ~= "off")
    lg.Layout.Tile = 'east';
end
nexttile(1);
title(plotColumnNames(1));
ylabel(plotRowNames(1),'FontWeight','bold');
nexttile(2);
title(plotColumnNames(2));
nexttile(3);
title(plotColumnNames(3));
nexttile(4);
ylabel(plotRowNames(2),'FontWeight','bold');
hold off
exportgraphics(tiled,erase(saveName,"/")+".png");
close;
end

function plotFitSets(fits, plotXlabel, plotYlabel, plotTitle, plotColumnNames,
plotRowNames, conditions, saveName)
tiled = tiledlayout(2,3);
fig = gcf;
fig.Position(3:4) = fig.Position(3:4)*1.5;
```

```
fig.Position(1:2) = [0,0];
tiled.TileSpacing = 'compact';
tiled.Padding = 'compact';
title(tiled, plotTitle);
ylabel(tiled, plotYlabel);
xlabel(tiled, plotXlabel);
colours = [ 0,0,0;
            1,0,0;
            0,1,0;
            0,0,1;
            0.5,0.5,0.5;
            0.5,0,0;
            0,0.5,0];
for i = 1:size(fits,1)
    for j = 1:6
        nexttile(j);
        hold on;
        h = plot(fits{i,j});
        for k = 1:4
            h(k).Color = colours(i,:);
        end
        h(3).Annotation.LegendInformation.IconDisplayStyle = "off";
        h(4).Annotation.LegendInformation.IconDisplayStyle = "off";
        delete(h(1));
        title("");
        xlabel("");
        ylabel("");
        legend("off");
    end
end
lg = legend(conditions,'Location','best');
if(conditions ~= "off")
    lg.Layout.Tile = 'east';
end
nexttile(1);
title(plotColumnNames(1));
ylabel(plotRowNames(1),'FontWeight','bold');
nexttile(2);
title(plotColumnNames(2));
nexttile(3);
title(plotColumnNames(3));
nexttile(4);
ylabel(plotRowNames(2),'FontWeight','bold');
hold off
exportgraphics(tiled,erase(saveName,"/")+".png");
close;
end

function statExport(fits,groupings, labels, saveName)
R2 = [];
RMSE = [];
CohensD = [];
pval = [];
fStat = [];
for location = 1:size(fits,2)
```

```
    for stiffness = 2:size(fits,1)-1%dont iterate over the grouped fit or control
trial
        R2 = [R2;fits{stiffness,location}.Rsquared.Adjusted];
        RMSE = [RMSE;fits{stiffness,location}.RMSE];
        CohensD = [CohensD;effectSize(fits{1,location},fits{stiffness,location})];
        fitStats = anova(fits{stiffness,location},'summary');
        pval = [pval;fitStats{"Model","pValue"}];
        fStat = [fStat;fitStats{"Model","F"}];
    end
end
rowNames = [];
stiffnesses = [];
for group = 1:length(groupings)
    for stiffness = 2:length(labels)
        rowNames = [rowNames;groupings(group)];
    end
    stiffnesses = [stiffnesses;labels(2:end).'];
end
stats = table(rowNames,stiffnesses,R2,RMSE,pval,fStat,CohensD);
writetable(stats,saveName+".xlsx");
end

function result = effectSize(control, test)
minX =
max(control.VariableInfo{"angle","Range"}{1}(1),test.VariableInfo{"angle","Range"}{
1}(1));%take innermost bounds of functions for integral limits
maxX =
min(control.VariableInfo{"angle","Range"}{1}(2),test.VariableInfo{"angle","Range"}{
1}(2));
fun = @(x) feval(control,x) - feval(test,x);
averageDiff = abs(integral(fun,minX,maxX))/(maxX-minX);%the average difference
between the functions
pooledRMSE = sqrt(((control.NumObservations-1)*control.MSE + (test.NumObservations-
1)*test.MSE)/(control.NumObservations+test.NumObservations-2));
result = averageDiff/pooledRMSE;
end
```

Data Collection

```
classdef DataCollectionAppv2 < matlab.apps.AppBase

    % Properties that correspond to app components
    properties (Access = public)
        UIFigure                      matlab.ui.Figure
        TabGroup                      matlab.ui.container.TabGroup
        ConnectTab                    matlab.ui.container.Tab
        WinchControlEditField         matlab.ui.control.EditField
        WinchControlEditFieldLabel    matlab.ui.control.Label
        SendButton                    matlab.ui.control.Button
        SaveButton                    matlab.ui.control.Button
        SaveLocationEditField         matlab.ui.control.EditField
        SaveLocationEditFieldLabel    matlab.ui.control.Label
        BrowseButton                  matlab.ui.control.Button
        ConnectionStatusLamp          matlab.ui.control.Lamp
        ConnectionStatusLampLabel     matlab.ui.control.Label
        ConnectButton                 matlab.ui.control.Button
```

```
        COMPortDropDown                 matlab.ui.control.DropDown
        COMPortDropDownLabel            matlab.ui.control.Label
        CalibrationTab                  matlab.ui.container.Tab
        Areacm2EditField                matlab.ui.control.NumericEditField
        Areacm2EditFieldLabel           matlab.ui.control.Label
        BrowseButton_2                  matlab.ui.control.Button
        FileNameEditField               matlab.ui.control.EditField
        FileNameEditFieldLabel          matlab.ui.control.Label
        WriteButton                     matlab.ui.control.Button
        AppliedWeightgEditField         matlab.ui.control.NumericEditField
        AppliedWeightgEditFieldLabel    matlab.ui.control.Label
        ExportCalibrationButton         matlab.ui.control.Button
        Read1sButton                    matlab.ui.control.Button
        UIAxes                          matlab.ui.control.UIAxes
        DebugTab                        matlab.ui.container.Tab
        TextArea                        matlab.ui.control.TextArea
    end


    properties (Access = private)
        arduino % Description
        calibration
        rawCalibration = {}
    end

    methods (Access = private)

        function arduinoDisconnect(app)
            app.TextArea.Value = [app.TextArea.Value; "Lost Connection to Arduino"];
            app.ConnectionStatusLamp.Color = [1,0,0];
        end

        function packetAvailable(app)
            reading     =     hex2dec(split(regexprep(readline(app.arduino),'([0-9A-
F]{3})([0-9A-F]{1,3})','$1 $2'),{' '}));
            %timeStamp = reading(1);
            app.arduino.UserData(end+1,1:61) = reading(1:61);
        end
    end


    % Callbacks that handle component events
    methods (Access = private)

        % Code that executes after component creation
        function startupFcn(app)
            app.COMPortDropDown.Items = serialportlist("available");
        end

        % Drop down opening function: COMPortDropDown
        function COMPortDropDownOpening(app, event)
            app.COMPortDropDown.Items = serialportlist("available");
        end

        % Button pushed function: ConnectButton
```

```
        function ConnectButtonPushed(app, event)
            try
                app.arduino                                                  =
serialport(app.COMPortDropDown.Value,2000000,"Timeout",1);
                app.ConnectionStatusLamp.Color = [0,1,0];
                app.arduino.UserData = [];
                app.arduino.ErrorOccurredFcn = @(~) arduinoDisconnect(app);
                configureCallback(app.arduino,"byte",32,@(~,~)
packetAvailable(app));
            catch err
                app.TextArea.Value = [app.TextArea.Value; err.identifier];
            end
        end

        % Button pushed function: BrowseButton
        function BrowseButtonPushed(app, event)
            file = uiputfile('*.csv','Select/Create File');
            if file ~= 0
                app.SaveLocationEditField.Value = file;
                app.SaveButton.Enable = "on";
            end
        end

        % Button pushed function: SaveButton
        function SaveButtonPushed(app, event)
            writematrix(app.arduino.UserData,app.SaveLocationEditField.Value);
            app.SaveLocationEditField.Value                                  =
regexprep(app.SaveLocationEditField.Value,'[0-
9]{3}',sprintf('%03d',str2double(regexp(app.SaveLocationEditField.Value,'[0-
9]{3}','match'))+1));
            app.arduino.UserData = [];
        end

        % Button pushed function: Read1sButton
        function Read1sButtonPushed(app, event)
                write(app.arduino,"1000",'string');
        end

        % Button pushed function: ExportCalibrationButton
        function ExportCalibrationButtonPushed(app, event)
            assignin('base','calibration',app.calibration);
            assignin('base','arduino',app.arduino.UserData);
            assignin('base','calibrationRaw',app.rawCalibration);
            writematrix(app.calibration, app.FileNameEditField.Value);
        end

        % Button pushed function: WriteButton
        function WriteButtonPushed(app, event)
            if(size(app.arduino.UserData,1) >= 1000)
                means = mean(app.arduino.UserData(end-999:end,1:end));
                app.calibration(end+1,:)                                     =
[(app.AppliedWeightgEditField.Value*9.81/1000)/(app.Areacm2EditField.Value/10000),m
eans];
```

```
                app.rawCalibration(end+1,:)                                          =
{(app.AppliedWeightgEditField.Value*9.81/1000)/(app.Areacm2EditField.Value/10000),a
pp.arduino.UserData(end-999:end,1:end)};%app.arduino.UserData(end-999:end,2:end);
                if size(app.calibration, 1) == 1
                    for i = 2:61
                        scatter(app.UIAxes,app.calibration(1),app.calibration(i));
                        hold(app.UIAxes,"on");
                    end
                else
                    for i = 2:61
                        plot(app.UIAxes,app.calibration(:,1),app.calibration(:,i));
                        hold(app.UIAxes,"on");
                    end
                end
                hold(app.UIAxes,"off");
            end
        end

        % Button pushed function: BrowseButton_2
        function BrowseButton_2Pushed(app, event)
            file = uiputfile('*.csv','Select/Create File');
            if file ~= 0
                app.FileNameEditField.Value = file;
                app.ExportCalibrationButton.Enable = "on";
            end
        end

        % Button pushed function: SendButton
        function SendButtonPushed(app, event)
            write(app.arduino, app.WinchControlEditField.Value,"string");
        end
    end

    % Component initialization
    methods (Access = private)

        % Create UIFigure and components
        function createComponents(app)

            % Create UIFigure and hide until all components are created
            app.UIFigure = uifigure('Visible', 'off');
            app.UIFigure.Position = [100 100 640 480];
            app.UIFigure.Name = 'MATLAB App';

            % Create TabGroup
            app.TabGroup = uitabgroup(app.UIFigure);
            app.TabGroup.Position = [1 1 640 480];

            % Create ConnectTab
            app.ConnectTab = uitab(app.TabGroup);
            app.ConnectTab.Title = 'Connect';

            % Create COMPortDropDownLabel
            app.COMPortDropDownLabel = uilabel(app.ConnectTab);
            app.COMPortDropDownLabel.HorizontalAlignment = 'right';
```

```
            app.COMPortDropDownLabel.Position = [40 388 59 22];
            app.COMPortDropDownLabel.Text = 'COM Port';

            % Create COMPortDropDown
            app.COMPortDropDown = uidropdown(app.ConnectTab);
            app.COMPortDropDown.Items = {'Arduino COM Port'};
            app.COMPortDropDown.DropDownOpeningFcn      =      createCallbackFcn(app,
@COMPortDropDownOpening, true);
            app.COMPortDropDown.Position = [114 388 100 22];
            app.COMPortDropDown.Value = 'Arduino COM Port';

            % Create ConnectButton
            app.ConnectButton = uibutton(app.ConnectTab, 'push');
            app.ConnectButton.ButtonPushedFcn        =        createCallbackFcn(app,
@ConnectButtonPushed, true);
            app.ConnectButton.Position = [240 388 100 23];
            app.ConnectButton.Text = 'Connect';

            % Create ConnectionStatusLampLabel
            app.ConnectionStatusLampLabel = uilabel(app.ConnectTab);
            app.ConnectionStatusLampLabel.HorizontalAlignment = 'right';
            app.ConnectionStatusLampLabel.Position = [371 388 103 22];
            app.ConnectionStatusLampLabel.Text = 'Connection Status';

            % Create ConnectionStatusLamp
            app.ConnectionStatusLamp = uilamp(app.ConnectTab);
            app.ConnectionStatusLamp.Position = [489 388 20 20];
            app.ConnectionStatusLamp.Color = [1 0 0];

            % Create BrowseButton
            app.BrowseButton = uibutton(app.ConnectTab, 'push');
            app.BrowseButton.ButtonPushedFcn         =         createCallbackFcn(app,
@BrowseButtonPushed, true);
            app.BrowseButton.Position = [409 27 100 23];
            app.BrowseButton.Text = 'Browse';

            % Create SaveLocationEditFieldLabel
            app.SaveLocationEditFieldLabel = uilabel(app.ConnectTab);
            app.SaveLocationEditFieldLabel.HorizontalAlignment = 'right';
            app.SaveLocationEditFieldLabel.Position = [178 27 81 22];
            app.SaveLocationEditFieldLabel.Text = 'Save Location';

            % Create SaveLocationEditField
            app.SaveLocationEditField = uieditfield(app.ConnectTab, 'text');
            app.SaveLocationEditField.Editable = 'off';
            app.SaveLocationEditField.Position = [274 27 128 22];

            % Create SaveButton
            app.SaveButton = uibutton(app.ConnectTab, 'push');
            app.SaveButton.ButtonPushedFcn          =          createCallbackFcn(app,
@SaveButtonPushed, true);
            app.SaveButton.Enable = 'off';
            app.SaveButton.Position = [524 27 100 23];
            app.SaveButton.Text = 'Save';
```

```
            % Create SendButton
            app.SendButton = uibutton(app.ConnectTab, 'push');
            app.SendButton.ButtonPushedFcn          =          createCallbackFcn(app,
@SendButtonPushed, true);
            app.SendButton.Position = [240 345 100 23];
            app.SendButton.Text = 'Send';

            % Create WinchControlEditFieldLabel
            app.WinchControlEditFieldLabel = uilabel(app.ConnectTab);
            app.WinchControlEditFieldLabel.HorizontalAlignment = 'right';
            app.WinchControlEditFieldLabel.Position = [24 345 77 22];
            app.WinchControlEditFieldLabel.Text = 'WinchControl';

            % Create WinchControlEditField
            app.WinchControlEditField = uieditfield(app.ConnectTab, 'text');
            app.WinchControlEditField.Position = [116 345 100 22];

            % Create CalibrationTab
            app.CalibrationTab = uitab(app.TabGroup);
            app.CalibrationTab.Title = 'Calibration';

            % Create UIAxes
            app.UIAxes = uiaxes(app.CalibrationTab);
            title(app.UIAxes, 'Calibration Data')
            xlabel(app.UIAxes, 'Weight (g)')
            ylabel(app.UIAxes, 'Analog Reading')
            zlabel(app.UIAxes, 'Z')
            app.UIAxes.Position = [27 23 567 175];

            % Create Read1sButton
            app.Read1sButton = uibutton(app.CalibrationTab, 'push');
            app.Read1sButton.ButtonPushedFcn         =         createCallbackFcn(app,
@Read1sButtonPushed, true);
            app.Read1sButton.Position = [141 328 100 23];
            app.Read1sButton.Text = 'Read 1s';

            % Create ExportCalibrationButton
            app.ExportCalibrationButton = uibutton(app.CalibrationTab, 'push');
            app.ExportCalibrationButton.ButtonPushedFcn    =   createCallbackFcn(app,
@ExportCalibrationButtonPushed, true);
            app.ExportCalibrationButton.Enable = 'off';
            app.ExportCalibrationButton.Position = [135 207 111 23];
            app.ExportCalibrationButton.Text = 'Export Calibration';

            % Create AppliedWeightgEditFieldLabel
            app.AppliedWeightgEditFieldLabel = uilabel(app.CalibrationTab);
            app.AppliedWeightgEditFieldLabel.HorizontalAlignment = 'right';
            app.AppliedWeightgEditFieldLabel.Position = [23 367 103 22];
            app.AppliedWeightgEditFieldLabel.Text = 'Applied Weight (g)';

            % Create AppliedWeightgEditField
            app.AppliedWeightgEditField      =      uieditfield(app.CalibrationTab,
'numeric');
            app.AppliedWeightgEditField.Limits = [0 Inf];
            app.AppliedWeightgEditField.Position = [141 367 100 22];
```

```
            % Create WriteButton
            app.WriteButton = uibutton(app.CalibrationTab, 'push');
            app.WriteButton.ButtonPushedFcn         =         createCallbackFcn(app,
@WriteButtonPushed, true);
            app.WriteButton.Position = [141 289 100 23];
            app.WriteButton.Text = 'Write';

            % Create FileNameEditFieldLabel
            app.FileNameEditFieldLabel = uilabel(app.CalibrationTab);
            app.FileNameEditFieldLabel.HorizontalAlignment = 'right';
            app.FileNameEditFieldLabel.Position = [67 250 59 22];
            app.FileNameEditFieldLabel.Text = 'File Name';

            % Create FileNameEditField
            app.FileNameEditField = uieditfield(app.CalibrationTab, 'text');
            app.FileNameEditField.Editable = 'off';
            app.FileNameEditField.Position = [141 250 100 22];

            % Create BrowseButton_2
            app.BrowseButton_2 = uibutton(app.CalibrationTab, 'push');
            app.BrowseButton_2.ButtonPushedFcn        =        createCallbackFcn(app,
@BrowseButton_2Pushed, true);
            app.BrowseButton_2.Position = [258 249 100 23];
            app.BrowseButton_2.Text = 'Browse';

            % Create Areacm2EditFieldLabel
            app.Areacm2EditFieldLabel = uilabel(app.CalibrationTab);
            app.Areacm2EditFieldLabel.HorizontalAlignment = 'right';
            app.Areacm2EditFieldLabel.Position = [56 407 70 22];
            app.Areacm2EditFieldLabel.Text = 'Area (cm^2)';

            % Create Areacm2EditField
            app.Areacm2EditField = uieditfield(app.CalibrationTab, 'numeric');
            app.Areacm2EditField.Limits = [0 Inf];
            app.Areacm2EditField.Position = [141 407 100 22];

            % Create DebugTab
            app.DebugTab = uitab(app.TabGroup);
            app.DebugTab.Title = 'Debug';

            % Create TextArea
            app.TextArea = uitextarea(app.DebugTab);
            app.TextArea.Editable = 'off';
            app.TextArea.Position = [15 27 609 402];

            % Show the figure after all components are created
            app.UIFigure.Visible = 'on';
        end
    end

    % App creation and deletion
    methods (Access = public)

        % Construct app
```

```
        function app = DataCollectionAppv2

            % Create UIFigure and components
            createComponents(app)

            % Register the app with App Designer
            registerApp(app, app.UIFigure)

            % Execute the startup function
            runStartupFcn(app, @startupFcn)

            if nargout == 0
                clear app
            end
        end

        % Code that executes before app deletion
        function delete(app)

            % Delete UIFigure when app is deleted
            delete(app.UIFigure)
        end
    end
end
```

Appendix B – Arduino Code

Sensor Controller

```
#include <SPI.h>
#include "printf.h"
#include "RF24.h"
const int sensorPins[] = { A0, A1, A2, A3, A4 };
const int selectorPins[] = { 44, 42, 40, 38, 36, 34, 32, 30, 28, 26, 24, 22
};
#define CE_PIN 46
#define CSN_PIN 48
#define LED_IR 7
#define LED_RED 5
#define LED_GREEN 3
#define MOTOR1_PIN 25
#define MOTOR2_PIN 27
RF24 radio(CE_PIN, CSN_PIN);
uint8_t address[][6] = { "Addr1", "Addr2" };
#define SIZE 31
byte buffer[SIZE];
int bufferPosition = 0;

void setup() {
  //initiate status LEDs
  pinMode(LED_BUILTIN, OUTPUT);
  pinMode(LED_RED, OUTPUT);
  pinMode(LED_GREEN, OUTPUT);
```

```
  initADC();
  //initiate motors
  pinMode(MOTOR1_PIN, OUTPUT);
  pinMode(MOTOR2_PIN, OUTPUT);
  initNRF24();
  for (int i : sensorPins) {
    pinMode(i, INPUT);
  }
  for (int i : selectorPins) {
    pinMode(i, OUTPUT);
  }
}

void loop() {
  int ID = 0;
  prepareBuffer(ID);
  for (int i = 0; i < 12; i++) {
    digitalWrite(selectorPins[i], HIGH);
    for (int j = 0; j < 5; j++) {
      int reading = analogRead(sensorPins[j]);
      writeToBuffer(reading);
      if ((bufferPosition - 1) / 2 == 15) {
        radio.writeFast(&buffer, SIZE);
        bool ok = radio.txStandBy();
        /*if (!ok) {  //check if connection lost
          stop();
          analogWrite(LED_RED, 125);
          digitalWrite(LED_GREEN, LOW);
        }*/
        uint8_t pipe;
        if (radio.available(&pipe)) {
          byte ack;
          radio.read(&ack, 1);
          switch (ack) {
            case 0b00000000:
              stop();
              analogWrite(LED_GREEN, 125);
              digitalWrite(LED_RED, LOW);
              break;
            case 0b00000001:
              spoolUp();
              analogWrite(LED_GREEN, 125);
              digitalWrite(LED_RED, LOW);
              break;
            case 0b00000010:
              spoolDown();
              analogWrite(LED_GREEN, 125);
              digitalWrite(LED_RED, LOW);
              break;
              case 0b01000000:
              //no clue why this keeps showing up
              break;
            default:
              stop();
              analogWrite(LED_GREEN, 125);
              analogWrite(LED_RED, 125);
              break;
```

```
        }
      } else {
        stop();
        analogWrite(LED_RED, 125);
        digitalWrite(LED_GREEN, LOW);
      }
      ID++;
      prepareBuffer(ID);
    }
  }
  digitalWrite(selectorPins[i], LOW);
 }
}

void prepareBuffer(byte ID) {
  buffer[0] = ID;
  bufferPosition = 1;
}

void writeToBuffer(int value) {
  buffer[bufferPosition] = highByte(value);
  buffer[bufferPosition + 1] = lowByte(value);
  bufferPosition += 2;
}

void spoolUp() {
  digitalWrite(MOTOR1_PIN, HIGH);
  digitalWrite(MOTOR2_PIN, LOW);
}

void spoolDown() {
  digitalWrite(MOTOR2_PIN, HIGH);
  digitalWrite(MOTOR1_PIN, LOW);
}

void stop() {
  digitalWrite(MOTOR1_PIN, LOW);
  digitalWrite(MOTOR2_PIN, LOW);
}

void initADC() {
  //set ADC clock prescaler
  ADCSRA &= ~(bit(ADPS0) | bit(ADPS1) | bit(ADPS2));  //clear bits
  //ADCSRA |= bit(ADPS1) | bit(ADPS2);  //  64 prescale on ADC clock
  ADCSRA |= bit(ADPS2);  //  16
  analogReference(EXTERNAL);
  analogRead(sensorPins[0]);   //make an analog reading to initialize the
hardware (25 clock cycles on first reading, 14 on subsequent)
}

void initNRF24() {
  if (!radio.begin()) {  //check if radio is working
    digitalWrite(LED_BUILTIN, HIGH);
    while (1) {}  // hold in infinite loop
  }
  radio.setPALevel(RF24_PA_MAX, true);
  radio.enableDynamicPayloads();
```

```
  radio.enableAckPayload();
  radio.setDataRate(1);
  radio.openWritingPipe(address[1]);
  radio.openReadingPipe(1, address[0]);
  radio.flush_rx();
  radio.stopListening();
}
```

Receiver

```
#include <SPI.h>
#include "RF24.h"

#define CE_PIN 7
#define CSN_PIN 8
#define TRIG 3

RF24 radio(CE_PIN, CSN_PIN);

uint8_t address[][6] = { "Addr1", "Addr2" };
#define SIZE 31
byte buffer[SIZE];
int packet[61];
int timeStamp = 0;
unsigned long lastTime;

void setup() {
  Serial.begin(2000000);
  pinMode(TRIG, INPUT);
  initNRF24();
  attachInterrupt(digitalPinToInterrupt(TRIG), sendPacketISR, FALLING);
}

void loop() {
  if (Serial.available() > 0) {
    int distance = Serial.readString().toInt();
    spool(distance);
  }
  byte ack = 0b00000000;
  if (millis() - lastTime <= 6) {
    ack = 0b00000001;
  } else {
    timeStamp = 0;
  }
  radio.writeAckPayload(1, &ack, 1);
  if (radio.available()) {      // is there a payload?
    radio.read(&buffer, SIZE);  // fetch payload from FIFO
    preparePacket();
  }
}

void preparePacket() {
  for (int i = 1; i <= 15; i++) {
    packet[buffer[0] * 15 + i] = buffer[i * 2 - 1] << 8 | buffer[i * 2];
  }
}
```

```
void sendPacketISR() {
  packet[0] = timeStamp;
  timeStamp++;
  for (int i = 0; i < 61; i++) {
    Serial.print(packet[i], HEX);
    Serial.print(" ");
  }
  Serial.println();
  lastTime = millis();
}

void spool(int distance) {
  unsigned long start = millis();
  while (start + abs(distance) > millis()) {
    byte ack = 0b00000001;
    if (distance < 0) {
      ack = 0b00000010;
    }
    radio.writeAckPayload(1, &ack, 1);
    if (radio.available()) {      // is there a payload?
      radio.read(&buffer, SIZE);  // fetch payload from FIFO
    }
  }
}

void initNRF24() {
  if (!radio.begin()) {
    Serial.println(F("radio hardware is not responding!!"));
    while (1) {}  // hold in infinite loop
  }
  radio.setPALevel(RF24_PA_MAX, true);  // enable LNA
  radio.enableDynamicPayloads();
  radio.enableAckPayload();
  radio.setDataRate(1);
  radio.openWritingPipe(address[0]);
  radio.openReadingPipe(1, address[1]);
  radio.flush_rx();
  radio.startListening();
}
```

Appendix C – Statistical and Effect Size Measures

Table C-1: Statistical and effect size results of the linear regressions fitted to the relative displacement of the limb segments and brace with longitudinal rotation at the shank interface permitted.

	Spring Stiffness	Adj. R2	RMSE	Cohen's D
Shank Transversal	1.2N/rad	0.25	0.69	2.62
	0.6N/rad	0.22	1.04	1.12
	0N/rad	0.39	0.53	2.08
Shank Longitudinal	1.2N/rad	0.49	1.35	1.37
	0.6N/rad	0.19	3.73	0.03
	0N/rad	0.31	2.32	0.61
Shank Sagittal	1.2N/rad	0.95	0.69	5.80
	0.6N/rad	0.79	2.15	2.60
	0N/rad	0.71	1.45	1.40
Thigh Transversal	1.2N/rad	0.42	1.06	0.82
	0.6N/rad	0.13	4.20	0.88
	0N/rad	0.35	5.50	1.29
Thigh Longitudinal	1.2N/rad	0.32	0.45	3.26
	0.6N/rad	0.30	0.62	3.23
	0N/rad	0.58	0.74	0.61
Thigh Sagittal	1.2N/rad	0.71	0.25	1.26
	0.6N/rad	0.66	0.43	1.08
	0N/rad	0.29	0.33	0.44

Table C-2: Statistical and effect size results of the linear regressions fitted to the thigh pressures with longitudinal rotation at the shank interface permitted.

	Spring Stiffness	Adj. R2	RMSE	Cohen's D
Proximal Lateral	1.2N/rad	0.06	241.68	1.81
	0.6N/rad	0.13	112.98	8.06
	0N/rad	0.22	151.50	0.72
Proximal Central	1.2N/rad	0.13	385.87	1.39
	0.6N/rad	0.35	187.05	5.11
	0N/rad	0.54	172.61	1.23
Proximal Medial	1.2N/rad	0.02	348.22	2.67
	0.6N/rad	0.07	211.27	0.38
	0N/rad	0.23	216.04	3.44
Distal Lateral	1.2N/rad	0.06	268.69	1.57
	0.6N/rad	0.10	128.34	6.54
	0N/rad	0.20	162.68	0.13
Distal Central	1.2N/rad	0.10	377.81	0.13
	0.6N/rad	0.31	181.56	1.99
	0N/rad	0.52	156.33	2.06
Distal Medial	1.2N/rad	0.03	339.63	1.75
	0.6N/rad	0.08	199.79	1.25
	0N/rad	0.22	203.92	4.21

Table C-3: Statistical and effect size results of the linear regressions fitted to the shank pressures with longitudinal rotation at the shank interface permitted.

	Spring Stiffness	Adj. R2	RMSE	Cohen's D
Proximal Lateral	1.2N/rad	0.44	213.71	6.02
	0.6N/rad	0.55	210.74	6.44
	0N/rad	0.28	241.40	5.35
Proximal Central	1.2N/rad	0.91	8.59	4.06
	0.6N/rad	0.45	16.86	4.17
	0N/rad	0.67	14.39	4.37
Proximal Medial	1.2N/rad	0.75	846.68	1.19
	0.6N/rad	0.26	1386.37	2.47
	0N/rad	0.44	1008.90	3.88
Distal Lateral	1.2N/rad	0.55	143.82	4.71
	0.6N/rad	0.41	202.04	3.72
	0N/rad	0.10	164.23	5.97
Distal Central	1.2N/rad	0.86	5.38	4.13
	0.6N/rad	0.31	11.61	3.89
	0N/rad	0.62	7.74	5.04
Distal Medial	1.2N/rad	0.17	422.90	1.45
	0.6N/rad	0.03	646.28	1.69
	0N/rad	0.05	771.03	0.74

Table C-4: Statistical and effect size results of the linear regressions fitted to the relative displacement of the jig limb segments and brace with longitudinal translation at the shank interface permitted.

	Spring Stiffness	Adj. R2	RMSE	Cohen's D
Shank Transversal	2kN/m	0.06	0.76	1.28
	1kN/m	0.13	0.59	2.25
	0N/m	0.02	0.46	2.78
Shank Longitudinal	2kN/m	0.68	2.10	0.77
	1kN/m	0.65	1.37	0.44
	0N/m	0.80	0.76	2.30
Shank Sagittal	2kN/m	0.76	0.78	0.17
	1kN/m	0.87	0.55	2.06
	0N/m	0.92	0.38	2.22
Thigh Transversal	2kN/m	0.23	3.50	0.16
	1kN/m	0.41	4.00	1.17
	0N/m	0.39	4.05	0.49
Thigh Longitudinal	2kN/m	0.88	0.61	2.06
	1kN/m	0.84	0.49	0.14
	0N/m	0.92	0.37	0.77
Thigh Sagittal	2kN/m	0.38	0.21	2.94
	1kN/m	0.51	0.87	1.28
	0N/m	0.35	0.20	2.10

Table C-5: Statistical and effect size results of the linear regressions fitted to the relative displacement of the human limb segments and brace with longitudinal translation at the shank interface permitted.

	Spring Stiffness	Adj. R2	RMSE	Cohen's D
Shank Transversal	0N/m	0.87	2.62	5.53
	1kN/m	0.95	1.37	5.72
Shank Longitudinal	0N/m	0.69	2.50	0.38
	1kN/m	0.72	2.29	0.67
Shank Sagittal	0N/m	0.60	2.97	2.34
	1kN/m	0.60	2.33	2.41
Thigh Transversal	0N/m	0.63	2.14	0.39
	1kN/m	0.50	1.89	0.08
Thigh Longitudinal	0N/m	0.29	2.24	3.61
	1kN/m	0.26	2.03	3.72
Thigh Sagittal	0N/m	0.85	2.60	4.32
	1kN/m	0.85	2.57	4.53

Table C-6: Statistical and effect size results of the linear regressions fitted to the thigh pressures with longitudinal translation at the shank interface permitted.

	Spring Stiffness	R2	RMSE	Cohen's D
Proximal Lateral	2kN/m	0.41	117.08	4.15
	1kN/m	0.17	165.79	1.38
	0N/m	0.12	375.63	0.96
Proximal Central	2kN/m	0.27	189.93	5.51
	1kN/m	0.11	318.78	3.25
	0N/m	0.36	330.10	0.91
Proximal Medial	2kN/m	0.26	154.42	3.82
	1kN/m	0.07	304.65	1.87
	0N/m	0.09	251.37	3.39
Distal Lateral	2kN/m	0.39	123.13	3.58
	1kN/m	0.16	174.21	1.00
	0N/m	0.08	425.38	1.10
Distal Central	2kN/m	0.25	171.72	2.28
	1kN/m	0.10	284.10	1.41
	0N/m	0.15	430.46	1.77
Distal Medial	2kN/m	0.27	145.66	2.22
	1kN/m	0.07	274.72	1.08
	0N/m	0.08	259.48	3.76

Table C-7: Statistical and effect size results of the linear regressions fitted to the jig shank pressures with longitudinal translation at the shank interface permitted.

	Spring Stiffness	R2	RMSE	Cohen's D
Proximal Lateral	2kN/m	0.72	123.66	5.14
	1kN/m	0.17	327.81	3.57
	0N/m	0.09	191.30	4.60
Proximal Central	2kN/m	0.94	6.51	6.35
	1kN/m	0.82	11.10	3.33
	0N/m	0.95	18.76	2.63
Proximal Medial	2kN/m	0.84	474.57	3.38
	1kN/m	0.55	1182.29	1.33
	0N/m	0.78	753.55	2.83
Distal Lateral	2kN/m	0.57	85.79	6.55
	1kN/m	0.29	139.28	6.47
	0N/m	0.24	182.14	5.68
Distal Central	2kN/m	0.89	4.98	5.61
	1kN/m	0.77	6.94	3.89
	0N/m	0.96	10.09	1.65
Distal Medial	2kN/m	0.77	229.29	0.51
	1kN/m	0.23	623.20	0.02
	0N/m	0.63	376.01	1.23

Table C-8: Statistical and effect size results of the linear regressions fitted to the human shank pressures with longitudinal translation at the shank interface permitted.

	Spring Stiffness	Adj. R2	RMSE	Cohen's D
Shank Transversal	0N/m	0.57	148.90	1.79
	1kN/m	0.66	145.84	0.46
Shank Longitudinal	0N/m	0.62	63.06	6.81
	1kN/m	0.75	38.89	7.80
Shank Sagittal	0N/m	0.31	1327.22	3.07
	1kN/m	0.58	949.03	2.72
Thigh Transversal	0N/m	0.33	103.39	3.35
	1kN/m	0.53	100.78	2.20
Thigh Longitudinal	0N/m	0.61	39.73	9.27
	1kN/m	0.77	24.82	9.65
Thigh Sagittal	0N/m	0.52	457.42	5.87
	1kN/m	0.71	381.97	5.25

Table C-9: Statistical and effect size results of the linear regressions fitted to the relative displacement of the limb segments and brace with sagittal rotation at the shank interface permitted.

	Spring Stiffness	R2	RMSE	Cohen's D
Shank Transversal	1.2N/rad	0.11	0.64	0.85
	0.6N/rad	0.13	0.78	0.28
	0N/rad	0.20	0.64	1.60
Shank Longitudinal	1.2N/rad	0.71	1.45	0.72
	0.6N/rad	0.84	1.42	1.79
	0N/rad	0.78	1.47	0.08
Shank Sagittal	1.2N/rad	0.64	0.75	0.83
	0.6N/rad	0.46	1.34	0.40
	0N/rad	0.91	0.81	2.57
Thigh Transversal	1.2N/rad	0.18	1.63	0.55
	0.6N/rad	0.54	3.55	1.14
	0N/rad	0.32	4.37	0.79
Thigh Longitudinal	1.2N/rad	0.80	0.64	0.88
	0.6N/rad	0.65	1.24	0.66
	0N/rad	0.32	0.62	2.54
Thigh Sagittal	1.2N/rad	0.42	0.19	2.42
	0.6N/rad	0.57	0.23	0.35
	0N/rad	0.93	0.17	1.96

Table C-10: Statistical and effect size results of the linear regressions fitted to the thigh pressures with sagittal rotation at the shank interface permitted.

	Spring Stiffness	R2	RMSE	Cohen's D
Proximal Lateral	1.2N/rad	0.33	216.30	2.18
	0.6N/rad	0.57	81.15	6.99
	0N/rad	0.60	109.82	0.71
Proximal Central	1.2N/rad	0.07	653.98	0.07
	0.6N/rad	0.66	176.83	2.65
	0N/rad	0.19	175.83	6.14
Proximal Medial	1.2N/rad	0.03	750.20	0.64
	0.6N/rad	0.33	141.22	2.75
	0N/rad	0.17	263.18	5.22
Distal Lateral	1.2N/rad	0.35	216.04	2.65
	0.6N/rad	0.54	83.65	6.36
	0N/rad	0.62	110.01	2.39
Distal Central	1.2N/rad	0.11	425.80	1.11
	0.6N/rad	0.58	168.98	0.41
	0N/rad	0.00	156.59	4.05
Distal Medial	1.2N/rad	0.02	773.68	0.34
	0.6N/rad	0.33	129.16	3.25
	0N/rad	0.19	230.03	6.01

Table C-11: Statistical and effect size results of the linear regressions fitted to the shank pressures with sagittal rotation at the shank interface permitted.

	Spring Stiffness	R2	RMSE	Cohen's D
Proximal Lateral	1.2N/rad	0.18	178.24	6.24
	0.6N/rad	0.01	250.14	3.30
	0N/rad	0.50	182.84	5.21
Proximal Central	1.2N/rad	0.83	4.86	7.76
	0.6N/rad	0.83	12.05	2.59
	0N/rad	0.89	12.72	1.61
Proximal Medial	1.2N/rad	0.22	1026.28	0.76
	0.6N/rad	0.43	1119.31	2.69
	0N/rad	0.70	624.81	5.36
Distal Lateral	1.2N/rad	0.21	114.17	7.21
	0.6N/rad	0.25	305.83	2.45
	0N/rad	0.58	122.17	4.59
Distal Central	1.2N/rad	0.68	4.25	6.63
	0.6N/rad	0.72	7.70	3.43
	0N/rad	0.87	6.63	3.29
Distal Medial	1.2N/rad	0.23	405.18	0.73
	0.6N/rad	0.15	575.52	1.98
	0N/rad	0.28	365.47	4.95

Table C-12: Statistical and effect size results of the linear regressions fitted to the relative displacement of the limb segments and brace with sagittal translation at the shank interface permitted.

	Spring Stiffness	**R2**	**RMSE**	**Cohen's D**
Shank Transversal	2kN/m	0.04	0.49	1.37
	1kN/m	0.09	0.47	1.58
	0N/m	0.11	0.58	1.27
Shank Longitudinal	2kN/m	0.85	1.07	0.51
	1kN/m	0.91	0.95	0.89
	0N/m	0.84	1.37	0.54
Shank Sagittal	2kN/m	0.69	0.94	0.74
	1kN/m	0.66	0.94	0.13
	0N/m	0.86	0.75	1.62
Thigh Transversal	2kN/m	0.24	5.48	0.49
	1kN/m	0.20	5.95	0.70
	0N/m	0.19	3.46	0.53
Thigh Longitudinal	2kN/m	0.61	0.94	0.19
	1kN/m	0.65	1.30	1.11
	0N/m	0.63	0.98	0.14
Thigh Sagittal	2kN/m	0.69	0.20	0.10
	1kN/m	0.30	0.35	0.62
	0N/m	0.93	0.13	0.73

Table C-13: Statistical and effect size results of the linear regressions fitted to the relative displacement of the limb segments and brace with sagittal translation at the shank interface permitted.

	Spring Stiffness	Adj. R2	RMSE	Cohen's D
Shank Transversal	0N/m	0.87	2.62	5.53
	1kN/m	0.95	1.37	5.72
Shank Longitudinal	0N/m	0.69	2.50	0.38
	1kN/m	0.72	2.29	0.67
Shank Sagittal	0N/m	0.60	2.97	2.34
	1kN/m	0.60	2.33	2.41
Thigh Transversal	0N/m	0.63	2.14	0.39
	1kN/m	0.50	1.89	0.08
Thigh Longitudinal	0N/m	0.29	2.24	3.61
	1kN/m	0.26	2.03	3.72
Thigh Sagittal	0N/m	0.85	2.60	4.32
	1kN/m	0.85	2.57	4.53

Table C-14: Statistical and effect size results of the linear regressions fitted to the thigh pressures with sagittal translation at the shank interface permitted.

	Spring Stiffness	R2	RMSE	Cohen's D
Proximal Lateral	2kN/m	0.73	101.20	0.28
	1kN/m	0.50	139.79	1.85
	0N/m	0.44	131.62	1.01
Proximal Central	2kN/m	0.51	161.73	5.83
	1kN/m	0.51	179.66	4.79
	0N/m	0.24	269.58	2.45
Proximal Medial	2kN/m	0.11	307.68	3.06
	1kN/m	0.42	116.84	8.16
	0N/m	0.14	219.83	5.03
Distal Lateral	2kN/m	0.68	110.47	2.50
	1kN/m	0.50	138.55	3.49
	0N/m	0.38	150.65	2.27
Distal Central	2kN/m	0.50	148.28	2.25
	1kN/m	0.51	156.85	1.00
	0N/m	0.18	273.33	0.11
Distal Medial	2kN/m	0.11	277.91	3.43
	1kN/m	0.48	97.68	7.81
	0N/m	0.14	209.42	4.04

Table C-15: Statistical and effect size results of the linear regressions fitted to the jig shank pressures with sagittal translation at the shank interface permitted.

	Spring Stiffness	R2	RMSE	Cohen's D
Proximal Lateral	2kN/m	0.39	198.28	7.60
	1kN/m	0.16	324.44	4.07
	0N/m	0.42	201.92	5.39
Proximal Central	2kN/m	0.93	6.07	4.77
	1kN/m	0.85	14.06	1.26
	0N/m	0.92	7.97	3.98
Proximal Medial	2kN/m	0.75	1055.71	0.64
	1kN/m	0.34	2362.76	0.10
	0N/m	0.76	630.35	3.64
Distal Lateral	2kN/m	0.10	152.09	6.75
	1kN/m	0.12	196.08	4.71
	0N/m	0.22	151.62	5.27
Distal Central	2kN/m	0.84	4.54	4.90
	1kN/m	0.79	8.17	2.24
	0N/m	0.85	4.89	4.87
Distal Medial	2kN/m	0.49	424.52	1.49
	1kN/m	0.19	713.43	0.75
	0N/m	0.21	421.22	2.45

Table C-16: Statistical and effect size results of the linear regressions fitted to the human shank pressures with sagittal translation at the shank interface permitted.

	Spring Stiffness	Adj. R2	RMSE	Cohen's D
Shank Transversal	0N/m	0.26	184.76	0.08
	1kN/m	0.19	170.41	1.74
Shank Longitudinal	0N/m	0.15	59.25	5.80
	1kN/m	0.12	68.90	3.51
Shank Sagittal	0N/m	0.06	1628.78	2.55
	1kN/m	0.16	1857.83	2.97
Thigh Transversal	0N/m	0.04	144.50	0.70
	1kN/m	0.25	135.48	1.13
Thigh Longitudinal	0N/m	0.11	39.00	7.03
	1kN/m	0.14	49.50	4.84
Thigh Sagittal	0N/m	0.15	678.61	4.73
	1kN/m	0.30	742.71	4.69

Table C-17: Statistical and effect size results of the linear regressions fitted to the relative displacement of the limb segments and brace with transverse rotation at the shank interface permitted.

	Spring Stiffness	R2	RMSE	Cohen's D
Shank Transversal	1.2N/rad	0.15	0.57	2.52
	0.6N/rad	0.29	0.55	3.02
	0N/rad	0.41	0.58	0.43
Shank Longitudinal	1.2N/rad	0.84	1.19	0.19
	0.6N/rad	0.78	1.15	0.84
	0N/rad	0.28	1.27	0.24
Shank Sagittal	1.2N/rad	0.92	0.73	3.74
	0.6N/rad	0.93	0.81	4.11
	0N/rad	0.97	0.43	4.36
Thigh Transversal	1.2N/rad	0.56	1.59	0.06
	0.6N/rad	0.75	1.50	1.11
	0N/rad	0.22	3.70	1.32
Thigh Longitudinal	1.2N/rad	0.72	0.34	2.90
	0.6N/rad	0.49	0.48	2.52
	0N/rad	0.72	0.38	2.11
Thigh Sagittal	1.2N/rad	0.84	0.17	0.49
	0.6N/rad	0.79	0.24	0.61
	0N/rad	0.75	0.20	0.33

Table C-18: Statistical and effect size results of the linear regressions fitted to the thigh pressures with transverse rotation at the shank interface permitted.

	Spring Stiffness	R2	RMSE	Cohen's D
Proximal Lateral	1.2N/rad	0.65	83.77	1.65
	0.6N/rad	0.42	175.42	1.17
	0N/rad	0.29	181.75	1.28
Proximal Central	1.2N/rad	0.28	140.96	0.31
	0.6N/rad	0.00	270.08	0.42
	0N/rad	0.03	319.66	2.20
Proximal Medial	1.2N/rad	0.06	196.73	1.19
	0.6N/rad	0.03	247.48	0.33
	0N/rad	0.02	337.40	2.27
Distal Lateral	1.2N/rad	0.57	90.20	0.19
	0.6N/rad	0.38	177.55	2.40
	0N/rad	0.18	251.43	1.59
Distal Central	1.2N/rad	0.24	132.51	3.38
	0.6N/rad	0.08	220.72	1.88
	0N/rad	0.02	414.20	1.57
Distal Medial	1.2N/rad	0.08	178.68	0.71
	0.6N/rad	0.04	209.94	1.03
	0N/rad	0.02	320.79	2.82

Table C-19: Statistical and effect size results of the linear regressions fitted to the shank pressures with transverse rotation at the shank interface permitted.

	Spring Stiffness	R2	RMSE	Cohen's D
Proximal Lateral	1.2N/rad	0.72	227.57	4.15
	0.6N/rad	0.71	204.48	6.22
	0N/rad	0.67	118.12	8.37
Proximal Central	1.2N/rad	0.90	21.32	1.19
	0.6N/rad	0.78	29.77	0.27
	0N/rad	0.90	9.40	4.12
Proximal Medial	1.2N/rad	0.64	495.45	7.52
	0.6N/rad	0.79	484.78	6.19
	0N/rad	0.94	506.94	2.15
Distal Lateral	1.2N/rad	0.57	217.03	4.51
	0.6N/rad	0.67	157.01	6.20
	0N/rad	0.72	80.93	9.49
Distal Central	1.2N/rad	0.83	14.01	0.62
	0.6N/rad	0.77	15.43	1.10
	0N/rad	0.85	5.17	4.84
Distal Medial	1.2N/rad	0.18	289.62	7.36
	0.6N/rad	0.19	481.40	3.94
	0N/rad	0.41	296.99	0.46

Table C-20: Statistical and effect size results of the linear regressions fitted to the relative displacement of the limb segments and brace with sagittal translation at the shank interface permitted.

	Spring Stiffness	R2	RMSE	Cohen's D
Shank Transversal	2kN/m	0.02	0.62	1.68
	1kN/m	0.03	0.47	0.68
	0N/m	0.10	0.70	0.64
Shank Longitudinal	2kN/m	0.83	1.31	0.36
	1kN/m	0.80	0.99	0.13
	0N/m	0.41	1.71	1.15
Shank Sagittal	2kN/m	0.86	0.49	1.31
	1kN/m	0.90	0.50	0.10
	0N/m	0.69	1.14	0.76
Thigh Transversal	2kN/m	0.37	4.26	0.72
	1kN/m	0.58	4.37	1.38
	0N/m	0.10	4.14	0.94
Thigh Longitudinal	2kN/m	0.87	0.32	0.21
	1kN/m	0.86	0.31	1.21
	0N/m	0.50	0.85	0.06
Thigh Sagittal	2kN/m	0.80	0.17	0.54
	1kN/m	0.59	0.19	0.80
	0N/m	0.42	0.24	1.37

Table C-21: Statistical and effect size results of the linear regressions fitted to the thigh pressures with transverse translation at the shank interface permitted.

	Spring Stiffness	R2	RMSE	Cohen's D
Proximal Lateral	2kN/m	0.32	90.27	8.48
	1kN/m	0.22	126.86	4.67
	0N/m	0.03	377.43	3.50
Proximal Central	2kN/m	0.08	252.47	1.18
	1kN/m	0.34	90.80	3.66
	0N/m	0.03	422.73	0.99
Proximal Medial	2kN/m	0.01	363.51	0.89
	1kN/m	0.07	144.71	6.99
	0N/m	0.02	659.30	0.16
Distal Lateral	2kN/m	0.23	114.33	5.55
	1kN/m	0.19	144.82	3.63
	0N/m	0.03	430.90	2.82
Distal Central	2kN/m	0.05	239.15	1.76
	1kN/m	0.27	87.24	1.20
	0N/m	0.02	389.75	0.56
Distal Medial	2kN/m	0.02	331.97	0.51
	1kN/m	0.11	136.93	3.64
	0N/m	0.02	556.82	0.78

Table C-22: Statistical and effect size results of the linear regressions fitted to the shank pressures with transverse translation at the shank interface permitted.

	Spring Stiffness	R2	RMSE	Cohen's D
Proximal Lateral	2kN/m	0.33	195.96	4.53
	1kN/m	0.07	455.88	2.46
	0N/m	0.49	212.62	4.20
Proximal Central	2kN/m	0.72	8.09	4.31
	1kN/m	0.47	9.84	4.28
	0N/m	0.40	5.05	7.67
Proximal Medial	2kN/m	0.84	991.81	0.83
	1kN/m	0.86	541.06	5.71
	0N/m	0.57	1119.58	2.24
Distal Lateral	2kN/m	0.16	168.54	2.10
	1kN/m	0.16	208.36	3.65
	0N/m	0.27	243.42	0.99
Distal Central	2kN/m	0.66	4.71	4.05
	1kN/m	0.31	9.52	2.31
	0N/m	0.31	4.38	4.04
Distal Medial	2kN/m	0.56	566.50	0.60
	1kN/m	0.39	748.19	0.75
	0N/m	0.44	494.88	0.78

Table C-23: Statistical and effect size results of the linear regressions fitted to the relative displacement of the limb segments and brace with longitudinal rotation at the thigh interface permitted.

	Spring Stiffness	R2	RMSE	Cohen's D
Shank Transversal	1.2N/rad	0.02	0.46	2.73
	0.6N/rad	0.00	0.63	2.16
	0N/rad	0.05	0.77	1.22
Shank Longitudinal	1.2N/rad	0.80	0.76	2.24
	0.6N/rad	0.65	1.38	0.38
	0N/rad	0.68	2.10	0.77
Shank Sagittal	1.2N/rad	0.92	0.38	2.18
	0.6N/rad	0.87	0.54	2.01
	0N/rad	0.76	0.79	0.14
Thigh Transversal	1.2N/rad	0.39	4.05	0.49
	0.6N/rad	0.41	4.05	1.16
	0N/rad	0.23	3.53	0.15
Thigh Longitudinal	1.2N/rad	0.92	0.37	0.75
	0.6N/rad	0.84	0.49	0.10
	0N/rad	0.89	0.61	2.09
Thigh Sagittal	1.2N/rad	0.35	0.20	2.18
	0.6N/rad	0.54	0.86	1.35
	0N/rad	0.38	0.21	3.03

Table C-24: Statistical and effect size results of the linear regressions fitted to the thigh pressures with longitudinal rotation at the thigh interface permitted.

	Spring Stiffness	R2	RMSE	Cohen's D
Proximal Lateral	1.2N/rad	0.39	146.07	2.38
	0.6N/rad	0.38	142.83	5.37
	0N/rad	0.11	210.87	5.82
Proximal Central	1.2N/rad	0.67	173.12	1.17
	0.6N/rad	0.46	200.61	2.13
	0N/rad	0.50	192.93	2.40
Proximal Medial	1.2N/rad	0.34	172.82	3.47
	0.6N/rad	0.26	230.98	3.89
	0N/rad	0.15	237.25	0.47
Distal Lateral	1.2N/rad	0.38	152.17	1.75
	0.6N/rad	0.43	149.54	4.89
	0N/rad	0.11	236.36	5.02
Distal Central	1.2N/rad	0.61	161.29	0.79
	0.6N/rad	0.44	185.11	0.90
	0N/rad	0.42	181.54	0.22
Distal Medial	1.2N/rad	0.00	193.69	1.94
	0.6N/rad	0.27	211.24	3.59
	0N/rad	0.17	205.58	0.13

Table C-25: Statistical and effect size results of the linear regressions fitted to the shank pressures with longitudinal rotation at the thigh interface permitted.

	Spring Stiffness	R2	RMSE	Cohen's D
Proximal Lateral	1.2N/rad	0.34	273.39	5.66
	0.6N/rad	0.38	243.97	4.91
	0N/rad	0.34	199.60	6.90
Proximal Central	1.2N/rad	0.92	10.90	2.86
	0.6N/rad	0.79	20.86	0.68
	0N/rad	0.74	18.93	1.42
Proximal Medial	1.2N/rad	0.86	758.49	2.45
	0.6N/rad	0.78	931.32	2.00
	0N/rad	0.89	767.20	1.13
Distal Lateral	1.2N/rad	0.08	259.65	3.00
	0.6N/rad	0.05	214.23	3.11
	0N/rad	0.33	184.77	3.74
Distal Central	1.2N/rad	0.91	6.05	3.37
	0.6N/rad	0.78	11.48	1.01
	0N/rad	0.76	9.89	1.51
Distal Medial	1.2N/rad	0.64	381.14	1.97
	0.6N/rad	0.58	478.51	1.33
	0N/rad	0.78	387.84	0.20

Table C-26: Statistical and effect size results of the linear regressions fitted to the relative displacement of the limb segments and brace with longitudinal translation at the thigh interface permitted.

	Spring Stiffness	R2	RMSE	Cohen's D
Shank Transversal	2kN/m	0.14	0.25	1.42
	1kN/m	0.26	0.23	1.39
	0N/m	0.11	0.25	1.13
Shank Longitudinal	2kN/m	0.96	0.78	2.26
	1kN/m	0.93	1.09	1.79
	0N/m	0.97	0.68	2.68
Shank Sagittal	2kN/m	0.92	0.27	1.32
	1kN/m	0.85	0.37	2.52
	0N/m	0.86	0.39	1.15
Thigh Transversal	2kN/m	0.91	1.52	1.39
	1kN/m	0.95	1.35	3.15
	0N/m	0.96	1.05	3.41
Thigh Longitudinal	2kN/m	0.96	0.34	3.18
	1kN/m	0.97	0.33	4.93
	0N/m	0.97	0.32	4.06
Thigh Sagittal	2kN/m	0.90	0.12	1.17
	1kN/m	0.74	0.24	0.54
	0N/m	0.84	0.25	0.74

Table C-27: Statistical and effect size results of the linear regressions fitted to the thigh pressures with longitudinal translation at the thigh interface permitted.

	Spring Stiffness	R2	RMSE	Cohen's D
Proximal Lateral	2kN/m	0.28	165.74	5.30
	1kN/m	0.50	153.94	6.32
	0N/m	0.33	189.90	4.48
Proximal Central	2kN/m	0.52	116.48	8.63
	1kN/m	0.40	157.34	6.68
	0N/m	0.00	296.88	3.74
Proximal Medial	2kN/m	0.29	192.95	5.78
	1kN/m	0.38	143.85	7.07
	0N/m	0.01	484.08	2.52
Distal Lateral	2kN/m	0.28	178.07	4.38
	1kN/m	0.50	162.16	5.38
	0N/m	0.29	214.55	3.82
Distal Central	2kN/m	0.47	127.41	4.96
	1kN/m	0.35	164.21	3.83
	0N/m	0.05	340.00	2.43
Distal Medial	2kN/m	0.28	189.25	4.77
	1kN/m	0.38	139.95	6.34
	0N/m	0.01	485.96	2.42

Table C-28: Statistical and effect size results of the linear regressions fitted to the shank pressures with longitudinal translation at the thigh interface permitted.

	Spring Stiffness	R2	RMSE	Cohen's D
Proximal Lateral	2kN/m	0.40	124.63	5.62
	1kN/m	0.08	225.42	3.93
	0N/m	0.21	236.52	3.74
Proximal Central	2kN/m	0.95	14.48	2.79
	1kN/m	0.95	14.74	2.22
	0N/m	0.97	10.31	0.80
Proximal Medial	2kN/m	0.83	771.90	1.43
	1kN/m	0.67	776.46	3.71
	0N/m	0.71	937.72	2.74
Distal Lateral	2kN/m	0.22	126.58	4.19
	1kN/m	0.46	179.58	3.19
	0N/m	0.19	149.71	3.27
Distal Central	2kN/m	0.95	8.27	2.01
	1kN/m	0.94	9.91	1.09
	0N/m	0.96	7.51	0.36
Distal Medial	2kN/m	0.75	255.74	2.92
	1kN/m	0.49	329.10	4.71
	0N/m	0.62	341.58	3.63

Table C-29: Statistical and effect size results of the linear regressions fitted to the relative displacement of the limb segments and brace with sagittal rotation at the thigh interface permitted.

	Spring Stiffness	R2	RMSE	Cohen's D
Shank Transversal	1.2N/rad	0.57	0.31	0.35
	0.6N/rad	0.77	0.18	0.34
	0N/rad	0.82	0.18	0.48
Shank Longitudinal	1.2N/rad	0.96	1.00	3.46
	0.6N/rad	0.98	0.57	3.52
	0N/rad	0.97	0.73	3.73
Shank Sagittal	1.2N/rad	0.53	0.36	3.49
	0.6N/rad	0.78	0.22	4.85
	0N/rad	0.48	0.39	2.71
Thigh Transversal	1.2N/rad	0.79	2.64	1.40
	0.6N/rad	0.92	1.48	2.40
	0N/rad	0.93	1.50	2.59
Thigh Longitudinal	1.2N/rad	0.86	0.69	1.80
	0.6N/rad	0.99	0.21	5.24
	0N/rad	0.98	0.29	3.93
Thigh Sagittal	1.2N/rad	0.73	0.21	0.75
	0.6N/rad	0.87	0.10	1.46
	0N/rad	0.79	0.25	0.54

Table C-30: Statistical and effect size results of the linear regressions fitted to the thigh pressures with sagittal rotation at the thigh interface permitted.

	Spring Stiffness	R2	RMSE	Cohen's D
Proximal Lateral	1.2N/rad	0.25	156.60	4.47
	0.6N/rad	0.23	179.28	3.20
	0N/rad	0.26	132.72	6.57
Proximal Central	1.2N/rad	0.44	221.88	3.29
	0.6N/rad	0.13	252.01	2.69
	0N/rad	0.37	170.39	5.62
Proximal Medial	1.2N/rad	0.26	185.74	7.41
	0.6N/rad	0.13	257.89	7.47
	0N/rad	0.43	120.66	11.47
Distal Lateral	1.2N/rad	0.25	176.12	4.37
	0.6N/rad	0.22	186.04	4.09
	0N/rad	0.24	143.53	5.96
Distal Central	1.2N/rad	0.33	215.20	2.41
	0.6N/rad	0.11	199.99	4.41
	0N/rad	0.28	172.01	3.18
Distal Medial	1.2N/rad	0.24	190.90	6.32
	0.6N/rad	0.14	217.01	8.61
	0N/rad	0.41	115.94	10.24

Table C-31: Statistical and effect size results of the linear regressions fitted to the shank pressures with sagittal rotation at the thigh interface permitted.

	Spring Stiffness	R2	RMSE	Cohen's D
Proximal Lateral	1.2N/rad	0.12	304.93	4.25
	0.6N/rad	0.68	121.85	6.49
	0N/rad	0.24	197.43	4.80
Proximal Central	1.2N/rad	0.89	9.81	6.02
	0.6N/rad	0.92	5.44	10.13
	0N/rad	0.93	8.44	5.71
Proximal Medial	1.2N/rad	0.90	259.63	8.95
	0.6N/rad	0.91	280.31	8.11
	0N/rad	0.87	430.92	7.32
Distal Lateral	1.2N/rad	0.31	122.35	9.70
	0.6N/rad	0.71	73.15	12.92
	0N/rad	0.16	94.97	12.06
Distal Central	1.2N/rad	0.88	6.60	6.14
	0.6N/rad	0.91	3.73	9.60
	0N/rad	0.94	5.02	6.54
Distal Medial	1.2N/rad	0.83	217.36	4.54
	0.6N/rad	0.94	143.15	4.63
	0N/rad	0.88	199.14	4.34

Table C-32: Statistical and effect size results of the linear regressions fitted to the relative displacement of the limb segments and brace with sagittal translation at the thigh interface permitted.

	Spring Stiffness	R2	RMSE	Cohen's D
Shank Transversal	2kN/m	0.70	0.35	0.40
	1kN/m	0.76	0.21	0.33
	0N/m	0.72	0.23	0.23
Shank Longitudinal	2kN/m	0.88	1.87	2.32
	1kN/m	0.98	0.55	3.55
	0N/m	0.97	0.67	3.23
Shank Sagittal	2kN/m	0.76	0.52	1.16
	1kN/m	0.95	0.19	2.45
	0N/m	0.80	0.48	0.68
Thigh Transversal	2kN/m	0.83	2.19	1.38
	1kN/m	0.96	0.95	3.30
	0N/m	0.87	1.83	2.14
Thigh Longitudinal	2kN/m	0.84	0.75	1.51
	1kN/m	0.98	0.21	3.44
	0N/m	0.79	0.62	0.54
Thigh Sagittal	2kN/m	0.89	0.31	2.06
	1kN/m	0.98	0.12	3.72
	0N/m	0.83	0.47	1.92

Table C-33: Statistical and effect size results of the linear regressions fitted to the thigh pressures with sagittal translation at the thigh interface permitted.

	Spring Stiffness	R2	RMSE	Cohen's D
Proximal Lateral	2kN/m	0.29	174.96	2.65
	1kN/m	0.23	143.00	8.49
	0N/m	0.45	117.83	9.42
Proximal Central	2kN/m	0.29	332.46	0.79
	1kN/m	0.33	164.51	6.72
	0N/m	0.67	99.51	9.34
Proximal Medial	2kN/m	0.09	364.59	1.68
	1kN/m	0.21	217.46	3.41
	0N/m	0.63	110.48	9.72
Distal Lateral	2kN/m	0.20	216.21	3.22
	1kN/m	0.20	175.88	7.12
	0N/m	0.44	128.95	8.95
Distal Central	2kN/m	0.17	355.50	1.27
	1kN/m	0.25	168.73	4.37
	0N/m	0.68	92.08	6.48
Distal Medial	2kN/m	0.08	361.83	2.07
	1kN/m	0.23	208.74	3.27
	0N/m	0.69	101.98	9.13

Table C-34: Statistical and effect size results of the linear regressions fitted to the shank pressures with sagittal translation at the thigh interface permitted.

	Spring Stiffness	R2	RMSE	Cohen's D
Proximal Lateral	2kN/m	0.36	221.99	5.52
	1kN/m	0.36	176.28	5.92
	0N/m	0.06	256.59	4.54
Proximal Central	2kN/m	0.88	22.12	0.30
	1kN/m	0.89	14.07	2.17
	0N/m	0.73	23.96	1.38
Proximal Medial	2kN/m	0.82	487.32	7.71
	1kN/m	0.88	314.34	9.00
	0N/m	0.71	487.75	8.22
Distal Lateral	2kN/m	0.11	152.07	8.10
	1kN/m	0.30	97.80	10.14
	0N/m	0.25	111.77	9.84
Distal Central	2kN/m	0.86	15.24	0.49
	1kN/m	0.87	9.28	2.99
	0N/m	0.74	13.37	2.23
Distal Medial	2kN/m	0.68	320.36	5.91
	1kN/m	0.72	255.25	5.50
	0N/m	0.52	321.18	5.12

Table C-35: Statistical and effect size results of the linear regressions fitted to the relative displacement of the limb segments and brace with transverse rotation at the thigh interface permitted.

	Spring Stiffness	R2	RMSE	Cohen's D
Shank Transversal	1.2N/rad	0.94	0.16	0.86
	0.6N/rad	0.89	0.19	0.29
	0N/rad	0.91	0.20	0.68
Shank Longitudinal	1.2N/rad	0.97	0.71	3.14
	0.6N/rad	0.97	0.60	1.68
	0N/rad	0.96	0.80	1.77
Shank Sagittal	1.2N/rad	0.90	0.15	6.01
	0.6N/rad	0.89	0.15	6.62
	0N/rad	0.92	0.12	7.18
Thigh Transversal	1.2N/rad	0.77	1.42	0.08
	0.6N/rad	0.61	2.20	0.36
	0N/rad	0.82	1.30	0.46
Thigh Longitudinal	1.2N/rad	0.67	0.67	0.15
	0.6N/rad	0.87	0.37	0.86
	0N/rad	0.66	0.62	0.27
Thigh Sagittal	1.2N/rad	0.89	0.13	0.29
	0.6N/rad	0.74	0.13	2.04
	0N/rad	0.83	0.12	0.79

Table C-36: Statistical and effect size results of the linear regressions fitted to the thigh pressures with transverse rotation at the thigh interface permitted.

	Spring Stiffness	R2	RMSE	Cohen's D
Proximal Lateral	1.2N/rad	0.20	218.48	2.26
	0.6N/rad	0.07	173.35	7.84
	0N/rad	0.17	273.74	1.83
Proximal Central	1.2N/rad	0.39	293.24	1.65
	0.6N/rad	0.02	318.99	2.50
	0N/rad	0.15	459.22	1.80
Proximal Medial	1.2N/rad	0.15	318.45	2.21
	0.6N/rad	0.03	340.51	1.81
	0N/rad	0.09	440.65	1.69
Distal Lateral	1.2N/rad	0.14	240.53	2.66
	0.6N/rad	0.05	201.84	7.98
	0N/rad	0.12	298.84	1.93
Distal Central	1.2N/rad	0.29	283.95	2.09
	0.6N/rad	0.02	217.02	3.97
	0N/rad	0.09	443.65	1.58
Distal Medial	1.2N/rad	0.13	301.60	2.83
	0.6N/rad	0.04	261.82	2.85
	0N/rad	0.08	422.60	1.84

Table C-37: Statistical and effect size results of the linear regressions fitted to the shank pressures with transverse rotation at the thigh interface permitted.

	Spring Stiffness	R2	RMSE	Cohen's D
Proximal Lateral	1.2N/rad	0.64	115.17	12.77
	0.6N/rad	0.83	100.00	13.33
	0N/rad	0.14	148.58	9.12
Proximal Central	1.2N/rad	0.59	5.03	12.20
	0.6N/rad	0.21	5.97	10.95
	0N/rad	0.86	3.05	8.10
Proximal Medial	1.2N/rad	0.44	353.17	7.56
	0.6N/rad	0.33	645.01	3.62
	0N/rad	0.47	632.27	2.73
Distal Lateral	1.2N/rad	0.78	103.76	9.37
	0.6N/rad	0.82	97.25	10.61
	0N/rad	0.63	118.97	6.56
Distal Central	1.2N/rad	0.57	4.43	9.90
	0.6N/rad	0.21	5.50	9.01
	0N/rad	0.84	2.91	4.34
Distal Medial	1.2N/rad	0.71	180.96	6.36
	0.6N/rad	0.56	304.23	2.90
	0N/rad	0.74	258.63	0.97

Table C-38: Statistical and effect size results of the linear regressions fitted to the relative displacement of the limb segments and brace with transverse translation at the thigh interface permitted.

	Spring Stiffness	R2	RMSE	Cohen's D
Shank Transversal	2kN/m	0.14	0.91	0.43
	1kN/m	0.72	0.31	2.79
	0N/m	0.10	1.07	0.46
Shank Longitudinal	2kN/m	0.86	1.79	2.84
	1kN/m	0.97	0.80	4.33
	0N/m	0.69	3.34	1.34
Shank Sagittal	2kN/m	0.62	0.83	0.97
	1kN/m	0.81	0.39	0.61
	0N/m	0.54	0.66	1.12
Thigh Transversal	2kN/m	0.45	3.41	0.18
	1kN/m	0.79	2.28	0.59
	0N/m	0.62	3.05	1.60
Thigh Longitudinal	2kN/m	0.95	0.36	2.12
	1kN/m	0.97	0.30	2.99
	0N/m	0.85	0.71	1.46
Thigh Sagittal	2kN/m	0.56	0.27	0.21
	1kN/m	0.64	0.16	0.93
	0N/m	0.30	0.32	0.98

Table C-39: Statistical and effect size results of the linear regressions fitted to the thigh pressures with transverse translation at the thigh interface permitted.

	Spring Stiffness	R2	RMSE	Cohen's D
Proximal Lateral	2kN/m	0.11	194.29	6.28
	1kN/m	0.16	189.51	3.03
	0N/m	0.22	163.00	2.86
Proximal Central	2kN/m	0.02	329.09	3.40
	1kN/m	0.23	331.40	1.72
	0N/m	0.32	249.02	2.05
Proximal Medial	2kN/m	0.07	290.36	5.20
	1kN/m	0.00	469.23	2.48
	0N/m	0.13	268.53	3.64
Distal Lateral	2kN/m	0.13	205.33	6.09
	1kN/m	0.15	204.06	2.55
	0N/m	0.20	180.49	3.21
Distal Central	2kN/m	0.02	309.29	2.72
	1kN/m	0.19	333.09	0.05
	0N/m	0.25	243.23	1.58
Distal Medial	2kN/m	0.06	291.37	4.72
	1kN/m	0.07	444.35	1.67
	0N/m	0.11	262.09	3.29

Table C-40: Statistical and effect size results of the linear regressions fitted to the shank pressures with transverse translation at the thigh interface permitted.

	Spring Stiffness	R2	RMSE	Cohen's D
Proximal Lateral	2kN/m	0.48	152.44	8.50
	1kN/m	0.46	156.93	7.87
	0N/m	0.27	230.21	8.69
Proximal Central	2kN/m	0.87	5.11	9.43
	1kN/m	0.71	5.64	12.05
	0N/m	0.67	6.19	11.39
Proximal Medial	2kN/m	0.82	425.78	8.00
	1kN/m	0.77	307.07	10.09
	0N/m	0.65	589.07	7.96
Distal Lateral	2kN/m	0.44	126.14	9.34
	1kN/m	0.60	94.49	10.28
	0N/m	0.69	123.75	11.43
Distal Central	2kN/m	0.83	3.85	8.71
	1kN/m	0.66	4.80	10.34
	0N/m	0.69	3.92	11.66
Distal Medial	2kN/m	0.86	191.70	6.51
	1kN/m	0.64	289.90	5.27
	0N/m	0.59	393.04	5.06

Appendix D – Experimental Data

Shank Longitudinal Rotational

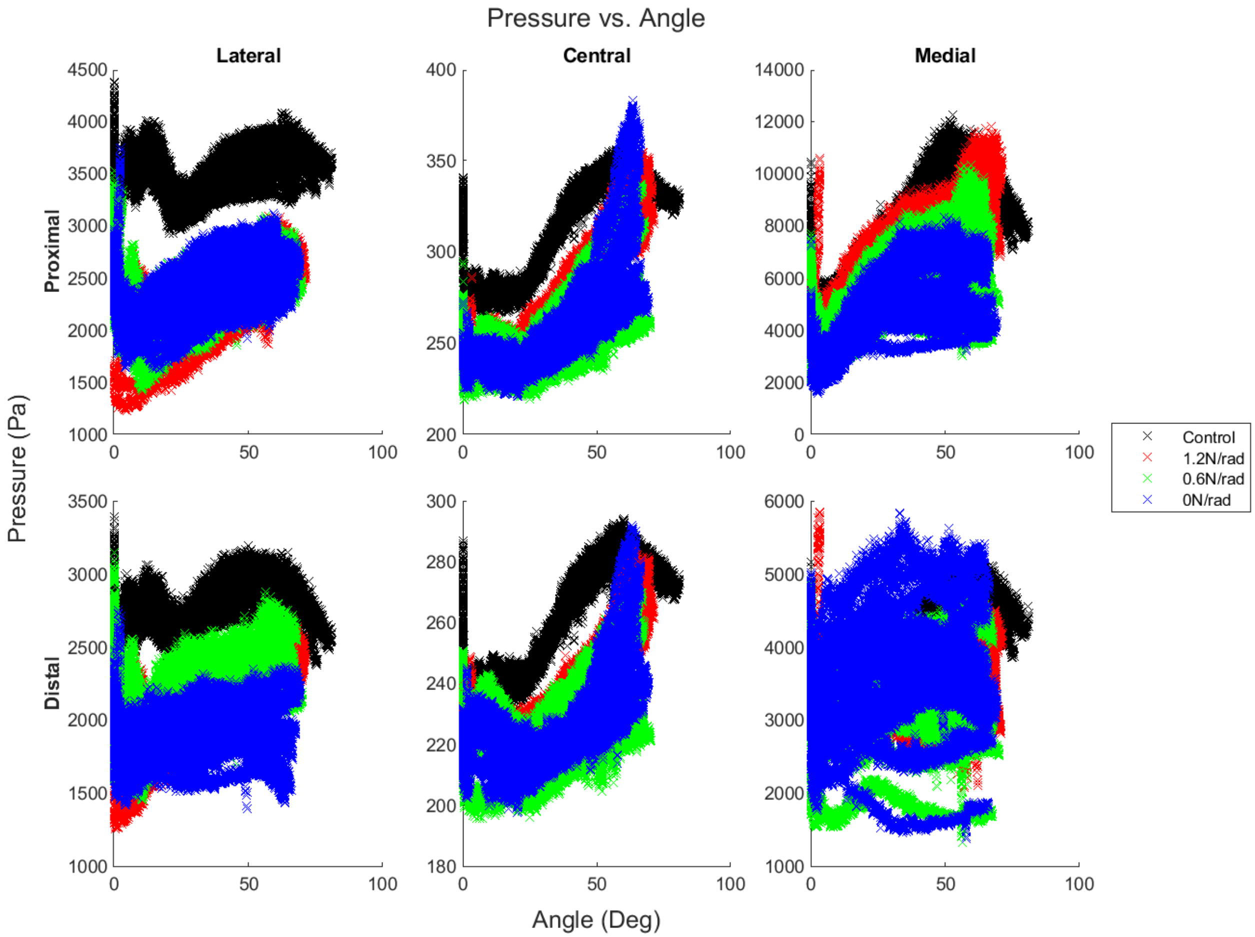

Figure D.1: Pressure readings on the shank with longitudinal rotation permitted on the shank interface.

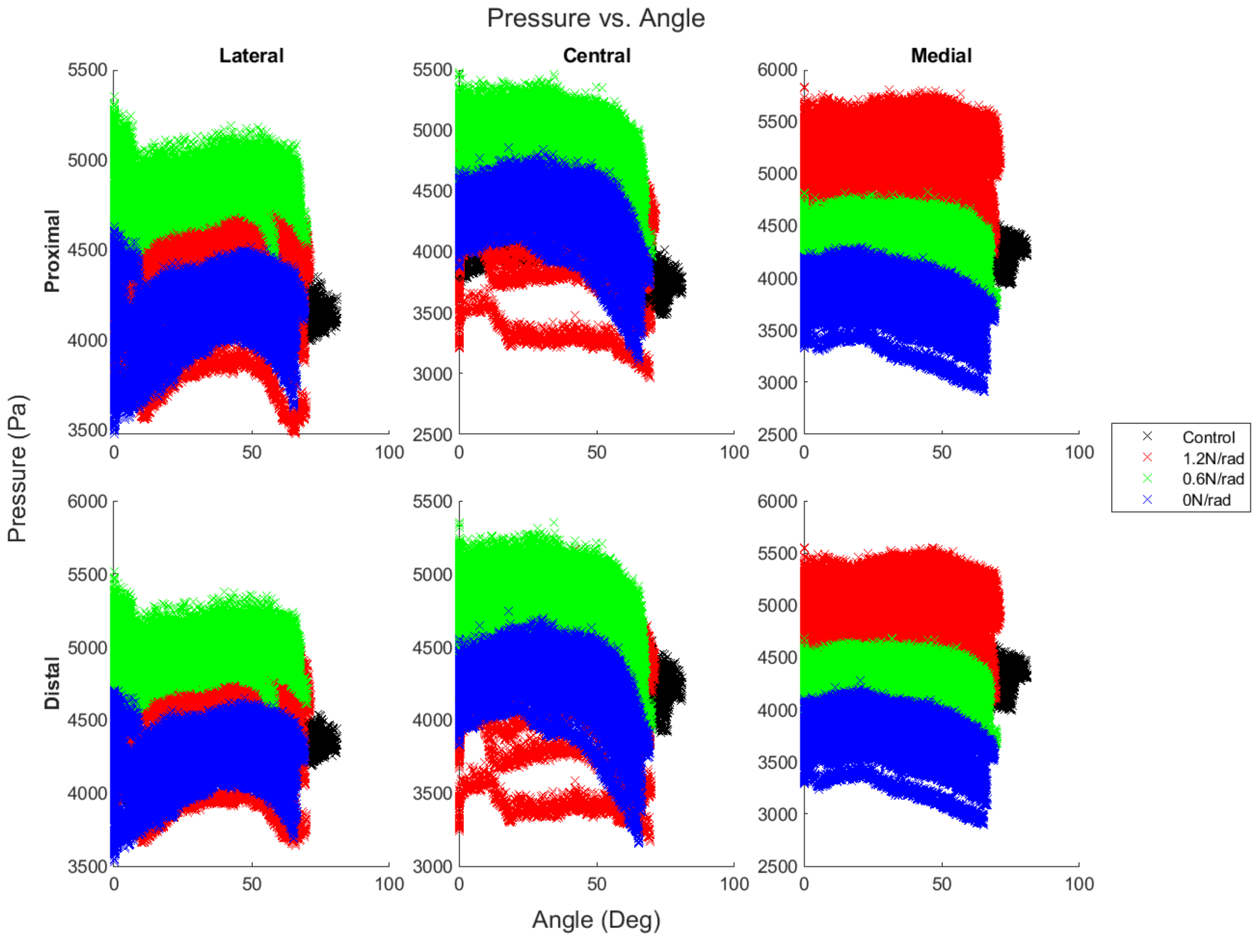

Figure D.2: Pressure readings on the thigh with longitudinal rotation permitted on the shank interface.

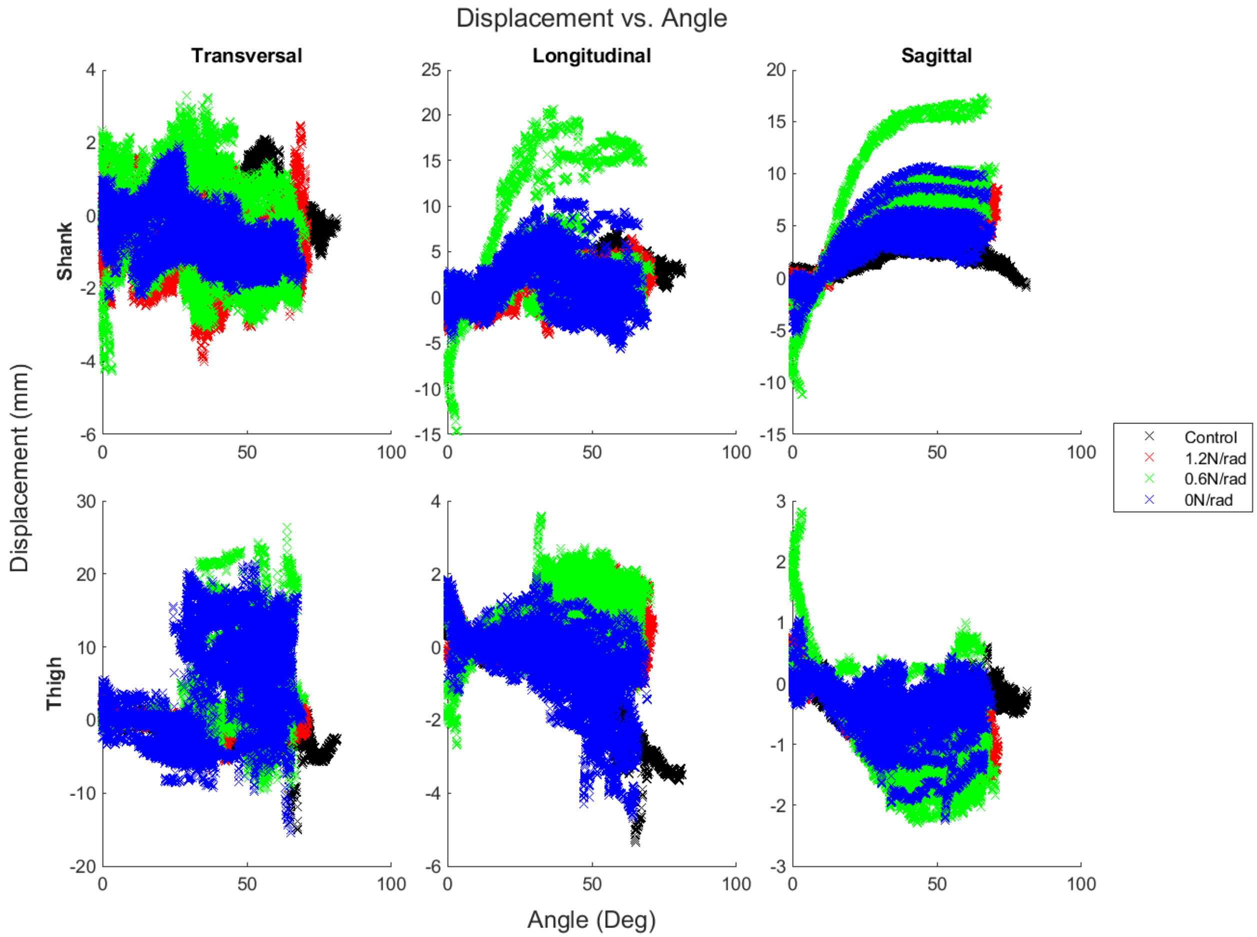

Figure D.3: Relative displacements of the limb segments and brace with longitudinal rotation at the shank interface permitted.

Shank Longitudinal Translational

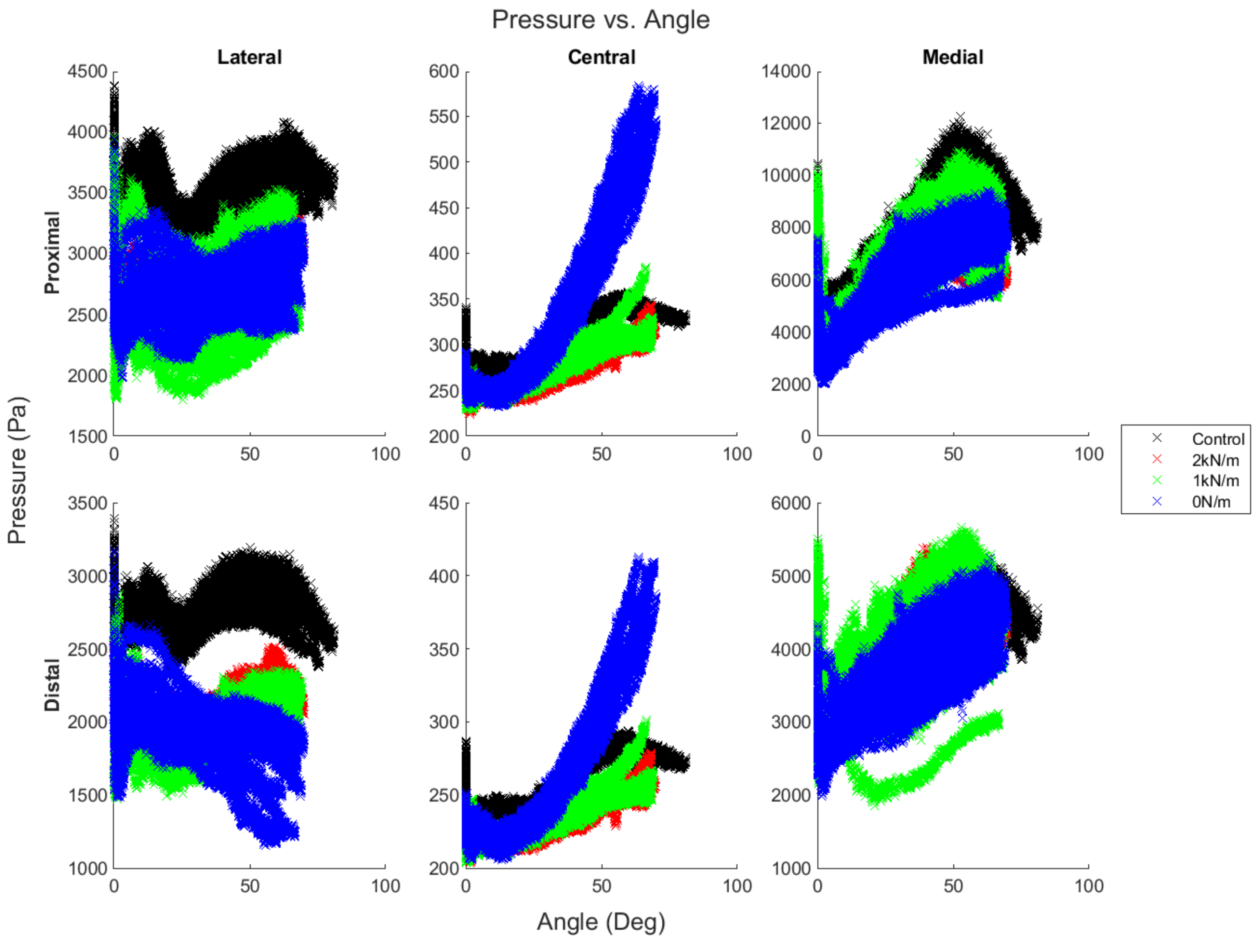

Figure D.4: Pressure readings on the shank with longitudinal translation permitted on the shank interface.

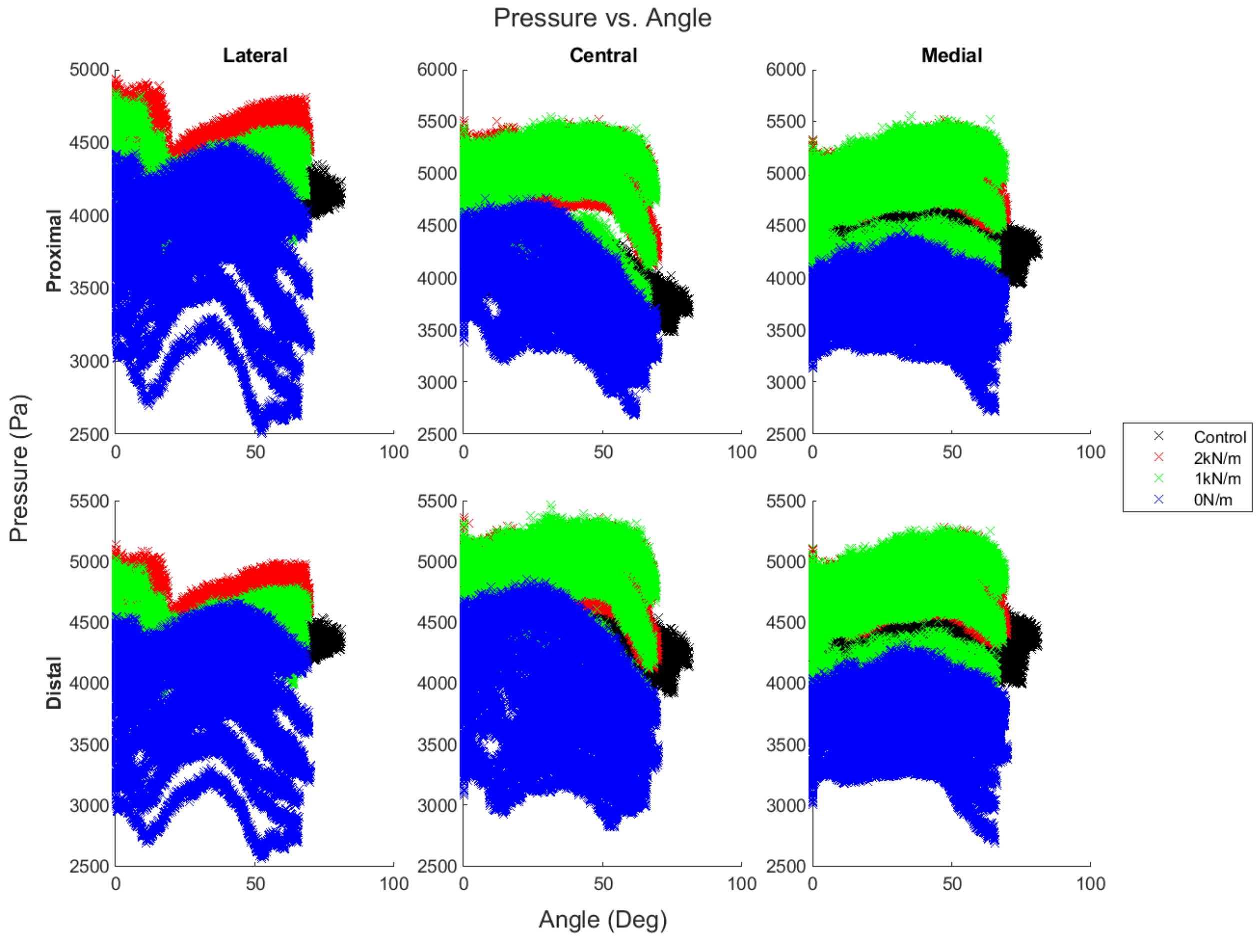

Figure D.5: Pressure readings on the thigh with longitudinal translation permitted on the shank interface.

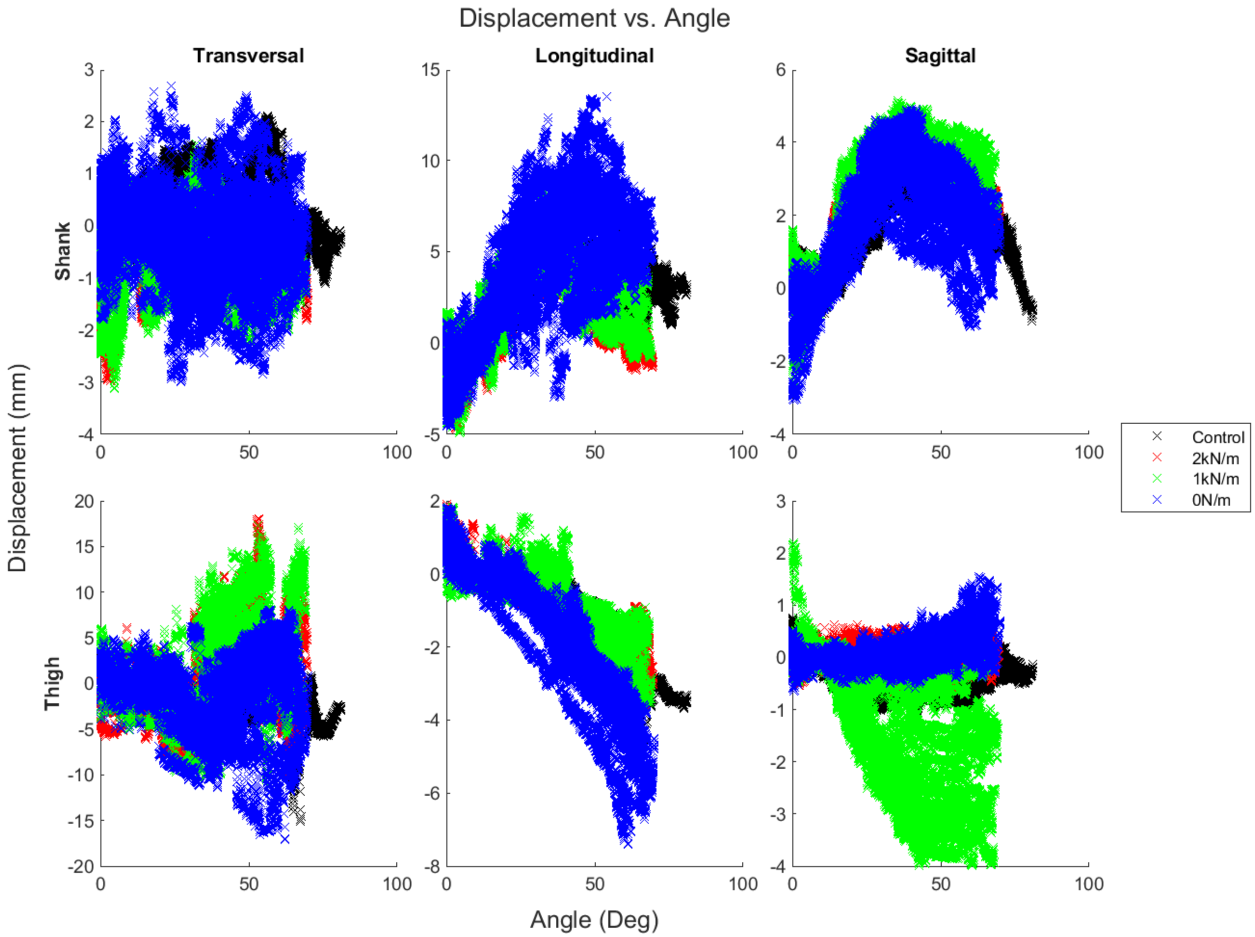

Figure D.6: Relative displacements of the limb segments and brace with longitudinal translation at the shank interface permitted.

Shank Sagittal Rotational

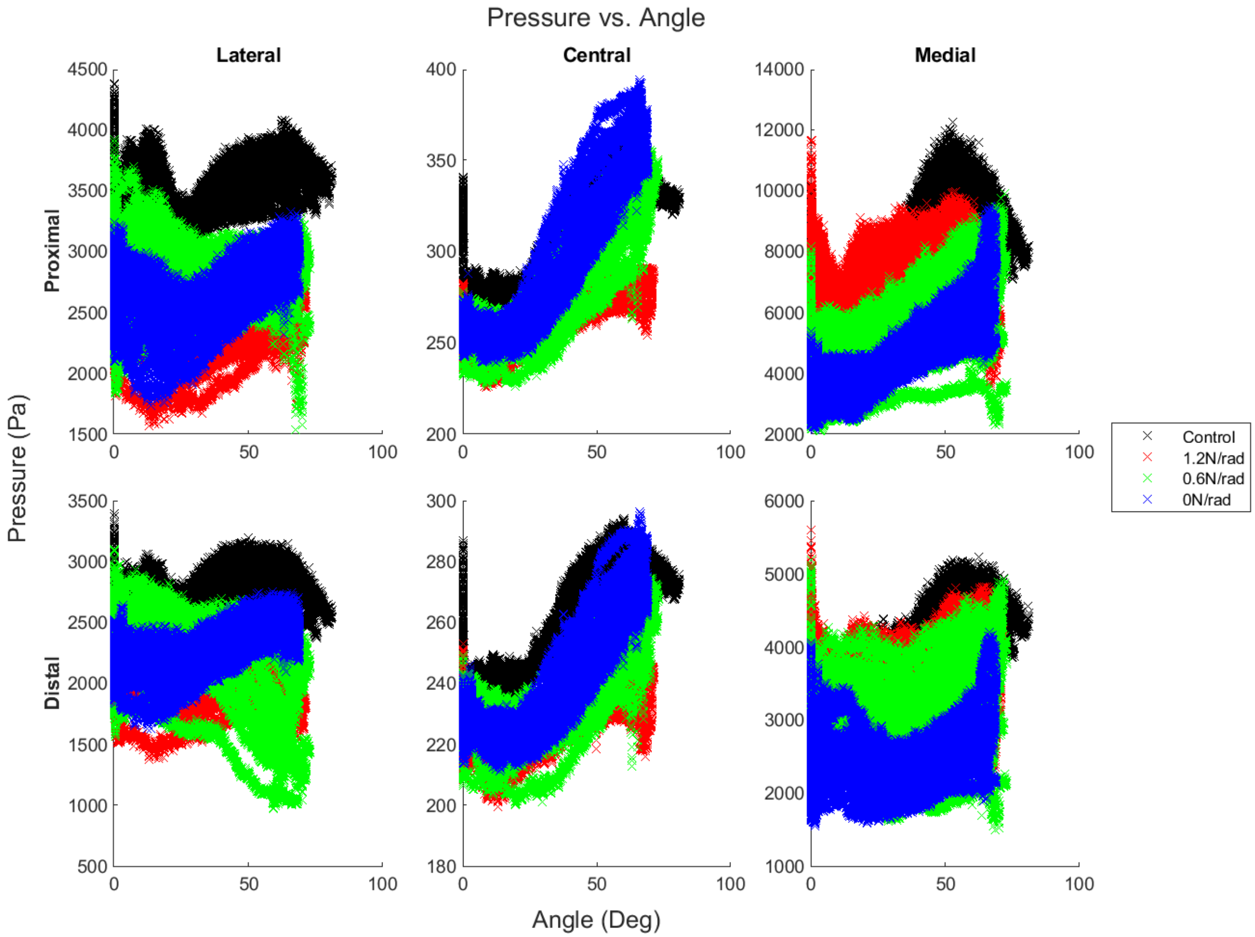

Figure D.7: Pressure readings on the shank with sagittal rotation permitted on the shank interface.

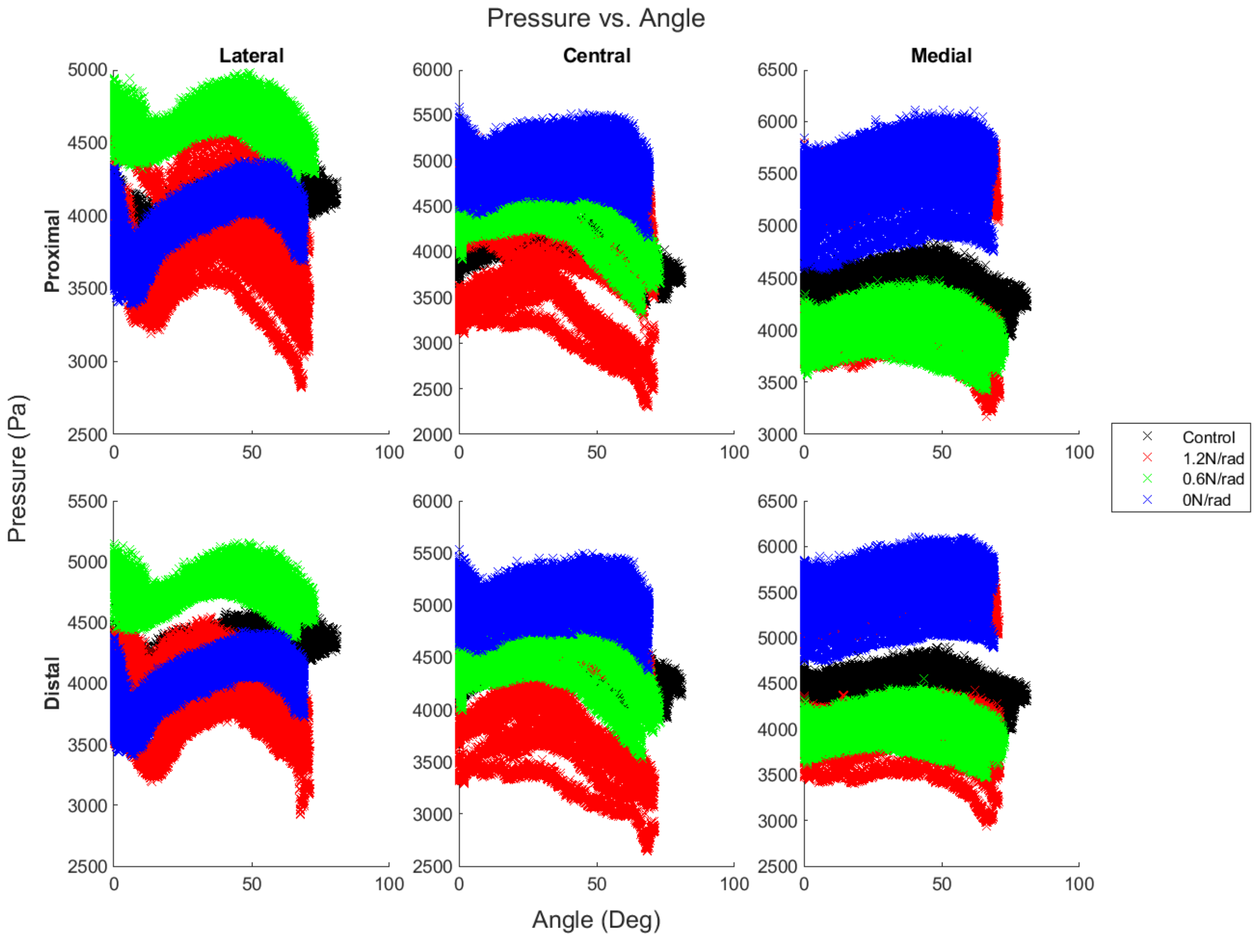

Figure D.8: Pressure readings on the thigh with sagittal rotation permitted on the shank interface.

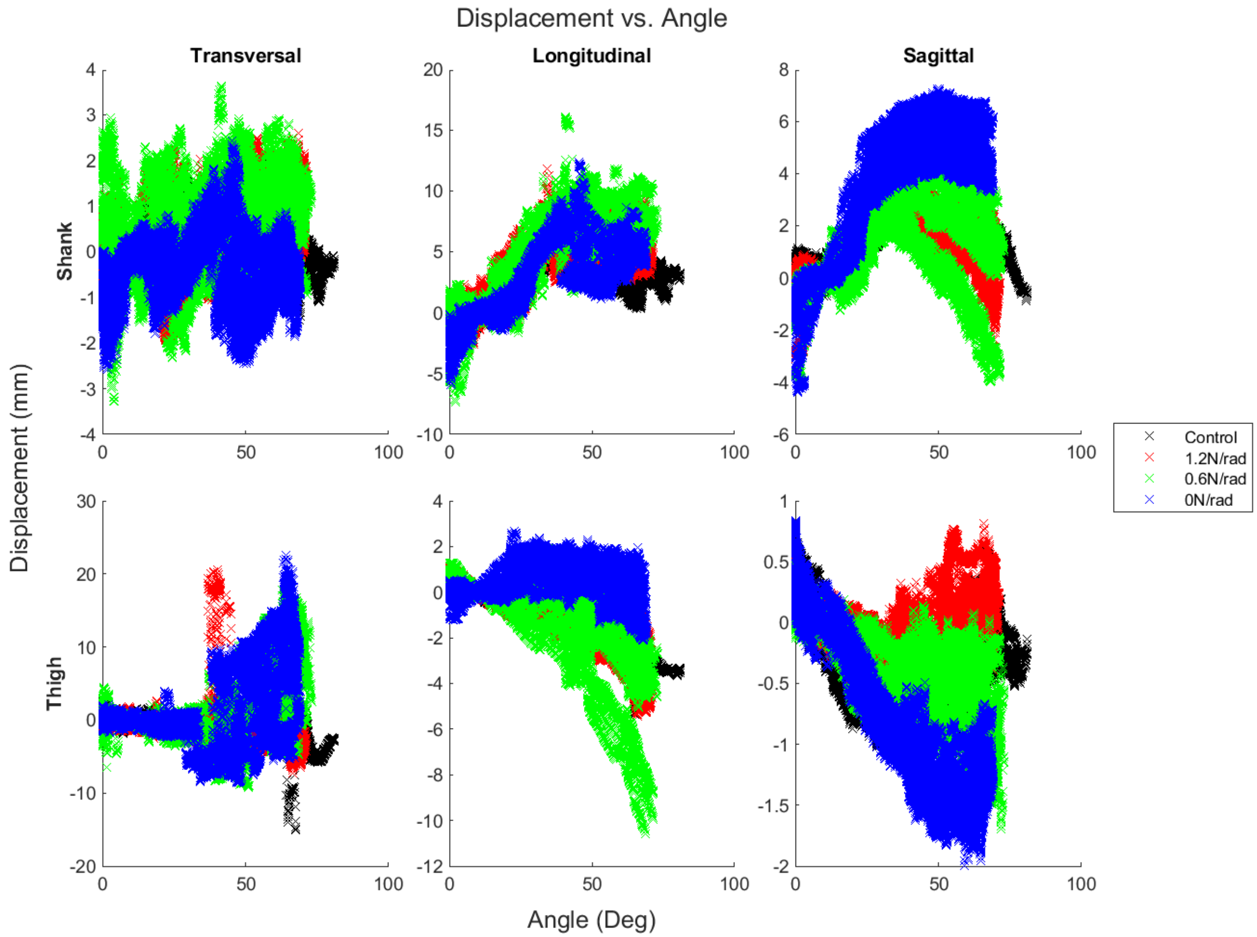

Figure D.9: Relative displacements of the limb segments and brace with sagittal rotation at the shank interface permitted.

Shank Sagittal Translational

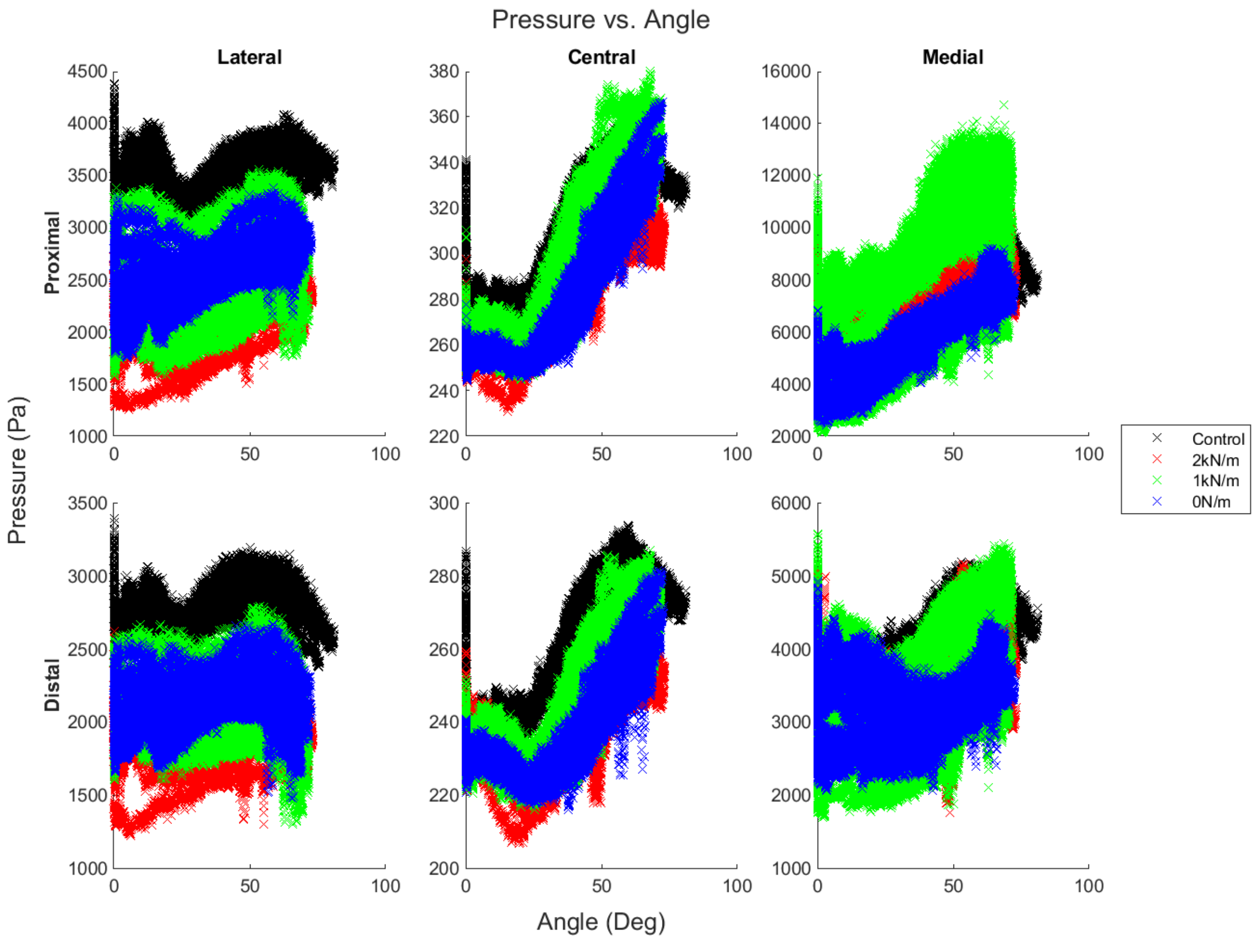

Figure D.10: Pressure readings on the shank with sagittal translation permitted on the shank interface.

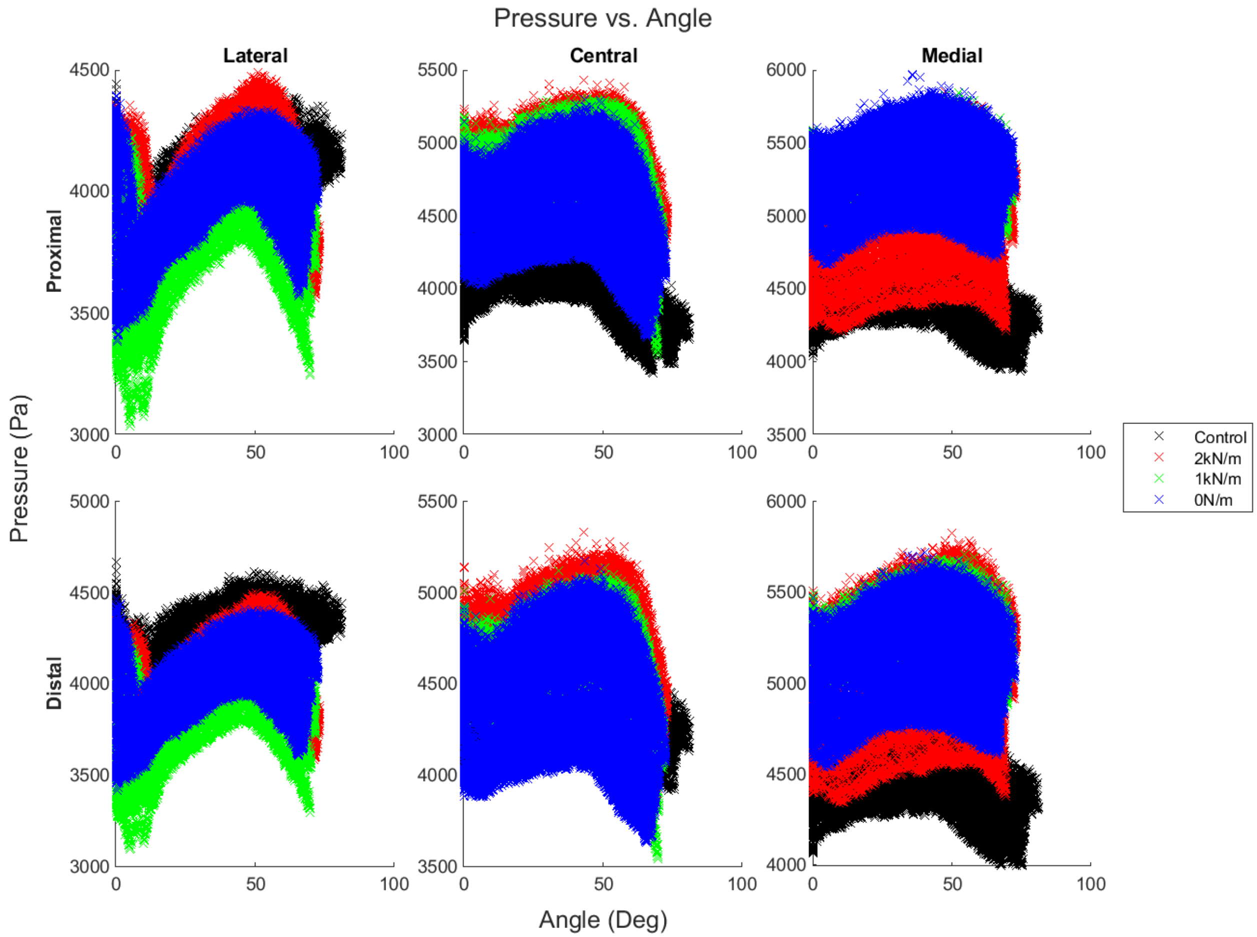

Figure D.11: Pressure readings on the thigh with sagittal translation permitted on the shank interface.

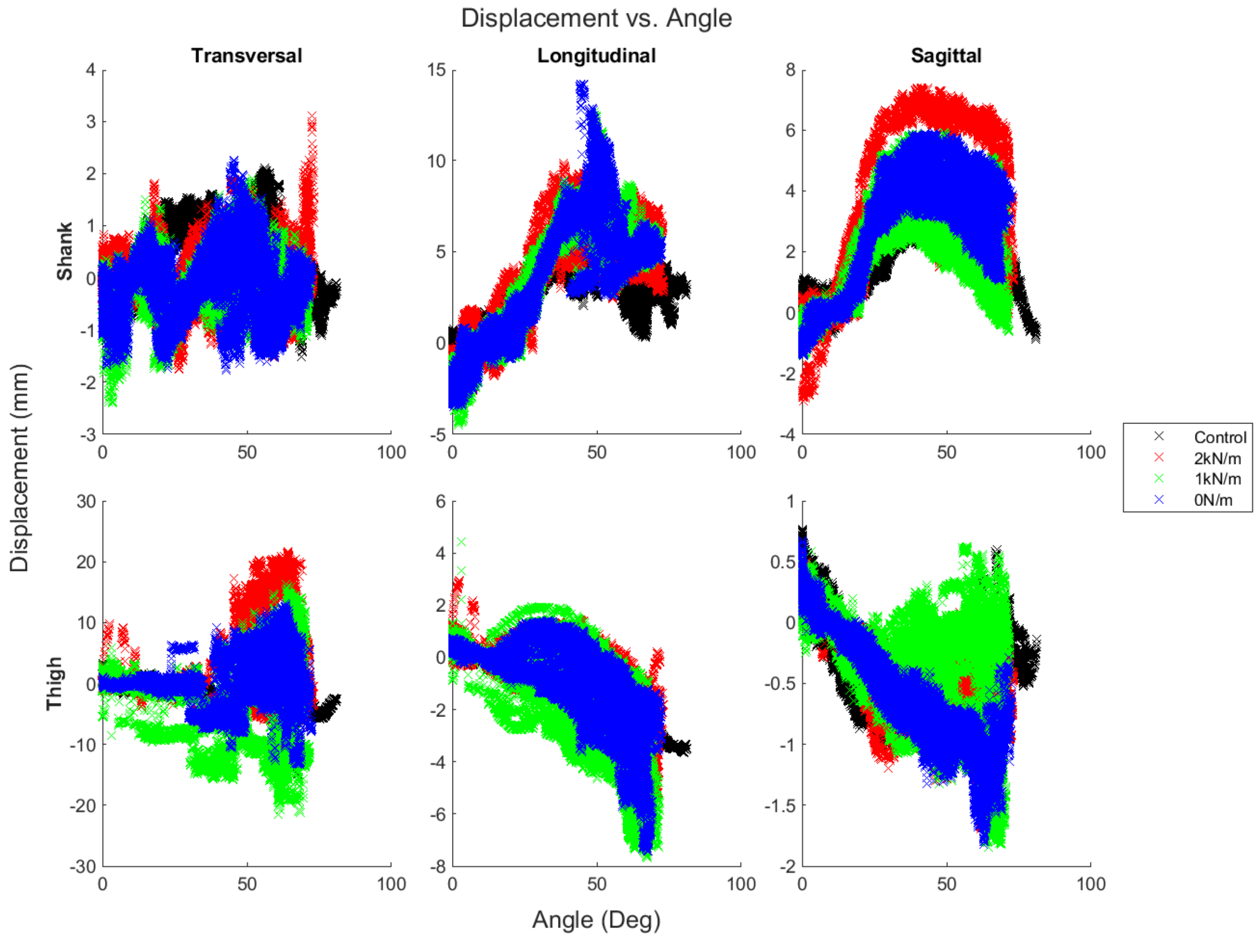

Figure D.12: Relative displacements of the limb segments and brace with sagittal translation at the shank interface permitted.

Shank Transverse Rotational

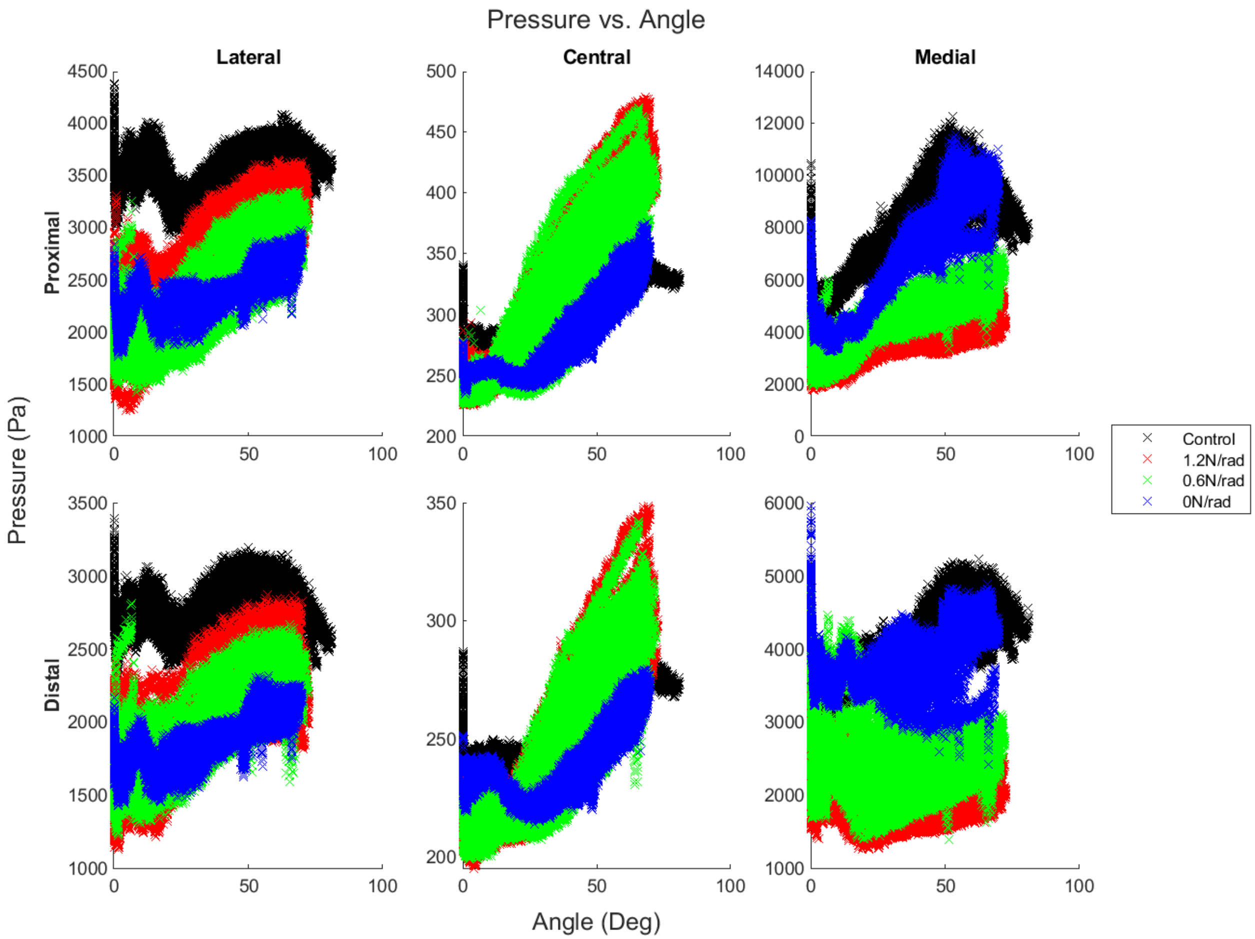

Figure D.13: Pressure readings on the shank with transverse rotation permitted on the shank interface.

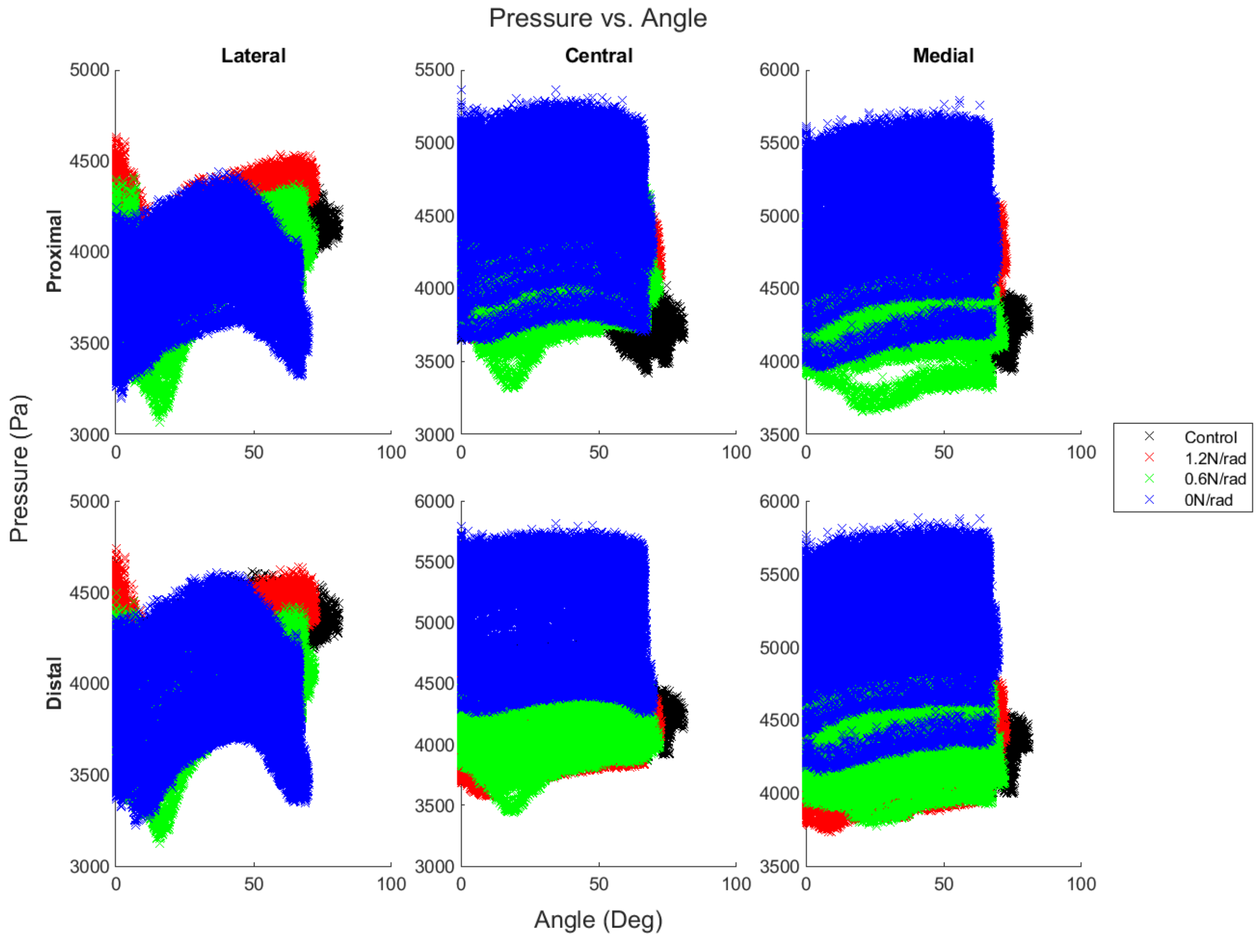

Figure D.14: Pressure readings on the thigh with transverse rotation permitted on the shank interface.

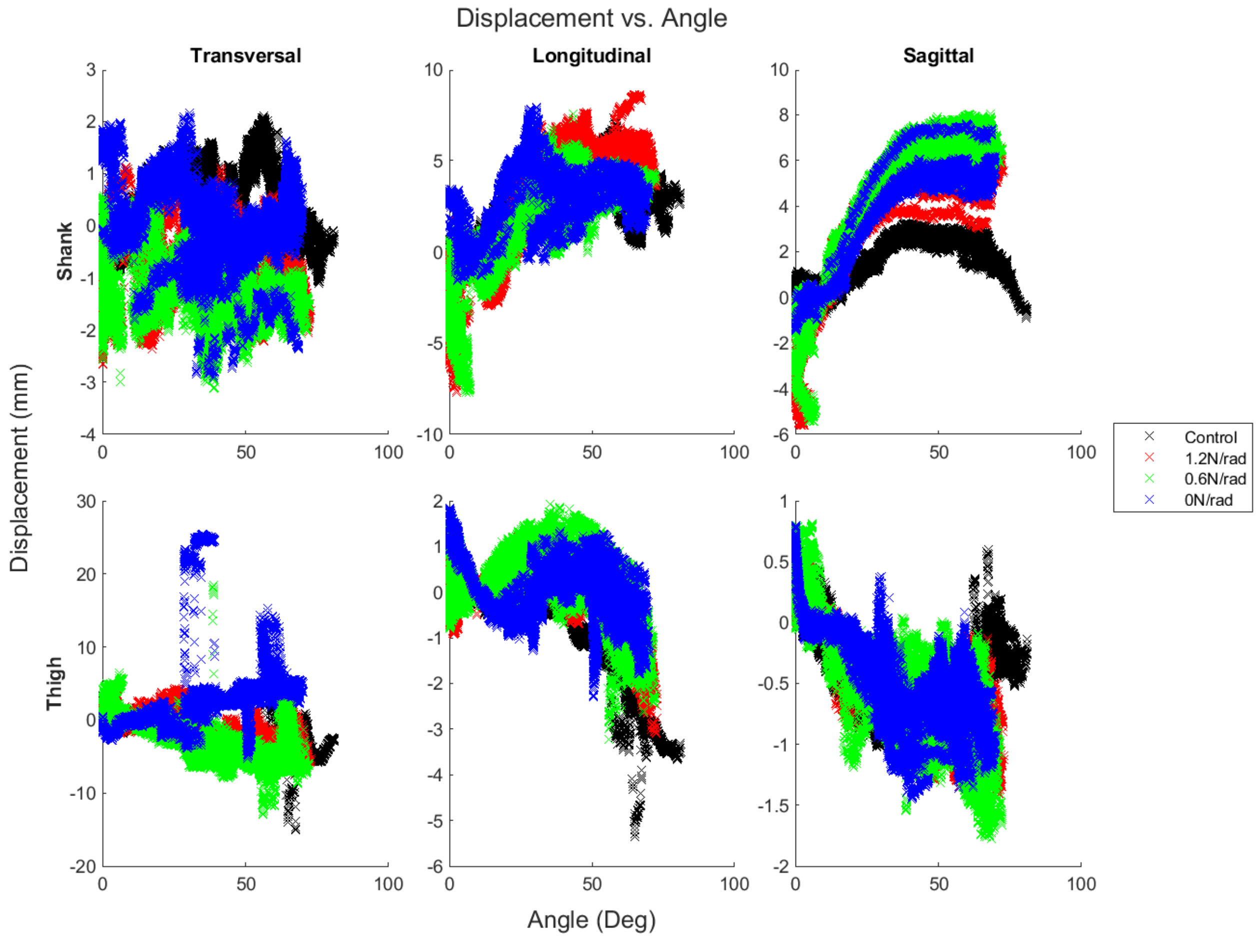

Figure D.15: Relative displacements of the limb segments and brace with transverse rotation at the shank interface permitted.

Shank Transverse Translational

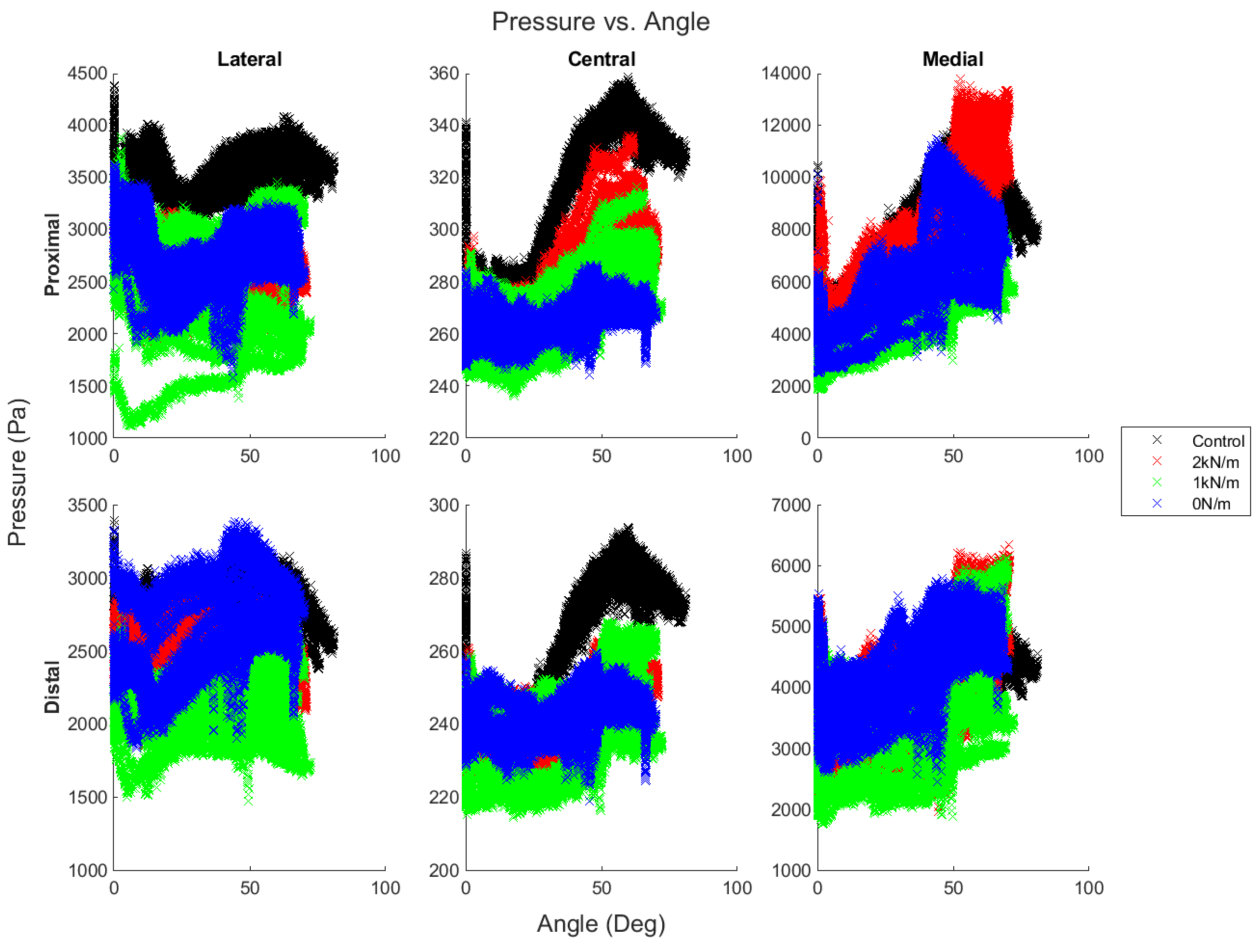

Figure D.16: Pressure readings on the shank with transverse translation permitted on the shank interface.

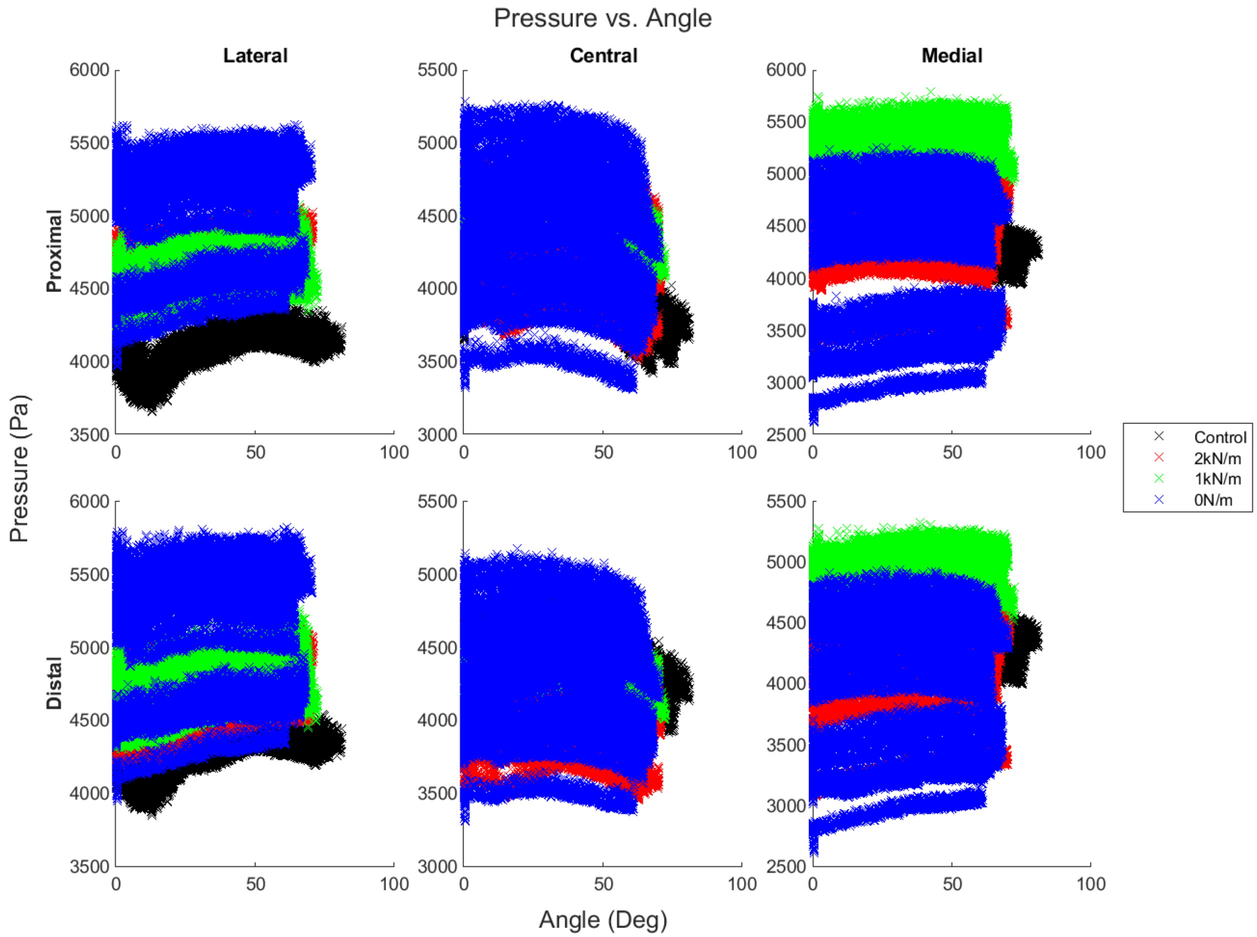

Figure D.17: Pressure readings on the thigh with transverse translation permitted on the shank interface.

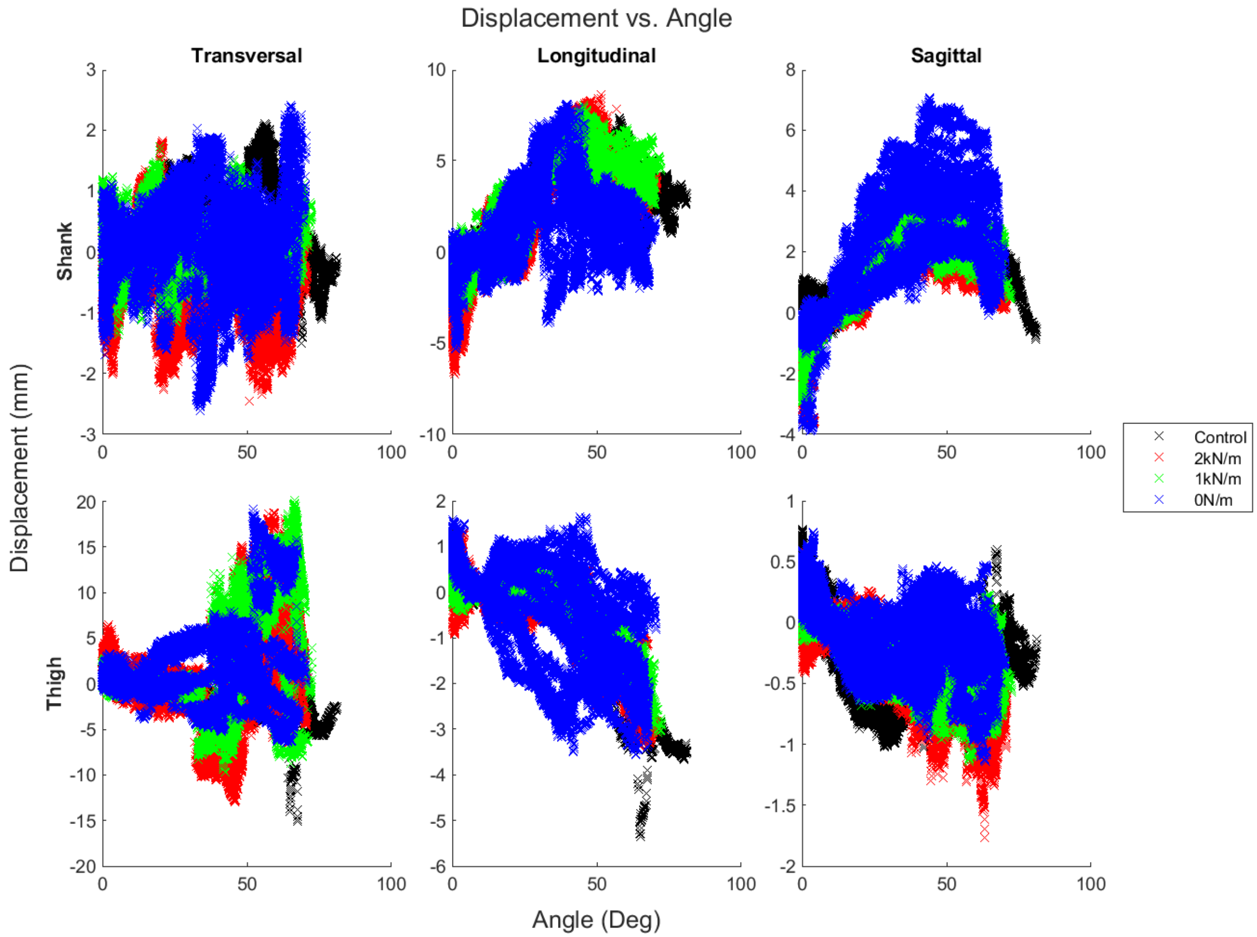

Figure D.18: Relative displacements of the limb segments and brace with transverse translation at the shank interface permitted.

Thigh Longitudinal Rotational

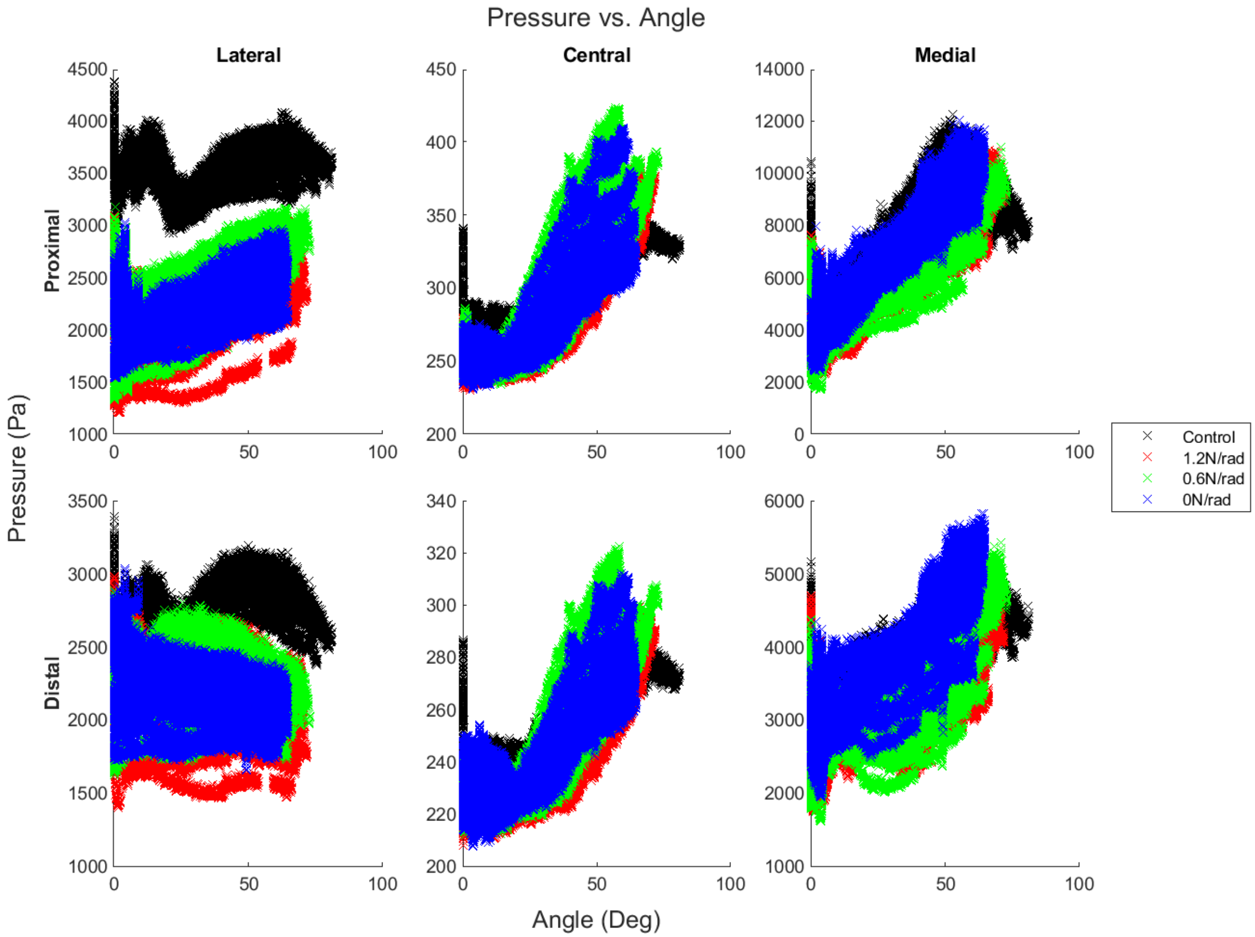

Figure D.19: Pressure readings on the shank with longitudinal rotation permitted on the thigh interface.

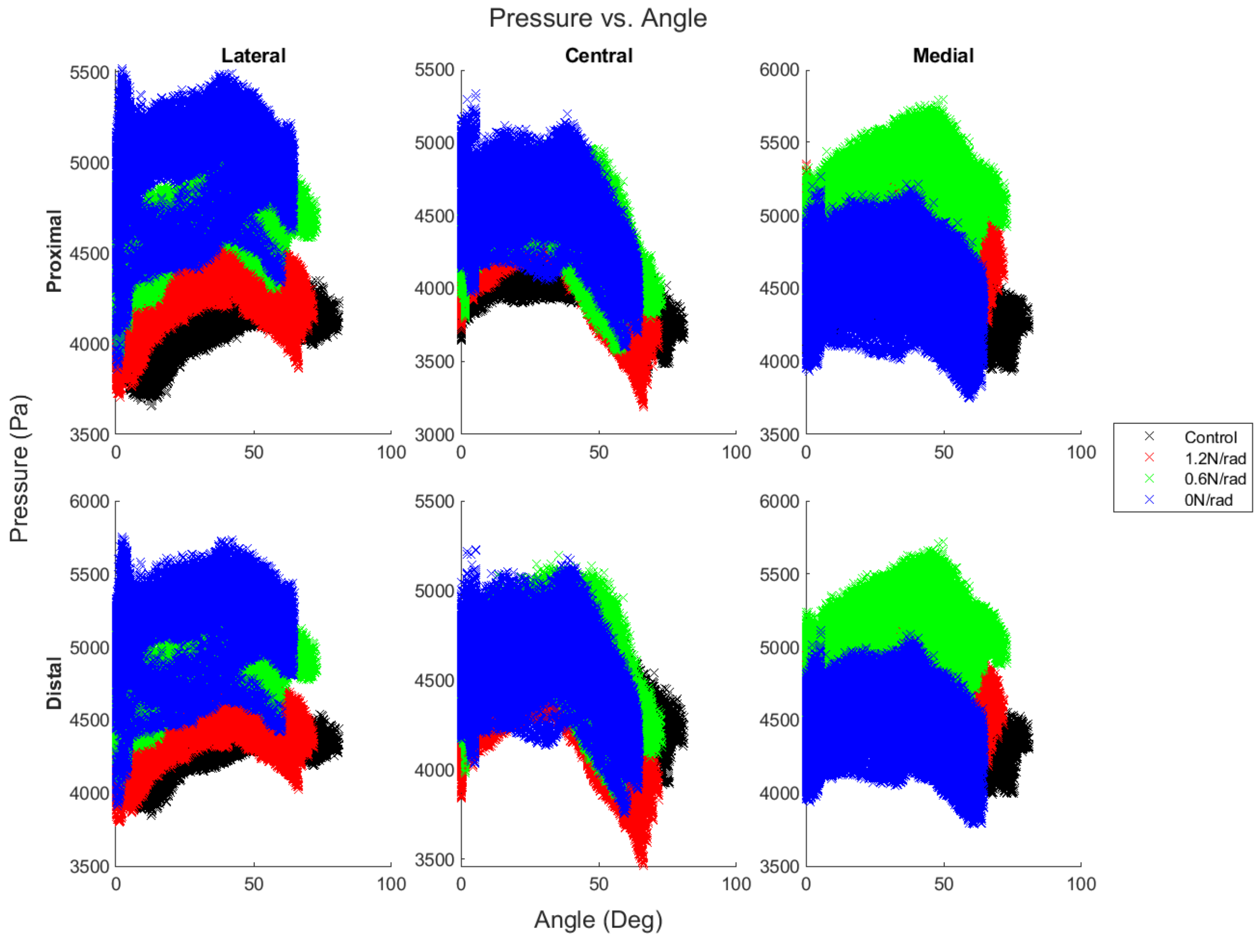

Figure D.20: Pressure readings on the thigh with longitudinal rotation permitted on the thigh interface.

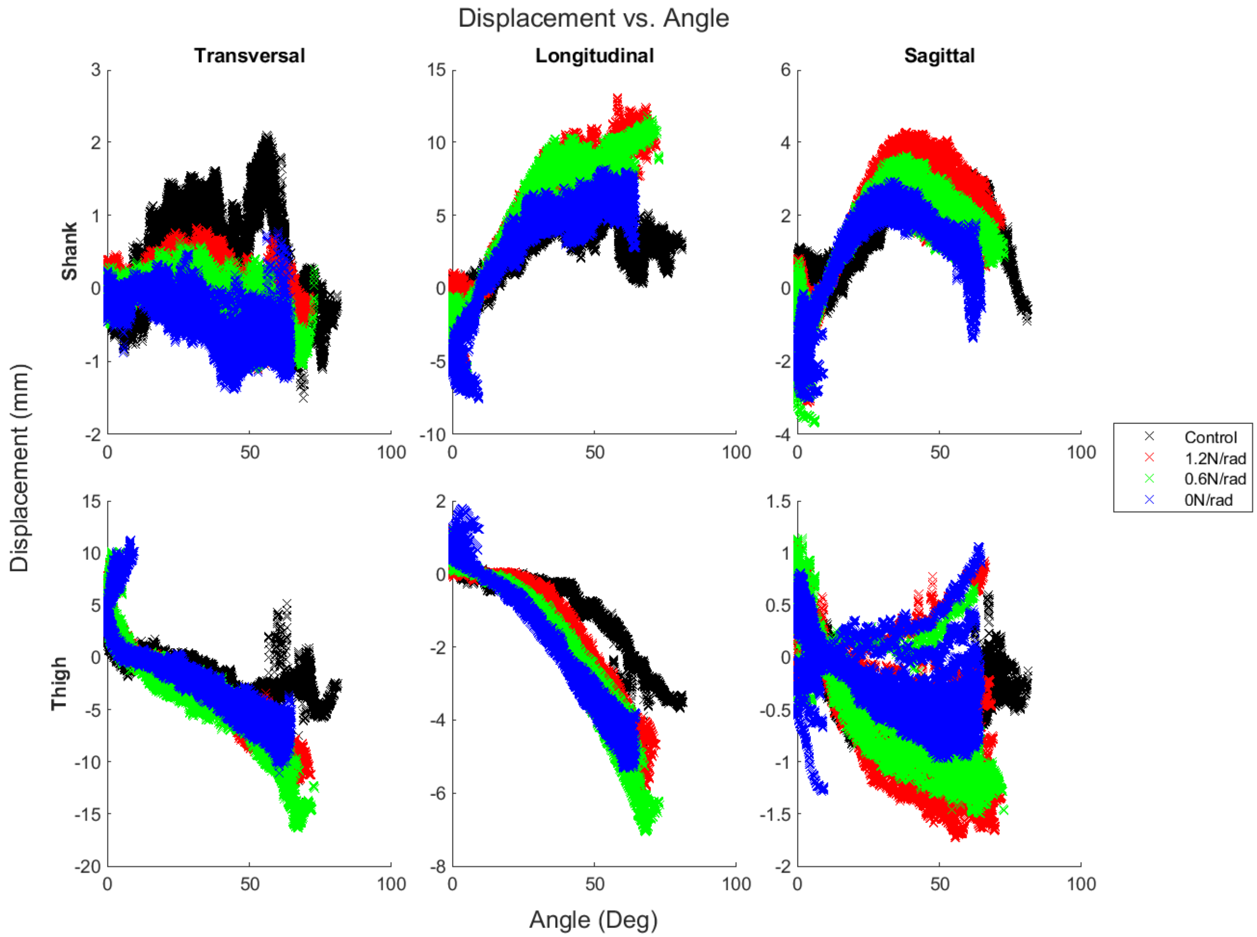

Figure D.21: Relative displacements of the limb segments and brace with longitudinal rotation at the thigh interface permitted.

Thigh Longitudinal Translational

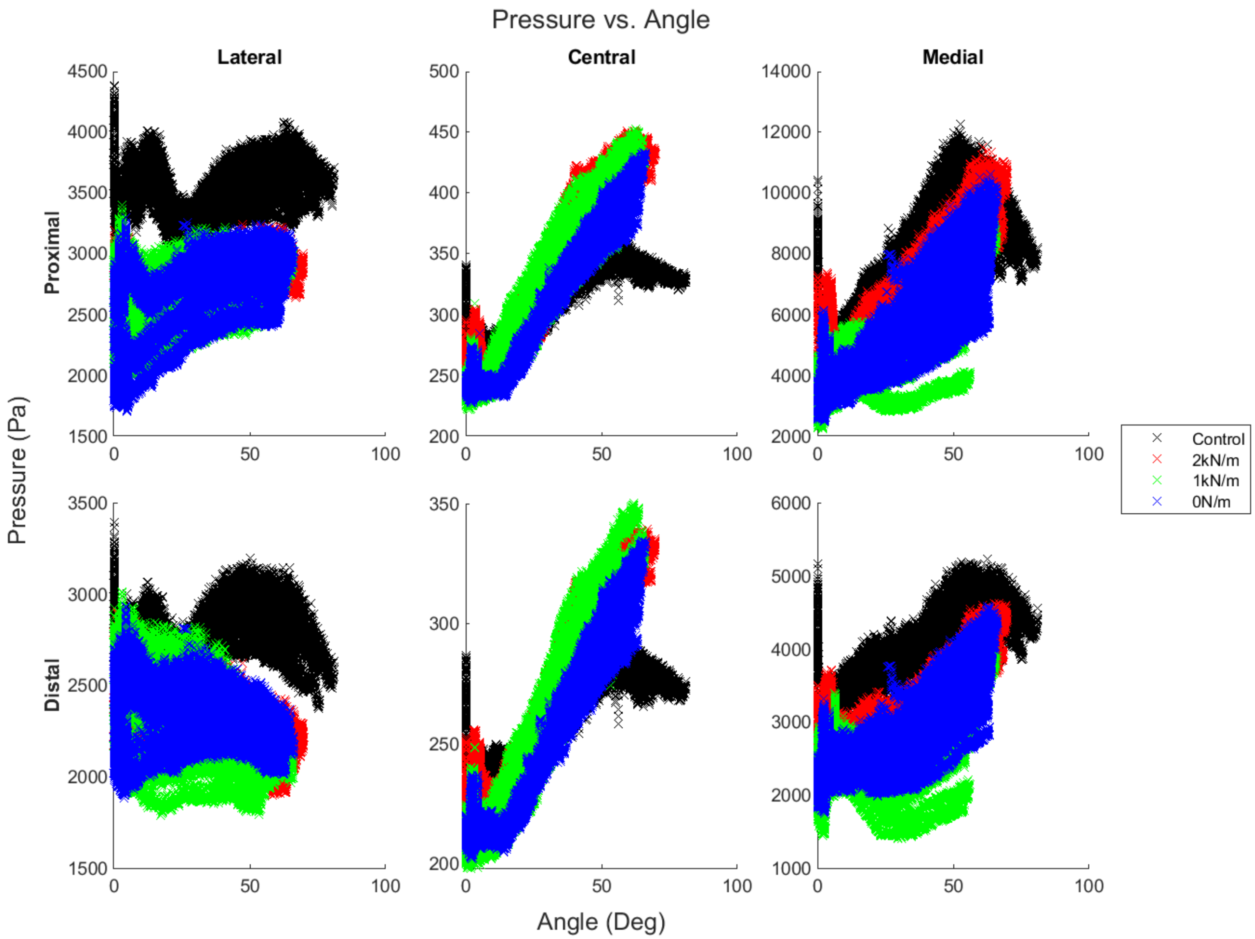

Figure D.22: Pressure readings on the shank with longitudinal translation permitted on the thigh interface.

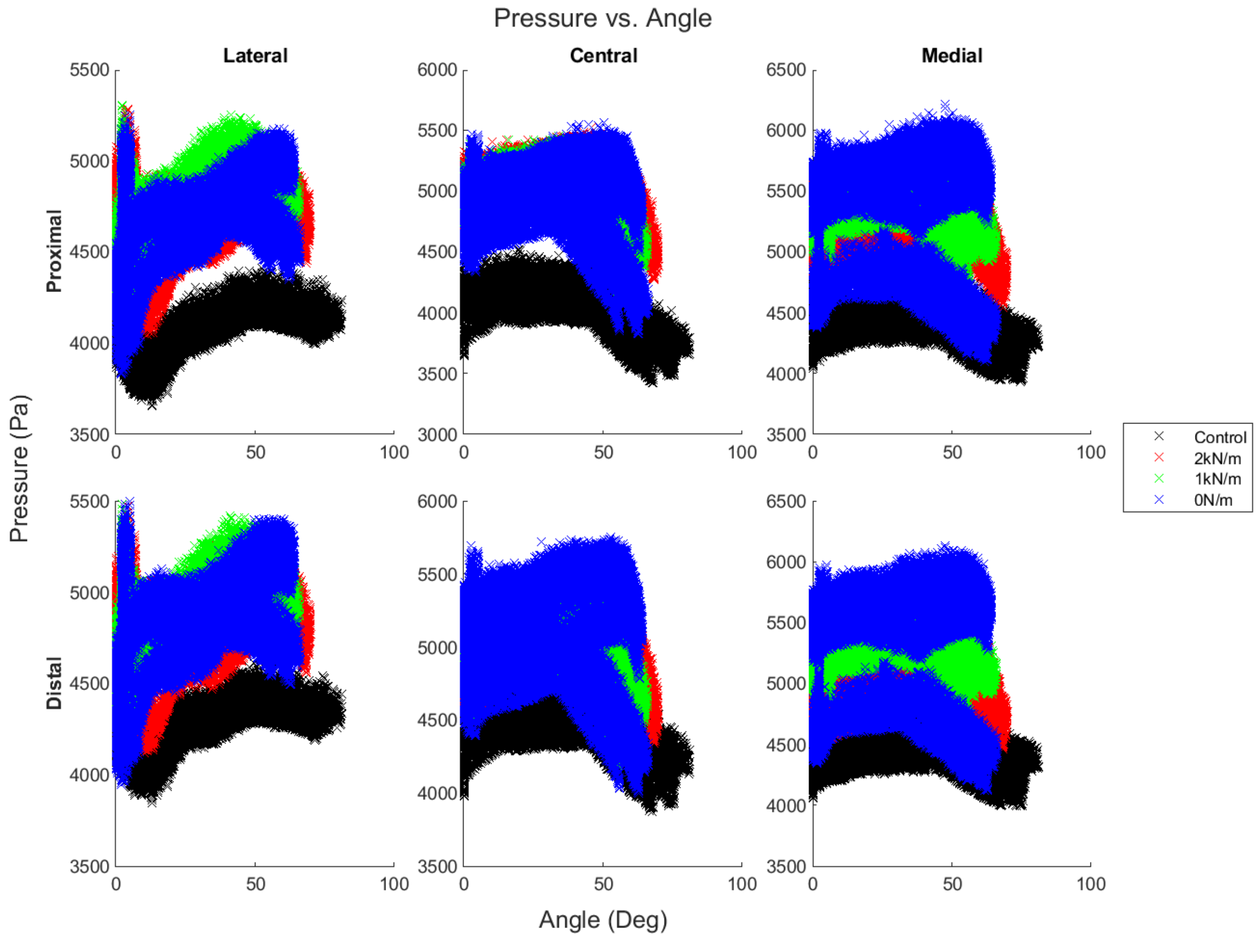

Figure D.23: Pressure readings on the thigh with longitudinal translation permitted on the thigh interface.

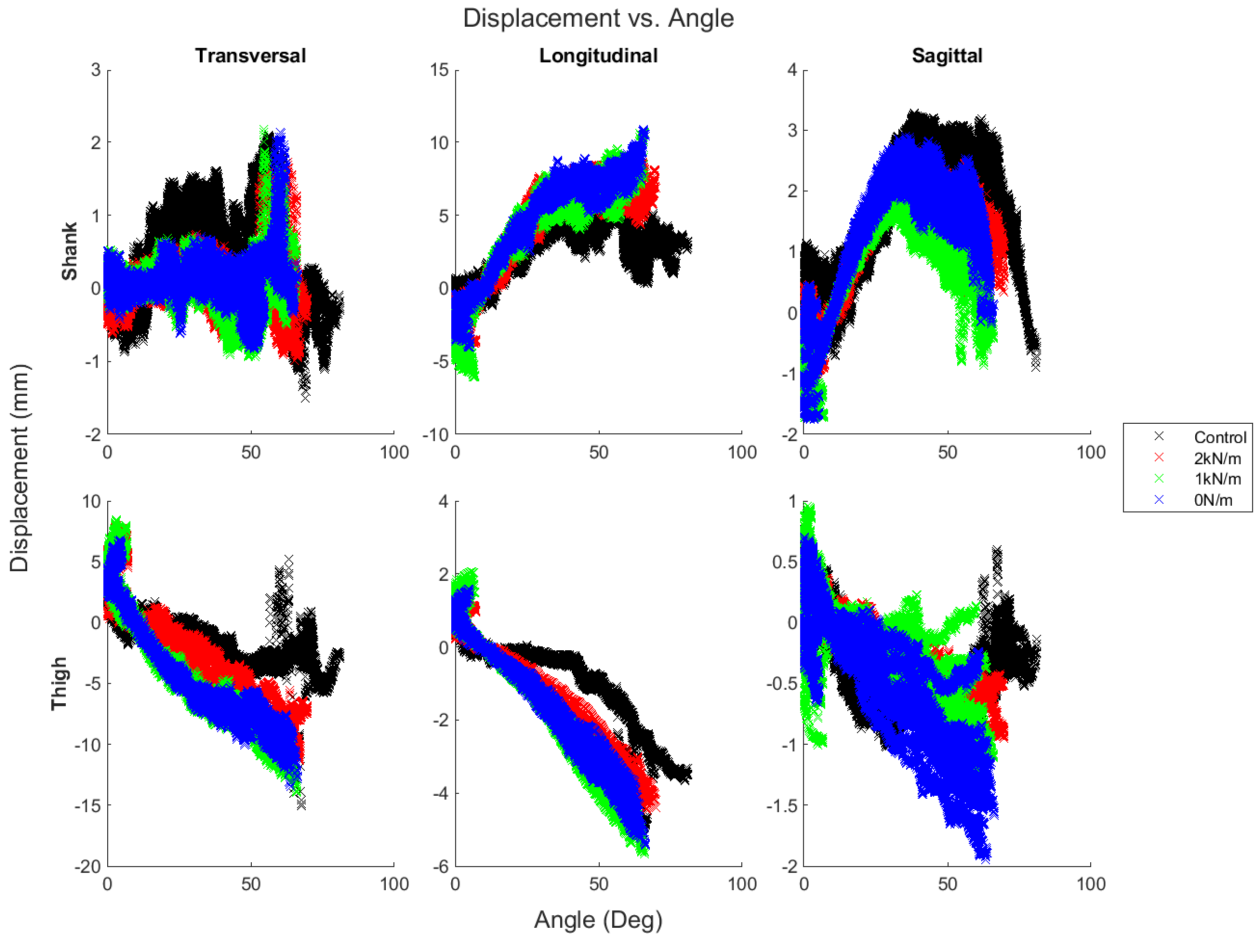

Figure D.24: Relative displacements of the limb segments and brace with longitudinal translation at the thigh interface permitted.

Thigh Sagittal Rotational

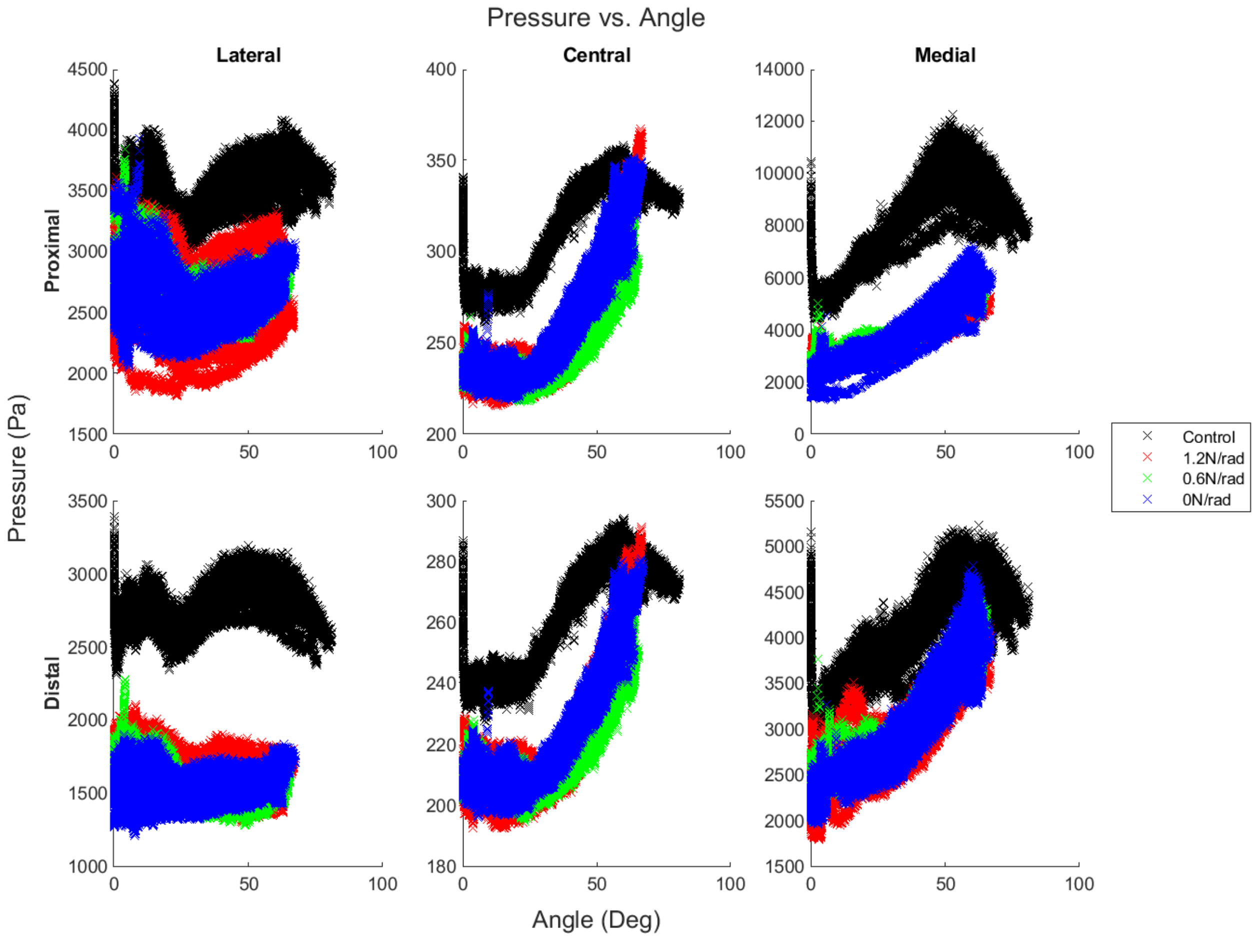

Figure D.25: Pressure readings on the shank with sagittal rotation permitted on the thigh interface.

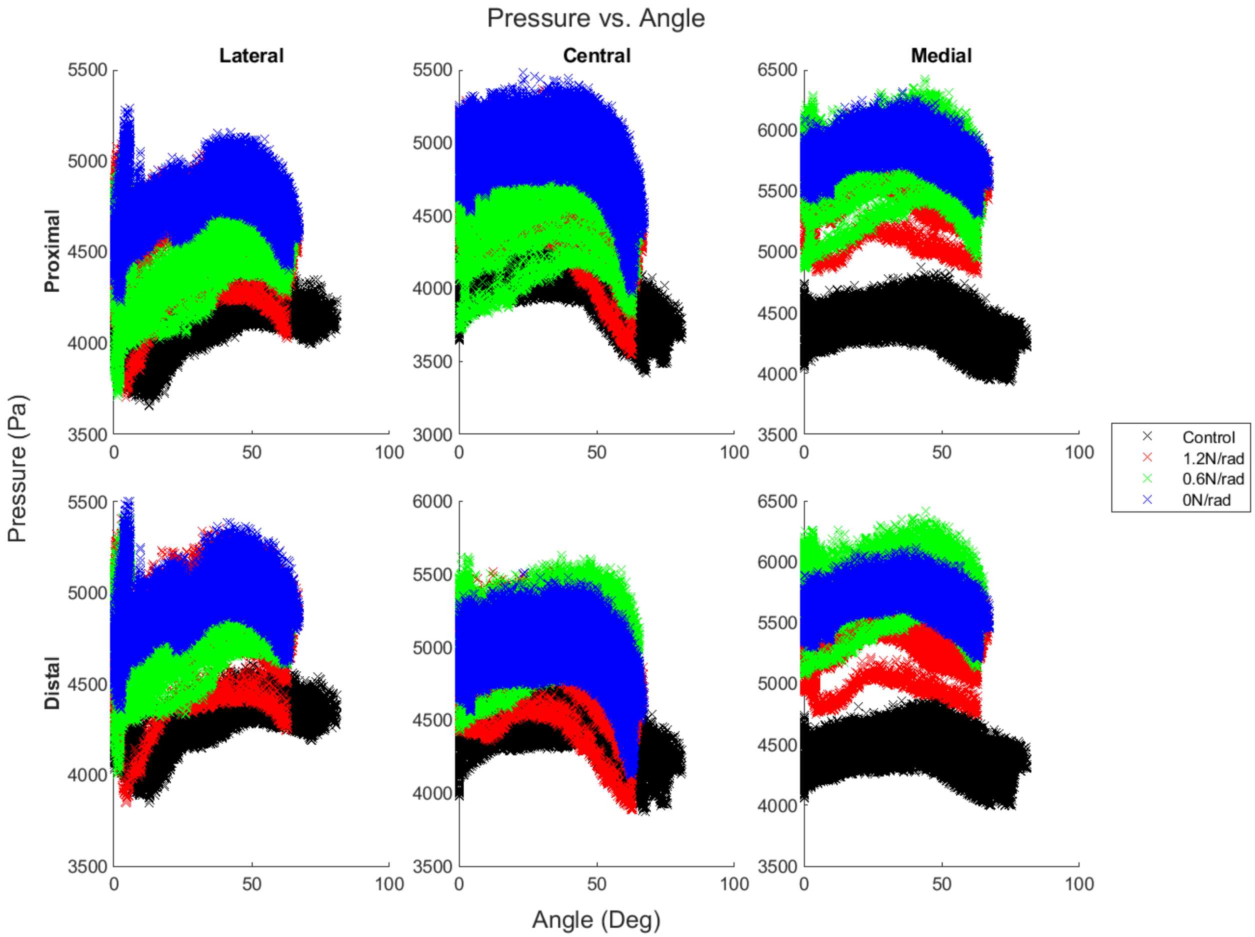

Figure D.26: Pressure readings on the thigh with sagittal rotation permitted on the thigh interface.

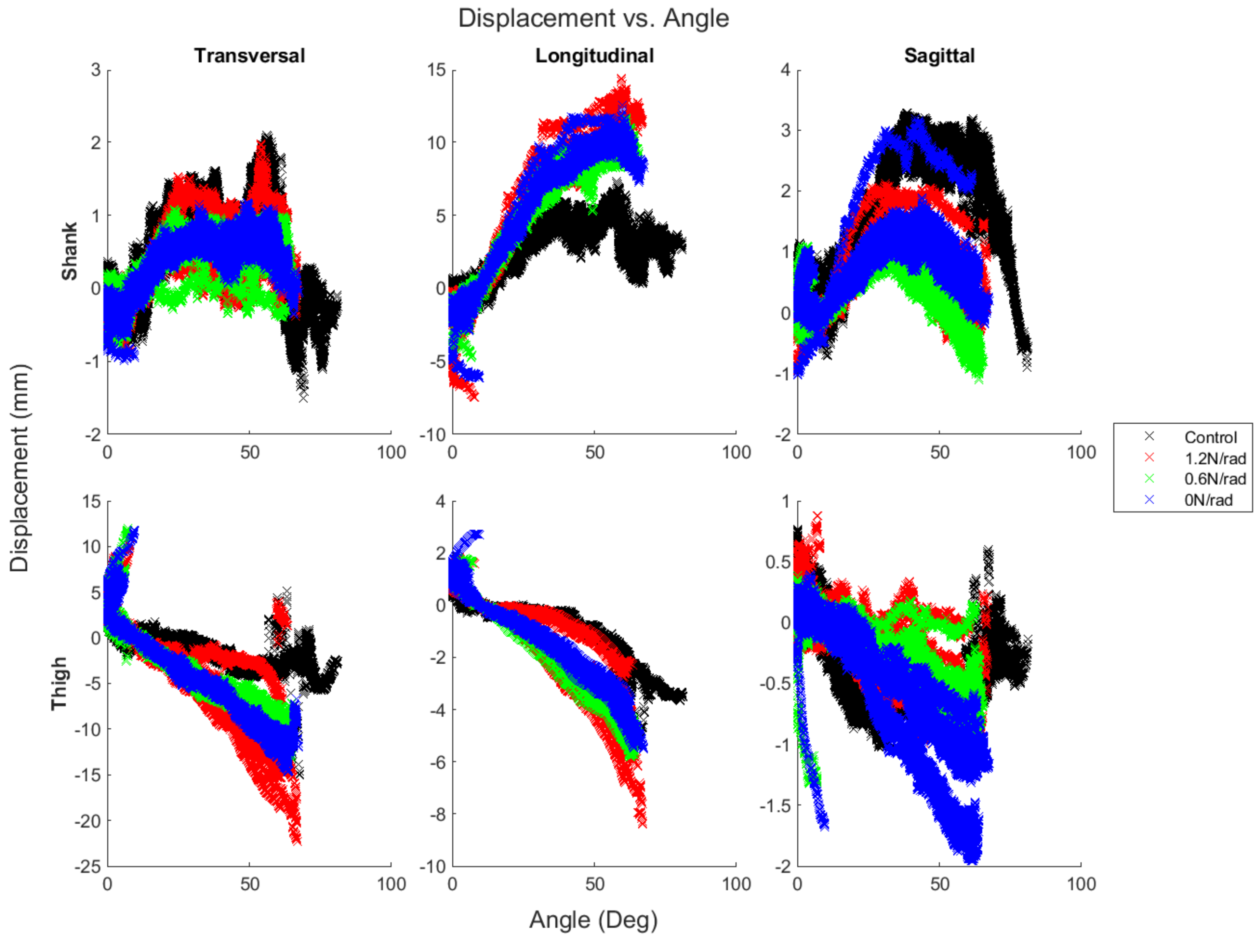

Figure D.27: Relative displacements of the limb segments and brace with sagittal rotation at the thigh interface permitted.

Thigh Sagittal Translational

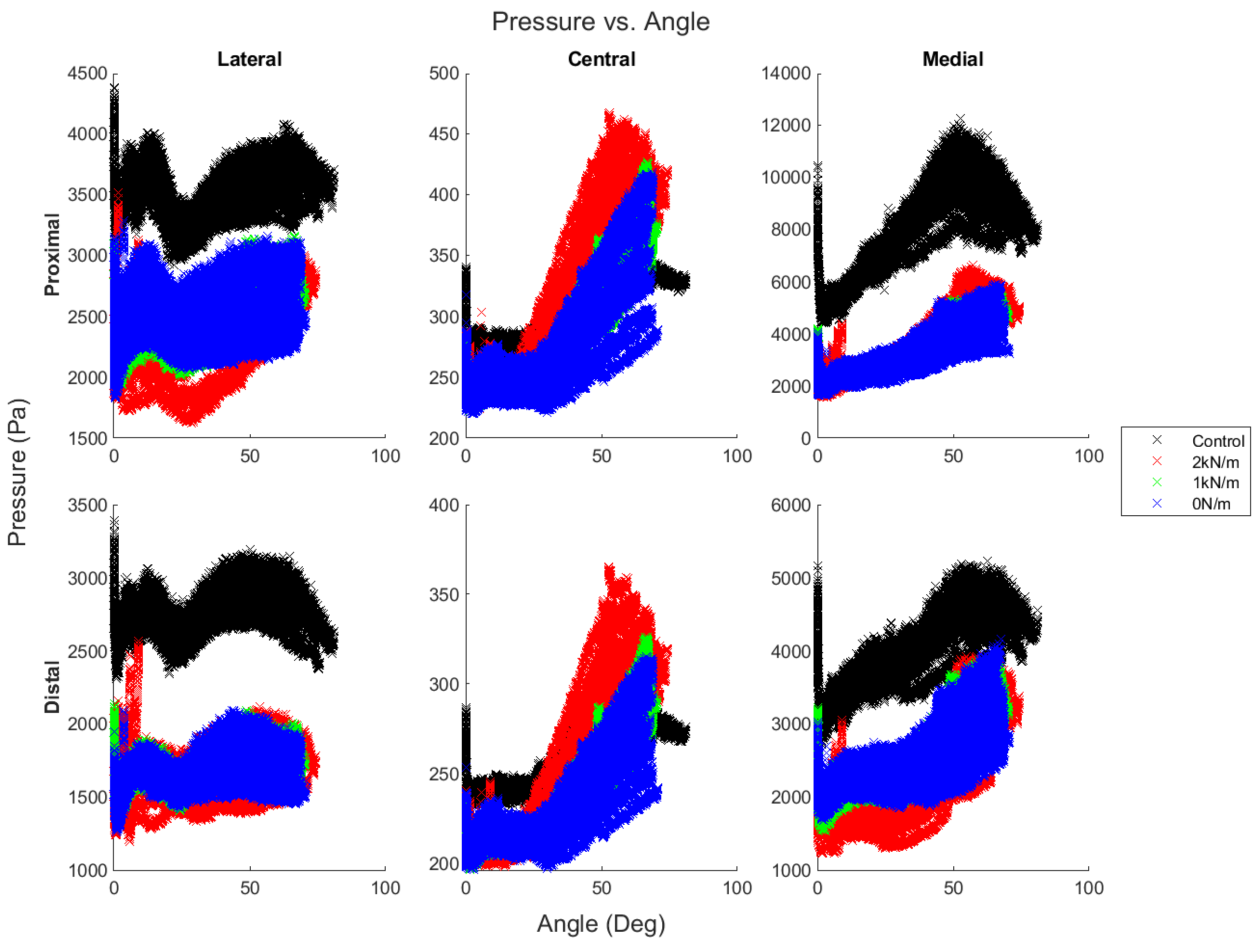

Figure D.28: Pressure readings on the shank with sagittal translation permitted on the thigh interface.

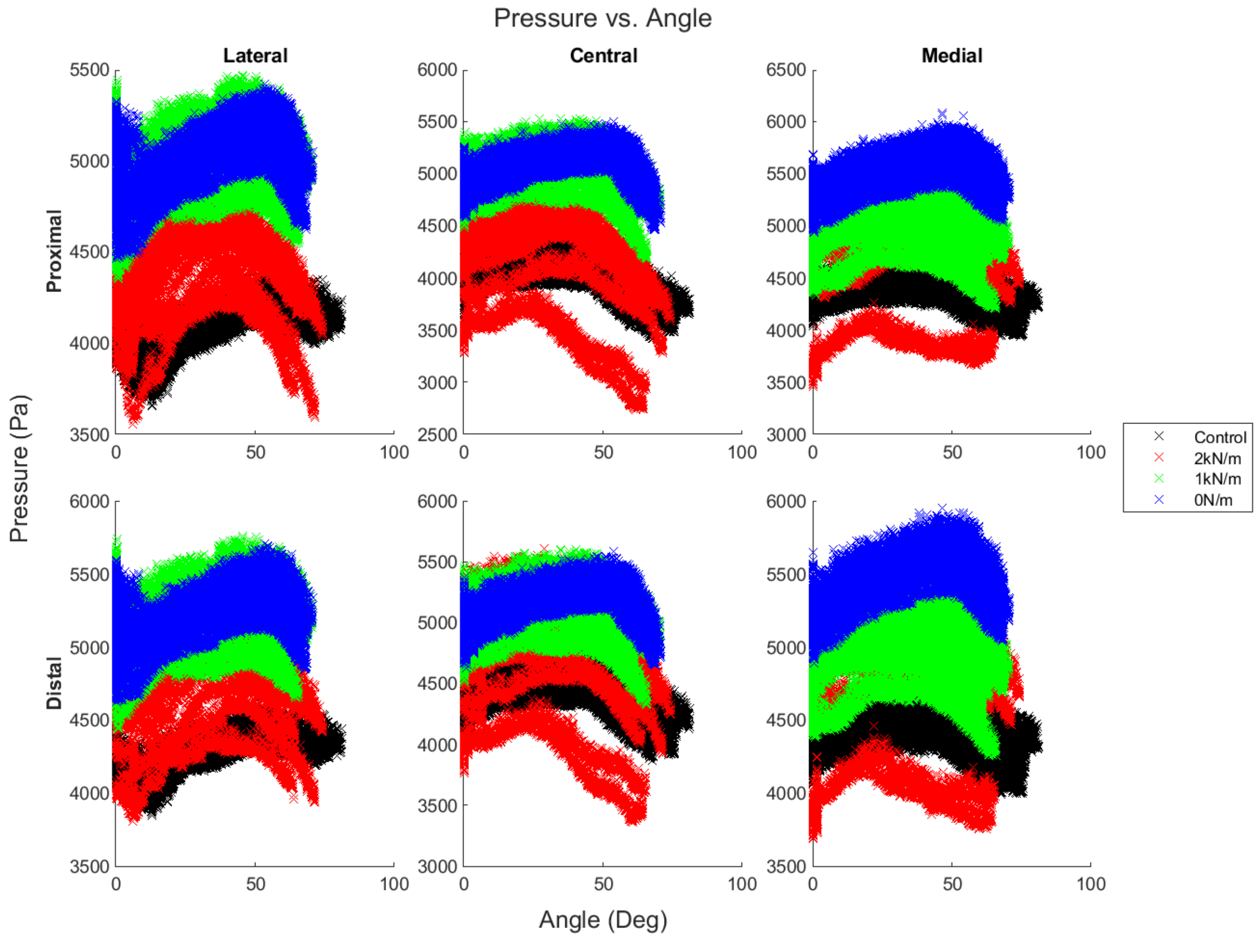

Figure D.29: Pressure readings on the thigh with sagittal translation permitted on the thigh interface.

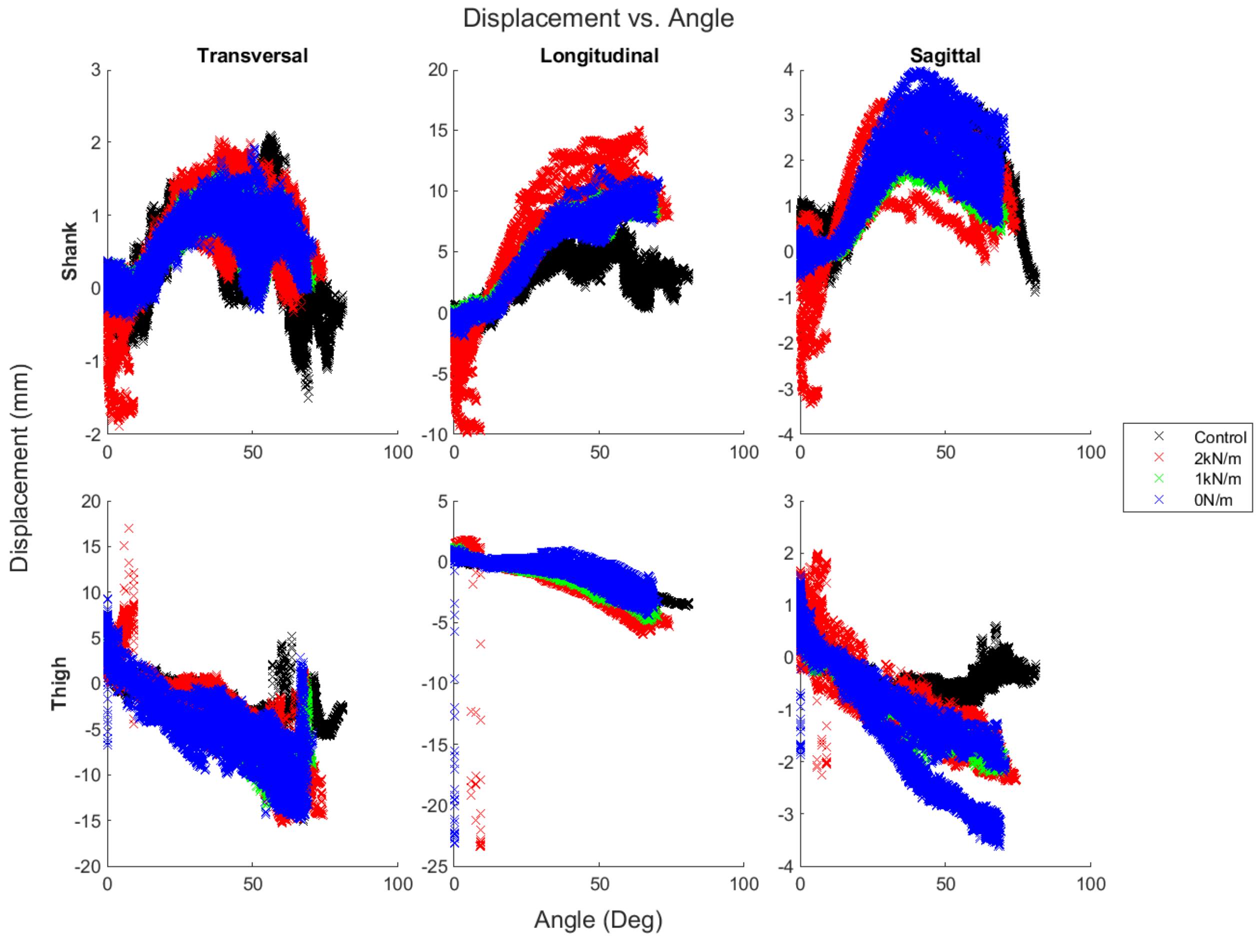

Figure D.30: : Relative displacements of the limb segments and brace with sagittal translation at the thigh interface permitted.

Thigh Transverse Rotational

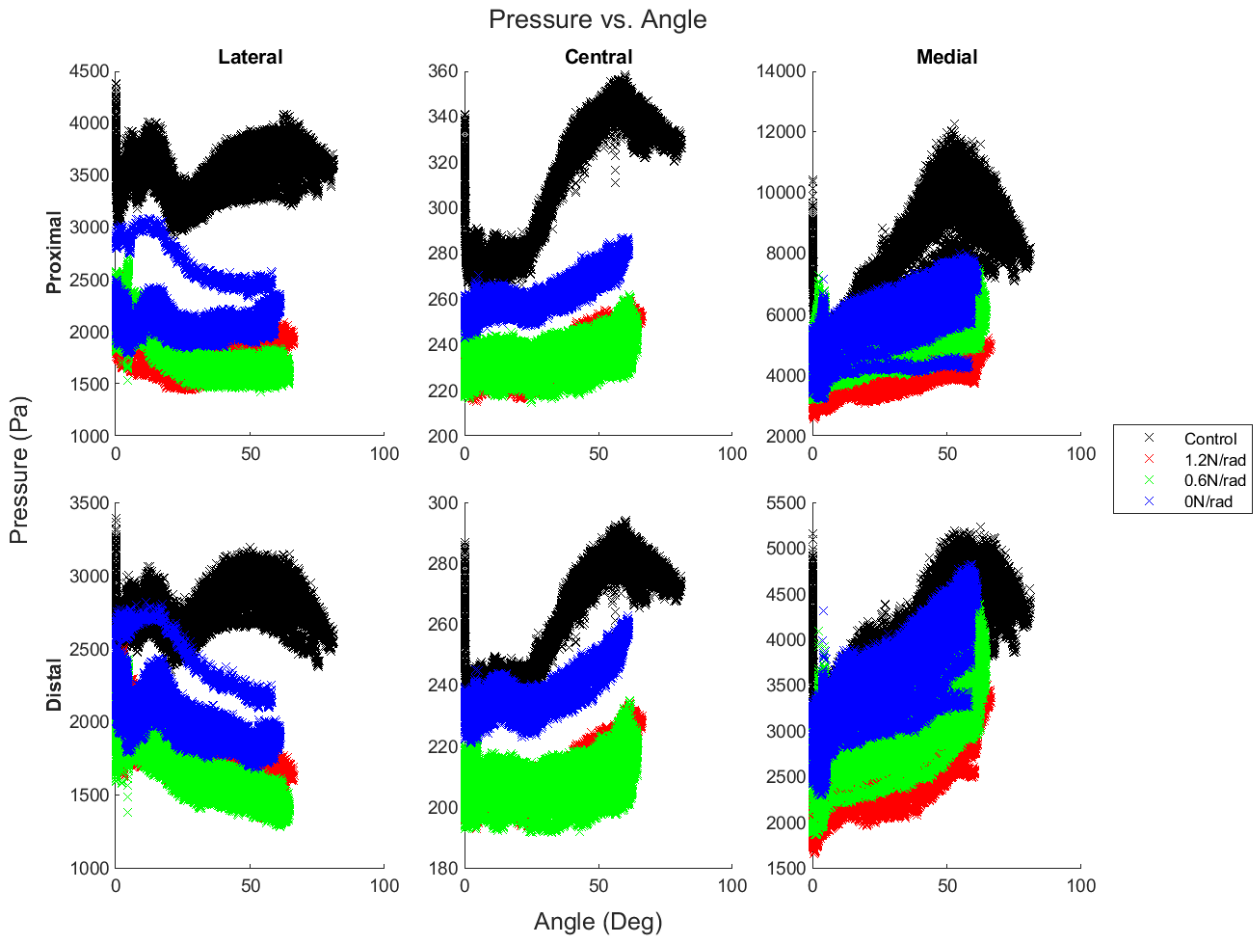

Figure D.31: Pressure readings on the shank with transverse rotation permitted on the thigh interface.

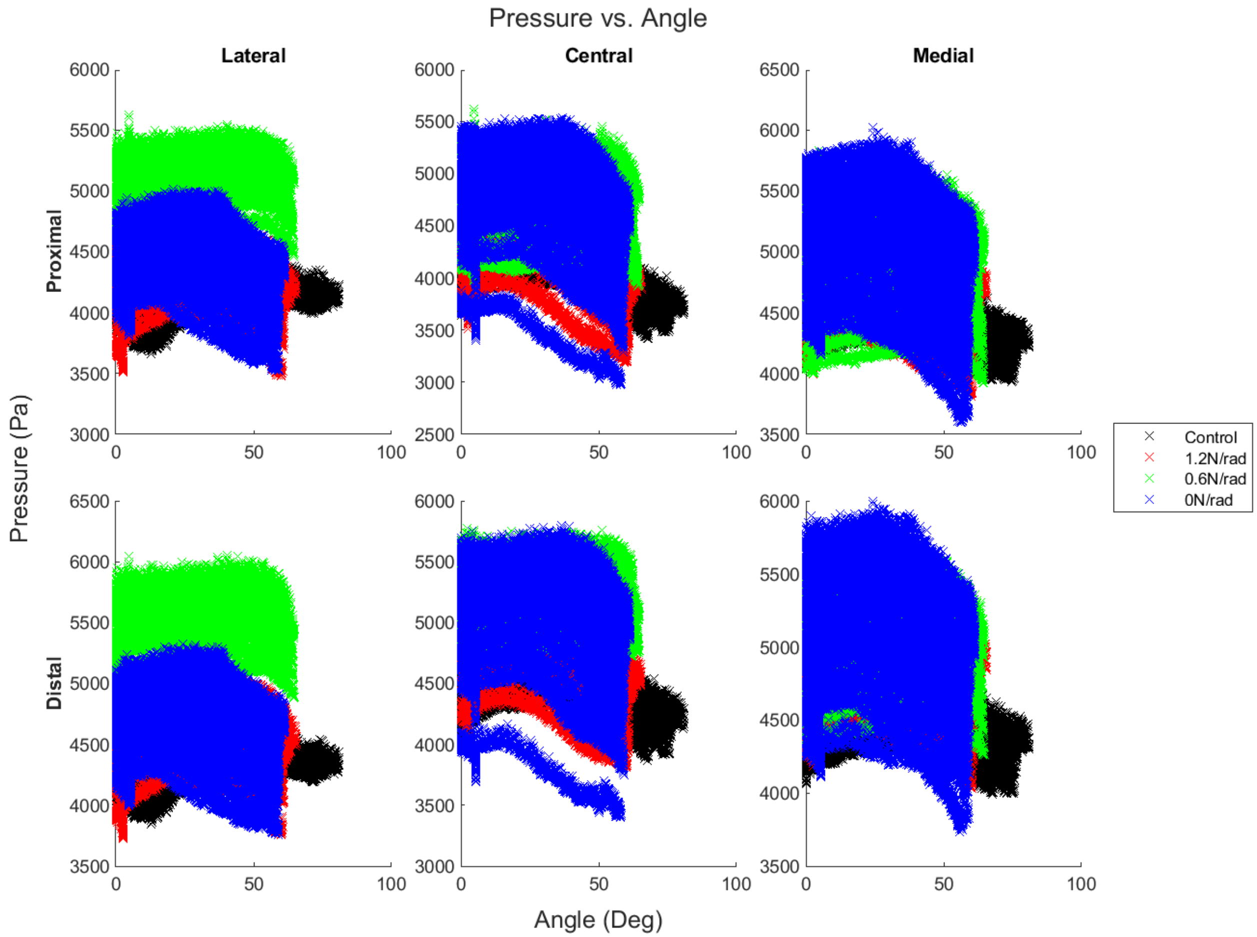

Figure D.32: Pressure readings on the thigh with transverse rotation permitted on the thigh interface.

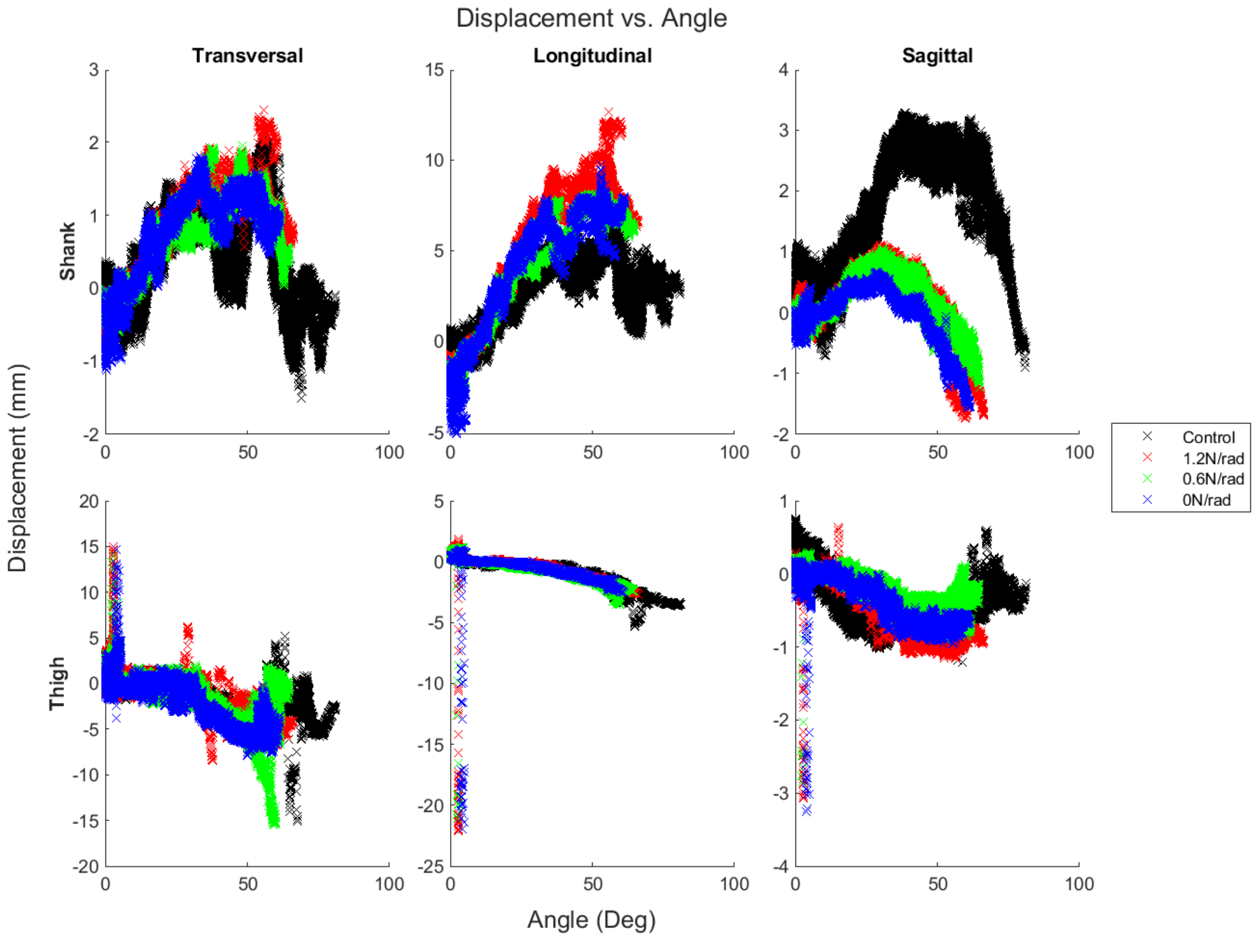

Figure D.33: Relative displacements of the limb segments and brace with transverse rotation at the thigh interface permitted.

Thigh Transverse Translational

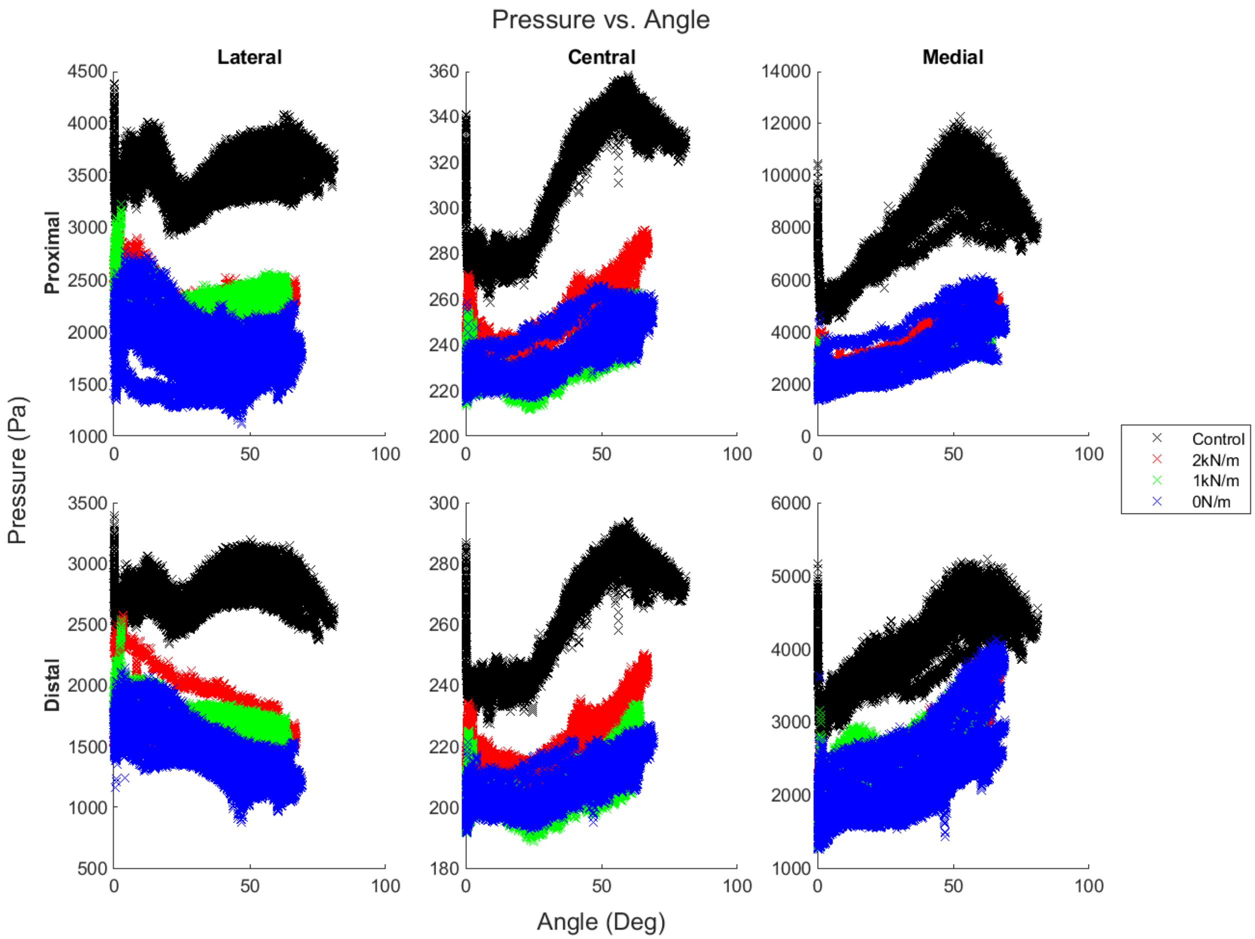

Figure D.34: Pressure readings on the shank with transverse translation permitted on the thigh interface.

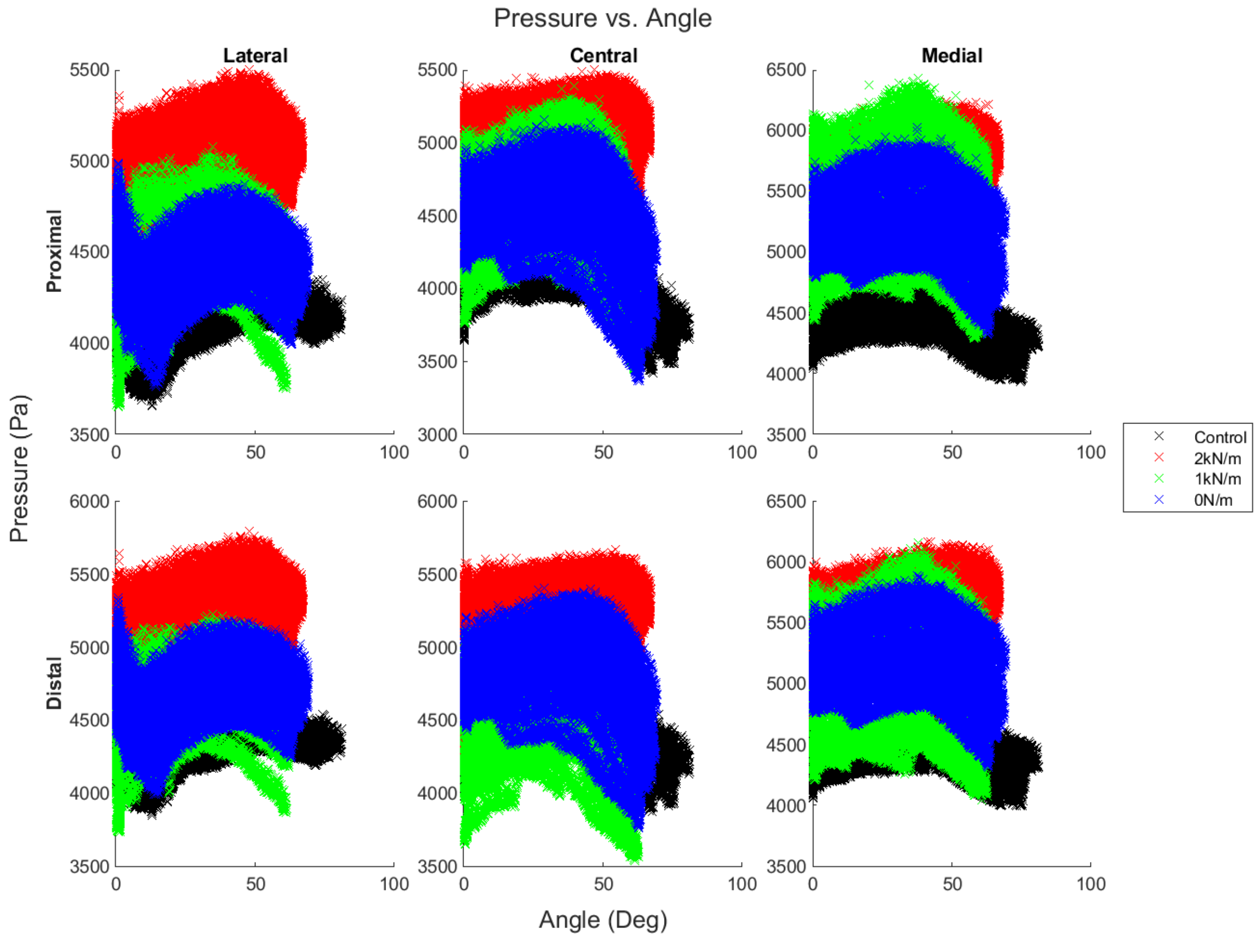

Figure D.35: Pressure readings on the thigh with transverse translation permitted on the thigh interface.

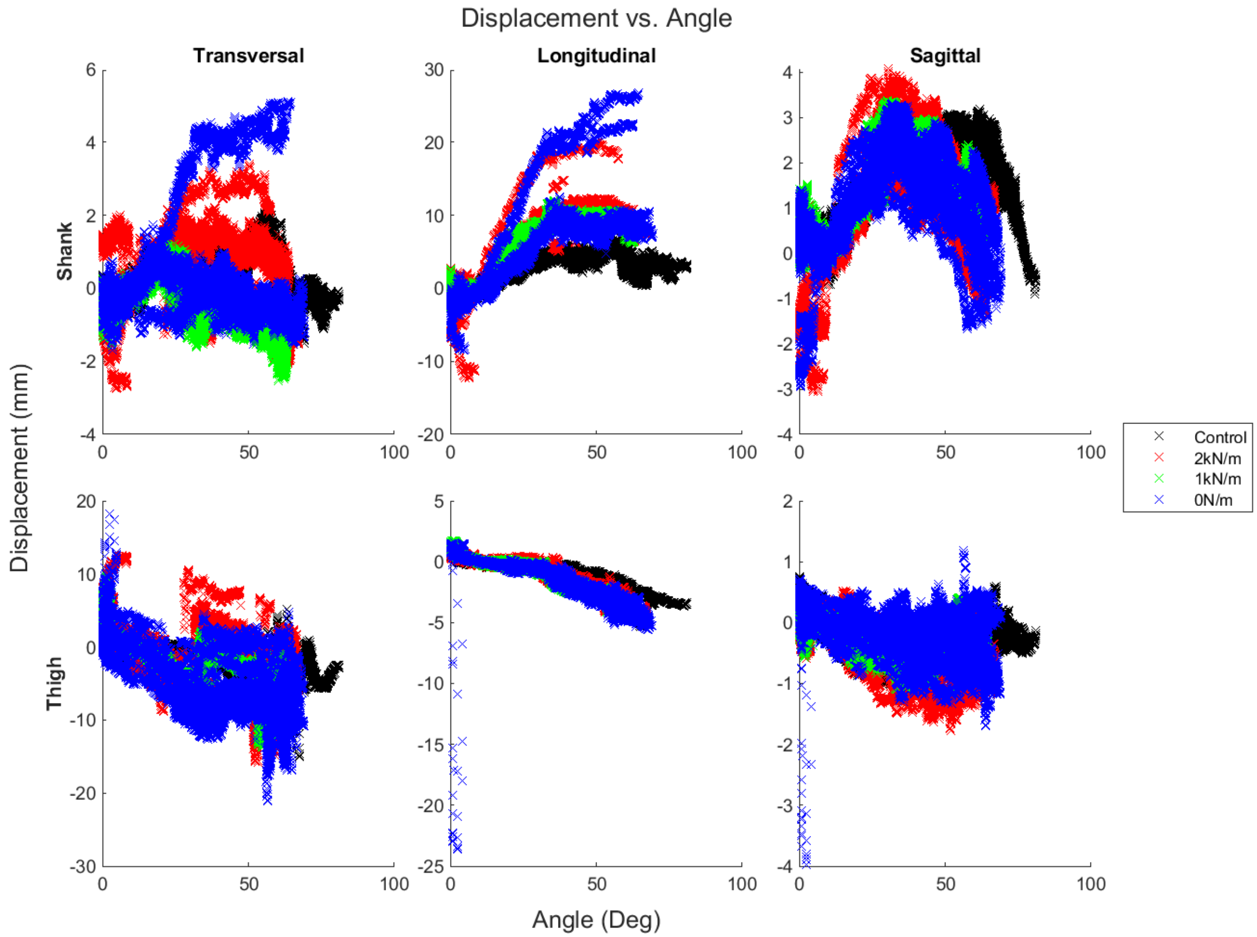

Figure D.36: Relative displacements of the limb segments and brace with transverse translation at the thigh interface permitted.

Appendix E – Ethics Certificate

26/06/2023

Université d'Ottawa
Bureau d'éthique et d'intégrité de la recherche

University of Ottawa
Office of Research Ethics and Integrity

CERTIFICAT D'APPROBATION ÉTHIQUE | CERTIFICATE OF ETHICS APPROVAL

Numéro du dossier / Ethics File Number	H-06-23-9326
Titre du projet / Project Title	Experimental characterization of passive degrees of freedom in a knee exoskeleton connection mechanism
Type de projet / Project Type	Thèse de maîtrise / Master's thesis
Statut du projet / Project Status	Approuvé / Approved
Date d'approbation (jj/mm/aaaa) / Approval Date (dd/mm/yyyy)	26/06/2023
Date d'expiration (jj/mm/aaaa) / Expiry Date (dd/mm/yyyy)	25/06/2024

Équipe de recherche / Research Team

Chercheur / Researcher	Affiliation	Role
Kaleb MANNION	Département de génie mécanique / Department of Mechanical Engineering	Chercheur Principal / Principal Investigator
Marc DOUMIT	Département de génie mécanique / Department of Mechanical Engineering	Superviseur / Supervisor

Conditions spéciales ou commentaires / Special conditions or comments

550, rue Cumberland, pièce 154
Ottawa (Ontario) K1N 6N5 Canada

550 Cumberland Street, Room 154
Ottawa, Ontario K1N 6N5 Canada

613-562-5387 • 613-562-5338 • ethique@uOttawa.ca / ethics@uOttawa.ca
www.recherche.uottawa.ca/deontologie | www.recherche.uottawa.ca/ethics

26/06/2023

Université d'Ottawa

Bureau d'éthique et d'intégrité de la recherche

University of Ottawa

Office of Research Ethics and Integrity

Le Comité d'éthique de la recherche (CÉR) de l'Université d'Ottawa, opérant conformément à l'*Énoncé de politique des Trois conseils* (2014) et toutes autres lois et tous règlements applicables, a examiné et approuvé la demande d'éthique du projet de recherche ci-nommé.

L'approbation est valide pour la durée indiquée plus haut et est sujette aux conditions énumérées dans la section intitulée "Conditions Spéciales ou Commentaires". Le formulaire « Renouvellement ou Fermeture de Projet » doit être complété quatre semaines avant la date d'échéance indiquée ci-haut afin de demander un renouvellement de cette approbation éthique ou afin de fermer le dossier.

Toutes modifications apportées au projet doivent être approuvées par le CÉR avant leur mise en place, sauf si le participant doit être retiré en raison d'un danger immédiat ou s'il s'agit d'un changement ayant trait à des éléments administratifs ou logistiques du projet. Les chercheurs doivent aviser le CÉR dans les plus brefs délais de tout changement pouvant augmenter le niveau de risque aux participants ou pouvant affecter considérablement le déroulement du projet, rapporter tout évènement imprévu ou indésirable et soumettre toute nouvelle information pouvant nuire à la conduite du projet ou à la sécurité des participants.

The University of Ottawa Research Ethics Board, which operates in accordance with the *Tri-Council Policy Statement* (2014) and other applicable laws and regulations, has examined and approved the ethics application for the above-named research project.

Ethics approval is valid for the period indicated above and is subject to the conditions listed in the section entitled "Special Conditions or Comments". The "Renewal/Project Closure" form must be completedfour weeks before the above-referenced expiry date to request a renewal of this ethics approval or closure of the file.

Any changes made to the project must be approved by the REB before being implemented, except when necessary to remove participants from immediate endangerment or when the modification(s) only pertain to administrative or logistical components of the project. Investigators must also promptly alert the REB of any changes that increase the risk to participant(s), any changes that considerably affect the conduct of the project, all unanticipated and harmful events that occur, and new information that may negatively affect the conduct of the project or the safety of the participant(s).

Riana MARCOTTE
Responsable d'éthique en recherche / Protocol Officer
Pour/For **Daniel LAGAREC** Président(e) du/ Chair of the **Comité d'éthique de la recherche en sciences de la santé et sciences / Health Sciences and Sciences Research Ethics Board**

550, rue Cumberland, pièce 154 550 Cumberland Street, Room 154
Ottawa (Ontario) K1N 6N5 Canada Ottawa, Ontario K1N 6N5 Canada

613-562-5387 • 613-562-5338 • ethique@uOttawa.ca / ethics@uOttawa.ca
www.recherche.uottawa.ca/deontologie | www.recherche.uottawa.ca/ethics